ROOM USE ONLY

MAR 0 1 5 2012

INFRARED PHOTOELASTICITY;
PRINCIPLES, METHODS, AND APPLICATIONS

By

Gary Lee Cloud

AN ABSTRACT

Submitted to
Michigan State University
in partial fulfillment of the requirements
for the degree of

DOCTOR OF PHILOSOPHY

Department of Metallurgy,
Mechanics and Materials Science

1966

ABSTRACT

INFRARED PHOTOELASTICITY;
PRINCIPLES, METHODS, AND APPLICATIONS

By Gary Lee Cloud

An investigation was undertaken with the primary objective of extending photoelastic methods of stress analysis into the infrared portion of the electromagnetic spectrum. A review of the basic concepts and equations of photoelasticity serves to demonstrate that the methods of measurement of birefringence are not limited to the visible spectrum. Apparatus and techniques for observing and measuring birefringence in the infrared were developed. These methods were then employed in the study of stress birefringence in a broad range of wave lengths for various materials, including semiconductors.

Monochromatic radiation in the range of wavelengths between 405 nm and 1900 nm was obtained by selective filtering of spectral sources and isolation of a narrow band of wavelengths from white radiation through the use of interference filters. Type HR Polaroid sheet served to polarize the infrared radiation, and discs of half-wave retardation materials were used singly and stacked as quarter-wave plates for the spectral region between 0.7μ and 1.9μ. Plane-wise observation of birefringence was accomplished with an infrared converter, and results were recorded photographically in the visible and infrared up to 1.2μ using special infrared films. Pointwise sensing techniques were developed for the measurement of birefringence in the

spectral range between 1.2μ, the practical limit of imaging devices, and 1.9μ. A goniometric method of fractional isochromatic order determination was improved and employed in the quantitiative studies of material behavior.

The stress birefringence of Columbia Resin CR-39 and Palatal P-6 was investigated in the visible and near infrared by planewise measurements. The stress-optical properties of polycarbonate resin between 1.1 and 1.9 microns wavelength were measured with the point-sensing and compensation techniques. Preliminary observation and measurement of stress-induced birefringence in silicon were accomplished with the infrared converter and point-sensor systems. The physical and technological implications of the stress birefringence of this nontransparent semiconductor are very interesting. Additional limited experimentation with amorphous selenium showed that this material may also prove useful for instrumentation.

It is known that for many materials the order of isochromatic is not simply inversely proportional to wave length. This dependence of the photoelastic coefficients on wavelength is called dispersion of birefringence in analogy to a similar phenomenon occurring in optics. Examination of past descriptions of dispersion, which are partially arbitrary, shows them to be inadequate in view of progress in photoelasticity, spectroscopy and polymer physics. New measures of dispersion were developed. Using these new ideas, the dispersion of birefringence of CR-39, P-6, and polycarbonate were derived from the calibration data. It was found that the stress-optic coefficient for

CR-39 changes by about 5% in the visible spectrum. The coefficient for P-6 changes by 11% in the same range, indicating that serious errors could result if constant coefficients were used in tests involving more than one wavelength. The dispersion of birefringence may be closely related to structural changes at microscopic levels, and, thus, might serve as an indicator of mode of deformation as well as of material behavior. The birefringence and dispersion of P-6 were found to depend on sign as well as magnitude of stress. Continued investigation of these problems and others suggested by the research will contribute immediately to the technology and application of photoelasticity in addition to providing insight into material behavior and the physical basis of induced birefringence.

INFRARED PHOTOELASTICITY;
PRINCIPLES, METHODS, AND APPLICATIONS

By

Gary Lee Cloud

A THESIS

Submitted to
Michigan State University
in partial fulfillment of the requirements
for the degree of

DOCTOR OF PHILOSOPHY

Department of Metallurgy,
Mechanics and Materials Science

1966

G41482
1-9-67

ACKNOWLEDGEMENT

The author expresses his sincere appreciation to Dr. Jerzy T. Pindera for his suggestion of the experimental problem and his guidance and support of the research. The dedicated efforts of Dr. George E. Mase, who advised the author throughout his course of study and the preparation of the dissertation, are gratefully acknowledged. Finally, the author wishes to thank the members of his doctoral committee, Dr. Lawrence E. Malvern, Dr. William A. Bradley, and Dr. Robert H. Wasserman, for their encouragement and direction.

TABLE OF CONTENTS

Article			Page
1.	Statement of the Problem		1
	1.1.	Summary of Development of Photoelasticity	1
	1.2.	Purpose and Scope of the Investigation	3
	1.3.	Review of Related Literature	4
2.	Techniques of Investigation		9
	2.1.	The Photoelastic Method	9
		2.1.1. Nature of Light and the Electromagnetic Spectrum	9
		2.1.2. Refraction, Retardation, Birefringence	14
		2.1.3. Birefringence in Deformable Bodies	18
		2.1.4. The Equations of Photoelasticity	22
		2.1.5. Optical Dispersion and Dispersion of Birefringence	30
	2.2.	Infrared Photoelasticity Apparatus and Technique	35
		2.2.1. Optical Systems Used	35
		2.2.2. Elements of the Optical Systems	37
		2.2.3. Measurement of Fractional Isochromatic Order	63
3.	Determinations of Optical Behavior of Materials		73
	3.1.	Descriptions of Materials and Testing Procedures	73
		3.1.1. Tensile Calibration of CR-39 in Visible and Near Infrared	73
		3.1.2. Tests of Palatal P-6	79
		3.1.3. Birefringence of Polycarbonate between 1 and 2 microns	83
		3.1.4. Preliminary Investigations of Birefringence of Semiconductors	88
	3.2.	Treatment of Data and Presentation of Results	90
		3.2.1. Calibration of P-6 and CR-39	90
		3.2.2. Calibration of Polycarbonate	100
		3.2.3. Dispersion of Birefringence of CR-39, P-6, and Polycarbonate	102
		3.2.4. Birefringence of Semiconductors	115

Article Page

4. Discussion and Conclusion 117

4.1. Summary of Techniques and Apparatus 117
4.2. Material Behavior 121
4.3. Continuation of the Research 134

Bibliography 136

LIST OF FIGURES

Number	Title	Page
2.1	The Electromagnetic Spectrum	144
2.2	Infrared Polariscope Arrangements	145
2.3	Photoelastic Apparatus for the 1-2 Micron Region.	146
2.4	Emission of Helium Lamp in Infrared	147
2.5	Transmission of Representative Interference Filters.	148
2.6	Infrared Sensing Circuit	149
2.7	Reduction of Error in Measurement of Fractional Isochromatic Order	150
3.1	CR-39 Model, Stress Distribution, Load History	151
3.2a	Isochromatic Pattern in CR-39 Model for λ = 546nm with Linear Polarization	152
3.2b	Isochromatic Pattern in CR-39 Model for λ = 1083nm with Linear Polarization	153
3.3	Ring Model of Cured Palatal P-6, Load History . .	154
3.4	Isochromatic Pattern in P-6 Ring for λ = 1083nm with Circular Polarization.	155
3.5	Beam Model of Cured Palatal P-6, Load History .	156
3.6a	Isochromatic Pattern in P-6 Beam for λ = 546nm with Circular Polarization	157
3.6b	Isochromatic Pattern in P-6 Beam for λ = 405nm with Linear Polarization	158
3.6c	Isochromatic Pattern in P-6 Beam for λ = 668nm with Linear Polarization	159
3.7	Disc Model of Polycarbonate, Load History	160
3.8	Fringe Order for Constant Wavelength and Calculated Stress Along Axis of Portion of CR-39 Model.	161

LIST OF FIGURES (continued)

Number	Title	Page
3.9	Fringe Order Per Unit Thickness for Constant Wavelengths in P-6 Beam	162
3.10	Fringe Order Per Unit Thickness for Constant Wavelength in P-6 Ring	163
3.11	Retardation Per Unit Thickness Along Axis of CR-39 Model for Various Wavelengths	164
3.12	Retardation Per Unit Thickness for Constant Wavelengths and Stress by Curved Beam Theory for P-6 Beam	165
3.13	Retardation Per Unit Thickness for Constant Wavelengths in P-6 Ring.	166
3.14	Fringe Order and Retardation Per Unit Thickness versus Stress for Constant Wavelength in CR-39. .	167
3.15	Examples of Fringe Order Per Unit Thickness at Constant Wavelength Versus Stress From Curved Beam Theory for P-6 Beam.	168
3.16	Fringe Order for Constant Wavelength Versus Corrected Stress in Polycarbonate	169
3.17	Representative Retardation Per Unit Thickness at Constant Wavelengths Versus Corrected Stress in Polycarbonate.	170
3.18	Spectral Transmittance of Polycarbonate.	171
3.19	Normalized Retardation versus Wavelength and Frequency for CR-39	172
3.20a	Representative Normalized Retardation Versus Wavelength for P-6	173
3.20b	Representative Normalized Retardation Versus Frequency for P-6.	174

LIST OF FIGURES (continued)

Number	Title	Page
3.21	Normalized Retardation Versus Wavelength for Polycarbonate for $1\mu < \lambda < 2\mu$	175
3.22a	Dispersion of Birefringence versus Wavelength for CR-39.	176
3.22b	Dispersion of Birefringence versus Frequency for CR-39.	177
3.23a	Dispersion of Birefringence versus Wavelength for P-6	178
3.23b	Dispersion of Birefringence versus Frequency for P-6	179
3.24	Stress Birefringence in Silicon	180

LIST OF TABLES

Number	Title	Page
2.1	Monochromatic Radiation Sources and Filters . . .	44
2.2	Manufacturers Specifications, Varo Inc., Model 5500C Detect-IR-scope	52
2.3	Photographic Films	54
4.1	Stress Optical Data in Infrared for Polycarbonate Resin	126

LIST OF APPENDICES

Article	Title	Page
A	Representative Measurements and Corrected Data for P-6 Beam at λ = 546 nm	181
B	Dimensions of Tapered CR-39 Model and Computation of Stress	182
C	Radius of Curvature and Stress in P-6 Beam . . .	183
D	Computation of Stress Difference in Polycarbonate Disc.	185
E	Illustrative Determination of Fractional Isochromatic Order in Polycarbonate Disc	186
F	Illustrative Normalized Retardation Data and Its Statistical Treatment for CR-39	187

LIST OF SYMBOLS

$\overline{E}$	Electric Intensity
$\overline{B}$	Magnetic Induction
K	Dielectric coefficient
μ	Magnetic permeability
v	Velocity of electromagnetic wave
C	Velocity of light in a vacuum
λ	Wavelength of radiation
μ	Micron = 10^{-6} meter
nm	Nanometer = 10^{-9} meter = millimicron
ν	Radiation frequency, cps
$\overline{\nu}$	Wave number
n	Absolute index of refraction
d	Thickness of parallel refractive plate
z	Distance along optical path
R_1, R_2	Absolute retardation of rays vibrating in principal planes 1 and 2
n_o	Absolute index of refraction of medium surrounding optical system (usually air)
n_1, n_2	Absolute indices of refraction corresponding to principal planes
R	Relative retardation
m	Isochromatic order
σ_1, σ_2	Principal stress
ϵ_1, ϵ_2	Principal strain
$\sigma_{\ell\ell}$	Maximum value of stress in linear range on basis of accepted deviation from linearity (0.5%, 1%, etc.) and given time

ϵ_{ll}	Maximum value of strain in linear range on basis of accepted deviation from linearity (0.5%, 1%, etc.) and given time
c_1, c_2	Absolute stress-optical coefficients
C_σ	Stress-optical coefficient
C_ϵ	Strain-optical coefficient
S_σ	Material stress-optical coefficient for d = 1 cm
n_λ	Absolute index of refraction at wavelength λ
n_F, n_C, n_D	Absolute indices of refraction referred to F, C, D Fraunhofer Lines
e	Quarter-wave plate error in wavelength
$\Delta n = n_1 - n_2$	Difference between indexes of refraction of rays vibrating in principal planes; a measure of birefringence
Δn°	Unit birefringence (for σ = 1 kg/mm^2)
R°	Unit relative retardation, unit retardation
r	Normalized relative retardation, normalized retardation
D	Dispersion of birefringence
D_λ°	Normalized dispersion of birefringence in terms of wavelength
D_ν°	Normalized dispersion of birefringence in terms of frequency

1. Statement of the Problem

1.1. Summary of Development of Photoelasticity

The discovery by Sir David Brewster in 1816 of stress-induced birefringence in glass established the beginnings of an optical method of experimental stress analysis. Brewster's discovery went almost unnoticed for nearly a century until Coker and Filon (10) and others began to develop this interesting physical phenomenon into a useful and powerful tool for science and engineering. Fundamentally, the method rests upon the measurement of the artificial double refraction in a material through the use of polarized light and the subsequent relating of this birefringence to the state of stress or strain in the material.

Since the time of Coker and Filon and their contemporaries, the photoelastic method has been greatly expanded in usefulness and technique, and it has been applied to a multitude of academic and practical problems. The mention of all significant works in the field of photoelastic analysis is neither necessary nor appropriate here. Comprehensive bibliographies are to be found in the classical work already cited, and in the book by Wolf (78) as well as the handbook edited by Hetenyi (29).

The disciplines of experimental mechanics and related areas of materials science have undergone considerable transformation in recent years. Photoelasticity has served and should continue to serve as a simple, inexpensive and straightforward method for

partially determining the state of stress or strain in simple and complicated structural shapes. The technique and application of the method is continually being refined and extended. A few of the writings which may be indicative of the general trend of thought include the works of Haberlund on the photoelastic analysis of plates (26), Kuske on wave propagation and the physical modeling of birefringent phenomena (41, 42), Schwieger on impact and photo-elastic coatings (71), Pindera in rheology and material behavior (58, 59, 60), and, of course, a multitude of others. Reference to one of the bibliographies mentioned above or current review papers and articles (25, 61) will further illustrate the range of endeavor in the application and improvement of photoelasticity.

A second aspect of the contemporary development of experimental mechanics appears in the form of a closer affiliation with what might be termed the basic sciences. Experimental methods of field analysis are generally drawn from fundamental physical phenomena. Examples include the disproportionately large change in resistance of a wire upon stretching, piezoelectric effects, sonic transmission and reflection, magnetostriction, and stress-induced double refraction (piezobirefringence). Many times the unifying basis of the physical measurements becomes lost or ignored in the bifurcation of packaged publishable research problems and the complications surrounding the technique of obtaining data and translating it into meaningful form. Doubtless, the closer alliance of the technology and application of measurement with the physical basis of the measure-

ment will contribute significantly in both areas. The experimental methods and the analysis of results will be simplified, improved, and extended, while the basic science will receive the benefit of experience, additional data, and the resulting improvement in understanding of physical phenomena.

One phase of the broadening of the base and the range of application of photomechanics is the utilization of a band of radiation which is wider than the visible spectrum. Such endeavor may be expected to contribute to the technique and range of application of photoelastic measurement. It should also furnish an addition to the catalogs of physical data. Then, taken as a part of the whole, there should result an increased understanding of the puzzling phenomenon of birefringence. Finally, this inquiry should lead to an improved conception of the relationships between structure, environment, history, and observed behavior of materials. Apart from the academic, the import of such understanding for the analysis and synthesis of material and for structural design is great. The extension of the photoelastic method outside the visible light spectrum forms the subject of this work.

1.2. Purpose and Scope of the Investigation

In view of the possible benefits derivable from such a study and the limited past inquiry into the problem, an investigation was undertaken with the primary purpose of extending photoelastic stress analysis into the infrared portion of the electromagnetic spectrum and establishing the physical and technological validity of the result.

The fundamental goal was to be approached through pursuit of a number of secondary experimental objectives:

1. To develop reliable apparatus, methods, and techniques for performing quantitative photoelastic investigations in the spectral region from the short wavelength limit of visible light up to about 2.0 microns wavelength.

2. To obtain preliminary stress-birefringence data for certain photoelastic materials from limited calibration tests using infrared radiation.

3. To improve the method of description of dispersion of birefringence and to measure the dispersion of certain materials over the visible and infrared ranges in accordance with the proposed definitions; also to make preliminary studies of the effects of stress and strain field upon the dispersion of birefringence.

4. To conduct limited studies of the stress-birefringence of various materials which are not transparent to visible light, in particular the semiconductors, and to inquire into their suitability for use as photoelastic materials in the given spectral range.

1.3. Review of Related Literature

The records of past investigations which are directly related to the measurement of birefringence in the long-wave region are limited in quantity. However, there exists much information in areas associated with the development of apparatus and techniques and the interpretation of results of infrared photoelastic investigations. Some of the significant and more comprehensive references will be

cited here. Other works of more retricted application are referred to in the sections of this report where they contribute most to the subject under discussion.

In 1957, Drechsler and Schreiner (17) used infrared radiation for the observation of stress-birefringence in certain polymers. The results were obtained through the use of light whose wavelengths extended continuously through the spectral range between the minimum wavelength transmitted by their visible light blocking filter and the upper limit of the light source and the sensing devices. Observation and photography were accomplished by means of a device which converted an image formed by infrared radiation of up to about 850 nanometers wavelength into a visible replica. The analysis was qualitative in nature. E. Hausmann and G. Junghamel in 1962 (28) published information on their more quantitative investigations into infrared photoelasticity. In the experiments described in the abstract of the last mentioned presentation, an infrared converter was employed to observe photoelastic patterns in simple, thin models made of polyvinyl chloride and ebonite. These materials are transparent to visible light only in thicknesses smaller than those used in the experiments. Nonmonochromatic radiation at a central wavelength of about 800 nanometers was used. A contribution of quite a different sort is due to Dietzel, Deeg, and Amrhein (15), who demonstrated the existence of double refraction of microwave radiation in a ceramic material.

Infrared radiation has been used in the observation of birefringence generated by internal structure, residual stresses and

slip in crystals. Dash (13) describes his experiments in relating the residual birefringence in silicon crystals, which are generally not transparent to visible light, to the crystal structure and growth process. Nonmonochromatic infrared light of somewhat less than one micron was used, and an infrared converter facilitated observation. Appel and Pontarelli (3) described an infrared crystallographic polariscope in an unpublished lecture. Besse and Desvignes (4) also developed an infrared polariscope for studies of crystal structure and behavior. Apparently, none of these latter investigations were concerned with the detection of birefringence which was artifically induced by stress. This problem has been pursued by Prussin and Stevenson (68), who measured the strain-optic coefficients of silicon crystals using an infrared converter and nonmonochromatic radiation at about 1.2 μ wavelength. Jacob and Schmidt-Tiedermann (34) used a similar technique in determining thermally-induced stresses in semiconductor junctions. The last-mentioned authors cite three other papers which describe measurements of the piezobirefringence of silicon (23, 30, 24). Apparently the experimental methods were similar, but the results differ widely.

Although there exists relatively little information directly related to the specific area of longwave photoelasticity, considerable data on the use of longwave radiation in other areas of science are available. Infrared light has become very important because of its suitability for use in the detection of hot bodies, alarm systems, and penetration of a broad class of materials. At the more fundamental

level, infrared spectroscopy has developed into a most useful tool for the analysis of material composition and structure. These and other military, scientific, and industrial applications of infrared radiation have led to the extraordinary development of the technology and theory associated with the generation, processing, and detection of longwave radiation. As a further result, an immense variety of apparatus for infrared studies is available commercially. Thus, although the application of infrared radiation to photoelastic stress analysis may have been neglected, the tools and knowledge are immediately available.

It is not practical to discuss here even a representative number of the recent books and papers dealing with the various aspects of infrared technology. Mention of only a few of these is sufficient for understanding of the work at hand. The comprehensive work of Jamieson and his associates (35) serves as a text of theory and a catalog of technological data, as does the book by Kruse, McGlauchlin and McQuistan (40). More elementary is the text by Hackforth (27). Interesting and useful data in the area of infrared technology, and other fields as well, is contained in the encyclopedic collection of Landolt-Börnstein (43) and the standard handbooks such as the one published by the American Institute of Physics (2) and that edited by Condon and Odishaw (11).

The basic works and bibliographies in photoelasticity have already been mentioned. Additionally, there is the concise work by Jessop and Harris (37) and also Frocht's classic text (20). Shurcliff's treatment (75) of the subject of polarized light places this matter upon

a firm mathematical and conceptual foundation within the limits of electromagnetic theory.

The science of optics is closely allied with the subject of photoelasticity. The classical and profound treatment of the subject by Born and Wolf (8) is most useful for its development of optics from the electromagnetic field equations. Among the many basic texts treating geometrical optics, the one by Sears (72) is mentioned only because of its simplicity, correctness, and general availability.

2. Techniques of Investigation

2.1. The Photoelastic Method

The measurement of stress-or-strain-induced birefringence using polarized visible light has been highly developed, and the techniques and theory have been treated extensively by many authors. Duplication of this information is neither appropriate nor necessary here. But, for the sake of completeness and to clearly establish the basis for extending photoelasticity into the longwave region, it is desirable to discuss briefly the nature of light, the equations of photoelasticity, the techniques of measurement, typical apparatus, and certain aspects of material behavior which are pertinent to the original investigation.

2.1.1. Nature of light and the electromagnetic spectrum

The exact nature of light is a question that has long puzzled scholars and scientists. Quite apart from this question, the problem of developing a system for the adequate description of the nature and the behavior of light has also received much study. For most purposes of photoelasticity, it is sufficient to consider light, including visible, ultraviolet, and infrared, as well as other forms of radiation such as heat and radio waves to be energy in the form of transverse electromagnetic waves. At any time, the wave train constituting a "ray" of radiation can be completely described by two vectors which are perpendicular to the direction of the ray and to each other. The first vector, $\overline{E}$, is usually called the

electric intensity vector, while the second, $\overline{B}$, is ordinarily known as the magnetic induction. Starting with the fundamental physical quantity known as "charge" and Coulomb's experimental law, the laws governing the behavior of a field of electromagnetic waves can be developed rationally. This electromagnetic field theory, which serves to describe the behavior of light waves, is based on a system of equations worked out by several investigators, then refined, extended, and systemized by James Clerk Maxwell in 1873. The treatment of the propagation of light waves by Maxwell's equations is simplified considerably because the wavelength of "light" is ordinarily negligible in relation to the other dimensions in common optical systems. The behavior of light is discussed from the viewpoint of electromagnetic theory in the comprehensive book by Born and Wolf (8). Coker and Filon (10) treat the matter especially as it is related to photoelasticity.

Emphasis must be given to the fact that field theory is only a workable method for describing without contradiction most observable phenomena associated with the transmission, reflection and propagation of light. The system is not complete, nor does it contain an expression of the exact physical nature of this radiation. Neither does the theory adequately explain the effects of light in changing the electrical conductivity of certain materials (photo-conductive or photoresistive), generating electron emission in others (photoemissive), being generated by electron bombardment in luminescent materials, exciting a voltage in some materials (photovoltaic), or even changing the magnetic properties of another class

of substances (photoelectromagnetic). These and other effects of radiation are partially explained by quantum wave mechanics in which light is considered to be composed of bundles or "photons" of energy. This theory provides a way of describing certain effects of light. It fails to account for certain other aspects of behavior. which are well described by field theory. In order words,, two methods of describing the behavior of light exist. Neither method is complete or sufficient, but they do not contradict one another or experimental observation. Both fail to express the fundamental nature of the radiation. This troublesome lack of completeness and consistency in the description of the nature of radiant energy and its interaction with bodies results from the restrictions on human senses and understanding. The picture is complete; man can see only a small part of it and he must rationalize the rest.

As will be seen, the various phenomena associated with birefringence are adequately described on the basis of electromagnetic field theory. The exception, for part of this work, is that a quantum affect of light is used in measuring the intensity of radiation. This exception must go unattended as something observable and useful but presently beyond precise physical description.

In a nonconducting medium which is free of electric charge, Maxwell's equations require that the electric vector $\overline{E}$, which is characteristic of the field, satisfy the wave equation:

$$\nabla^2 \overline{E} = K\mu \frac{d^2\overline{E}}{dt^2} \qquad (2.1)$$

For this equation, $K\mu = \frac{1}{v^2}$, where v is the velocity of propagation of the wave. It is the speed of light or any other electromagnetic disturbance, and in a vacuum it is found to be very nearly 3×10^{10} cm/sec. The values of K, the dielectric coefficient, and μ, the magnetic permeability, in the above equations depend on the choice of units.

A solution to the wave equation (2.1) may be taken in the form:

$$\overline{E} = \overline{F} \cos \frac{2\pi}{\lambda} (x - vt) \qquad (2.2)$$

This solution represents a harmonic plane wave of wavelength λ which is propagated in the x-direction with velocity v. $\overline{F}$ is a vector independent of x and t which specifies the amplitude and plane of the wave. Such a wave may be thought of as the simplest solution to the governing equation. Light rays which are not planar and/or which are composed of more than one wavelength can be described by a vector sum of more than one solution to the wave equation. If the medium is a conductor, the analysis is more complex, but will yield results which, within the limit of the present work, are the same.

As mentioned, the travelling wave of eq. (2.2) always lies in a single plane. Such a wave is said to be linearly polarized, the term "plane polarized" being ambiguous.

Associated with each train of light waves is a wavelength λ and velocity v. These two quantities are related to the frequency ν of the wave by the basic wave relation:

$$v = \nu\lambda \tag{2.3}$$

Since the frequency of a wave is constant, the wavelength must change directly with any changes in velocity which may occur when the wave passes from one medium into another.

The effect of electromagnetic waves upon human senses depends upon the wavelength or the frequency of the wave. The wavelength of light from ultraviolet through infrared is most conveniently expressed in terms of the micron ($1\mu = 10^{-6}$ meter) or the millimicron ($1 m\mu = 10^{-9}$ meter = 1 nanometer). In these units, ordinary visible light covers the range from about 0.4 micron through approximately 0.7 micron. The infrared range begins at about 0.7 micron and extends three decades up to the neighborhood of 1 millimeter, where short radio waves begin. The so-called radiant energy and radio spectral regions are known to overlap, and the two types are distinguished only by their sources, whether black body or electrical oscillator. The usual units for frequency of a wave are cycles per second (cps) designated ν, and wave number $\bar{\nu}$. The frequency, wave number and wavelength of radiation are related to each other and to the velocity of light in a vacuum as follows:

$$\nu(\text{cps}) = \frac{C(\mu/\text{sec})}{\lambda(\mu)} = \frac{3\text{x}10^{14}(\mu/\text{sec})}{\lambda(\mu)} \tag{2.4a}$$

$$\bar{\nu}(\text{cm}^{-1}) = \frac{1}{\lambda(\text{cm})} = \frac{\nu(\text{cps})}{C(\text{cm/sec})} \qquad (2.4b)$$

A chart showing the frequencies and wavelengths corresponding to the various regions of the electromagnetic spectrum is given in Fig. 2.1 along with an expanded diagram of the visible and infrared portions important to this investigation.

In this report, the term "light" will be applied to radiation of any wavelength whose primary function is illumination.

2.1.2. Refraction, Retardation, Birefringence

The rate at which a light wave travels through a transmitting medium depends only on the nature of the medium. In fact, the governing wave equation (2.1) indicates that the velocity of propagation of any electromagnetic wave through a material depends only on the dielectric constant and magnetic permeability of the material. The ratio of the speed of light in a vacuum to the speed of light in a particular material is known as the absolute index of refraction, n, of that material. The index ordinarily varies with the wavelength of light:

$$n_\lambda = \frac{C}{v} \qquad (2.5)$$

If a light ray passes through a parallel plate of refracting material, the ray will emerge from the plate in a position behind or ahead of the position which would have been occupied if the ray had not been disturbed. If d is the thickness of the plate whose index of refraction is n_1, and if n_o is the index of refraction of the material surrounding the plate, then the distance by which the refracted ray lags behind its unrefracted position is:

$$R_1 = (n_1 - n_o) \frac{d}{n_o} \qquad (2.6)$$

This is the "absolute retardation" of the ray of light by the refracting plate which is immersed in a refracting medium. To avoid ambiguity, the "relative refractive index" will not be used here.

In certain materials, the refractive index varies with orientation. An analysis of the transmission of an electromagnetic wave through such an anisotropic medium is outside the scope of this writing. The problem has been treated by several authors including, for example, Coker and Filon (10). For this work it is sufficient to observe that the propagation of a light wave through an optically anisotropic material can be described in terms of the refractive indexes corresponding to a certain set of orthogonal axes in the material. These are known as the principal axes and may be thought of as the axes around which the refractive indexes vary in a symmetrical manner. The indexes of refraction belonging to these principal axes may be termed the principal values of the refractive index. It can be shown that a material having unequal principal refractive indexes can transmit only light which is linearly polarized along the principal axes normal to the path of the light. The two polarized rays will travel through the medium at velocities dependent upon the refractive indexes corresponding to the principal axes in the plane of the wave front. These principal axes in the plane of the wave front and their respective refractive indexes are directly related to, but are not generally the same as the principal axes and principal indexes of the medium. The relationship depends upon the

direction of the light ray, and the two sets of axes and indices are the same only if the light path is along one of the principal axes of the transmitting material.

Suppose now that a ray of light is passed normally through a plane parallel plate of thickness d and made of material which is optically anisotropic. Let the principal values of the refractive index in the plane of the plate be n_1 and n_2, the two being unequal. Upon striking the plate, the ray will be polarized into components along the principal optical axes of the plate. The two components of the original ray will traverse the plate at different speeds, and upon leaving the plate, one component will be retarded with respect to the other. If the components could be separated from each other upon emergence from the plate, then two rays of mutually perpendicular linearly polarized light would be obtained. The Nicol Prism and certain other polarizers are based on this principle. Dichroic type polarizers, of which Polaroid sheet is an example, function in a similar manner. But, instead of separating the two rays, the dichroic polarizer simply absorbs one of them.

If the ray incident upon the plate is not polarized, meaning that it consists of a random assortment of polarized components, then the polarized components emerging from the plate will recombine (unless artificially separated) into a ray without a constant preferred orientation of the electric vector. The effects of the anisotropic material upon the unpolarized incident ray cannot be detected by ordinary means.

Suppose, however, that the ray incident upon the plate having unequal refractive indexes is linearly polarized. This ray will be resolved by the plate into two components bearing a known relationship to the original ray. The two components will each be retarded by the plate by amounts which may be computed from formula (2.6) for the absolute retardation due to a refracting plate.

$$R_1 = (n_1 - n_o)\frac{d}{n_o} \qquad R_2 = (n_2 - n_o)\frac{d}{n_o} \qquad (2.7)$$

The difference between these two values of absolute retardation represents the amount by which one component of the ray is retarded with respect to the other. This "relative retardation", R , is dependent on n_o, the refractive index of the surrounding medium. This fact is often ignored.

$$R = R_1 - R_2 = (n_1 - n_2)\frac{d}{n_o} \qquad (2.8)$$

The eye cannot determine whether or not light is polarized nor can it detect changes in phase of light waves. Thus, the light emerging from the plate just described will appear to be no different than the light entering the plate. In turn, the unaided eye cannot distinguish this from common unpolarized radiation. However, the state of polarization of the light leaving the plate differs from the known state of polarization of the incident ray. This difference can be detected and measured.

A plate of material whose principal refractive indexes differ is said to be doubly refracting or "birefringent". The detection and

measurement of the relative retardation produced between the components of a polarized ray passing through such a material forms the basis of the photoelastic method.

2.1.3. Birefringence in Deformable Bodies

Certain materials are naturally birefringent, and slabs of these materials retard light rays in the same manner as the birefringent plate of the previous section. Natural crystalline substances which are doubly refracting include Calcite (or Iceland Spar; $Ca0 \cdot C0_2$) and Sodium Nitrate ($NaN0_3$) as the most common examples. Both of these crystals are used in the manufacture of birefringence type polarizers such as the Nicol prism.

In another broad class of materials, the birefringence can be induced by stress or deformation. Materials which exhibit this property of stress or strain birefringence include glass, many plastics, certain rubbers, semiconductors, and some fluid materials. This type of birefringence is a property of a large number of transparent materials, although the birefringence may be small enough to be unnoticeable.

The birefringence-producing interactions between the elements of a material's structure and stress are not yet clearly known. Models of the material behavior have been developed on the basis of the diphase theory (20) and a multiphase theory (41), but these are meant to serve only as representations rather than explanations or descriptions. Other investigators, for instance Persoz (56) and Rao (70), have concluded that in certain molecular structures the birefringence may be due to stretching of certain molecular groups and also to the

reorientation of some anisotropic side chains. The stretching birefringence and orientational birefringence may add or oppose one another, or one of them may be missing entirely, depending on the material and the conditions of the test. It is on such a basis that the presence of a second-order transition point and other diphase phenomena may be justified for real materials. Another approach is discussed by Blumstein (7), who analytically extends the chemist's concept of rubber photoelasticity to the epoxy resins. Further discussion of the microscopic mechanism of birefringence is not within the limitations of the present investigation. But the question must be diligently studied, both analytically and experimentally, in order to place photoelasticity on a sound scientific basis and also to contribute to the knowledge of material structure.

Although artificial double refraction cannot yet be firmly related to changes in material, it can be connected to the history of stress and/or strain at a point through experimentally derived relationships. For example, if σ_1 and σ_2 are the principal stresses at a point in a two-dimensional "momentarily linearly elastic" plate of optically sensitive material (generalized plane stress problem), then it can be shown experimentally that the principal axes of refraction correspond to the principal stress axes. A polarized ray will, when passed through the plate, be split into two components along the principal stress axes while passing through the plate, and the two components will be retarded absolutely and with respect to one another. The absolute retardations can be expressed in terms of the absolute photoelastic coefficients, c_1 and

c_2, which are generally functions of stress, strain, time, and wavelength of radiation. The equations are

$$R_1 = (c_1\sigma_1 + c_2\sigma_2)\, d \qquad (2.9a)$$

$$R_2 = (c_2\sigma_1 + c_1\sigma_2)\, d \qquad (2.9b)$$

The relative retardation is the difference of R_1 and R_2. In terms of the absolute coefficients, this relative retardation is:

$$R = (c_1 - c_2)(\sigma_1 - \sigma_2)\, d \qquad (2.10)$$

Comparing (2.10) with (2.8), it seems reasonable to write

$$\frac{n_1}{n_o} = c_1(\sigma_1 - \sigma_2) \text{ and } \frac{n_2}{n_o} = c_2(\sigma_1 - \sigma_2) \qquad (2.11)$$

The absolute coefficients have been only rarely used in photoelasticity up to the present. The relative retardation is usually related to the stress state by means of an empirical stress-optical coefficient C_σ, which is related to the absolute coefficients by

$$C_\sigma = c_1 - c_2 \qquad (2.12)$$

The expression for relative retardation then becomes:

$$R = C_\sigma(\sigma_1 - \sigma_2)\, d \qquad (2.13)$$

Alternatively, the relative retardation may be written in terms of strain at a point through use of the experimentally-derived strain-optical coefficient, C_ϵ.

$$R = C_\epsilon(\epsilon_1 - \epsilon_2)\, d \qquad (2.14)$$

If the expressions for relative retardation in terms of stress and strain are to be identical, then the principal axes of stress and strain must be coincident. If methods based on birefringence measurement are to be extended to problems involving large deformation and flow where the stress and strain axes may be different, then the interpretation of data and the meaning of the coefficients becomes more complex. The photoelastic analysis of such problems has been adequately formulated for only the simplest cases.

The interpretation of birefringence measurements in terms of stress or strain is not a primary purpose of this investigation. Wherever this problem must be considered, discussion will be restricted to "momentarily linearly elastic" material behavior. This means that the birefringence, stress, and strain are linearly related at the time of measurement. The stress-optical and strain-optical coefficients are then functions only of time and wavelength of radiation. The restriction to a linear range suggests the problem of detecting the occurrence of nonlinear behavior. More will be said on this particular problem later in this writing. The definition of "momentarily linear elastic" behavior and calibration data are presented in the works of Pindera(58, 59, 60). A summary of past investigations, additional data, and the definition of the limit of the linear range of behavior are presented by Pindera and Kiesling (64).

The coefficients relating retardation and stress or strain are generally complicated functions of material and its history, time, stress, strain, temperature, and wavelength of the light used. In

practice, the coefficients are usually developed experimentally by measuring under controlled conditions the relative retardation produced by a specimen in which the stress or strain field is known. The results of such a calibration test can be used to explore unknown stress states through measurements of retardation. From what has been said of the relationships between the stress field and the principal refractive axes and the magnitude of the birefringence, one would expect that the photoelastic method will yield information on principal stress orientation and difference in magnitude of principal stresses in a two dimensional body. The equations governing this measurement are presented in the following section.

2.1.4. The Equations of Photoelasticity

Double refraction is measured through determination of the relative retardation between two components of a ray of polarized light that is passed through the birefringent body. The phenomenon of destructive interference of light is useful in this measurement of relative retardation, which is usually a very small quantity. The equations describing the light transmitted through two polarizing plates with a model between have been presented in different forms by many authors. The equations must be briefly re-examined here for three reasons. First, it should be demonstrated that the equations are applicable throughout the electromagnetic spectrum. Secondly, the equations for the case of parallel polarizing plates, (without quarter-wave plates) are not ordinarily presented, since it is not common to utilize this arrangement of the polariscope. Much

of the data presented here was obtained with linear polarization and with polarizers both parallel and crossed. All the data must be properly interpreted. Finally, one of the methods of measuring small values of relative retardation required knowledge of the general relationship between light intensity and the relative inclinations of polarizers and model.

The development of the governing equations may begin with consideration of the ray emerging from the first polarizer. If this ray has a wavelength λ, travels in the z direction with velocity v in a medium (usually air) having refractive index n_o, and is polarized in the yz plane, then the electric vector describing this radiation is:

$$\overline{E} = \overline{A} \cos \frac{2\pi}{\lambda} (z - vt) \hat{j} \qquad (2.14)$$

When the ray falls normally upon a stressed birefringent plate whose principal stresses, σ_1 and σ_2, are inclined at angles ϕ and $\phi + 90^\circ$ to the x axis, the ray will be split into components along the principal stress axes, and the two components will propagate through the plate at different velocities v_1 and v_2. Writing separately the scalar components:

$$E_1 = E \sin \phi = A \cos \frac{2\pi}{\lambda} (z - v_1 t) \sin \phi \qquad (2.14a)$$

$$E_2 = E \cos \phi = A \cos \frac{2\pi}{\lambda} (z - v_2 t) \cos \phi \qquad (2.14b)$$

Here, attenuation of the wave due to reflection and absorption and also changes in phase which may occur at interfaces are neglected.

They are not assumed zero but rather are assumed to be equal for the two components of the original ray.

After traversing the thickness, d , of the plate, each component of the ray will have been retarded and the magnitudes of the orthogonal electric vectors describing the rays emerging from the plate are:

$$E_1 = A \cos \frac{2\pi}{\lambda} [z - vt - (n_1 - n_o)\frac{d}{n_o}] \sin \phi \qquad (2.15a)$$

$$E_2 = A \cos \frac{2\pi}{\lambda} [z - vt - (n_2 - n_o)\frac{d}{n_o}] \cos \phi \qquad (2.15b)$$

The vector sum of the two components represents the electric vector of the emergent ray. The particular nature of this vector will be discussed shortly. For the moment, consider the ray which will emerge from a second polarizer which is placed with its transmitting axis at an angle θ with the original axis of polarization in the path of the ray whose components are now travelling at equal velocities but out of phase. The analyzer (the second polarizer) will transmit only those components which are parallel to its axis. The electric vector of the linearly-polarized emerging ray will be inclined at angle θ to the axis of the first polarizer, and its magnitude will be:

$$E = A \cos \frac{2\pi}{\lambda} [z - vt - (n_1 - n_o)\frac{d}{n_o}] \sin \phi \sin (\theta + \phi)$$
$$+ A \cos \frac{2\pi}{\lambda} [z - vt - (n_2 - n_o)\frac{d}{n_o}] \cos \phi \cos (\theta + \phi) \qquad (2.16)$$

which becomes after considerable manipulation,

$$E = A \sin\left[\frac{\pi}{\lambda}(n_1 - n_2)\frac{d}{n_o}\right](\sin\theta \sin 2\phi - \cos\theta \cos 2\phi)$$

$$\sin\frac{2\pi}{\lambda}\left(z - vt - \frac{n_1 + n_2 - 2n_o}{2}\frac{d}{n_o}\right) +$$

$$A \cos\left[\frac{\pi}{\lambda}(n_1 - n_2)\frac{d}{n_o}\right]\cos\theta$$

$$\cos\frac{2\pi}{\lambda}\left(z - vt - \frac{n_1 + n_2 - 2n_o}{2}\frac{d}{n_o}\right) \qquad (2.17)$$

The emergent light wave is thus seen to be the scalar sum of two rays of equal wavelength out of phase by $\frac{\pi}{2}$ and with amplitude depending on the retardation in the birefringent plate and the orientation of the polarizer, analyzer and stress axes. The general expression is not amenable to straightforward physical interpretation. It is useful and instructive to examine the result for two special cases. First, with polarizer and analyzer crossed, $\theta = 90^o$, and the magnitude of the electric vector reduces to:

$$E = A \sin\left[\frac{\pi}{\lambda}(n_1 - n_2)\frac{d}{n_o}\right]\sin 2\phi$$

$$\sin\frac{2\pi}{\lambda}\left(z - vt - \frac{n_1 + n_2 - 2n_o}{2}\frac{d}{n_o}\right) \qquad (2.18)$$

This is clearly a travelling wave of wavelength λ and amplitude dependent upon the relative retardation and the orientation of the stress axes. The amplitude, and thus the intensity, of the wave is zero if:

(1) $\phi = 0, \frac{\pi}{2}$; that is, if the polarizers are aligned with with the principal stresses in the birefringent plate. This phenomenon serves as a device for determining principal stress directions.

(2) $\frac{(n_1 - n_2)\, d}{\lambda_o\, n} = m = 0$ or an integer. This serves to measure relative retardation, $(n_1 - n_2)\, d$, in terms of the wavelength of radiation used.

Now, for $\theta = 0^o$, that is with polarizers parallel, the magnitude of the electric vector of the emergent wave is:

$$E = -A \sin\left[\frac{\pi}{\lambda}(n_1 - n_2)\frac{d}{n_o}\right]\cos 2\phi$$

$$\sin\frac{2\pi}{\lambda}\left(z - vt - \frac{n_1 + n_2 - 2n_o}{2}\,\frac{d}{n_o}\right) +$$

$$A\cos\left[\frac{\pi}{\lambda}(n_1 - n_2)\,\frac{d}{n_o}\right]$$

$$\cos\frac{2\pi}{\lambda}\left(z - vt - \frac{n_1 + n_2 - 2n_o}{2}\,\frac{d}{n_o}\right) \qquad (2.19)$$

This indicates that the resulting electric vector consists of two separate component waves out of phase by $\frac{\pi}{2}$. The amplitude of one wave depends only on relative retardation and the other depends on retardation and stress direction. The magnitude of the resultant wave is zero only when both components are zero simultaneously. This occurs only when $\phi = \frac{\pi}{4}$ and $\frac{(n_1 - n_2)}{\lambda\, n_o}\, d = \frac{m}{2}$, m an integer. If the elements are properly aligned, such a system can be used in addition to the crossed system for the determination of relative retardation. Such a measurement with light field linear polarization is not common in photoelasticity. The calculations also show that the retardations common to both rays as they pass through refractive media do not affect the results. These common phase shifts can be eliminated by a suitable coordinate transformation, but in practice they are usually ignored entirely. Only the relative phase differences must be considered.

Suppose now that the stressed birefringent plate is not uniformly birefringent. This would occur if the stress field varied. The crossed linear polariscope would not transmit rays which passed through points in the model where the stresses were properly inclined or where the relative retardation was an integer multiple of the wavelength. An image of the plate constructed with the rays transmitted through the polariscope would show two sets of dark lines. One set, called the isoclinics, would be the locus of points at which the principal stress directions coincide with the directions of polarizer and analyzer. The second family is the locus of points where the relative retardation equals integral multiples of the wavelength,

$$R = (n_1 - n_2)\frac{d}{n_o} = m\lambda, \quad m = 0, 1, 2, \ldots \tag{2.20}$$

These lines of constant relative retardation are termed whole-order isochromatic fringes. They serve to indicate lines in the plate along which the stress (or strain) has reached certain discrete values. If C_σ is the so-called stress-optical coefficient, then

$$\sigma_1 - \sigma_2 = \frac{m\lambda}{C_\sigma d} \tag{2.21}$$

If polarizer and analyzer are placed parallel, dark lines will show up in an image of the plate only in those areas where the principal stresses are inclined 45^o to the polarizer axis and where the relative retardation is a half-integer multiple of the wavelength. These lines are termed half-order isochromatic fringes. Along such a fringe,

$$R = (n_1 - n_2)\frac{d}{n_o} = \frac{m}{2}\lambda \ , \quad m = 1, 2, \ldots \ . \tag{2.22}$$

the corresponding stresses are:

$$\sigma_1 - \sigma_2 = \frac{m\lambda}{2C_\sigma d} \tag{2.23}$$

These stress values are seen to be midway between the values given by the whole-order fringes. The two sets of isochromatics taken together thus give a plot of principal stress difference (or strain difference) at a network of points in the plate. Values of stress difference at points in between the isochromatics can be found by interpolation or compensation. When these are coupled with the stress directions found from the isoclinic fringes by suitable computation, the complete stress field can be mapped. That is, σ_1, σ_2 and their inclinations can be determined for any point in the birefringent plate. Much has been written regarding the interpretation of photoelastic fringe patterns. Further discussion here will serve no purpose within the limited scope of the investigation.

Returning now to equation (2.15) for the components of light emerging from the birefringent plate, consider the special case when $(n_1 - n_2)\frac{d}{n_o} = \frac{\lambda}{4}$ and $\phi = 45^\circ$. If $\hat{p}$ and $\hat{q}$ are the unit vectors along the principal axes, the electric vector can be written as follows:

$$\overline{E} = \frac{\sqrt{2}}{2} A \left\{ \cos \frac{2\pi}{\lambda} \left[z - vt - (n_1 - n_o)\frac{d}{n_o} \right] \hat{p} \right.$$

$$\left. + \cos \frac{2\pi}{\lambda} \left[z - vt - (n_1 - n_o)\frac{d}{n_o} + \frac{\lambda}{4} \right] \hat{q} \right\}$$

Eliminating the retardation common to both components by a coordinate change and introducing an identity:

$$\overline{E} = \frac{\sqrt{2}}{2} A[\cos \frac{2\pi}{\lambda}(z - vt)\,\hat{p} - \sin \frac{2\pi}{\lambda}(z - vt)\,\hat{q}] \qquad (2.20)$$

The two components are thus identical but out of phase by $\frac{\pi}{2}$. The magnitude of the vector is found by the Pythagorean Theorem to be constant. The inclination of the vector with the $\hat{p}$ axis is

$$\alpha = -\frac{2\pi}{\lambda}(z - vt) \qquad (2.21)$$

At any instant, the orientation of the light vector varies uniformly with position z on the optical axis, that is, it describes a circular helix. Otherwise, for fixed z, the light vector rotates uniformly with time and so describes a circle. Radiation which can be described by (2.20) is said to be circularly polarized. The birefringent plate which produced the circularly polarized light from that which was plane polarized is termed a quarter wave plate.

Circularly polarized light serves two useful functions in photoelastic measurements. First, it can be used to remove the orientational dependence of extinction of radiation which exists in a polariscope employing only linear polarizers. This use is well described in the standard texts and handbooks. The linear polariscope is converted to circular by insertion of quarter-wave plates between polarizer and stressed plate and between analyzer and stressed plate. The equations governing the use of the circular polariscope do not have to be re-examined here, since the data used quantitatively in this work were taken using linear polarization. In general, these

equations are slightly simpler in form than those presented for the linear system.

The second important use of circular polarization is for precise determination of relative retardation at a prescribed point in a birefringent plate. The isochromatic fringe patterns obtained with the crossed or parallel polariscope indicate the locus of points where the retardations are integral and half-integral multiples of wavelength. The retardation at points between whole and half-order isochromatics can be found by two methods of goniometric compensation in which quarter wave plates are used. The two methods are discussed thoroughly in the literature (36, 47). A slight modification of one of these methods was used in this investigation, and the procedure and equations will be discussed where appropriate in a later section. The errors which may result from imperfect quarter-wave plates will also be mentioned.

2.1.5. Optical Dispersion and Dispersion of Birefringence

For a given state of stress and time, the birefringent properties of materials depend to a certain limited extent upon the wavelength or frequency of the radiation used in its measurement. That is to say, the order, m, of isochromatic fringe as expressed by equations (2.20 - 2.23) of the preceding section cannot be considered to be inversely proportional to the wavelength. Unfortunately, this simple proportionality is still often assumed.

The degree to which the stress-birefringence of a material depends on wavelength may be expressed in terms of the principal refractive indices, n_1 and n_2; the absolute stress-optical

coefficients, c_1 and c_2; or the relative stress-optical coefficient, C_σ. The corresponding strain-birefringence coefficients could also be used. In order to attain complete understanding of the phenomena of double-refraction and dispersion, the variation of the absolute coefficients and of refractive index with wavelength must be explored. These absolute quantities have been used only rarely in photoelasticity up to now. Hence, this discussion will be restricted to the relationship between the frequency or wave-length of radiation and the relative stress-optical coefficient.

The dependence of the relative retardation upon the vibrational frequency of radiation is commonly called the dispersion of birefringence, because it results from the same basic physical phenomena as the dependence of the refractive index, n, on the radiation frequency. This variation of n with wavelength is known as optical dispersion or, simply, dispersion. The dispersive effect in glasses and other materials is useful in a prism, for example, since it allows the prism to separate colors. The same effect detracts from the usefulness of a lens, and much effort is expended in developing lenses which have a minimum of chromatic dispersion. The term dispersion was first applied in the area of photoelasticity by H. Ambronn (1), and it is now in common use.

Part of this investigation was concerned with the measurement and adequate description of dispersion of birefringence. As yet, there has been little agreement among the various investigators as to the best method of presenting dispersion data and the proper

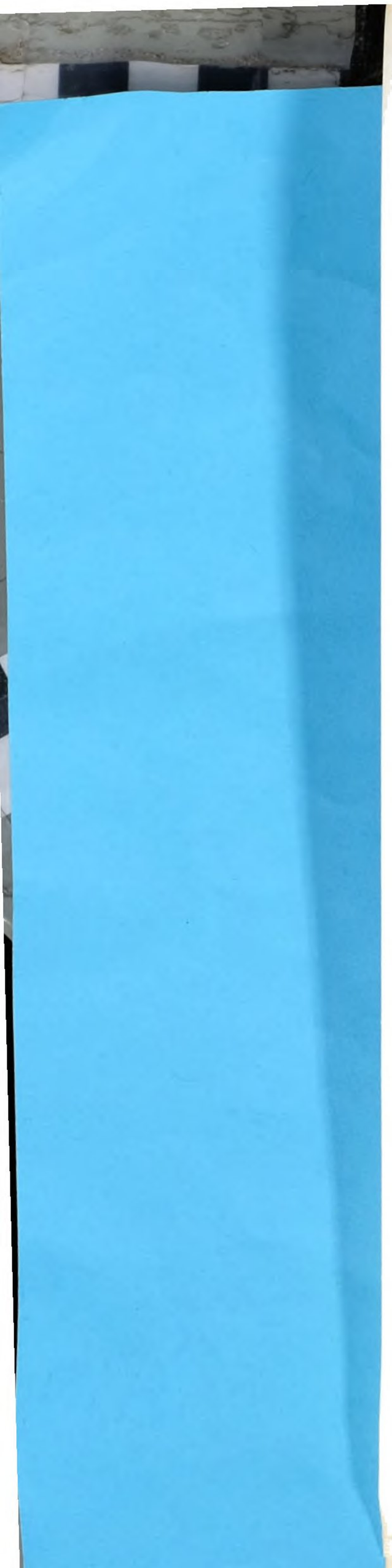

interpretation of the data. Neither is experimental information very complete or conclusive. Hence, the results and ideas of various researchers must be examined briefly here. Also, since the dispersion of birefringence is so closely allied with the much better known phenomenon of ordinary optical dispersion, much can be gained from a short discussion of some accepted definitions of the dispersive power of glasses.

There are a variety of arbitrary definitions of optical dispersive power. Examples include the "relative dispersion," which is expressed in terms of the indices of refraction at the wavelengths of certain Fraunhofer lines,

$$\frac{n_F - n_C}{n_D - 1} \tag{2.21a}$$

and the "partial dispersion":

$$\frac{n_\lambda - n_D}{n_C - n_F} \tag{2.21b}$$

A more general measure of dispersion involves the derivative of the quantity under consideration with respect to the independent variable. On this basis, the optical dispersion of a medium is defined as the rate of change of the index of refraction with respect to radiation frequency or, respectively, wavelength:

$$\frac{dn}{d\nu} \tag{2.22a}$$

$$\frac{dn}{d\lambda} \tag{2.22b}$$

In the general case, the refractive index changes with radiation frequency, and normally the index increases with increasing

frequency. That is,

$$\frac{dn}{d\lambda} < 0 , \qquad \frac{dn}{d\nu} > 0 \tag{2.23}$$

This type of dispersion is called normal dispersion.

It is known that under special circumstances in a narrow range of frequencies near absorption bands, that is to say in regions of resonant frequencies for the material, the refractive index of transparent materials decreases with increasing frequency:

$$\frac{dn}{d\lambda} > 0 , \qquad \frac{dn}{d\nu} < 0 \tag{2.24}$$

This phenomenon is called anomalous dispersion. According to the theory of molecular optics, it results from the frequency dependence of the molecular polarizability (11, 8).

The dispersion of birefringence of certain photoelastic materials, including mainly glasses but also celluloid and gelatin, has been investigated by several authors. A comprehensive survey of research work done in this field and a related bibliography is presented in the classical work of Coker and Filon (10). These authors found that for many glasses the variation of stress-optical coefficient with color is, on the whole, closely fitted by the formula:

$$C_\sigma = \frac{C_o}{1 - (\lambda_o/\lambda)} \tag{2.25}$$

where C_o and λ_o are constants for any given glass. In fact, these constants indirectly describe the dispersion of birefringence. It may be pointed out that the above formula was used for non-creeping glasses.

E. Monch in his paper (49) proposed the following relation as a measure of the dispersion of birefringence:

$$D = \frac{(m\lambda)_{Na} - (m\lambda)_{Hg}}{(m\lambda)_{Na}} \qquad (2.26)$$

where the indexes Na and Hg denote the yellow sodium line and the blue mercury line, respectively. In a later paper (53), E. Monch and R. Lorek used the same formula in relating the dispersion of birefringence to red light (λ = 655 nm) and the blue mercury line (λ = 436 nm).

The same measure of dispersion of birefringence is used by Monch, Hartmann, Jira, and Lorek (50, 51, 52, 38, 45), who attempted to relate the degree of plastic deformation to the dispersion of birefringence for several plastics. Positive results were obtained only for celluloid. For this material, the dispersion as expressed by formula (2.26) may be considered a measure of plastic distortion. This result confirms those published in 1924 by A. Ramspeck (69). He found that in the elastic range the dispersion of birefringence in celluloid is normal, with the stress-optical coefficient for red being about 3% smaller than for violet. However, beyond the elastic limit, C_σ for red is greater than that for violet.

Unfortunately, such a definite relationship does not exist for several other model materials. This has been demonstrated by R. Lorek (45) for several polyester resins of Leguval type and by J. T. Pindera (62, 63) for allyl polyester resin CR-39 and unsaturated polyester resin P-6. These negative results should be interpreted

to mean only that the relation between inelastic deformation and the dispersion of birefringence measured according to formula (2.26) has not yet been found. Typical measurements of the dispersion of birefringence as reported by different authors are presented in the papers cited above. Especially interesting is the presence of anomalous dispersion first discovered by Filon (10).

The definitions developed for this investigation into the dispersion of birefringence of representative materials are presented along with the data in Chapter 3.

2.2. Infrared Photoelasticity Apparatus and Technique

2.2.1. Optical Systems Used

The visible radiation which is ordinarily used in photomechanic investigations comprises only a very narrow portion of the complete electromagnetic spectrum. Certain optical effects which are readily observable under visible illumination should also be apparent with nonvisible radiation provided the human senses are extended by suitable apparatus and the optical interactions are not limited to certain wavelengths. Examination of the photoelastic equations presented indicates no limitation to the visible portion of the spectrum. Thus, with appropriate techniques, meaningful measurements of birefringence could be taken in other spectral regions. The actual methods used would depend on the wavelengths used. The important thing is that the functions served are the same in all spectral regions.

The experimental investigations considered here were carried out in the range of wavelengths from visible violet to two microns. A basic difference in the techniques of recording data necessitated the use of three different optical systems. Sketches of the systems are presented in Figure 2.2, and photographs of the optical bench are shown in Figure 2.3. The first of these systems are used for investigations through visible up to 0.7μ, and was basically no different than the polariscopes commonly used for photoelastic investigations in visible light. The second system, quite similar to the first (Figure 2.2a), was used for the 0.7 through 1.2μ range. Both these systems provided means of planewise observation and measurement of birefringence. The third system, shown in Figure 2.2b and Figure 2.3a - 2.3c served for the pointwise measurement of birefringence. It was developed for the extension of photoelastic measurement up to the 2 micron limit of this investigation, although, in principle, the approach is not limited to any particular wavelength range. The reasons for the particular configuration of this system will be discussed shortly.

The following paragraphs describe the optical elements and techniques used for performing the basic functions in the various polariscope systems. Suggestions for improvement and for the extension of the method into other spectral regions are also presented. The chapter closes with a discussion of the special methods used to measure fractional fringe orders and record data.

2.2.2. Elements of the Optical Systems

A. Light Sources and Filters

The first item of apparatus required in any polariscope is a source of radiation. This radiation should be nearly monochromatic. Several different wavelengths should be available, and the radiation should be as intense as possible.

The most common method of producing intense monochromatic light is through the isolation of certain bands from the emission of spectrally pure sources. Such sources generally consist of lamps containing small amounts of certain gaseous or metallic chemical elements. Proper electrical excitation will cause the elements to emit energy at wavelengths characteristic of the element. This phenomenon is that commonly used in the spectroscopic chemical identification of materials. When the emission lines are separated from one another by selective filtering, monochromatic radiation results. For most lamps of this type, the emission lines of useful intensity occur between deep ultraviolet and 1.5 microns.

For this investigation, a low-pressure Mercury-vapor lamp (General Electric, H-4) and a low-pressure Helium lamp (Philips, 93098) were used as two of three sources of radiation in the visible and near infrared spectral ranges. The emission characteristics of this particular Mercury lamp, as well as other Mercury lamps, are well known (66). The characteristics of the Helium lamp in the infrared region are not readily available. Usually the output of spectral lamps differs to a limited extent from the spectroscopic emission of the elements involved due to effects of pressure, impurities, presence of electrodes, etc. The emission of both spectral lamps in

the near infrared was determined by means of an infrared spectrometer (Perkin-Elmer, Model 137-G). This device is intended to be used in measuring the infrared transmission characteristics of materials for identification purposes. The instrument was used as an emission spectroscope by blocking the light path in the sample side of the optical system and using mirrors to inject light from the lamps. The result is a plot which compares the lamp emission to the emission of the standard source (glo-bar) inside the instrument over the wavelength range from 0.85 to 2.5 microns. The results of these measurements agreed well with published data. Of particular interest is the output of the Helium lamp. According to spectroscopic tables, the emission spectrum of Helium in the infrared consists of three very intense lines whose wavelengths are very close together. For practical purposes, that is for low resolution of wavelengths, the emission is one narrow band centered at 1.083 microns. The absence of other lines close by allows this line to be easily isolated. Figure 2.4 shows a representative plot of the emission of the Helium lamp, copied from those obtained with the Perkin-Elmer spectrometer.

Since the Helium and Mercury lamps were also used as sources of monochromatic visible light in accordance with common practice, their emission in this range was checked with an ordinary prism-type emission spectroscope (Hilger, No. D-26.303, 26222). The measurements agreed well with the characteristics usually ascribed to these lamps.

Sources of radiation which is to some degree continuous over a broad portion of the electromagnetic spectrum are very common, since every body at temperature greater than absolute zero is an emitter of such radiation. The intensity of radiation and the span of wavelengths are functions only of the temperature and surface and shape characteristics. The basic emission law describes the radiation from what is known as the ideal blackbody, and the emission of real, imperfect bodies can be described in terms of blackbody emission. Such emitters of radiation which is continuously distributed with respect to wavelength form useful sources of infrared light. By proper choice of body and temperature, the emission can be centered in any given span of wavelengths. A ribbon of tungsten wire or a carbon resistor, for example, if heated to about 1000^{o} Kelvin, will emit radiation with wavelengths distributed between 0.66 microns and 60 microns, with the peak emission at 3.2 microns. If monochromatic light is required, it must be selectively filtered from the "white", or continuously distributed light by filters or by means of a monochromater. The most serious problem associated with the use of spectrally-continuous sources of longwave radiation is that of obtaining great enough intensity. Ideally, any wavelength can be produced. Unfortunately, as the temperature of the emitter is decreased in order to obtain longer wavelengths, the intensity of the radiation also decreases. Waves as long as 1 cm have been produced by simple blackbody radiation, but they were almost undetectable (35). At wavelengths above about 1 mm, reasonably intense radiation must usually be obtained by electronic resonance such as is used in ordinary radio circuits.

Two spectrally-continuous sources of radiation were used in the present investigation. The first was a General Electric "Point-O-Light" lamp. This is basically a 100 watt incandescent lamp whose tungsten ribbon is closely wound in order to concentrate the source of radiation into a small area. The result is quite intense white light with wavelengths ranging from about 400 nm up to a maximum of about 3μ. The other continuum source, which was particularly well suited for the production of intense visible and infrared radiation, was a Sylvania "Concentrated Arc" lamp, type K100P. Although rated at only 100 watts, the total emission of this lamp comes from an arc whose diameter is only 0.059 in (1.5 mm), giving a brillance of 24,500 candles per square inch. The spectral distribution of such a lamp is quite uniform from near ultraviolet through several microns. A direct current power supply which also provided the required 2000 volts for ignition was supplied with the lamp.

Various other sources which are similar in principle to those described here can be employed in infrared optical systems. Papoular (55) describes the use of a water-cooled Mercury-vapor lamp as a source of radiation in the 15-100 cm^{-1} range. Here the hot bulb rather than the arc acts as the emitter. The same author also has developed an oven with an aperture which acts as a black-body radiator. Devices based on the same principle are available commercially.

Regardless of the apparatus used to produce radiation, some sort of filtering is usually required in order to meet the requirement that the light be monochromatic. Many methods of selective filtering

of radiation have been investigated and developed, and these are well described in the extensive literature on the subject. Filters are conveniently characterized on the basis of their transmission curves as "wide bandpass" or "narrow bandpass". The latter term may be applied to filters which transmit a band of wavelengths which is narrow enough to be taken as monochromatic for the purpose at hand. Wide-band filters transmit a wider span of wavelengths, and are intended to be used in blocking off a portion of the spectrum. Special types of wide bandpass filters are the low-pass type, which transmits radiation below a certain wavelength, and the high-pass variety which transmits above a certain wavelength. These terms are only descriptive, and actual plots of transmission versus wavelength are required for the precise description and evaluation of light filters.

Several filters of each type were used in this research effort. Initially, for the isolation of emission lines from the spectrally pure sources, wide-band filters of high-pass, low-pass, and controlled band width types were used singly and in combination. These filters were mostly of the "transmission", "color", or "Wratten" type which transmit certain colors and absorb all others. Their construction, use, and specifications are described in detail in the excellent pamphlet by Eastman Kodak (39). Many other types of transmission-absorption filters, many of them simply aqueous solutions of common chemicals, are described by Landolt-Borstein (43) and North American Philips (57), in addition to the common physics and optics textbooks and handbooks. Plyer and Ball (65) describe the use of deposited films of tellurium, bismuth, antimony, and

magnesium oxide as transmission filters for the infrared. Other authors (74, 6) present similar information on plastics and organic dyes.

Transmission-absorption filters which pass only a very narrow band of wavelengths are difficult to manufacture or obtain. When monochromatic light must be obtained by isolating closely spaced spectral emission lines or a narrow wavelength band from continuum radiation, then either a monochromator or narrow band-pass "interference" filter must be employed. The filters are usually preferred when intensities must be high. Such filters consist of several layers of dielectric materials having carefully controlled thicknesses, rather than the one layer characteristic of transmission filters. The thickness, number, and material of the layers depends on the peak wavelength and bandwidth desired. The simultaneous occurrence of selective reflection, absorption and destructive and constructive interference within the layers causes the combination to transmit only the chosen band of wavelengths. Often the primary wavelength is accompanied by sidebands which are harmonics or subharmonics of the center wavelength.

Several interference type filters which were supplied by three different manufacturers were used for experimentation in the visible and infrared ranges in conjunction with the various light sources. The characteristics of two filters which are representative of those used are shown in Figure 2.5. The data plotted in Figure 2.5a for Optics Technology filter no. 160-1-145 is from spectrometer plots supplied by the maker. The other plot (2.5b) for Infrared

Industries filter no. NB-156-0-(1) was obtained with the Perkin-Elmer spectrometer previously described in the paragraphs on lamps.

Table 2.1 summarizes the apparatus used for producing the radiation used in the investigation. (see page 44).

Of the sources listed, two require further comment. First, the radiation centered at 853 nm is not truly monochromatic. Superposition of the transmission of the filter, the output of the lamp, and the photographic film used with this combination (Kodak 1R135) indicates that the combination has a band pass centered at about 853 nm with a half-width of 36 nm, or 4%. This bandwidth is sufficiently narrow to make possible a measurement in the region between 707 nm and 1083 nm, although the accuracy of measurement would certainly be less than that obtained with more nearly monochromatic light. Secondly, the combination listed for a wavelength of 707 nm actually includes a second weaker line at 728 nm. The effects of this added radiation were small enough so that no difficulties arose.

B. Lens

With most practical polariscopes, at least one lens is required to cause the rays of light to converge to a projection device or else to form an image of the birefringent plate upon a screen. A second lens is usually used to collect and collimate the radiation from the light source. Several additional lenses may be employed to improve the overall quality of the optical path. The sketches in Figure 2.2

Table 2.1. Monochromatic Radiation Sources and Filters

λ nm	ν 10^{14} cps	$\bar{\nu}$ 10^{4} cm^{-1}	Lamps	Filter
405	7.40	2.47	Mercury, H-4	Zeiss Jena (Schott) 267406
436	6.88	2.29	Mercury, H-4	Zeiss Jena (Schott) 013213
546	5.49	1.83	Mercury, H-4	Zeiss Jena (Schott) 050025 or Kodak 74
578	5.19	1.73	Mercury, H-4	Zeiss Jena (Schott) 373635 or Kodak 22
587	5.11	1.70	Helium, Philips 93098	Zeiss Jena (Schott) 373635
668	4.49	1.50	Helium, Philips 93098	Kodak 92
707	4.24	1.41	Helium, Philips 93098	Kodak 89-B
853	3.51	1.17	Incandescent or Mercury	Kodak 87-C
1083	2.77	0.92	Helium, Philips 93098	Kodak 87-C
1100	2.73	0.909	Sylvania Arc, K100p	Zeiss Jena B8105/8
1145ω	2.62	0.873	Sylvania Arc, K100p	Optics Technology 160
1244	2.41	0.804	Sylvania Arc, K100p	Optics Technology 822
1348	2.22	0.742	Sylvania Arc, K100p	Optics Technology 283
1446	2.07	0.692	Sylvania Arc, K100p	Optics Technology 382
1550	1.93	0.645	Sylvania Arc, K100p	Optics Technology 1101
1560	1.92	0.641	Sylvania Arc, K100p	Infrared Industries NB-156-0-(1)
1650	1.82	0.606	Sylvania Arc, K100p	Optics Technology 227
1900	1.58	0.526	Sylvania Arc, K100p	Infrared Industries NB-190-0-(1)
2490	1.20	0.402	Sylvania Arc, K100p	Infrared Industries NB-249-0-(1)

show two such lens systems as they were developed for this investigation.

As may be expected, lenses suitable for the visible portion of the electromagnetic spectrum may not function well in the infrared due to changes in transmission characteristics of the lens material and variations in refractive index with wavelength (optical dispersion). More precisely, the transmission of ordinary optical glass is down to 10% at about 3μ wavelength. Special glasses have been developed which transmit longwave radiation well. Examples include fused quartz and high-silicate glasses, calcium aluminate glass, arsenic trisulfide glasses, and other commercially available modified glasses. Extensive data on these glass materials and others are given in references already cited. In general, this class of materials can be made to function as windows, prisms and lenses up to somewhere between 4 and 10 microns wavelength.

Due to the cost of special glasses and their reduced transmission, other materials should be considered for lenses to be used beyond about 3μ. The material should be transparent in the desired wavelength range, it must have a suitable and preferably uniform refractive index in this range, and it must be readily available, hard, easily worked, non-toxic and stable. Among materials which meet these requirements to varying degrees are calcite, sodium chloride, silver chloride, magnesium oxide, barium titanate, magnesium fluoride and zinc sulfide. The last two materials are marketed commercially by Kodak under the trade names Irtran I and Irtran II, respectively, and they are well suited to the manufacture of lens.

More recently, a type of glass which is highly doped with selenium has been successful for use in the extended wavelength range. This material is known commercially as Servofrax and is a development of Servo Corporation of America. This company also markets a variety of lenses for use at up to 16 microns.

Another possible source of inexpensive infrared lenses is described in detail by Gebbie and Cannon and others (21, 16, 22) and has been verified in the course of this research. The element selenium occurs in an amorphous form which is transparent between 0.6μ and 25μ wavelength. The refractive index at about 1 micron is 2.5 Lenses of this material can be machined from blanks or, more simply, cast from the melt in a pyrex mold. The mechanical characteristics of this material are good, but they can be improved by adding a trace of arsenic. The resulting material is more glass-like and is useful to about 25 microns, with a deep absorption band at 12.7μ (35).

C. Polarizers

The most common methods of polarization of light utilize the phenomenon of double refraction. Two such methods were described in Section 2.1.2 of this report. The first of these is to simply separate two orthogonally polarized rays of light (Nicol Prism, etc), while the other approach is to use birefringent crystals which also absorb one of the rays as they travel through the crystal. Polarizing filters which are based on the latter effect, which is known as dichroism, are presently the most common due to their extensive development,

low cost, large size and ready availability. Dichroic polarizers which consist of a sheet of plastic carrying a multitude of properly aligned microcrystals of dichroic material are marketed commercially under the patents of the Polaroid Corporation. This company supplies an excellent brochure (67) containing full descriptions and samples of their polarizing materials.

Polaroid dichroic sheet polarizers were used exclusively in the investigation reported upon here. In the visible region, type HN32 Polaroid material in 13" diameter discs was used. These discs were sandwiched between glass sheets and mounted in aluminum rings which allowed calibrated rotational freedom.

Type HR Polaroid filters were employed in the infrared range between 0.7μ and the 2μ limit of these filters. HR polarizers are of the dichroic type, but they differ considerably in construction from the types used for visible light. They are provided in glass laminated squares (presently also unlaminated) in sizes up to 4" maximum. Pairs in two sizes, 2" and 4", were mounted in calibrated aluminum rotating rings and used in the infrared phases of the research.

The axes of polarization of all polaroids used in this study were aligned with respect to the protractor markings on the carrier rings through use of the known zero-degree isoclinic existing in a disc in diametral compression. This method of calibration of the polariscope is described by Frocht (20) and others, and it is found to be a very sensitive and accurate device. Observation of the isoclinic in the infrared system was carried out with the aid of an

infrared converter to be described later, and the pattern was also photographed.

Other methods of polarization must be used at longer wavelengths. For the broad range between 0.7 and 25 microns, suitable polarizers are advertised by Hilger and Watts, Ltd. This device is said to function on the basis of selective transmission and reflection through films of crystalline selenium which are properly oriented with respect to the optical path (Brewster's angle). Polarizers which work in a similar way in a more limited range of wavelengths can be constructed of one or more plates of dark glass or other infrared dielectric materials such as silver chloride. The principle upon which these polarizers act is well-known and has been often used in the visible region when more sophisticated polarizers were not available.

A polarizer which operates on the "picket fence" idea has been developed by Bird and Parrish (5). This filter consists of a very fine wire grid, formed by vacuum deposition on a plastic master, and it polarizes very efficiently at wavelengths from 2μ to well beyond 15μ. Mitsuishi and his associates (48) have made a polarizer of a stack of polyethylene sheets of appropriate thicknesses which serves from 14μ through 200μ except for the material absorption bands. Certain crystals of semiconductors are known to be optically anisotropic. Possibly polarizers could be manufactured from these materials if they are uniformly birefringent or dichroic.

D. Quarter-wave Plates

For the spectral range of wavelengths between visible red and 2 microns, circularly polarized light was produced from linearly polarized light by straightforward extension of the methods commonly used in the visible range. This technique calls for the use of a sheet of birefringent material which, when oriented at 45^{o} to the polarization axes, will split a linear polarized beam into two equal components and retard one component with respect to the other by 1/4 of the wavelength of the light. For this purpose various materials such as polyvinyl-alcohol, mica, or stressed glass can be used. If the relative retardation is not exactly $\lambda/4$, then elliptically polarized light results. Ordinarily the use of imperfect circular polarized light does not create error in photoelastic measurements (47). If imperfect quarter-wave plates are used in the goniometric compensation methods of fringe order measurements, then certain errors do arise. These will be discussed and calculated where appropriate in this report.

Polaroid Corporation supplies sheets of retardation material which produce relative retardations of any specified value up to about 1/4 micron. Material producing the latter extreme of retardation is called half-wave retardation material for the visible region. If a sheet of the material behaved the same in near infrared as in visible, it could be expected to serve as a $\lambda/4$ plate for the infrared range around 1 micron. This was found to be the case, and the half-wave material was extensively used for circular polarization in the infrared. As the investigation was extended up toward 2 microns

wavelength, the error in such a plate became too large to be ignored. For example, at 2μ, the half-wave retardation material would act as a λ/8 retarder, resulting in a serious loss in system efficiency and possible increase of second-order errors and dichroic effects. Since the sheets seemed to transmit and retard properly at these wavelengths, it became apparent that more than one sheet of various retardation materials could be stacked with their optical axes aligned in order to obtain plates which produced more nearly the required retardation of λ/4. The error could be minimized by use of properly chosen sheets producing different retardation. For this investigation two sheets of the half-wave material were successfully used to produce a λ/4 retarder for the range of wavelengths between 1.5 and 2μ.

In actual practice, 5-inch discs of the retardation material were clamped in retaining rings with the optical axes of the material aligned with a peg on the periphery of the ring. The plates could then be inserted at will into the optical system by slipping them into supporting holders which were provided with a slot to accommodate the pegs. The supporting holders were similar to the polarizer rings and provided complete facility for calibrated angular rotation of the λ/4 plates. The system was simple and performed efficiently up to the 2 micron limit of transmission of the retardation material.

E. Sensors

The fundamental requirement in the measurement of birefringence with a polariscope is to measure variations in light

intensity with changes in load, location on the birefringent plate, time, or relative position of the optical axes of polarizer, principal stresses, and quarter-wave retarders. This observation of intensity can be carried out planewise, meaning the relative retardation may be observed at every point in the plate simultaneously, or the measurement may be made pointwise and the doubly refracting plate scanned. The advantages of planewise observation are obvious. Unfortunately, this technique cannot be used except in a certain narrow range of wavelengths, and point-by-point methods must eventually be employed. Variations of both methods were used in the investigation under consideration. Since they differed considerably, they will be discussed separately.

The planewise observation of data is most desirable for photoelastic analysis. The approach is based upon observation of the fringe pattern, that is the locus of points of zero intensity, in an image of the stressed birefringent model. The observation may be directly by eye, by viewing through an intermediate device such as a screen or ground glass, or by photographing the image.

Direct visual observation of the fringe pattern has the distinct advantage of immediacy, and the disadvantage of producing no permanent record from which precise measurements can be taken. In the visible spectrum, this observation is accomplished by placing the field lens close to the birefringent model, then placing the eye at the focal point of the lens, which then acts as a magnifying glass. Another approach is to cast a real image of the model upon a reflective screen or translucent plate.

Such simple procedures are, of course, not adequate in the infrared range where special devices and techniques must be used for direct observation.

One such device which makes immediate visual observation of infrared phenomena possible is the infrared converter. This apparatus is a refinement of the well known "snooperscope" or "sniperscope" developed for military and law-enforcement activity. At the heart of the device is an infrared converter tube which is powered by a small high-voltage, low-current power supply. The converter tube consists of a photo cathode which emits electrons from the portions of its area which are subjected to infrared radiation. These electrons are electrically accelerated and focused to fall upon an electroluminescent anode screen in the same pattern at which they left the cathode. The electroluminescent screen, of course, converts the energy of the electrons to visible radiation, producing a visible image of the infrared image. The image of the infrared illuminated scene is cast upon the cathode by means of suitable optics. The infrared converter used in this study was a high resolution type manufactured by Varo, Inc. Its characteristics are listed in the following table.

Table 2.2.

Manufacturer's Performance Specifications

Varo Inc., Model 5500C Detect-IR-scope

Spectral response	0.4μ to 1.2μ (S-1)
Peak response	0.8
Magnification	1:1
Resolution	5.5 minutes minimum
Linear Distortion	8% maximum at 12° from field center
Focus range	1' to infinity

The performance of this instrument, which is of high quality, is seriously limited for scientific work by its rather narrow spectral response and the distortion and lack of resolution. It represents the simplest of only a very few possibilities for infrared photoelastic observation, and the device proved invaluable in the present investigation.

For accurate measurement and later reference, it is desirable to have a permanent record of the photoelastic pattern. This record is best obtained photographically in a certain limited band of wavelengths. The method has long been used for photoelastic research in the visible range of the spectrum. For the recording of fringe patterns in the infrared, two photographic techniques may be proposed, and both were used to some extent in the experimental research.

The first method used was direct photography of the image of the birefringent model through the field lens of polariscope. The present availability of films and camera lenses which may be used in the infrared limits photography to about 1.2 microns wavelength. The broad wavelength range used here necessitated the use of several different types of film during any one test. These are listed in Table 2.3 for each wavelength up to the limit of 1.08μ. Processing of negatives was in accord with manufacturers' specifications.

Table 2.3.

Photographic Films

λ, nm	film type
405	Kodak Plus-x or Panatomic-x
436	Kodak Plus-x or Panatomic-x
546	Kodak Plus-x or Panatomic-x
578	Kodak Plus-x or Panatomic-x
587	Kodak Plus-x or Panatomic-x
668	Kodak Plus-x or Panatomic-x
707	Kodak High Speed Infrared
853	Kodak IR 135
1083	Kodak Type I-Z Spectroscopic

Of particular interest is the use of Infrared Spectroscopic Film Type I-Z which was donated by Eastman Kodak for trial. This film is intended for use in detecting infrared radiation. It is not commonly employed for imaging. This film proved very useful, as it is the only film available for photography in this extended region. The results were limited only slightly by the very slow film speed and rather large grain size. The camera used was a Nikon F, 35 mm, with lenses chosen to match the optical system, which was slightly different for each experiment.

The second technique for recording the fringe pattern was to use the camera in conjunction with the infrared image converter already described. The 35mm Nikon F camera was coupled with the eyepiece of the converter by means of the telemicroscope adaptor supplied for this camera. Pictures were then taken of the visible image on the converter's luminescent screen using ordinary panchromatic

films. The results were acceptable, but not as good as those obtained by direct photography with infrared film. The lower quality was due to the distortion and lack of resolution in the optics of the converter. The system could be improved to a point by careful design of the apparatus used to couple converter and camera. Such a conversion-photography system might prove best for use above the 1.2μ limit of films should suitable infrared converter tubes become available.

One other planewise recording technique was tried in this work. This involved the use of screens which luminesce visibly when exposed to infrared radiation. The principles and preparation of infrared photoluminescent materials are well-known (18, 19, 44) since they received a great deal of attention in the 1940's before converter tubes were developed to the point of usefulness. It would seem possible to construct a screen which would convert infrared radiation to visible by coating a ground glass, for example, with a paint composed of powdered luminescent material in a binder. The infrared photoelastic image could then be observed visually or photographed with ordinary film. Another possibility which has been successfully employed in infrared emission spectroscopy is to coat an ordinary film plate with such a material. The material glows when an infrared image falls on the plate, and the plate is thus exposed. It should be mentioned that most of the luminescent materials (as opposed to, say photoemissive materials) must first be excited by exposure to gamma rays, x-rays, or ultraviolet up to about 350 nm wavelength. The material may then glow, and the infrared radiation extinguish the glow (photoquench), or the material

may emit visible light only when subjected to infrared radiation after excitation.

Here, first efforts were with an infrared luminescent screen obtained from Eastman Kodak. This device is simply a card which seems to be impregnated with the luminescent material and then coated with plastic. It is apparently intended for checking the emission of near infrared lasers, which, of course, provide very intense radiation. The intensities in the infrared polariscope were not great enough to cause the screen to luminesce. But, the polarized and unpolarized monochromatic infrared radiation would bring about luminescence of a rather low intensity. With stronger light sources, the simple card would perhaps serve well for visual observation of infrared photoelastic fringe patterns. In addition to the Kodak screen, an infrared phosphor was compounded according to one of the recipes in one of the references mentioned (44). This particular photoluminescent material was made by heating for one hour a wet mixture of 20 g zinc sulfide and 0.9 g manganese chloride and salt flux to the fusion temperature of 1000°C in a nitrogen atmosphere. The resulting powder, after excitation by ultraviolet, did phosphoresce when exposed to infrared. The efficiency of the material appeared to be of the same order as that of the Kodak screen. The theoretical limit of use of phosphors is about 2μ wavelength. If more efficient chemical converters could be developed, they may prove to be the only methods of planewise observation between the 1.2μ photographic limit and 2μ.

Closed circuit television provides another interesting approach to the problem of planewise observation with longwave radiation. Radio Corporation of America is at the time of this writing developing a vidicon (television camera) tube which will respond to radiation of up to 2.8 microns wavelength. The projected cost of this tube is rather high in comparison to that of other data-recording apparatus, and the associated television circuitry would have to be furnished. If the cost of such a system could be justified in terms of the benefits of the results obtained, this device would make possible the immediate observation and permanent recording, on magnetic tape or photograph, of static and dynamic photoelastic phenomena through visible and up to the extended wavelength limit mentioned. The wavelength span would be over eight times the visible bandwidth. The technique should be seriously considered for future application in this and other areas of research.

Since the practical limit of available imaging systems is at about 1.2 microns, investigations at longer wavelengths must employ pointwise light sensing techniques. The sensing element around which such a system is constructed may be a phototube, photoconductor, or some other device which produces a signal, usually electrical, when subjected to a change of light flux. If such a sensor were placed at a given point in an image of the birefringent plate in a polariscope, it would generate a signal related to the intensity of light passing through the point in the plate corresponding to the chosen point in the image. This satisfies the basic requirements of photoelastic measurement. Recent military and industrial interest has furnished impetus to the

development of various sensing elements and systems adaptable for use in the polariscope. Only the system developed for experimentation plus a few suggestions for improvement can be considered here out of the near infinity of possibilities.

As mentioned, the planar imaging techniques available for this work were applicable up to 1.2 microns maximum. The investigation was to be extended up to the 2 micron limit of the polarizers. Thus, a point sensing system for the range of wavelengths between 1.2μ and 2μ had to be developed. On the basis of spectral response, availability, cost, sensitivity, and time constant, an infrared photoconductive sensor manufactured by Infrared Industries was chosen. This is a lead sulfide sensor with a square sensing area measuring 0.5 mm x 0.5 mm. The maximum dimension of the sensitive area of the device is $\sqrt{2}$ x 0.5 mm = 0.71 mm. If the image of the photoelastic model being tested is n times larger than the model itself, the sensor receives light from a point on the model whose maximum dimension is 0.71/n mm. Even with magnifications of only 1 or 2 times, the sensing area may be considered to be a point relative to the other dimensions of ordinary models.

The lead sulfide sensor is one whose resistance changes with changes in intensity of incident light. A circuit which converted this resistance change to an easily-processed voltage signal was developed. The circuit diagram is shown in Figure 2.6. This circuit was enclosed in a small aluminum box along with the sensor.

Connections were provided for power and signal plus a small hole for the admission of radiation were provided in the box, which may be seen in the photographs of Figure 2.3. The sensing circuit was intended to make the output signal as independent as possible from fluctuations in the supply voltage. To reduce electrical noise, it was found desirable to use batteries as the bias voltage source. The nominal bias for the sensor proper is specified by the maker to be about 33 vdc. To reduce noise still further without decreasing sensitivity unduly, that is, to improve the signal-to-noise ratio, the sensor bias was reduced to values somewhat below nominal. Various values were used, but most experimentation was carried out with a power supply of 22.5 v, which gave a sensor bias of about 10 v.

The output of the sensing circuit is a voltage whose variation with practical changes in light intensity was on the order of 10^{-6} volts, so extensive amplification of the signal was necessary. To allow the required high amplification and to reduce the noise resulting from cell and circuit components, the "lock-on" amplifying technique was used. This method requires that the information of interest be used to modulate a fixed frequency AC carrier signal. The amplifier can then be tuned to the carrier frequency, and the variation in the amplitude of that signal monitored. Noise at frequencies outside the bandpass of the amplifier is rejected. Use of a narrow bandpass filter or amplifier results in maximum improvement in the signal/noise figure. Ordinary amplitude modulation broadcast radio will be recognized as a special application of this general approach to information processing.

In practice, the carrier signal in an optical sensing system is

best created by chopping the light beam at a constant known frequency. In a polariscope or other system where polaroid filters can be introduced, this chopping is best done by rotating one polarizer with respect to the other. A sinusoidal carrier results. However, since the measurements performed in this work involved manual manipulation of the analyzer, a separate device for chopping the light beam had to be introduced. This element of the optical system consisted of an aluminum chopping blade placed normal to the optical axis and rotated at nearly constant speed of 960 rpm by means of a Hurst permanent-magnet hysteresis-type synchronous motor. The blade carried a row of 20 holes near its periphery arranged so that the width of each hole was about equal to the distance between holes. The blade was located at a focal point of the optical system. The blade then functioned as a shutter, switching the light on and off at a known frequency of about 340 cps. The time constant of the sensor was short enough (< 1 μ-sec) so that it responded quite faithfully to the variations in light. Thus, if nothing further disturbed the light beam, the output of the sensing circuit was a voltage varying with time in a waveform closely approximating a square wave whose frequency was 340 cps. The first and largest Fourier component of this square wave would be a sinusoidal wave at the first harmonic of 340 cps. This component could be isolated and amplified at will with suitably tuned amplifiers and filters.

Now, if there was introduced into the optical path a material whose transparency varied at a rate considerably less than the carrier frequency, its effect would be to change the maximum amplitude of the chopped light beam. The output of the sensor would

then be an amplitude modulated square wave. The amplifier output would indicate the changes in transparency of the material as variations of amplitude of the first sinusoidal component of the carrier. For the problem at hand, of course, the object whose transparency changed was just the combination of polarizers, birefringent plate and quarter-wave plates. The transparency changes were due to birefringence in the plate. If the polariscope system was arranged to give dark field, whole-order isochromatics in the area of the image covered by the sensor would ideally appear at the system output as a 340 cps sine wave of zero amplitude.

The amplifier used in this study was a General Radio Co. type no. 1232-A tuneable amplifier with gain variable up to 120 db, and 3 db bandpass of 6% of the center frequency. The extremely sharp peak of the gain-frequency characteristic caused some difficulty because slight variations in chopping frequency appeared as variations in output. This problem was minimized but not eliminated by the motor used. Incorporated into the amplifier is a voltmeter which indicates the rms output voltage. Essentially then, this meter indicated light intensity for a given amplifier gain setting. For each set of readings, the gain was set to give a maximum output of about 0.8 volt, the maximum output being 1 volt before clipping of the waveform begins to occur. The output of the system was also monitored on a Hewlett-Packard Oscilloscope. This was particularly useful in checking frequency variations and preliminary adjustment of the system.

The pointwise technique indicates only the intensity of light passed by a small area of the model. In order to observe the photoelastic fringe pattern in the whole model, it would be necessary to scan the image of the model, plotting voltage (light intensity) versus position. This could be accomplished by incorporating into the amplifier output a demodulator which in turn could be coupled to an oscilloscope or one axis of an x-y recorder. The position indication could be obtained by a slide-wire potentiometer or differential transformer in the scanning mechanism. A still greater improvement would result from moving the model itself with respect to the fixed optical system. Intensity variations in the optical field then would not affect the readings. Also, a much narrower and more intense beam and a more compact optical system could be used, since there is no need to illuminate the whole model at once. The loading system used provided complete facility for horizontal and vertical motion of the loaded model, so the optical system was designed with this latter approach in mind.

Rather than use the sensing system to measure absolute light intensity, results were improved by using it to indicate only relative intensity. Relative retardations in the birefringent plate were then measured through the use of compensation methods. In this way, accurate determination of fractional fringe order was possible without concern for a known or fixed relationship between system voltage output, light intensity, and fringe order. The compensation method used will be pursued further in Section 2.2.3.

F. Optical Bench and Loading

The optical bench and loading frame used in this research were designed and built at Michigan State University. The bench is of heavy cast iron girder construction with facility for leveling and lateral movement. The optical elements of the polariscope are mounted on heavy plates which slide on the smooth rails of the bench. The loading frame is readily adaptable to any type of loading system, and it may be moved in its plane independently of the optical bench. The photographs of Figure 2.3 show clearly the construction of these items of apparatus.

2.2.3. Measurement of Fractional Isochromatic Order

The equations developed in Section 2.1.4 indicate that for given relative retardation in a birefringent plate, the isochromatic order, m, becomes smaller as the wavelength of light used in its measurement is increased. With very long wavelengths and/or with materials of low optical sensitivity, the exact relative retardation at a point in a model cannot be accurately determined by simple interpolation between whole- and half-order isochromatic fringes. Under such conditions, improved measurements of relative retardation can be obtained through the use of one of several methods of compensation. Accurate fractional fringe order measurement was especially important for the calibration studies performed at long wavelengths as part of this investigation.

A number of methods of fractional fringe order measurement, or compensation, have been developed. The best known methods require that an auxiliary device, usually a calibrated retarding plate,

be placed in the optical path adjacent to the point in the model where the retardation is to be determined. Two other useful methods of fractional fringe order measurement are based on rotation of one of the polarizing elements in the optical system. These goniometric methods have the advantages of simplicity and no requirement for auxiliary equipment. Basically the same in principle and manipulation, the methods are known by the names of the men who developed them. Mindlin (47) and Jessop (36) have analyzed the errors in the two methods, and Jessop shows that the errors inherent in the Senarmont technique are always smaller than those of the Tardy method. (This fact seems to be not widely recognized, and many investigators use the least accurate method purposely with the mistaken notion that the method involving 2-quarter wave plates is always most accurate.)

Both the Tardy and Senarmont techniques require rotation of the analyzer of the polariscope to produce zero light intensity at the point on the model where the partial fringe order is desired. The methods, then, are basically "null location" methods, and they are ideally suited to systems where the presence or intensity of light is detected electronically. In this investigation, a slight variation of the more accurate Senarmont method was used for calibration measurements of longer wavelengths. Thus, it is necessary to examine briefly the procedures and governing equations.

Let a polarized ray of monochromatic light fall upon a birefringent plate of thickness d whose principal axes are inclined at 45^{o} to the polarization axis. Referring to equations (2.15), and recalling that retardations common to both components were shown

to be irrelevant, the components of the original ray as they emerge from the plate may be written in terms of the relative retardation:

$$E_1 = \frac{\sqrt{2}}{2} A \cos \frac{2\pi}{\lambda}[z - vt]$$

$$E_2 = \frac{\sqrt{2}}{2} A \cos \frac{2\pi}{\lambda}[z - vt - (n_1 - n_2)\frac{d}{n_o}]$$

Now, as the two component rays enter a quarter wave plate whose axes are at 45^o to the principal axes, that is parallel and perpendicular to the polarizer axis, each component will be divided into subcomponents by the quarterwave plate, and the resultant components as they enter the plate will be:

$$E_x = \frac{\sqrt{2}}{2} E_1 - \frac{\sqrt{2}}{2} E_2 \qquad (2.27a)$$

$$E_y = \frac{\sqrt{2}}{2} E_1 + \frac{\sqrt{2}}{2} E_2 \qquad (2.27b)$$

Upon traversing the plate, the rays will be retarded absolutely by a common amount and relative to one another by $\frac{\lambda}{4}$. The components leaving the plate may be described as

$$E_x = \frac{1}{2} A \{ \cos \frac{2\pi}{\lambda}[z - vt] - \cos \frac{2\pi}{\lambda}[z - vt - (n_1 - n_2)\frac{d}{n_o}]\}$$

$$E_y = \frac{1}{2} A \{ \cos \frac{2\pi}{\lambda}[z - vt - \frac{\lambda}{4}] + \cos \frac{2\pi}{\lambda}[z - vt - (n_1 - n_2)\frac{d}{n_o} - \frac{\lambda}{4}]\}$$

or,

$$E_x = - A \sin \frac{2\pi}{\lambda}[z - vt - \frac{n_1 - n_2}{2 n_o} d] \sin \frac{2\pi}{\lambda}[\frac{n_1 - n_2}{2 n_o} d] \qquad (2.28a)$$

$$E_y = A \sin \frac{2\pi}{\lambda}\left[z - vt - \frac{n_1 - n_2}{2n_o} d\right]$$

$$\cos \frac{2\pi}{\lambda}\left[\frac{n_1 - n_2}{2 n_o} d\right] \qquad (2.28b)$$

The rays are then passed through a second polarizer inclined at $(\frac{\pi}{2} - \theta)$ from the first polarizer, that is at angle θ from the configuration in which whole order isochromatics appear dark. The polarized ray leaving the polarizer will be the sum of part of each of the components leaving the quarter-wave plate:

$$E = E_x \cos \theta + E_y \sin \theta \qquad (2.29)$$

This becomes

$$E = - A \sin\left[\frac{2\pi}{\lambda}\left(\frac{n_1 - n_2}{2 n_o}\right) d - \theta\right]$$

$$\sin \frac{2\pi}{\lambda}\left[z - vt - \frac{n_1 - n_2}{2 n_o} d\right] \qquad (2.30)$$

The retardation of the wave leaving the analyzer is thus seen to be in the form of a single traveling wave whose intensity is the square of the amplitude,

$$I = A^2 \sin^2\left[\frac{\pi (n_1 - n_2) d}{\lambda n_o} - \theta\right] \qquad (2.31)$$

The intensity is zero when the argument of the expression vanishes or equals a multiple of 180^o. Only the first value is of any consequence.

$$\frac{\pi (n_1 - n_2) d}{\lambda n_o} - \theta = 0 \qquad (2.32)$$

Thus, if the various optical axes in a polariscope are properly oriented with respect to the principal stress axes at some point in a birefringent

plate, the amount of rotation of the analyzer from the crossed configuration required to produce zero intensity at the same point is proportional to the fraction of a whole isochromatic order existing at that point. The fraction, m_f, of a whole order of retardation is easily calculated.

$$m_f = \frac{n_1 - n_2}{\lambda n_o} d = \frac{\theta \text{ (rad)}}{\pi} = \frac{\theta^o}{180^o} \qquad (2.33)$$

If m_w is the next highest or next lowest whole fringe, the actual retardation at the point being considered is, in terms of fringe order:

$$m = m_w \pm \frac{\theta^o}{180^o} \qquad (2.34)$$

The direction of the principal stresses can be obtained from observation of the isoclinics at the point or points in the birefringent plate where the accurate measurement of retardation is desired. The nearest whole order may be determined by inspection of the isochromatic field or by watching the isochromatics develop, whichever is easier. After insertion of the quarter-wave plate and proper alignment of the axes of the optical elements, rotation of the analyzer until extinction of the light occurs will indicate the fractional order. The sign of the correction in equation (2.33) depends on the "handedness" of the quarter-wave plates, the material of the birefringent plate, and the direction of rotation. This is best established for each polariscope by preliminary tests on a known simple stress field such as exists in a tension or compression bar.

The pointwise light detection scheme used for the investigations in the longwave spectral range was especially compatible with the goniometric methods of fringe order measurement. With the polariscope properly arranged and with the sensing device located at the desired point in the image of the model, it would normally only be necessary to rotate the analyzer until the output of the sensing circuit, that is the amplitude of the sinusoidal voltage, was zero. The difference between preliminary and final values of the analyzer orientation indicates the fractional fringe order. At a certain loss of simplicity, the procedure was changed to overcome a procedural and system weakness and improve accuracy.

Expression (2.31) for the light intensity as a function of the relative retardation and inclination of the polarizer from the crossed position may be rewritten in terms of the deviation as:

$$I = \frac{1}{2} A^2 \{1 - \cos 2[\frac{\pi (n_1 - n_2) d}{\lambda n_o} - \theta]\} \qquad (2.33)$$

A plot of intensity versus the angular difference of the argument is thus a cosine curve whose amplitude varies between $I = 0$ and $I = 1/2\ A^2$. The Senarmont null detection technique reduces to a search for the values of the argument at which the intensity becomes zero. Otherwise stated, the problem is to determine the angle at which a sine or cosine curve reaches minimum amplitude by observation of the amplitude. Since the slope of such a curve is zero at the minimum, the problem is poorly conditioned to begin with. The detection of minimum amplitude is further complicated by noise in the intensity detection system. In most electronic systems,

including the intensity detection circuit used in this investigation, a certain small amount of random noise will appear at the output regardless of the signal amplitude. As the signal, in this case the light intensity, is reduced in magnitude, it will dip below the noise level and become undetectable at values greater than zero. This makes location of the angle at which zero intensity occurs a virtual impossibility. The possible error in determination of the angle may be rather large because of the shape of the curve at its minimum. This difficulty is represented pictorially in Figure 2.7a.

Better results can be obtained by measuring the angles on either side of the minimum where the amplitude reaches some arbitrarily assigned value and the slope of the curve is greater. Since the intensity is an even function of the difference between retardation and inclination of the polarizer, the average of the two values of angle thus obtained will represent the angle at which the intensity reaches the desired minimum. The greater accuracy results from both the averaging process and the reduction in the possible error in both measurements due to lessened effect of the noise. Reference to Figure 2.7b will clarify this point. Additional improvement will also result from rotating the analyzer such that the arbitrary amplitude is approached from, say, a greater value, so that the indeterminancy in the measurement of the two angles due to noise will oppose one another, and these errors will cancel in the average.

The procedures just described were employed with success in the experiments involving goniometric compensation with

the point-sensing techniques in the longwave region. In practice, the analyzer was rotated to give maximum output of the detection circuit, and the amplifier gain adjusted to give a meter reading of 80. The angle at which the amplitude of the output was minimum was measured as closely as noise in the system would allow. Then, the angles on each side of the minimum value at which the amplitude of the output reached an arbitrary value such as half of maximum, or 40 on the meter, were measured carefully, and these two values recorded. The average obtained was compared with the angle giving minimum output as a check. The two measurements were usually in good agreement, but scatter was appreciably less with the method of averaging the symmetrical points.

A complete discussion of the possible error in the compensation measurement is not feasible here. The intensity of available radiation, the transmission of the optical elements, and the sensitivity of the sensor varied with wavelength. The gain of the amplifier was adjusted to give the same output at each wavelength. The resulting large variations in system gain meant that the noise, and therefore, the signal-noise ratio varied with wavelengths used. Let it be sufficient to say that the errors were reduced as much as possible within the limits of the system and operator judgment. The scatter in measured data will give some indication of the failure to reduce random errors to absolute null.

One source of systematic error that could affect results in an undetectable way deserves further consideration. The derivation of the equations governing the Senarmont compensation technique rested on

the assumption that the quarter-wave plate used produced a relative retardation of exactly $\frac{\lambda}{4}$. It is well-known that errors in quarter-wave plates do not ordinarily affect the positions of isochromatic fringes in a stress or strain field (47). Still, to avoid possible secondary effects, isochromatic fringe data for this investigation were obtained using linear polarization. Fringe patterns obtained with the circular polariscope were used only for auxiliary purposes. The remaining question is how the quarter-wave plate errors contribute to errors in compensation measurements of fractional fringe order. The problem is especially important here, since, as will be recalled from previous discussions, half-wave plates for the visible spectrum were used singly or stacked to serve in the infrared range.

Jessop, in the paper already referenced (36), presents an analysis of errors in the Tardy and Senarmont methods of compensation. If e is the quarter wave plate error in wavelengths, the maximum system error (not operator error) in the latter method will be, in terms of wavelengths:

$$m_{actual} - m_{indicated} = \frac{1}{2}\pi e^2 \sin \frac{2\pi}{\lambda}(n_1 - n_2)\frac{d}{n_o} \qquad (2.34)$$

The nominal retardation of the quarter wave plates used was 0.277μ. One of them thus served as a perfect quarter wave plate at $\lambda = 4 \times 0.277 = 1.108\mu$, and two plates would serve at $\lambda = 2.216\mu$. The maximum error would occur at a value midway between these wavelengths, where it was necessary to change from one to two plates. The maximum error in retardation would then occur at

λ = 1.662. An ideal quarter-wave plate for this wavelength would produce a retardation of 0.4155μ. The actual plates produced retardation of 0.277μ and 0.554μ. The error then is 0.4155 - 0.277 = 0.554 - 0.4155 = $\pm$ 0.1375μ. The error in terms of wavelength is, thus,

$$e = \pm \frac{0.1385}{1.662} = \pm 0.0833$$

Using equation (2.34), the maximum reading error would then equal $1/2\,\pi\,(0.0833)^2$ = 0.0109 wavelengths. In other words, inaccuracies in the quarter-wave plates used would induce into the measurement of fractional fringe order a maximum error of 1% of one fringe. If the total isochromatic order at the point where the fringe order is being measured by the compensation technique had a value m, then the maximum measurement error due to the quarter-wave plates would be $\frac{1}{m}$ % . This source of error may be considered negligible within the limits of the experiments involving radiation of wavelengths between 1 and 2 microns.

3. Determinations of Optical Behavior of Materials

The experimental techniques which were developed for the performing of photoelastic investigations in the longwave spectral range were employed in experiments having several distinct but related purposes. These objectives included calibration at various wavelengths of three resins, the definition and measurement of dispersion of birefringence, and preliminary investigation into the birefringence of certain semiconductor materials.

3.1. Description of Materials and Testing Procedures

3.1.1. Tensile calibration of CR-39 in visible and near infrared

Representative stress-optical properties, including dispersion data, were obtained for the common birefringent plastic CR-39 from planewise measurements in the spectral range from the visible up to over one micron.

Columbia Resin CR-39, an allyl polyester resin, is probably at present the most widely used photoelastic material. Its optical sensitivity and transparency make it attractive for photoelastic use, even though it suffers seriously from high mechanical and optical creep and undesirable edge effects. The mechanical and birefringent properties of this material have been extensively explored by several investigators including Coolidge (12), Pindera (58, 62, 63), Clark (9) and Pindera and Kiesling (64). These previous investigations have consisted of calibration and creep tests using visible radiation. The present tests were intended to supplement existing data and provide preliminary indications of the optical properties of CR-39 in the infrared range.

The particular material studied was obtained in 3/8" thickness from Cast Optics Corporation. Tapered models were tested in tension after the method discussed by Frocht (20), developed by Pindera (62) and further improved by Pindera and Kiesling (64). This calibration technique calls for the use of a wedge-shaped model having a small wedge angle so that, under tensile loading, the stress state at any point consists of a radial tensile stress which is easily calculated. The gradient of stress over the length of the model allows a tensile stress-birefringence plot to be constructed from one set of observations on one model at any given time after loading. A sketch of the model tested is presented in Figure 3.1 along with a plot of the stress along the model axis and the load history.

The specimen was supported in the moveable loading frame described previously and loaded through a deadweight loading system. The loading lever of the system, designed and built for the photoelasticity laboratory, was one employing hardened knife edges at all load pivot points. The load was transmitted uniformly to the specimen through specially designed grips which clamped the enlarged ends of the model between serrated brass faces. Local effects which tend to fracture brittle plastic models near load application points were thus avoided. Each grip also provided means of moving the load application point perpendicularly to the load axis in order that the load could be precisely aligned with the model axis. The dead weight of 40.8 kg, which placed a load of 204.1 kg on the spcimen was applied gradually over a period of about 10 minutes. This was sufficient to create a maximum tensile

stress of 2.126 kg/mm^2 in the uniform neck of the specimen. The period of recording results was expected to be more than one hour, due to the necessity of changing apparatus for the various wavelengths of light used. In order to reduce the effects of creep during the recording period, data was not taken until 21 hours and again at 66 hours after loading. Only the results obtained at 66 hours were evaluated. A complete calibration would, of course, measure creep which took place throughout this time period. Data from similar experiments by a previous investigator (63) indicate that during the recording period, the optical-creep rate, $\frac{dm}{dt}$, should be less than 4×10^{-2} per hour at a stress level of 2.2 kg/cm^2 for light at λ = 436 nm. During the 3-hour data-recording period of this test, then, the change of maximum isochromatic order should be less than 0.75%. The tests were conducted under ambient laboratory conditions.

In order to measure relative retardation in the tapered model for the given load and time conditions, photoelastic fringe patterns were recorded photographically using monochromatic light at several wavelengths spread over a sprectral range of 0.678 microns. Chosen on the basis of availability and convenience at the time of testing were wavelengths of 405 nm, 436 nm, 546 nm, 578 nm, 587 nm, 668 nm, 707 nm, 853 nm, 1083 nm. The methods for obtaining monochromatic radiation at these wavelengths have been discussed in Section 2.2.2 and are summarized in Table 2.1 of this report. The variety of wavelengths means, of course, that it was necessary to change light sources and filters throughout the testing period. Within the limits imposed by

the necessity of changing light sources and other equipment the various wavelengths of light were taken in nonsystematic order so that the effects of creep during the recording period would at most appear in the data as scatter, rather than as a trend over the spectral range. Duplicate data obtained near the beginning of the recording period and again near the end indicated that the creep effects were well within the expected limits. The numerous filters used were mounted in an indexed filter wheel to facilitate speedy changes of color during the test.

The optical bench and lenses were arranged in accordance with the discussion of Chapter 2. Figure 2.2a shows the arrangement of the system for planewise observations. The condensing lens used in this portion of the study was a simple convex-convex type. The small ratio of focal length to diameter and resulting high distortion and chromatic aberration made it difficult to illuminate the field uniformly. Some of this difficulty with chromatism was overcome by moving the lens slightly for the different wavelengths. The field lens utilized was of plano-convex type with focal-length to diameter ratio of about 3. This simple lens, while of better quality than the condensing lens, created enough distortion so that some difficulties were encountered in the analysis of results.

Since both visible light and infrared radiation were employed, two different sets of polaroid and quarter-wave plates were required, and these also had to be switched during the data-recording period. The polarizers and quarter-wave plates used have already been described. Those for the visible radiation were of 13" diameter.

The 4" square size of the largest available infrared polarizers (HR sheet, glass-mounted) made it necessary to cover the rather large CR-39 model in segments, as will be described shortly. One layer of half-wave retardation material for the visible region was used for each of the two quarter-wave plates for the infrared range between 0.7 and 1.08 micron. Permanent recording of the photoelastic patterns in the loaded CR-39 model was accomplished photographically. Auxiliary observation in the portions of the test involving nonvisible light was possible through the use of the infrared converter. Both camera and converter were located at or near the focal point of the field lens. The location of this focus varied considerably over the extreme range of wavelengths due to chromatic dispersion in the lens, so the camera and converter had to be moved slightly with changes in wavelength to previously determined focal points along the optical axis. This was required to establish uniform illumination of the field and also to ensure that only rays passing normal to the plane of the model were used in constructing the image of the model on the film or converter cathode screen.

A 35 mm Nikon F camera with lens chosen to match the other optical elements was used in the recording of results. With a lens of 55 mm focal length, maximum image size was attained on the film when the camera was placed at the focus of the field lens and the field lens placed as little distance as possible, about 6", from the model. This camera and its lens, while of excellent optical quality, was also subject to the effects of chromatic dispersion. A special focusing mark is provided on the lens barrel for focusing with

near infrared radiation at about 0.8 micron. For focusing at 1.08 micron, another index mark was established that provided a correction in focus twice that prescribed for 0.8 microns. The various films required for photography over the extended spectral range have been summarized in Table 2.3 of Section 2.2.2. The film had to be changed along with polarizers, light sources, and filters in the course of the recording period. In order to change film, the camera had to be dismounted, the film changed in a light-tight bag, and the camera remounted, aligned, and focused at considerable expense of time. The camera aperture setting and shutter speeds depended on film, wavelength and optical system configuration. Nothing will be added by tabulating these here, but they varied between f22 at 1/250 sec for λ = 435 nm and f8 at 30 sec for λ = 1083 nm. Processing of the negatives was in accordance with manufacturer's instructions, with preference given to the methods giving highest contrast and smallest grain size.

The four-inch maximum field in the infrared system required that the photoelastic pattern in the large tapered CR-39 model be photographed in segments. To accomplish this, a pointer was attached to the loading frame which could be raised and lowered electrically with respect to the optical bench. Index lines were placed on a stationary scale attached to the base of the loading frame. These lines were placed so that when the pointer was aligned with them, the loading frame and model would be properly located with about 4" of the model in the polariscope field. In this way, slightly more than 1/3 of the model could be photographed at one time. By raising and lowering

the frame and model, the segments could be photographed in order. Enough overlap existed between the segments to allow the photographs to be properly matched. The matching process was facilitated by scratching gage lines on the surface of the specimen. Light and dark field pictures using both linearly and circularly polarized light were taken at each position on the model with one wavelength before changing wavelength and repeating the cyclic photography of the segments of the model. A total of 108 exposures was required to complete the test. Representative photographs of the isochromatic pattern in the head end of the model with radiation of 546 nm and 1083 nm are presented in Figure 3.2a and 3.2b. These patterns were obtained with linear polarization oriented at 45^{o} to the axis of the specimen. The 45^{o} isoclinic is readily apparent in the fillet above the uniform neck of the model.

3.1.2. Tests of Palatal P-6

Certain aspects of the mechanical-optical properties of the polyester resin Palatal P-6 were explored photoelastically in the visible and near infrared spectral range. The birefringent properties of this material in the visible range have been investigated by the authors previously cited in connection with their work with CR-39. These researchers found that P-6, which is not commonly used for photoelastic studies in the United States, possessed certain desirable characteristics including good light transmission, high optical sensitivity, and relative freedom from time-edge effects.

The material used in this study was donated by Badische Anilin and Soda-Fabrik (Germany) in the form of raw liquid resin. Sheets

of the polyester were formed by casting between glass plates a mixture of 100 parts fluid resin, 2 parts catalyst, and 0.05 parts accelerator. After hardening, the sheets were removed from the forms, aged 3 months, and then cured at 90°C for 40 hours. The heating and cooling rate of the curing cycle was set at a nearly uniform rate of 5°C/hr. The models were then machined from these sheets using standard methods.

Two different models were cut from different sheets of the P-6. Sketches of the models tested and their load histories appear in Figures 3.3 and 3.5. The circular ring having an outer diameter of 80 mm, inner diameter of 44 mm and thickness of 6.10 mm was tested in diameteral compression early in the course of the investigation. This particular test was directed towards a preliminary measurement of the dispersion characteristics of P-6, so the results are not as comprehensive as those obtained from the other experiments. The load of 320 pounds was applied to the specimen by means of a dead-weight lever system in a stationary frame. The load on the specimen was maintained at ambient laboratory conditions for 50 hours, at which time the birefringent pattern was recorded photographically over a period of 2.5 hours.

The optical system used in this first test of P-6 was essentially the same as that used in the test of CR-39 already described. Rather than the optical bench, the polariscope elements were supported on threaded rods mounted in drilled aluminum plates. The plates were themselves mounted on pedestals consisting of a telescoping aluminum column on a heavy steel base.

The photoelastic pattern in the P-6 ring was photographed with radiation of 6 different wavelengths. The methods described earlier were used to produce light having wavelengths of 405 nm, 436 nm, 546 nm, 578 nm, 853 nm, and 1083 nm. Photographic procedures were identical to those used in the tensile test of CR-39. Representative photographs may be seen in Figure 3.4.

The second model of Palatal P-6 resin tested was a beam 300 mm long by 38 mm deep and 6.05 mm thick. The model was loaded in pure bending with forces of 5.44 kg applied at each of the third points. The model was supported in the moveable loading frame used in the test of CR-39, and loaded through cylindrical pins which were held in place by vee-blocks. The lever arm supported on hardened knife edges was used to transfer the dead-weight load to the lower support of the model. The load was applied over a period of about 10 minutes. Recording of the data took place at 49 hours after loading. From the results obtained in the visible spectral region by the investigators already mentioned, the rate of optical creep of P-6 at the maximum stress level was $\frac{dm}{dt} < 2 \times 10^{-2}$ per hour for $\lambda = 435$ nm. Thus, during the time of recording data, the change of maximum isochromatic order was less than 0.3%. As with the test of CR-39, duplicate pictures taken at one wavelength early and late in the test indicated this estimate of the creep effects to be conservatively large.

The optical system used in this test of the P-6 beam was the same as that employed in the tensile test of CR-39, with the exception of the collimating lens and the field lens. The high distortion evident

in the lenses used in the previous tests indicated a need for higher quality optics. Matched convex-convex lenses of 33 cm diameter and 1 m focal length became available and were used in this experiment involving P-6. The large span of wavelengths used and the accompanying chromatic dispersion in the lens still necessitated the moving of the recording apparatus to the focal points for each wavelength, but the distortion in the image of the model and the uneven field illumination were effectively eliminated.

The birefringent patterns in the bent beam were recorded photographically with illumination having wavelengths of 405 nm, 436 nm, 546 nm, 578 nm, 587 nm, 668 nm, 707 nm, 853 nm, and 1083 nm. Auxiliary observation at the longer wavelengths was possible with the infrared converter. The techniques and experimental procedures were the same as those already described. Since a longer-focal-length field lens was used, it was necessary to use a camera lens having a focal length of 85 mm. This optical system allowed photography of the full length of the beam with visible radiation. In the infrared, only the central portion of the beam could be photographed due to the smaller size of the infrared polarizers. The negatives obtained at $\lambda = 1083$ with spectroscopic film were somewhat underexposed, and it was necessary to use a mercury intensifier to increase negative density to the point where good measurements could be obtained. Otherwise, processing of the films was as before. Pictures were obtained with both circular and linear polarization at each wavelength. Figures 3.6a - 3.6c show the isochromatic pattern in the beam at $\lambda = 546$ nm with

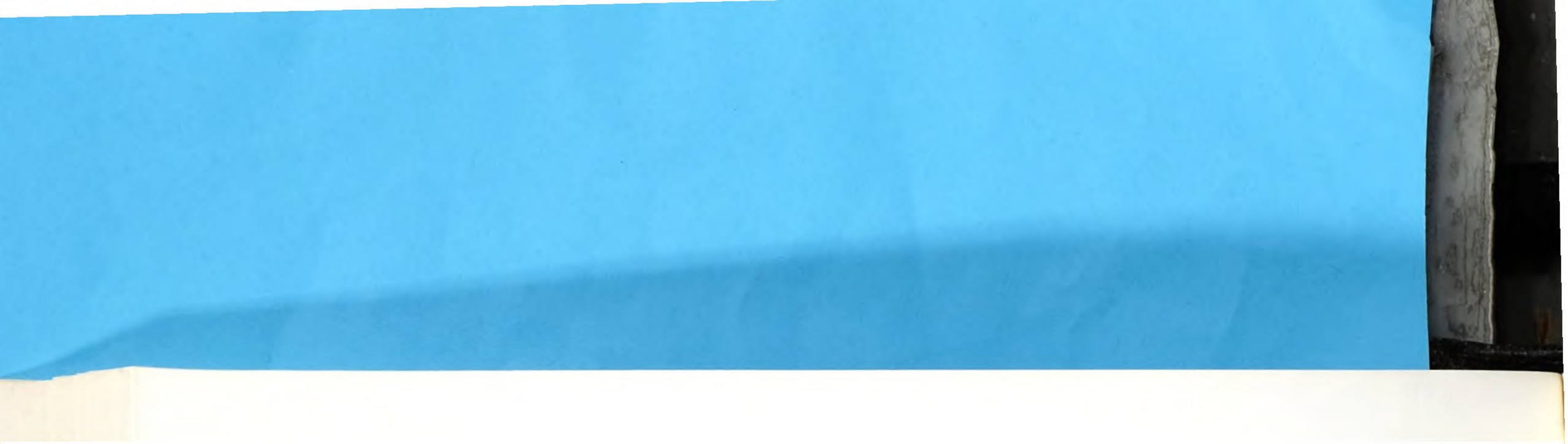

circular polarization, and at λ = 450 nm and λ = 668 nm with linear polarization. The dimensions of the beam and the large load used suggest the possibility that the beam may have buckled slightly during the test, thus changing the moment and stress distribution. The symmetry of the isochromatic patterns obtained with circularly - polarized light and the fact that the central isochromatics form closed loops indicate that buckling definitely did not occur.

3.1.3. Birefringence in Polycarbonate between 1 and 2 microns

Polycarbonate resin possesses a number of characteristics which make it attractive for use as a photoelastic and photoplastic model material. Ito (33) summarizes the basic properties of this material and proposes its use in studies involving elastic and plastic deformation. The optical sensitivity of the resin is higher than that of other photoelastic materials, and the same is true of its modulus of elasticity. Toughness and impact strength are also higher than that of linear polymers. Of particular interest is the fact that polycarbonate can be severely plastically deformed, even in the cold state, without affecting either strength of transparency.

Polycarbonate seemed especially attractive for this investigation, because, unlike several other common plastics, it was highly transparent (above ~ 75%) in the spectral region in which the study was to be carried out.

The model tested was a disc of 78.5 mm diameter and 4.26 mm thickness which was cut from a cylindrical billet of "Lexan", one of the commercial names applied to polycarbonate of 4-4-dioxphenyl propane and phosgen. The model and its load history are given in

Figure 3.7. Both sides of the rough plate sawed from the billet were faced in a lathe after turning the outer diameter. The disc was then polished as flat as possible on metallographic polishing plates using three grades of abrasive paper. Reasonably good optical surfaces were then produced by lapping the plate on rotating metallograph laps using linen and felt laps with 500 and 320 levigated alumina as the lapping medium. Some large scratches remained in the surfaces, but the small scratches were removed and the faces of the model did not tend to diffuse light. Observation of the model in a visible light polariscope indicated a residual stress pattern in the outer 1 cm of the disc which was probably caused by rapid cooling of the extruded billet. The residual stress pattern near the center of the model was not great. Since it did not interfere with the experimentation, no attempt was made to relieve the residual stresses by annealing.

The polycarbonate disc was loaded in diametral compression using an arrangement very similar to that used in loading the P-6 beam. Common procedure for calibrating a material by testing a disc in compression is to load the disc, wait the desired time, then record the fringe pattern or observe directly the birefringence at various points on the model where the stress can be easily calculated. Usually points on the horizontal and vertial diameters are chosen. A stress-fringe plot can then be constructed from the calculated stress spectrum and the observed birefringence. In this quantitative application of the pointwise sensing technique, the scanning procedure was not used, and the test was conducted in a

manner similar to the ordinary tensile test. That is, the relative retardation at a given point on the model was observed as the load was increased. Since the measuring and recording of fringe order for several different wavelengths at each load required about 0.5 hr. creep effects could lead to serious error. The effects of creep or the results can be minimized in a test of this sort by applying an increment of load, then waiting a specified time before recording results. If the time periods between recording birefringence at a given wavelength are always identical and the stresses were within the linear limit for the material, the deviations would be null. In this case, the stress-birefringence curve for each wavelength would correspond to a different testing time. If, on the other hand, the time periods were kept uniform and the several wavelengths taken in nonsystematic order, the experimental points would deviate from a smooth curve by no more than the amount of creep occurring during the recording period. This deviation could be reduced to near zero by extending the interval between increasing the load and beginning to measure birefringence. In any case, the smooth curves through the experimental points, which may be scattered some amount by creep effects, should represent the stress-retardation characteristic at each wavelength for the same time. If the material is not "momentarily-linear-elastic", the situation is more complex, but still meaningful.

The last described approach was used in the test under discussion. An increment of load was applied, the measurements of fringe order were begun after a period of 1 hour. The total interval between successive

increases of load was thus about 1.5 hours. There were some slight deviations from this schedule in the early phases of the experiment, as may be observed by reference to Figure 3.7. Maximum load on the specimen was limited to 108.8 kg due to difficulty with the loading apparatus. The resulting stress levels near the center of the disc were apparently within the linear limit, but very severe local deformation did take place near the pins through which the load was applied to the model. Load increments varied between 6.45 and 2.27 kg (1 to 5 lbs), and total testing time was 12.5 hours.

The optical system used in this investigation of the birefringence in polycarbonate with infrared radiation between 1μ and 2μ wavelengths has been described in Chapter 2 and pictured in Figures 2.2 and 2.3. The general techniques have also been discussed. After aligning the center of the disc with the optic axis of the polariscope, the 55 mm diameter achromatic field lens was adjusted to focus a magnified image of the model in the plane of the infrared sensor. Reasonably high light intensity was maintained by using an image which was 2.5 times larger than the object. Since the sensor had a sensing area of 0.5 mm square, the largest dimension of the area on the model over which the intensity was averaged by the sensor was $\frac{0.5}{2.5} \times 1.4 =$ 0.28 mm. The sensor was carefully aligned with the center of the image of the model as indicated by diametral lines scratched on the model surface. These lines were carried close to, but not through, the center of the model so as not to interfere with observation. This preliminary adjusting and focusing was done with visible radiation and checked in near infrared with the aid of the infrared converter. The

correction in positioning between visible (650 nm) and near infrared (1μ) was almost undiscernible, due no doubt to the use of small diameter achromatic lenses in the optical system. For assurance, the small adjustment in focus necessary between visible and near infrared was doubled to establish the approximate correction for the spectral region beyond 1 micron where visual observation was not feasible. Since imaging was not required, small errors in focus were of not great consequence. Laboratory temperature during the test was 20° C.

Relative retardation in the disc of polycarbonate was measured using radiation of eight different wavelengths. Chosen at the time of the experiment because of availability of filters, response of the sensor, and transmission of the optical system were wavelengths of 1.145μ, 1.244μ, 1.348μ, 1.446μ, 1.550μ, 1.56μ, 1.650μ, 1.90μ. After applying each increment of load and waiting the specified time, the fractional isochromatic order existing in the center of the model with radiation of each of the eight wavelengths was measured using the detection and goniometric compensation methods outlined in Section 2.2.3. The nearest whole-order isochromatic was determined by observing the changes in light intensity for one or another of the wavelengths as indicated by the output of the detection circuit while the load was being increased.

The spectral transmittance of polycarbonate in the 0.85 to 7.5μ range was obtained through the use of the Perkin-Elmer Model 137-G Spectrophotometer in its normal mode.

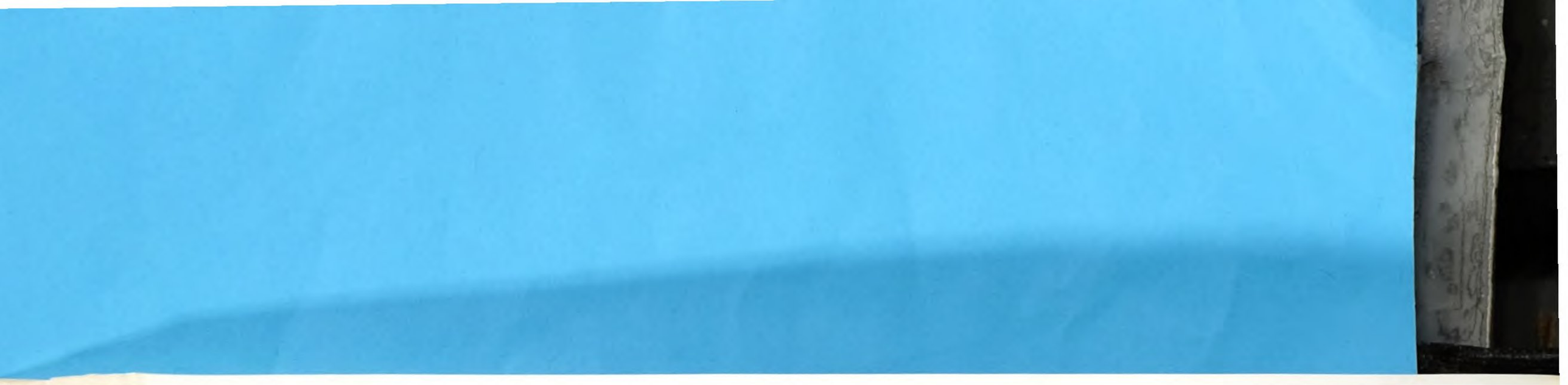

3.1.4. Preliminary Investigations of Birefringence of Semiconductors

Inquiry into the possibility of using materials which are not transparent to visible light for photoelastic studies using infrared radiation was begun by investigating the birefringent properties of two semiconductor materials. These two materials, selenium and silicon, were chosen because of their known transparency to infrared light and their similarity to common, brittle metallic structural materials. Also, these semiconductors have been shown to be birefringent to some limited extent by authors already mentioned (3, 13, 23, 24, 30, 34, 68).

The element selenium exists in several forms including two crystalline types and the amorphous form, which is of particular interest for optical applications. The latter type is easily produced by quenching the molten element to its freezing point. Its structure is similar to that of amorphous sulfur, as might be expected because of their relation in the periodic chart. In the melt, selenium exists as a fluid mixture of entangled chains of atoms. When quenched, this entangled chain structure is maintained, although the chains may take up some degree of preferred orientation with respect one one another (31, 32). The result is a solid which seems to bear some similarity to the chain structure of the polymers, but which also possesses some of the aspects of metallic crystalline forms. Amorphous selenium is known to transmit radiation between 0.6μ (deep visible red) to 25μ wavelength, with absorption bands at 13.5 and 20.5μ (35, 54). The material is quite stable, somewhat brittle, and the frozen form does not soften or begin to transform to the

crystalline until 50° C. As mentioned, birefringence caused by internal stresses created during crystallization has been observed.

For this experiment, discs of amorphous selenium having 50 mm diameter and 6.3 mm thickness were produced by casting. The mold consisted of a partial ring of aluminum which was sandwiched between pyrex plates. The molten selenium was poured into the mold through the opening in the ring and the whole assembly immersed in cold water to freeze the selenium. After solidification, the disc was separated from the mold and the sprue broken off. In this way good optical surfaces were produced, but cavitation in the disc due to shrinkage created considerable difficulty.

The disc model of selenium was supported and loaded in the same way as was the polycarbonate disc. The optical system was similar to that used for planewise test of CR-39. Observations were visual by means of the infrared converter at 0.850 microns radiation wavelength.

Silicon is a hard and brittle material which belongs to the same periodic group as selenium. It transmits radiation having wavelengths between about 1.1 and 25μ. A disc of this material having a diameter of 25 mm and thickness of 0.914 mm was loaded in diametral compression and the stress birefringence observed and measured. Since silicon transmits radiation whose wavelengths are within the sensitivity range of the infrared converter, this instrument was used to observe visually the photoelastic effects. Photography of the isoclinic and isochromatic fringes could also be accomplished with the converter.

The point sensing and compensation techniques were employed in the quantitative measurement of the stress-birefringence of silicon. The apparatus, stress calculations, and most experimental procedures were identical to those of the test of polycarbonate. In this case, the retardation was measured immediately following the application of an increment of load. The possibility of buckling the thin specimen limited the range of load which could be used. The small thickness of the specimen also caused the fringe order for the maximum load to be on the order of 0.1. Recalling the previous calculation of error in the compensation method, the possible error in measurement of the fringe order in the silicon disc might be as high as 10%.

In keeping with the organization of this report, the observations and measurements of birefringence in selenium and silicon are presented at the end of the following section. Various aspects of this and the other phases of the investigation are discussed further in Chapter 4.

3.2. Treatment of Data and Presentation of Results

3.2.1. Calibration of P-6 and CR-39

The stress-birefringence properties and dispersion of birefringence characteristics of P-6 and CR-39 for the near infrared and visible spectral range were obtained from the photographed isochromatic pattern through a simple but refined graphical procedure. First, the locations of the whole and half-order isochromatic fringes along the chosen cross section of each model were determined by measurement directly on the 35 mm negatives. A two-dimensional

measuring microscope manufactured by W. G. Pye and Co. Ltd. (England) was used for this measurement. The highest magnification, 20 x, was used and the centers of the isochromatic bands were generally well defined when the negatives were viewed through the microscope. Accuracy of the instrument is specified by the maker to be ± .01 mm when moved over its full range of 20 cm laterally and 10 cm longitudinally. The accuracy is said to be proportionately greater in relation to the smaller amount of traverse. Duplication of measurement on about one-fourth of the negatives indicated a minimum repeatability of measurement of ± .01 mm. Assuming the accuracy of the device is an order of magnitude greater for the small 35 mm negative, the repeatability in the more subjective process of locating the center of the isochromatics may be taken as the extreme measurement error. The value given above was more than sufficient for this work.

The negatives were illuminated during measurement by supporting the microscope over a fluorescent lamp, and usually a green Kodak filter was placed directly under the negative. Both whole and half order fringes were not located on all negatives. Where the light isochromatic on the negative (whole order for dark field, etc.) was very sharply defined and the fringes were closely spaced, only that isochromatic was located. Where the fringes were broad due to underexposure or other causes, both half and whole order were located by measurement, and often several observations were made and the results checked for consistency and then averaged.

To reduce the effects of chromatic dispersion and distortion in the polariscope lens system and unequal shrinkage in the variety of films used, the measurements from the negatives were normalized on the basis of the measured distance between gage lines which had been scribed on the specimens. These gage lines usually showed on the negatives, otherwise the extreme dimensions of the measured cross section of the model were used as the basis of the correction factor. The poorer lens used in the tests of the P-6 ring and the tapered CR-39 model introduced certain distortions which could not be completely nulled by linear magntification factors. These errors became apparent as consistent opposing deviations in the plotted results, and they were minimized by the graphical processing of the data.

Measurements of the isochromatic order in the tapered CR-39 model were taken along the longitudinal center line. For the P-6 ring, a horizontal radius was chosen as the cross section across which results were to be evaluated. The central cross section of the P-6 beam was selected for measurement. The chosen sections are indicated by heavy lines in the sketches of the various models presented in Figures 3.1, 3.3 and 3.5. It is worth mentioning again that measurements used for quantitative analysis were taken only from the pictures obtained with linearly-polarized radiation. A representative set of measurements and corrected data may be seen in Appendix A.

From the corrected measurements of the location of the isochromatics, plots of fringe order versus location on the cross section

were constructed for each model. The different curves corresponding to the various wavelengths used in any one test were plotted on the same sheet. Greatly reduced copies of some of these curves for the CR-39 model appear in Figure 3.8; those for the P-6 beam in Figure 3.9; and plots for the P-6 ring are shown in Figure 3.10. The original working plots were made in the largest practicable size using 24 in. x 36 in. graph paper for maximum resolution and accuracy. A smooth curve was drawn through the experimental points for each wavelength. In general, the deviations of the experimental points from the smooth curves were so small as to be insignificant with the scaling used. This reflects the consistent good results which might be expected from the technique of carefully measuring negatives with an instrument capable of high accuracy.

From the data and curves of fringe order versus location on the cross section, plots of relative retardation per unit thickness versus location were constructed by multiplying fringe order by the appropriate wavelength. Due to the smoothness and consistency in the measured and corrected data, this was used in developing the retardation curves, rather than using points read from the fringe order curves as would normally be the reason for employing the smoothing graphical technique. Essentially, this conversion from a plot of isochromatic order to one of retardation per unit thickness consists of introducing scale factors into the plots of isochromatic order at each wavelength in order to put them on a common basis. Dispersion of birefringence becomes apparent at this point, since the retardation plots for different radiation would be concurrent if

double refraction was independent of wavelength. The actual measurement of dispersion is discussed fully in later paragraphs.

The original working graphs of relative retardation per unit thickness versus location on the cross section of the model for constant wavelength of radiation were all made to large scale on 24" x 36" paper. Reductions of representative curves are given in Figures 3.11, 3.12 and 3.13 for each of the three models. Experimental points are not shown as they would only contribute a degree of confusion. However, all observed data, if shown, would lie within the width of the line used in drawing the smooth curves.

The stress along the longitudinal centerline of the tapered CR-39 model was calculated from the well known elasticity solution for a wedge with a concentrated force at the apex (76). The dimensions of the model were determined with the measuring microscope. These measured dimensions and the computation of stress are given in Appendix B. The results are plotted along with fringe order per unit thickness in Figure 3.8. The stress gradiation in the region of the fillet between the uniform neck of the model and the tapered portion was estimated by drawing a smooth curve between the stress level in the neck and the last point on the plot of the stress in the wedge where the isochromatic pattern indicated the theoretical solution justified. This portion of the graph and portions on succeeding plots derived from this smooth approximation are shown as dotted lines because of the decreased confidence in the evaluation of the stress in the fillet.

From the master diagrams, plots of fringe order per unit thickness and relative retardation per unit thickness versus stress

for constant wavelength were constructed. These are the calibration curves for CR-39 for the conditions of the test. Again, the original graphs were drawn to large scale on 24" x 36" paper. Diminished reproductions of the curves may be seen in Figure 3.14.

The curvature of the P-6 beam, which is apparent in the presented photographs, and the obvious shift of the zero order isochromatic plus variations in spacing of the isochromatics indicate that the stress in the beam cannot be calculated by ordinary beam theory and/or the strain-optic or stress-optic relationship is not linear over the range of stress and strain existing in the beam. Previous reports indicate that for the given stress range and other conditions of the test, the relative retardation-stress relationship for cured P-6 is linear (63). That is, the stress is lower than the linear limit and the material is behaving optically in a "momentarily linearly elastic" manner. If the stress-strain relationship could also be assumed to be momentarily linear, then exact or approximate elasticity solutions could be used for computing the stress in the curved beam.

In order to determine the radius of curvature of the deformed beam, the coordinates of three points on the curved centerline scratched on the model were determined from the negatives of the isochromatic photographs using the measuring microscope. Since the central portion of the beam was in uniform bending, the elastic curve should be a circular arc. The three known coordinates were sufficient to establish the location of the center of curvature and the radius of curvature. The value of the latter was 139 cm.

Knowing the radius of curvature, the bending moment, and the dimensions of the beam, the elastic bending stress could be calculated by a variety of methods. The Winkler-Bach Solution (73) for a curved beam is poorly conditioned for use with beams of shallow curvature, even though the basic assumption that cross sections of the beam remain plane is completely justified by the symmetry of the particular problem. The exact elasticity solution (14) is rather cumbersome. In view of the probable accuracy of the measurement of radius of curvature, it is doubtful that the increased labor is justified by the additional accuracy. An approximate solution which is developed by assuming a parabolic strain distribution and then applying least work principles is shown by Den Hartog (14) to provide accuracy superior to the Winkler-Bach solution for certain problems. Computational effort is minimum and the stress in a beam of large radius of curvature is easily calculated without the appearance of large errors due to minimal errors in the value of the curvature. The beam curvature measurements, sample calculations of stress by the approximate elastic solution, and an abbreviated table of values appears in Appendix C. As is apparent in the solution, the curved-beam correction terms amount to only about 1.5% of the total stress which would result from ordinary straight-beam theory for this problem. This is slightly more than the accepted maximum correction from the Winkler-Bach analysis of this beam. The computed stress is shown in Figure 3.12 along with retardation per unit thickness as a function of distance from the centroid of the cross section. The presented plot is a reduction of the 24" x 36" original. Even in the

reduced graph, the differences between the fringe-order plot and the stress plot are obvious. The shape is different and the point of zero stress does not correspond to the location of zero retardation. This suggests immediately a possible lack of clear correlation between retardation and stress and/or faulty calculation of the stress.

Proceeding further with the intent of exploring the stress-retardation relationship, a plot of these two quantities was constructed. This graph, presented in Figure 3.15, shows the values of fringe order per unit thickness at various distances from the beam axis as obtained from the graph of Figure 3.12 versus the stresses computed for corresponding locations on the cross section. The original plot was in the larger size, and the figure is a 1/3 reduction which includes only 3 of the 9 wavelengths. Points from the compression side of the beam were plotted separately from points on the tension side. Smooth curves could be drawn through the two sets of points separately. Both plots for each wavelength were curved over their whole length. The curvatures of the two were opposite and the two curves consistently crossed at about 2 kg/mm^2. The divergence of the curves above and below the crossing point was too great to be ignored. As suspected from qualitative examination of the isochromatic patterns, the experimental deviation could have been decreased only if the curvature correction had been greater. That is, the curves of m versus stress as calculated from an elasticity solution for the two halves of the beam would have been in close agreement had the radius of curvature been as small as about 15 cm, or one-tenth the measured value.

The inclusion of the small radial stress which is required for the exact solution would tend to bring the curves closer for part of their length, but would cause the remaining portions to drift further apart. This component of the stress involves only terms containing the natural logarithm of the ratio of two distances from the center of curvature to points on the beam. For the very shallow curvature of the curved beam, the radial stress must be very small. Also, this stress approaches zero in the outer fibers where the divergence of the measured data is greatest. Similarly, the imposition of tensile loading by the loading apparatus would have an effect opposite to that observed. The uniformity of the isochromatics in the central region of the beam indicated that this situation did not exist anyway. Nor can the variations be due to thickness variations. The slight variation in thickness (.002) of the cross section of the beam was almost entirely compensated by the lateral expansion during deformation. Measurement of the deformed cross section showed that the effects of thickness variation were less than 0.1%.

It must be concluded that the difference between the stress-optic curves derived from opposite sides of the P-6 beam is due to nonlinear relationships between stress, strain, and relative retardation. The symmetry of the problem implies that the central cross section remains plane, meaning that strain is proportional to distance from the centroidal axis within the limits of the small correction due to geometry change. Thus, the stress-strain-optic curves for the material and the conditions of the test must be quite complex. In particular, the properties of the material in tension must be different from those for compression. The subsequent redistribution of stress

and, separately, of birefringence invalidates any computation of stress based on elasticity theory, approximate or exact. This conclusion is supported by the dispersion of birefringence exhibited by this material. Verification of the result must await testing in simple tension and simple compression where the computation of stress is not ill-founded upon faulty assumptions. Such results are missing in the literature.

As previously mentioned, the test of the ring of P-6 was the first in this series of experiments to extend planewise photoelastic investigation into the near infrared. The conditions of the test were less carefully controlled, especially as regards load, than were the later tests which have already been discussed. The plots of fringe order per unit thickness and relative retardation per unit thickness as a function of position on a horizontal radius have been presented in Figures 3.10 and 3.13. These results indicate that, with proper calibration, photoelastic analysis of complex stress fields can be carried out with infrared radiation of up to 1μ wavelength. Since the stress-optical coefficients for the longer wavelengths and for the time of recording data in the test of the ring are lacking, it is not practicable to develop an experimental analysis of the stress distribution using infrared radiation for comparison with existing experimental solutions obtained with visible light. The similarity of the isochromatic distributions obtained with both visible and infrared radiation to each other and to those presented by Frocht (20) indicate qualitatively the correctness of the procedure.

Neither is it feasible to develop from the test of the ring stress-optic data which are within the limits of accuracy of the other tests of

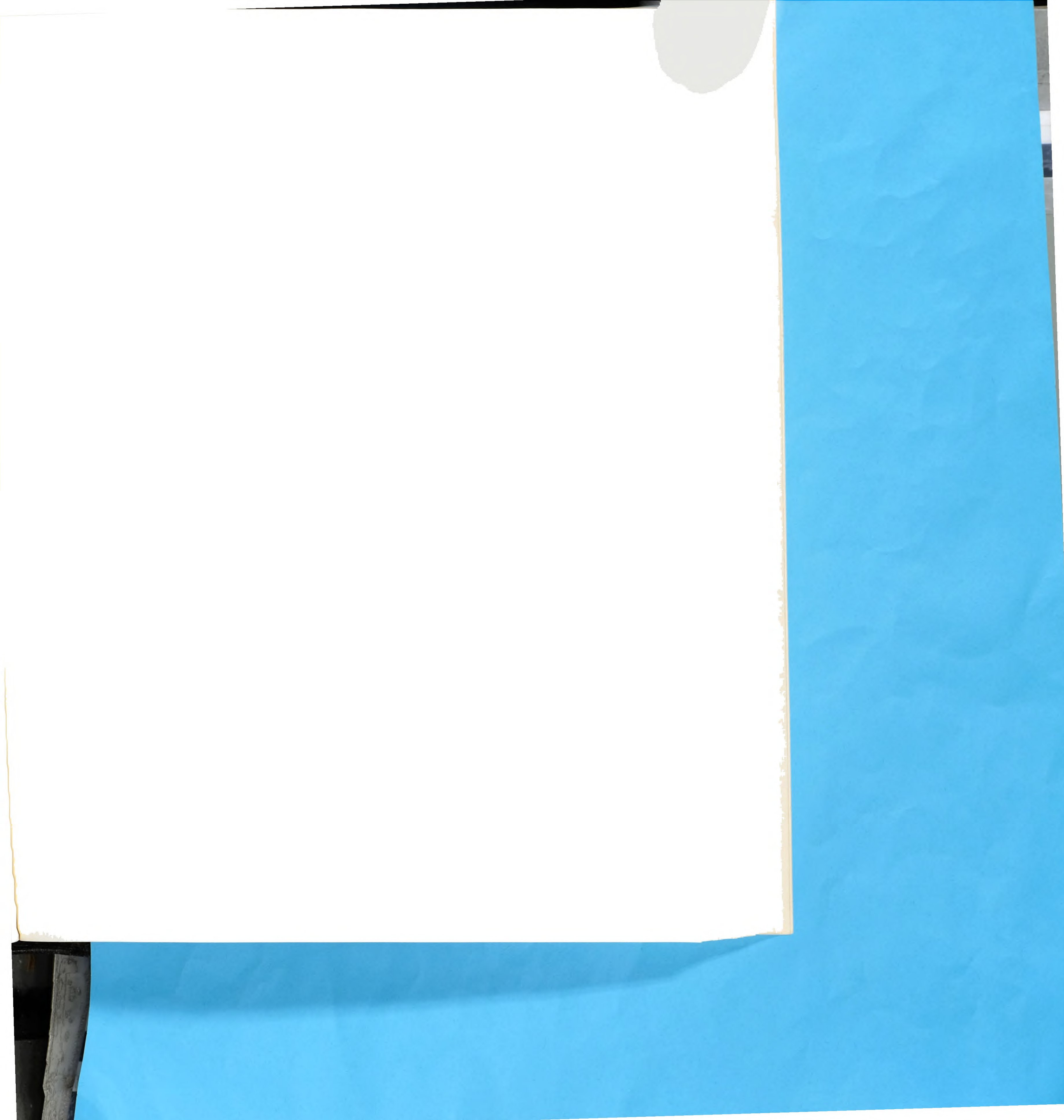

this investigation. Solutions giving the tangential stresses in a ring under diametral compression are well known (76), but there appears to be no convenient analytical solution for the radial stress. Both must be known in order to correlate their difference with the birefringence in the ring. The problem is further complicated by the probability that the stresses near the inner boundary of the ring were greater than the linear limit for the material and time of the test. The resulting redistribution of stress would seem to make difficult, if not impossible, the accurate analytical determination of stress.

In addition to providing graphical evidence of what may be expected from infrared photoelastic investigation of complicated stress fields, the test of the P-6 ring provided additional interesting information on the dispersion of birefringence of this material.

3.2.2. Calibration of Polycarbonate

The data from the test of the disc of polycarbonate are presented in Figure 3.16 as a plot of fringe order per centimeter thickness versus corrected stress for constant wavelengths and the particular load path used. The figure is a one-quarter reduction of the larger original. As will be recalled, this stress-optic information reported here is for the geometric center of the disc which was in diametral compression. The principal stresses at this point were calculated from the standard analytical solution (20, 76), and their algebraic difference taken as the independent variable. This calculation is given in Appendix D. The isochromatic order was the sum of the observed whole-order fringe plus the fractional order as

determined by the special goniometric compensation method developed for this investigation. The conversion from analyzer rotation and nearest whole fringe order observation to fractional orders of isochromatics is illustrated in the chart of Appendix E. Due to the presence of residual stress, residual birefringence, and the very small but undetermined initial load, the curves of fringe order versus theoretical stress did not pass through the origin. Rather, they converged at a point corresponding to zero fringe order at a stress difference of $-.016\ kg/mm^2$. The data was subsequently corrected by adding this value to the calculated difference between principal stresses, and later results were based on these corrected values. Smooth curves which best fitted the experimental data proved to be straight lines, as might be expected from the rather low level of applied stress and the short waiting periods.

Plots of relative retardation per unit thickness versus stress for the various wavelengths between 1μ and 2μ were constructed from the plots of fringe order per unit thickness. Since the $m-\sigma$ curves were linear, they could easily be transformed to retardation plots. The resulting graphs of retardation per unit thickness versus stress for constant wavelength were linear, of course, and their separation from one another indicates the dispersion of birefringence for polycarbonate in the given wavelength range. Reductions of typical of the original 24" x 36" plots of relative retardation versus stress may be seen in Figure 3.17.

The plot of the transmittance of this particular specimen of polycarbonate for the $0.85 - 2.5\mu$ region is given in Figure 3.18.

Additional measurements which were taken for the 2.5 - 7.5μ range of wavelengths indicated the material is not transparent there. This data indicated the range of wavelengths which could be used. Evidently such observation is limited to the visible through 1.6μ and 1.7 - 2.1μ regions, although photoelastic data from the narrow passband around 2.2μ might prove especially interesting. In addition to the practical function of indicating the range of usefulness of polycarbonate, the transmittance curve also gave preliminary indication of possible relationships between material structure and such phenomena as piezobirefringence and dispersion of birefringence.

3.2.3. Dispersion of Birefringence of P-6, CR-39, and Polycarbonate

The relationships between birefringence, wavelength or frequency of radiation, and stress which were derived from the photoelastic tests of CR-39, P-6 and polycarbonate resins made possible the investigation of the dependence of the double refraction of these materials upon the wavelength of light. This phenomenon, which is called dispersion of birefringence in analogy to a similar occurrence in optics, was described and defined previously in this report. Previous experimental results and analytical descriptions have also been discussed. In view of recent progress, these past methods of description seemed partially inadequate. New quantitative measures of photoelastic dispersion were developed, and these proposed methods of description are given following a discussion of the requirements which must be met. The results of the experiments are presented in accordance with the developed methods following a discussion of the relationships between the various photoelastic parameters and the quantities involved in dispersion measurements.

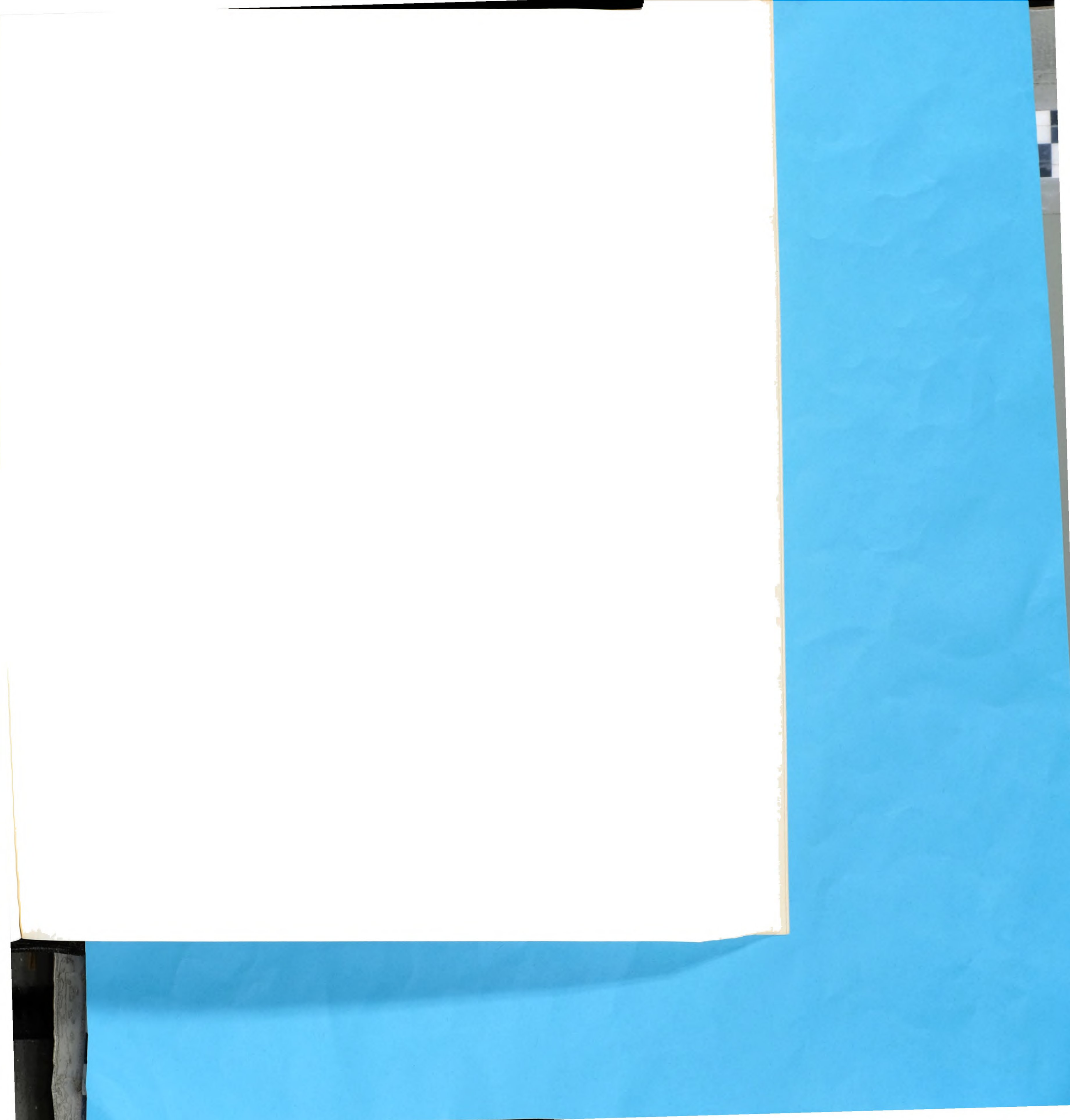

For a certain period of time after loading, birefringence is a linear function of the difference between the principal stresses or the principal strains. It seems that the dispersion of birefringence in this linear range of behavior should be independent of stress level. This has been demonstrated for Palatal P-6 and for CR-39 by J. T. Pindera (62, 63) on the basis of the formula (2.26) proposed by Mönch for the quantitative description of dispersion. But even in the linear range, dispersion of birefringence as expressed by formula (2.26) can be either dependent or independent of the time of loading.

The discrimination between linear and nonlinear behavior of model materials is one of the fundamental problems of mechanical model analysis (59). Related to this is the problem of models and materials which are suitable for investigations involving elasto-plastic deformations. Results previously cited show that the dispersion of CR-39 is constant with time, meaning it is uniform over the nonlinear and linear range of stress. The dispersion of cured P-6 has been found to be independent of stress level in the linear range, but it decreases with time. A rather particular relationship between dispersion and stress level exists for uncured P-6.

Considering the problem from the point of view of the structure of material and related optical properties, it seems that the lack of a clearly-defined relationship between the degree of plastic deformation and the dispersion of birefringence, such as that discovered by Mönch for celluloid, may result from an inadequate formulation of the

dispersion of birefringence. According to the equation of Mönch, the dispersion of birefringence is expressed as the relative change in birefringence in an arbitrary spectral range of 0.153 microns or 0.219 microns. There are two basic limitations of this measure. First, the spectral range is very narrow. Secondly, the spectral range is chosen quite arbitrarily, and it bears no relationship to the physical and optical phenomena occurring in the material in the linear and nonlinear range.

The formulas used in geometrical optics for the description of dispersion of optical glasses do not satisfy the special aspects of the dispersion of birefringence. Also, these definitions are referred to arbitrary spectral ranges which are bounded by certain Fraunhofer lines.

Coker and Filon described the dispersion of birefringence by a nonlinear function of wavelength which was similar to Hartmann's dispersion formula. They proved that their formula adequately described the optical properties of many glasses. However, as early as 1907, L. N. G. Filon found that in the visible spectral range some glasses exhibit irregularities which are similar to anomalous dispersion. Formula (2.25) appears to be quite satisfactory for glasses exhibiting only negligible creep and behaving linearly in practically the whole range of stress and strain at room temperature. The behavior of the plastics commonly used for general mechanical models, photoelastic models, and photoelastic coatings is much more complicated. For example, Pindera (62) shows that in the process of creep the stress-optical and strain-optical coefficients may approach

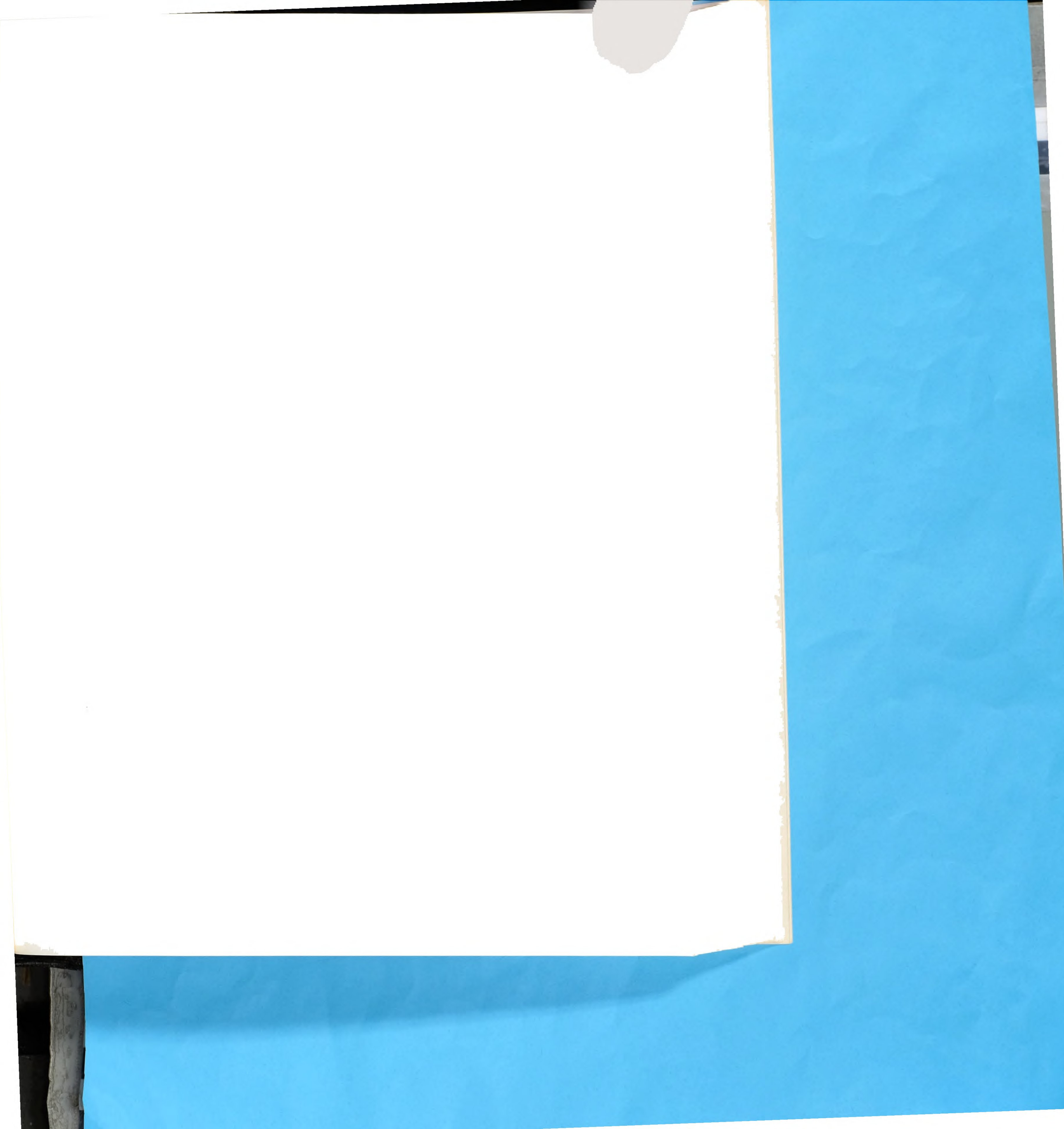

zero, while the dispersion of birefringence measured according to formula (2.26) remains essentially constant. The extensive data presented by T. D. Maksutova (46) on the relations between retardation, stress-optical coefficient, stress, strain, temperature, and material composition illustrate the very complicated nature of the involved phenomena. The extension of the photoelastic method into the longwave region makes it necessary to choose convenient, uniform, and adequate methods for the description of properties of photoelastic materials in linear and nonlinear stress ranges and over spectral ranges of 0.4 - 1.2 microns, 0.4 - 2.5 microns, and finally of 0.4 - 7 microns.

One important aspect of the present problem is to take into account recent progress in the theory of dispersion and spectroscopy of high polymers along with the previously established relations between the structure of polymers and their optical properties. This already has been expressed by J. T. Pindera (62) and by R. Van Geen (77). The new ideas and results presented by the last author go well beyond classical methods of photoelasticity and are outside the scope of the present work.

The proven existence of a kind of anomalous dispersion of birefringence, even in the visible spectral range, indicates strongly that not only the extrapolation but also the interpolation of dispersion curves may lead to erroneous results.

On the basis of the preceding short analysis, some suggestions for the adequate and convenient description of the dispersion of birefringence can be formulated.

The dispersion should be presented as a continuous function of frequency or wavelength of radiation in a possible wide spectral range. It should be referred to unit thickness and to unit stress or unit strain for a chosen time point on a creep or relaxation curve. It seems that the unit birefringence:

$$\Delta n^{o} = n_1 - n_2 \text{ , for unit stress,}$$

$$\Delta \sigma = \sigma_1 - \sigma_2 = 1 \text{ kg/mm}^2$$

may often be chosen as the basic quantity more conveniently than the coefficients C_σ and C_ϵ which would then be derived quantities. The relations for the dispersion of birefringence or the derived expressions should facilitate the distinguishing of linear and nonlinear behavior. Here, the term "linear range" may be taken to mean the region wherein the deviation from nonlinearity is less than 1% (64). Of course, it is important to present the dispersion in such a way that it would be easy to calculate the value of C_σ or C_ϵ (respectively, S_σ or S_ϵ) in a given spectral band.

To satisfy the above requirements, the following graphical descriptions were chosen:

1. Relative retardation versus wavelength and/or relative retardation versus radiation frequency for unit principal stress difference and unit thickness:

$$R^{o} = R^{o}(\lambda) \qquad \text{and/or}$$

$$R^{o} = R^{o}(\nu)$$

$$\text{for} \quad \sigma_o = 1 \text{ kg/mm}^2 \text{ and } d_o = 1 \text{ cm.}$$

These plots may be called "Unit Retardation Curves". In a linear range, these quantities may be expected to be independent of stress level but usually dependent on time.

2. Ratio of unit retardation for any wavelength to unit retardation for a standard wavelength versus wavelength or, respectively, frequency:

$$r = \frac{R^{o}(\lambda)}{R^{o}(\lambda_{o})} = r(\lambda)$$

$$r = \frac{R^{o}(\nu)}{R^{o}(\nu_{o})} = r(\nu)$$

where λ_{o} = 546.1 nm (green mercury line) and for a given time after loading with a constant force (t = constant). These curves will be termed "Normalized Retardation Curves." It is apparent that in the linear range this ratio should be independent of stress level but may depend on time.

3. Rate of change of normalized retardation versus radiation wavelength or frequency:

$$D_{\lambda}^{o} = \frac{dr}{d\lambda} = D^{o}(\lambda)$$

$$D_{\nu}^{o} = \frac{dr}{d\nu} = D^{o}(\nu)$$

The name applied to these quantities will be "Normalized Dispersion of Birefringence." Again, this quantity should not depend on stress magnitude in a linear range but may depend on time. This definition is analogous to a previously mentioned definition of optical dispersion.

4. Normalized dispersion of birefringence versus time during creep and relaxation for given λ or ν and several given stress levels. It is expected that these curves would indicate the effects of nonlinear behavior on the dispersion.

The important relationships which could be derived from the preceding list of basic curves would include:

1. Stress-optical coefficient and strain-optical coefficient versus radiation frequency or wavelength at constant time:

$$C_\sigma = C_\sigma(\nu) \quad \text{or} \quad C_\sigma = C_\sigma(\lambda)$$

$$C_\epsilon = C_\epsilon(\nu) \quad \text{or} \quad C_\epsilon = C_\epsilon(\lambda)$$

at t = constant.

2. Stress-optical coefficient and strain-optical coefficient versus time in creep and relaxation for chosen wavelengths:

$$C_\sigma = C_\sigma(t)$$

$$C_\epsilon = C_\epsilon(t)$$

for λ = constant.

According to the ideas expressed in papers (59) and (64), the curves discussed above achieve their full meaning if they are supplemented by curves which describe the range of linear relationship between stress, strain and birefringence:

$$\sigma_{\ell\ell} = \sigma_{\ell\ell}(t)$$

$$\epsilon_{\ell\ell} = \epsilon_{\ell\ell}(t)$$

$$m_{\ell\ell} = m_{\ell\ell}(t)$$

Several useful and interesting relationships between the involved quantities may be derived. Some of these are listed as follows:

Unit Retardation:

$$R^{o} = R \frac{\sigma_o}{\sigma_1 - \sigma_2} \frac{d_o}{d}$$

$$= \frac{d}{n_o}(n_1 - n_2) \frac{\sigma_o}{\sigma_1 - \sigma_2} \frac{d_o}{d}$$

$$= C_\sigma \, d_o \, \sigma_o = R^{o}(\lambda)$$

for t = constant

$$\sigma_o = 1 \text{ kg/mm}^2$$

$$d_o = 1 \text{ cm}$$

Normalized Retardation:

$$r = \frac{R^{o}(\lambda)}{R^{o}(\lambda_o)} = \frac{R(\lambda)}{R(\lambda_o)}$$

$$= \frac{(n_1 - n_2)_\lambda}{(n_1 - n_2)_{\lambda_o}} = \frac{\Delta n_\lambda}{\Delta n_{\lambda_o}} = \frac{C_\sigma(\lambda)}{C_\sigma(\lambda_o)} = r(\lambda)$$

for t = constant

In a linear range:

$$r(\lambda) = \frac{C_\sigma(\lambda)}{C_\sigma(\lambda_o)}$$

$$= \frac{C_\epsilon(\lambda)}{C_\epsilon(\lambda_o)}$$

for t = constant

Hence,

$$C_\sigma(\lambda) = C_\sigma(\lambda_o)\, r(\lambda)$$

Normalized Dispersion of Birefringence:

$$D = \frac{dr}{d\lambda} = \frac{1}{R(\lambda_o)} \frac{dR(\lambda)}{d\lambda}$$

$$= \frac{1}{(n_1 - n_2)_{\lambda_o}} \frac{d(n_1 - n_2)}{d\lambda}$$

$$= \frac{1}{\Delta n_{\lambda_o}} \frac{d(\Delta n)}{d\lambda} = D(\lambda)$$

for t = constant

In a linear range; for t = constant

$$D(\lambda) = \frac{1}{C_\sigma (\lambda_o)} \frac{d C_\sigma}{d\lambda}$$

$$= \frac{1}{C_\epsilon(\lambda_o)} \frac{d C_\epsilon}{d\lambda}$$

Mönch's Formula for dispersion of Birefringence:

$$D_{1,2} = \frac{R_{\lambda_1} - R_{\lambda_2}}{R_{\lambda_1}}$$

$$= \frac{m_1\lambda_1 - m_2\lambda_2}{m_1\lambda_1}$$

$$= 1 - (\frac{\lambda_2}{\lambda_1})(\frac{m_2}{m_1})$$

$$= 1 - \frac{(\Delta n)_2}{(\Delta n)_1}$$

$$= 1 - \frac{(C_\sigma)_{\lambda_2}}{(C_\sigma)_{\lambda_1}}$$

for t = constant.

Also:

$$D_{1,2} = 1 - \frac{r_2}{r_1}$$

Plots of normalized retardation versus wavelength and frequency of radiation were developed according to the above ideas from the graphs of fringe order and relative retardation versus either location on the cross section or stress for each of the three materials whose properties were investigated quantitatively. For CR-39 and P-6, the use of visible light in addition to infrared radiation allowed the taking of the mercury green spectral line at $\lambda = 546$ nm as the basis for the computation of normalized retardation. The relative retardation at each wavelength was divided by the retardation for $\lambda = 546$ nm for each of several different stress levels.

For CR-39, normalized retardation was computed for each of the 9 wavelengths and at 18 different stress magnitudes between 0 and 2.1 kg/mm^2. The normalized retardation for this material and for the conditions of the test seemed independent of stress level. Since no ordering of the 18 values of normalized retardation at each wavelength was apparent, the data was amenable to statistical treatment. The mean and RMS deviation (standard deviation) were computed for each group of 18 values. A sample of the data and the statistical calculations are given in Appendix F. The standard deviation, which represents a confidence limit of about 68%, and the extreme range of values obtained for the 18 stress levels up to 2.1 kg/mm^2 are shown in the plots of normalized retardation for CR-39, versus radiation wavelength, wave number and frequency. These are given in Figure 3.19 as reductions of the originals.

The dependence of the normalized retardation of Palatal P-6 upon radiation frequency, wave number and wavelength is indicated in the plots of Figure 3.20. The data for this material evidenced a peculiar relationship between the optical behavior, radiation wavelength, and sign and magnitude of stress. Because of the resultant ordering of the values of normalized retardation with stress, statistical treatment of the data was not appropriate. The values reported here are based on the average over the outer thirds of the beam tested. The deviations in this portion were generally not random, but the extremes of the values as indicated on the plots indicate that the averages are meaningful measures of the dispersion of birefringence over the corresponding stress ranges. The dependence of the normalized retardation upon the stress is readily apparent in the figure, and an average over the whole cross section of the beam would not be valid. The values obtained for the normalized retardation in the inner third of the beam were generally smaller than the values shown for the outer thirds.

Further testing would be required in order to establish clearly the relationship between stress and normalized retardation in P-6. As an indicator of what may be expected from such an investigation, values of normalized retardation extracted from the less complete study of the ring in diametral compression were compared with the data obtained from the beam. Shown on one of the graphs of Figure 3.20 are values of normalized retardation at locations on the cross section of the ring where the fringe order per unit thickness for $\lambda = 546$ nm was about equal to the fringe order per unit thickness

at the centers of the outer thirds of the beam and for the same wavelength. Presumably, the differences are due to the different nature of the stress field, the different conditions of the test, and also the multiplication of error inherent in this difficult measurement of the small differences between large values of relative retardation.

Because of the peculiar nature of the fluctuation of normalized retardation for both P-6 and CR-39 in the wavelength region between about 550 nm and 700 nm, these portions of the plots are shown as dotted lines. As will be discussed more fully later, these undulations may be due to anomalous dispersion, in which case the irregularity between the plotted points may be more drastic than shown.

The normalized retardation of polycarbonate as derived from the results of the calibration test in the spectral range between 1μ and 2μ is shown in Figure 3.21 as a function of wavelength. The values shown were derived from the plots of fringe order versus stress. Since these plots were linear for the limited stress range used, the normalized retardation was independent of stress. No measurements were taken with visible light, so the relative retardation at $\lambda_o = 1.145$ was used as the norm in constructing these plots. The scatter in experimental data at this wavelength was less than or equal to the deviations at the other wavelengths. The size of the experimental points shown in the figure is indicative of the extreme deviation in normalized retardation as calculated from the maximum separation of the experimental data points from the linear plots of fringe order versus stress at each wavelength. This places a bound on the extreme possible error in the determination of

the normalized retardation. A more realistic evaluation of the possible error would be based on the root mean square of the deviation (standard deviation) of the experimental data from the smoothed straight line curve.

The irregularities in the graphs of normalized retardation are similar to those of P-6 and CR-39, and also those presented by Filon (10) for glass. However, because of the decreased accuracy of this test and the lack of subsequent verification by further testing, the curve is shown dotted. Further improvement in testing would clearly define the exact nature of the behavior of polycarbonate. The presented data is perhaps indicative of what may be expected, and it should be considered only as a first approximation to the normalized retardation of this material.

The normalized dispersion of birefringence of P-6 and CR-39 was derived from tracings of the large original plots of normalized retardation of these two materials. This measure of dispersion is essentially the slope of the normalized retardation versus wavelength or frequency graphs. The slope was measured by using the well-known reflection technique to construct normals to the curves at several points along its length. More points were chosen in regions where the slope varied rapidly, and several trials were made at points in particularly troublesome portions of the curves, reversing the mirror for each trial. Inversion of the slope of the normal at each point yielded the slope of the normalized retardation curve at that point. These data appear plotted in Figure 3.22 and 3.23. The portions of the curves where the values of the normalized dispersion may be questioned are represented by dotted lines.

3.2.4. Birefringence of Semiconductors

The data resulting from the measurements of stress-birefringence in silicon were treated in the same manner as were the data for polycarbonate. Plots of the fringe order versus stress difference for wavelengths of 1.145, 1.348, 1.560, and 1.90 microns are presented in Figure 3.24. The original data was corrected so that the straight line plots might pass through the origin. The stress optical coefficients were computed from the slopes of the stress-optic curves. At $\lambda = 1.145\mu$, C_σ was found to be 12.5×10^{-4} kg^{-1}mm^2; for $\lambda = 1.348\mu$, $C_\sigma = 14.8 \times 10^{-4}$ kg^{-1} mm^2; for $\lambda = 1.560\mu$, $C_\sigma = 17.1 \times 10^{-4}$ kg^{-1}mm^2 and for $\lambda = 1.90\mu$, $C_\sigma = 20.8 \times 10^{-4}$ kg^{-1}mm^2.

The small thickness of the silicon disc limited the range of loads that could be applied without buckling and subsequent fracture of this brittle material. Since isochromatic order is proportional to load and to thickness, the maximum order of isochromatic observable in this test was about 0.18 fringes. Recalling the estimate of error in the goniometric compensation technique it is apparent that experimental deviations on the order of 10% might be expected in this particular study. The increased possibility of error shows clearly in the scatter of the experimental points in the graph. For this and other reasons, the curves of Figure 3.24 should be thought of only as the first approximation to the stress-optic characteristic of silicon.

Transmission of near infrared radiation by the amorphous selenium model was high, although partial crystallization in the slower-cooled central portion caused the light to be partially scattered. With no load on the model, photoelastic observation indicated two things of

interest. First, the model appeared to act as a retardation plate. With crossed polaroids, the model appeared light, and it nearly extinguished the infrared light with the light field arrangement of the polariscope. This retardation was apparent with both linear and circular polarization. Whether this was caused by the anisotropy and stresses from pouring and cooling, or it was a rotation of the light vector due to structure (optical activity), as is produced by aqueous solutions of sugar was not immediately apparent. Secondly, a birefringent pattern was noticed near the edges of the model. This was presumably due to residual stresses created by the rapid cooling of the portion of the model in contact with the aluminum mold. The birefringence due to cooling stresses has been observed previously by other investigators already mentioned.

No double refraction under externally applied loads was apparent in the selenium model. This was unexpected in view of earlier findings.

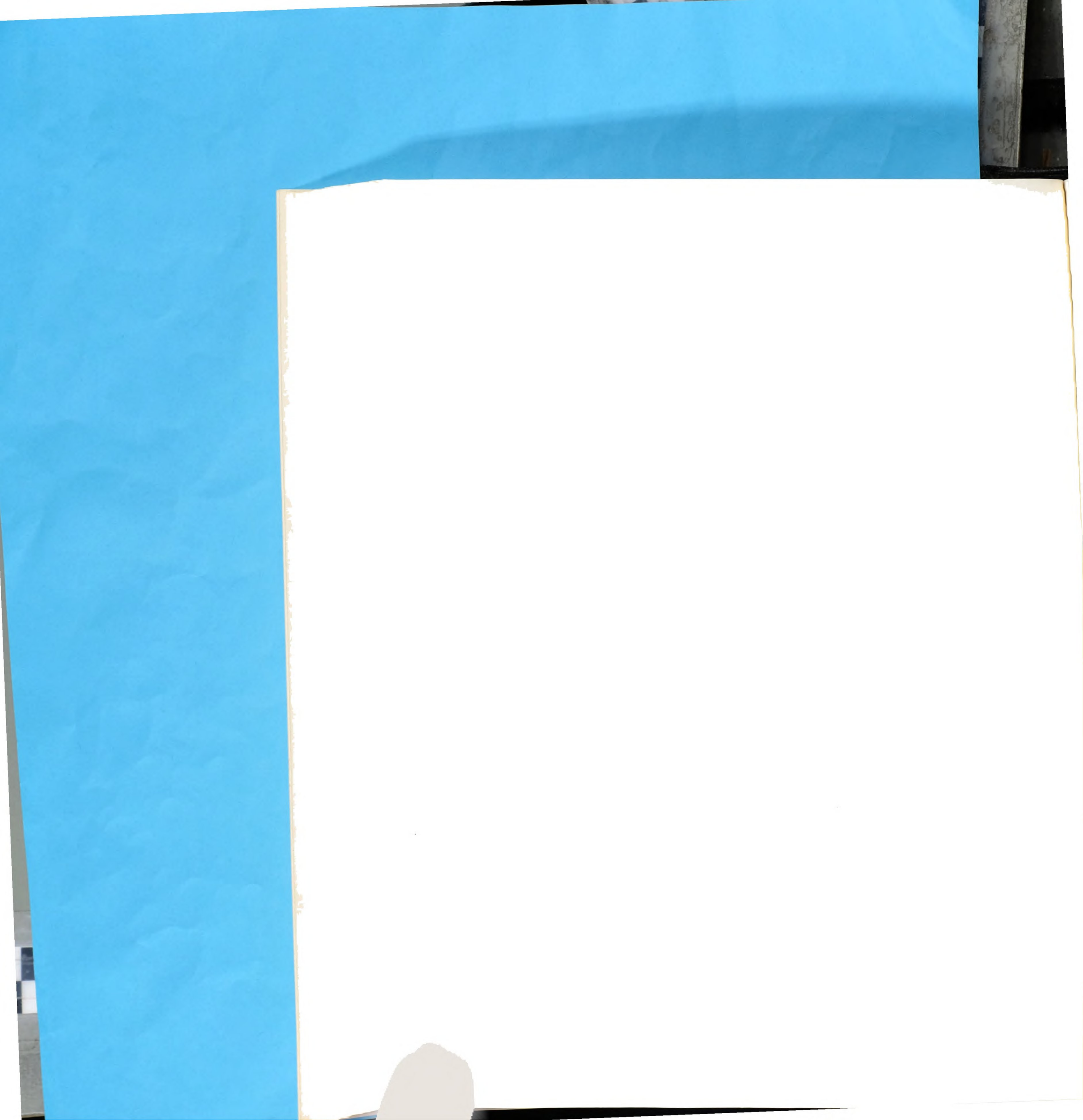

4. Discussion and Conclusion

The methods and results of this investigation, as presented in the previous chapters, may be examined for their contribution and deficiency in providing insight into the phenomenon of double refraction and its measurement. The original objectives of the experimental program were met, and some additional questions were answered. But more questions were created. The new information provides additional grounds for speculation about the nature and behavior of materials. The new questions can be answered only by continued experimental investigation.

4.1. Summary of Techniques and Apparatus

The birefringence of various materials was observed and measured using monochromatic radiation at several different wavelengths in the visible and near infrared spectral ranges. The fundamental character of the measurement and the interpretation of data in this extended range of wavelengths were identical to those which form the basis of all ordinary photoelastic investigations. Assuming that visible light, infrared radiation and radio waves, regardless of their true nature, may be considered to consist of electromagnetic waves whose behavior are described by Maxwell's equations, then the phenomena of double refraction and its measurement through the use of polarized light are not limited by wavelength.

While the governing photoelastic equations and the functioning of the optical system required for the observation and measurement of

birefringence are independent of the spectral range in which the work is being performed, the techniques and apparatus employed must necessarily change. The greatest modification is to the methods of sensing and recording the photoelastic pattern. Direct visual observation is limited to the relatively narrow range of wavelengths between 0.4 and 0.7 microns. This is also the spectral range in which most photoelastic analyses are performed. The improvement of photographic methods facilitated the direct planewise recording of results up to about 1.2 microns maximum wavelength. A device which converted an infrared image to a visible one was used for observations up to 1.3μ wavelength. The visible image in this converter could also be photographed, thus extending planewise recording up to about 1.3 microns, but the quality of results obtained was not as good as those derived from other methods. For the wavelength region beyond about 1.2 microns and up to 1.9 microns, point sensing methods were employed. The apparatus consisted of a very small infrared-sensitive photoconductive element which was used in conjunction with a circuit which sensed and measured the voltage drop across the light-variable resistor. The sensor, when placed in the plane of an image of a photoelastic model, indicated the variations in the light intensity transmitted by the area of the model corresponding to the point in the image at which the sensor was located. Scanning the image pointwise would furnish a complete map of the birefringent pattern in the model. This general method of pointwise detection should not be limited to any particular portion of the electromagnetic spectrum. The output of the sensing circuit could be calibrated directly

in terms of intensity and eventually of birefringence through use of the general photoelastic equations. The approach used here was more appropriate to a non-ideal system in which noise was present in that indications only of local minimum or maximum light intensity were required. This was sufficient for accurate measurement of fractional fringe orders by methods of goniometric compensation (analyzer rotation). In fact, the technique of goniometric compensation was improved so that the only requirement on the light sensing apparatus was that it dependably indicated the attainment of arbitrary pre-established levels of intensity. Examination of the equations which govern the analyzer rotation method showed that the transmitted intensity is an even function of the angular position of the analyzer when measured from the angle at which the intensity is minimum. The average of two angles on either side of the minimum where the transmitted intensities were equal provided a measurement of the angle at which the light was minimum. This method of averaging the symmetrical points was justifiably found to be more free from the errors due to system noise and operator error than the ordinary method of locating directly the angle of minimum intensity.

Three optical systems were developed. One was suited for the visible region, another for planewise investigation in the infrared, and another to be used with the pointwise method in the farther infrared. Monochromatic radiation was obtained by means of spectral lamps and interference filtering of white light. Ordinary polaroid sheet was used in the visible region, and type HR infrared polarizing material served byond 0.7μ wavelength. Circular polarization in the visible was

accomplished by the usual methods. Half-wave retardation plates served in the infrared up to about 1.6μ. Two of these plates were stacked in order to obtain more accurate circular polarization for the range of wavelength between 1.6μ and 2μ. The latter figure is nearly the practical transmission limit of this material. The errors in measurement of isochromatic order which could result from the errors in the quarter wave plates used for the given spectral range were shown to amount to about $\frac{1}{m}$%, where m is the fringe order.

The techniques and equipment developed served more than adequately the requirements of this early limited investigation into longwave photoelasticity. Refinement and sophistication are possible and necessary for continued experimentation in the spectral range of 0.4 to 2 microns wavelength and for the extension of the research up to the radio wavelengths. The results of the investigation indicate that this extension of photoelastic analysis further into the longwave region is physically possible and may be useful and enlightening in basic studies of rheology and material structure as well as for the solution of special stress analysis problems. The methods used here provide a basis from which to work, and several of the possibilities for further development of the apparatus have been described. The major problems to be met in the extension to longer wavelengths appear to be the production of monochromatic radiation of sufficient intensity and the associated problem of developing a sensing system of small enough area and adequate signal-to-noise ratio. The extended-range closed circuit television system and the longwave scanning radiometer

provide additional possibilities for planewise measurement in the far infrared spectral range.

4.2. Material Behavior

The test of Columbia Resin CR-39, which was mainly directed towards the measurement of dispersion of birefringence, provided representative values of stress-optical coefficients for this material under the particular conditions of the test. For stresses within the linear limit stress of about 1 kg/mm^2, for a temperature of 24^o C, at 66 hours after loading and for λ_o = 546 nm, the stress-optical coefficient, $C_\sigma(\lambda_o)$ was found to be 3.7×10^{-4} $kg^{-1}mm^2$. The corresponding material stress-fringe coefficient for a thickness of 1 cm, $S_\sigma(\lambda_o)$, was 0.15 kg/mm^2. The unit retardation for this material under the given conditions and for σ_o = 1 kg/mm^2 and 1 cm thickness was $R^o(\lambda_o)$ = 3.7 microns.

The stress-optical coefficients for the conditions of the test but for wavelengths other than λ_o = 546 nm may be computed from the presented dispersion data for CR-39. Figure 3.19 indicates that serious error may result from the assumption that the stress-optical coefficients are constant even within the limited visible spectrum. For the specimen tested, C_σ changed by about 5% between 405 nm and 650 nm wavelength, independent of stress level. This change would have to be taken into account in any test where light of more than one wavelength was used. Since the dispersion did not depend on stress, it is reasonable to expect that it would not depend on the other conditions of a test, at least within the linear range. If this

presumption can be justified experimentally, then the dispersion data may be used in conjunction with stress-optical coefficients more accurate than those presented here. Emphasis should be given the fact that accuracy of this measurement of dispersion of birefringence is not directly related to the accuracy of the determination of stress-optic behavior. This was due primarily to the errors in locating points on the specimen with respect to an absolute reference, which in turn resulted from the distortions of the inferior lens system and the necessity of observing the model in segments. The dispersion measurement required no such absolute location of points as long as the correspondence between points on different photographs of the same segment was established. This was easily and accurately accomplished regardless of the distortion in the images.

The results of the test of cured Palatal P-6 were not nearly as simple or well defined as were the results for CR-39. The data for this material evidenced a peculiar relationship between optical coefficients, wavelength of radiation, and sign and magnitude of stress. In the preceding chapter it was reasoned from the results summarized in Figures 3.10, 3.12 and 3.15 that the stress-optical coefficients and/or strain must depend on the sign of stress. This prohibits computation of the stress distribution in the beam or the ring by ordinary elasticity methods or correlation between calculated stress and birefringence. Hence, the optical coefficients could not be derived from the results of the tests. The normalized retardation and dispersion as functions of wavelength and frequency as reported here were based on average values taken over the outer thirds of the

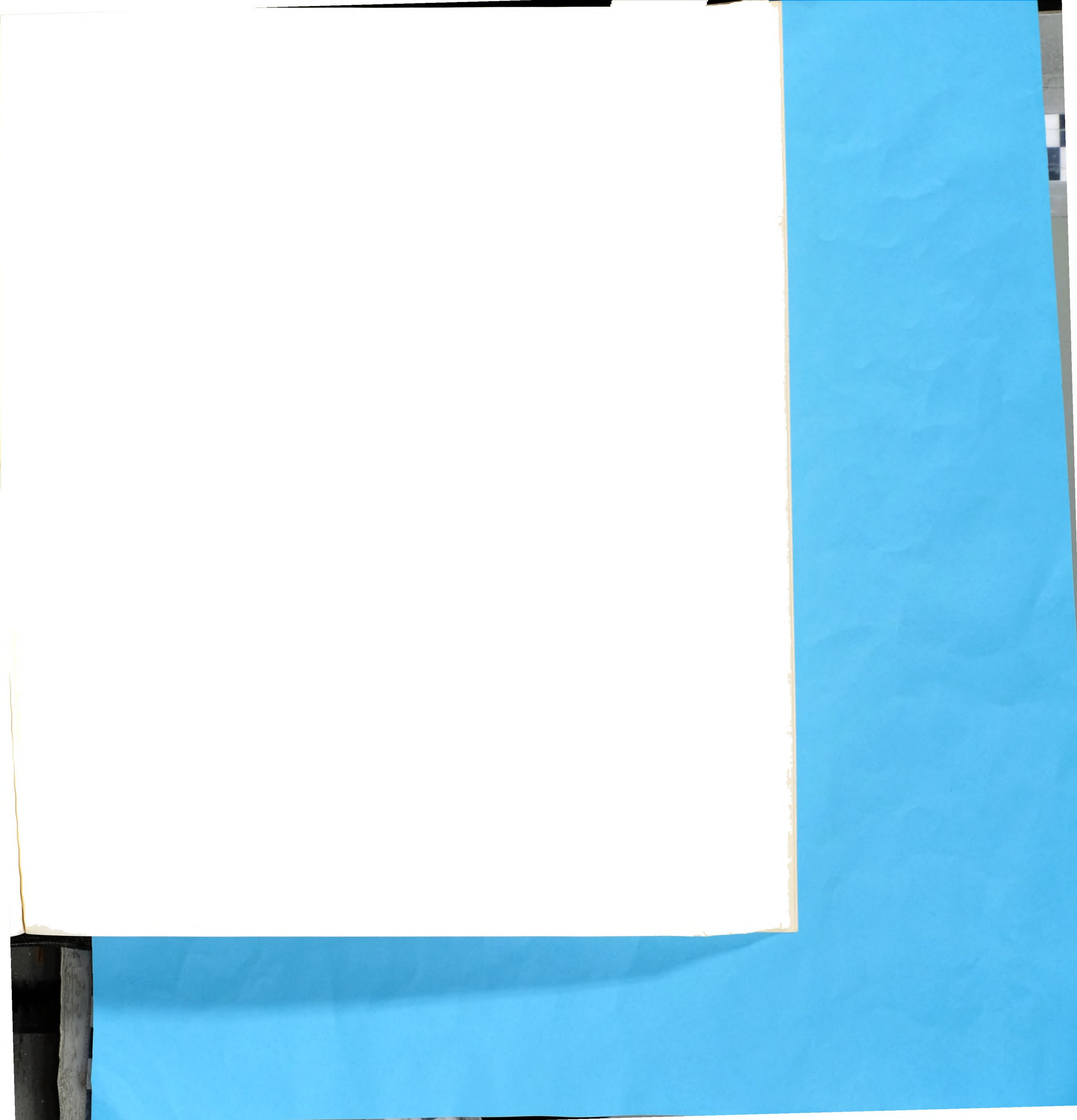

beam tested. The deviations were generally not random, but the ranges of values shown on the curves of Figures 3.20 and 3.23 indicate that the average is at least a meaningful measure of the dispersion of birefringence of P-6. The dependence of the normalized retardation on stress is readily apparent, and it would not be valid to take an average over the entire cross section of the beam. This particular behavior was verified by the initial, more limited test of the ring. Agreement was good considering the much different nature of the stress fields in the two specimens and the dependence of dispersion upon the stress field.

This apparent dependence of the optical properties of cured P-6 upon the character of the stress field appears partially contrary to the results reported by Pindera (62, 63) for this material. However, this author has observed a similar relationship between optical coefficients and stress for the uncured Palatal P-6. It seems most probable that the curing cycle used did not provide the optimum level of polymerization of this particular mixture of resin and catalyst. Rather, the polymerization was something between that of the uncured state and the nominal for cured resin. This opinion is strengthened by the fact that the value of the dispersion calculated by Mönch's formula (2.26) from the given data for both tension and compression agree well with each other (within 0.3%) and are both within 0.2% of the value given by Pindera for cured P-6 at the same stress and time. Further investigation under carefully controlled conditions are required in order to demonstrate more clearly the effects of resin mixture and curing upon the photoelastic properties. Perhaps this material will be

all the more interesting and useful because of its peculiar properties. The possibility of utilizing the variation in dispersion as a measure of sign and magnitude of elastic or plastic stress or strain, or only as an indicator of the presence of plastic deformation, is immediately apparent.

The data presented in Figures 3.20 and 3.23 show that the stress-optical coefficient of P-6, regardless of its actual value, changes by approximately 11% in the limited visible range. The use of a coefficient which is constant over any part of the spectrum would probably lead to quite significant error in experiments involving radiation of more than one wavelength.

The test of the disc of polycarbonate yielded values of the material optical coefficients at 8 different wavelengths in the spectral range from 1.145μ to 1.90μ. Since the stress-optic curves were linear, the material behaved as one momentarily linearly elastic, and the time after the placing an increment of load may be taken as the time of the test. The lack of data in the visible range prohibits the use of mercury green wavelength as the basis for calculating unit retardation and the reference wavelength for expression of the coefficients. The shortest wavelength of 1.145μ was chosen as the reference wavelength because of the minimal scatter in experimental data at this wavelength. Thus, for λ_o = 1.145 micron, time = 1.25 hrs., temperature = 20° C, the stress optical coefficient, $C_\sigma(\lambda_o)$, attained a value of 7.49×10^{-4} $kg^{-1}mm^2$; the material stress-fringe coefficient, $S_\sigma(\lambda_o)$, was 0.153 kg/mm^2 for 1 cm thickness; and the unit retardation $R^o(\lambda_o)$ for σ_o = 1 kg/mm^2 and d_o = 1 cm was 7.49 microns. These

results may be instructively compared to those obtained by Ito (33), although this author indicates neither the wavelength of light used nor the other conditions of the calibration test. He reports a stress-fringe coefficient of 1.0 fringe kg^{-1} mm. Assuming that the calibration experiment was conducted with visible light with λ = 546 nm, then the stress-optical coefficient would be $5.46 \times 10^{-4} kg^{-1} mm^2$. This value, while based on supposition of the actual conditions of test, is of the same order as the result of the present investigation. The difference is probably due to the unknown testing procedure and conditions, especially the wavelength of light used, and possibly to the presence of dispersion of birefringence. In this case the variation of the stress-optical coefficient with wavelength would be opposite to the decrease normally found. The dispersion would be of the anomalous type.

The average values of stress-optic coefficient, material stress-fringe coefficient, unit retardation, and normalized retardation of polycarbonate for the eight wavelengths are summarized in Table 4.1. The normalized retardation for polycarbonate has been presented in Figure 3.21. Since the stress-optic relationships for each wavelength were linear within the stress range employed, the coefficients and measures of the dispersion are independent of stress. The measured extreme variation of the stress-optical coefficients with wavelength or frequency in the spectral range is seen to be about 4%. This variation is only about twice the limit of accuracy of the particular test. Hence, the values of normalized retardation reported should be considered only the first approximation to the actual value. The dispersion data for P-6 and CR-39 suggest that this effect is decreased in the range

Table 4.1. Stress optical data in infrared for polycarbonate resin

Thickness = d_o = 1 cm = 1 kg/mm^2

Time = 1.25 hr.

Temperature = 20^o C

λ micron	R^o micron	r	C_σ 10^{-4} kg^{-1} mm^2	S_σ kg mm^{-2}
1.145	7.485	1.000	7.49	.153
1.244	7.487	1.000	7.49	.166
1.348	7.539	1.000	7.54	.179
1.446	7.358	0.983	7.36	.197
1.550	7.483	1.000	7.48	.207
1.560	7.384	0.987	7.38	.211
1.650	7.628	1.019	7.65	.216
1.90	7.318	0.978	7.32	.260

beyond 0.8μ. If polycarbonate behaves in a similar manner, its dispersion may be much greater in the visible range than in the band between 1 and 2 microns.

As was stated earlier, polycarbonate resin is very tough and impact resistant and can withstand extensive plastic deformation. If the complete stress-strain-optic-time law for this material can be found, it should serve for the photoelastic analysis of problems involving both elastic and inelastic deformations. The first and simplest problem of this type is one directed towards the detection of initiation of inelastic deformation and the indication of the elastic-plastic boundary. More complex analyses dealing with plastic flow would rest upon the material behavior and the extension of the similarity principles. Investigation along these lines was not within the limitations of this work, but one observation is worthy of mention. In the region of high plastic deformation under the loading points, the polycarbonate retained its optical transparency. This is different from the behavior of many ductile polymers which whiten and become opaque or translucent when severely deformed.

Of some interest is the consistent irregularity of the experimental normalized retardation curves of P-6, CR-39, and polycarbonate. The order of recording data during the various experiments indicates that these irregularities cannot have resulted from time effects. Although they may be partly caused by other experimental error, particularly in the case of polycarbonate, their appearance must be at least partially due to anomalous dispersion of birefringence. A similar behavior has been observed during extensive tests of glass

3453 by L. N. G. Filon (10). It should be pointed out that the presented plots of normalized retardation do not show other possible irregularities which may be important. The very presence of the fluctuations emphasizes the fact that the interpolation as well as the extrapolation of optical data can lead to serious errors unless the procedure is justified experimentally.

The source of anomalous dispersion and the reasons for its appearance are open to speculation. Two related possibilities present themselves. First, birefringence seems to result from variations in basic physical structure such as the changes in orientation or length of certain molecular or atomic groupings such as chains, side chains, or crystals (56). At different wavelengths or frequencies of radiation, the double refraction probably depends upon different structural groups. There is no reason why the transition from one group to another should be smooth or even continuous. On the basis of this simplified model, a plot of birefringence versus wavelength or frequency might be expected to have a jagged sawtooth form with unequal spacings and non-similar teeth. If the functioning of two or more groups overlap, then the plot may not lack continuity. Such a continuous change in dielectric constant within one group or between a series of structural units could contribute the property of normal or anomalous dispersion, either of the simple optical variety or as related to dispersion of birefringence.

The second factor which may serve as a source of irregularity of dispersion phenomena may be found in the effect upon light waves of molecular and atomic vibrations. The science of transmission

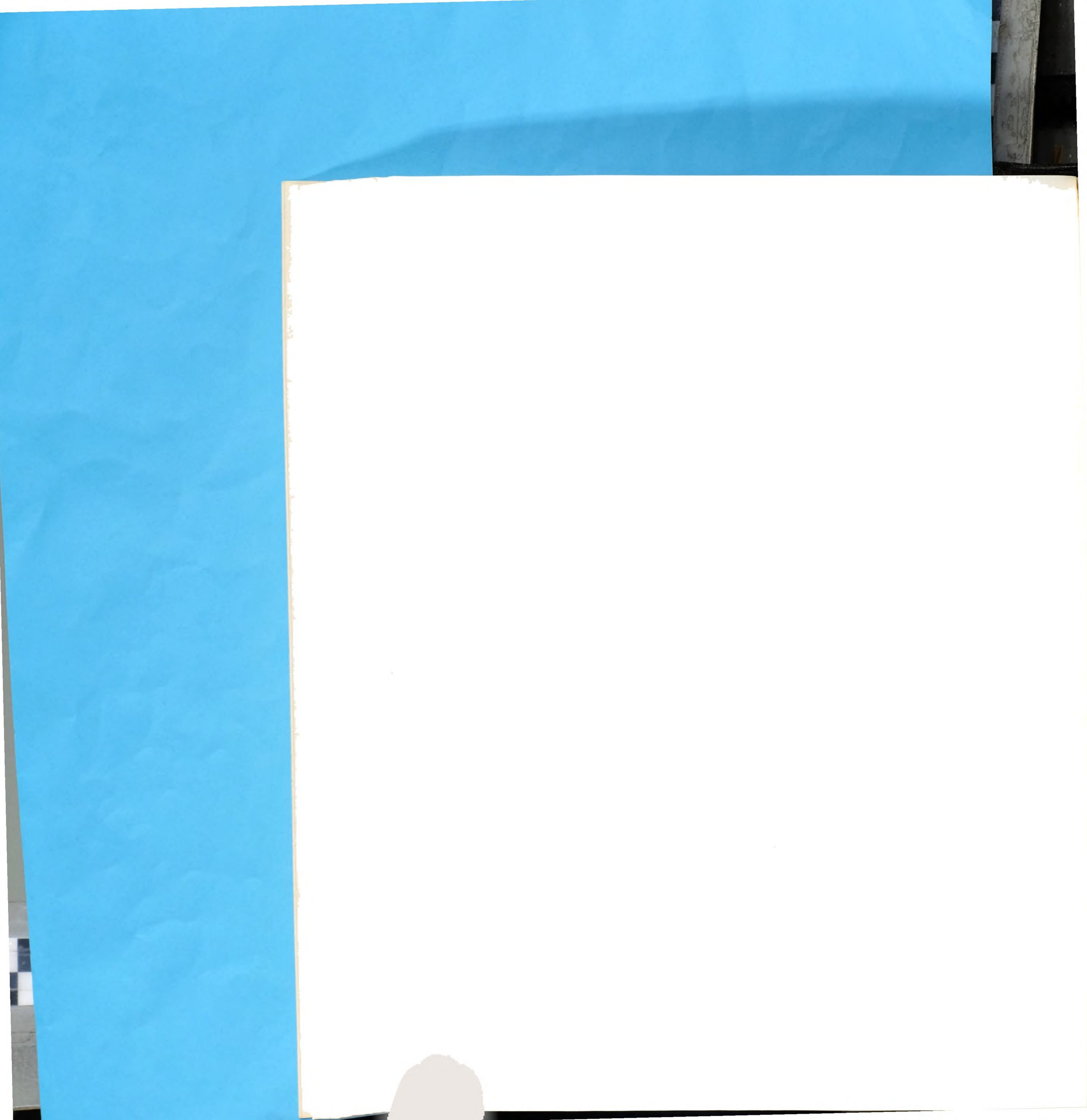

spectroscopy is based on the fact that light will be absorbed rather than transmitted by a medium when its frequency corresponds to a characteristic frequency of a natural mode of vibration of a molecular or atomic group contained in a transmitting medium. The association of absorption frequencies with molecular constituents provides a tool for the identification of compounds and the investigation of molecular structure. It is conceivable that the vibration of molecular groups contributes to the dispersive properties of materials. In particular, a condition of resonance between some element of the material structure and the radiation would logically disturb the double refraction properties in much the same way as it disturbs the transmittance and therefore the ordinary optical refraction. The part which molecular vibration plays in the appearance of the property of normal and, particularly, anomalous dispersion might be determined from correlation of dispersion data with infrared transmission spectroscopic information. Unfortunately, most transmission data for wavelengths between blue visible and about 1 micron yield little information about the bonds present in the photoelastic plastics such as P-6 and CR-39. In fact, transmittance curves for the shorter wavelengths are not generally available.

The normalized retardation of polycarbonate as shown in Figure 3.21 may be instructively compared to the spectral transmittance represented in Figure 3.18. While the results of the test of polycarbonate are not considered sufficiently accurate to warrant the construction of precise conclusions, a certain correlation between the plots is apparent. The greatest irregularities in normalized retardation seem to occur

near the absorption band around 1.66μ wavelength. The measurement at 1.65μ, very close to the absorption wavelength, deviated most from the other measurements. The trend of the other values of normalized retardation is generally to decrease with increased wavelength. That is, the dispersion is normal. The large value of normalized retardation near the absorption frequency creates an area of anomalous dispersion. The deviation seems too great to result from experimental errors. The results seem to indicate that improvement and extension of dispersion measurements and their subsequent comparison with spectroscopic data for various materials represents a promising and logical step along this course of experimentation.

Regardless of the factors which cause the properties of single and double refraction to depend upon wavelength and frequency of radiation, the investigation of this dependence will contribute to materials science and stress analysis in two ways. First, the relating of birefringence and dispersive properties, especially anomalous dispersion, to material composition and structure will eventually indicate strongly the source of the phenomenon of birefringence. What there is in a material that makes it birefringent is an interesting question from an academic viewpoint. Such correlation is also of practical interest, since it would facilitate the finding of other good photoelastic materials without extensive experimentation. It might also make possible the designing of new, more efficient birefringent materials.

Another possibility of more immediate practical significance is that extended investigation of dispersion should lead to knowledge of

possible relationships between dispersion and mode of deformation. Even if the real source of birefringence and dispersion cannot be pinpointed, the dispersion might depend on rearrangements of certain groups of molecules. This could be interpreted from a simple phenomenological point of view in terms of the diphase and multi-phase models of the structure of plastics. The results would be applicable to studies involving inelastic (including plastic and visco-elastic) behavior, three dimensional photoelasticity, and the design of rheological models which are more representative of real physical behavior.

Contribution to the understanding of physical properties such as stress birefringence and also to the practical application of photo-elasticity would be gained by the discovery and investigation of new materials which are doubly refracting in some spectral region. The possibility of finding such materials is expanded by the extension of the range of useable wavelengths. Conversely, the finding of materials which are transparent and birefringent in infrared or longer wave radiation adds to the probability of correlating photoelastic behavior with material structure.

Crystalline silicon, which was known to transmit light of wavelength longer than about 1.1μ, was found to be stress birefringent up to the 2μ limit of this work. Both isoclinics and isochromatics in a disc of this material were observed visually using the infrared converter, and the relationships between isochromatic order and stress were determined through use of the point sensing and compensation procedure. The stress optic coefficient for silicon was

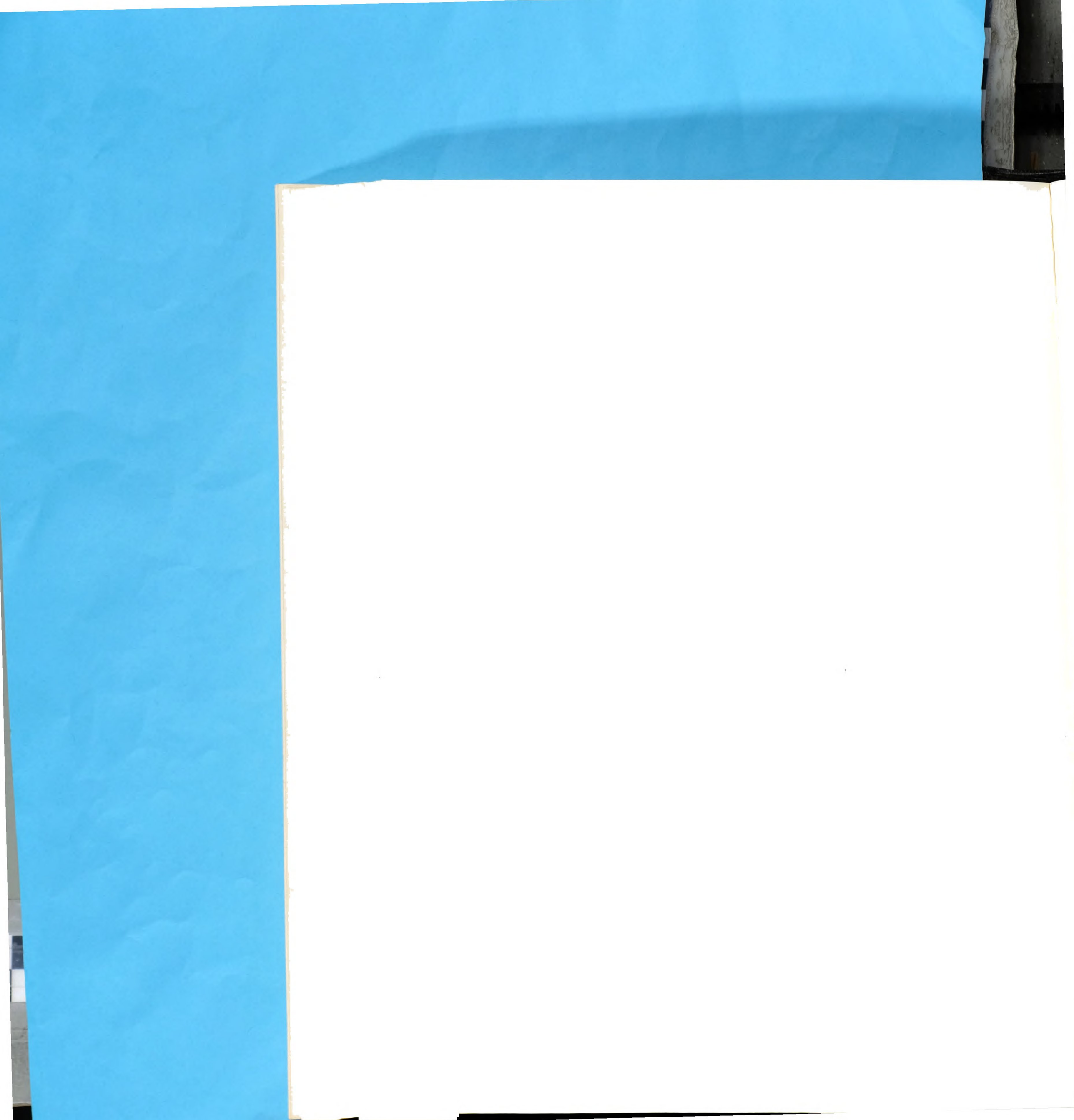

computed from the results present in Figure 3.24. For example, at $\lambda = 1.145\mu$, $C_\sigma = 12.5 \times 10^{-4}$ kg/mm^2, and at $\lambda = 1.90\mu$, $C_\sigma = 20.8 \times 10^{-4}$ kg/mm^{-2}. These values should be taken to be first approximations only, because of possible errors in the data resulting from the low isochromatic orders in the thin specimen. Mechanical and optical anisotropy of the crystal was also ignored.

Both silicon and amorphous selenium could be used to meet certain requirements in infrared instrumentation. A stressed plate of silicon, or a disc of naturally birefringent selenium could be made to serve as a quarter wave plate through the very wide transmission bands of wavelengths which are characteristic of these materials. These doubly-refracting materials might also serve as the core of beam-splitting or dichroic polarizers for the infrared range. Various other technological applications of the stress birefringence in infrared of silicon suggest themselves. These, along with extended discussion of the physical nature of birefringence in semiconductors, are not within the reasonable limits of this work.

Emphasis must be given the fact that the material tests carried out as part of this investigation were intended primarily as initial studies to demonstrate the validity of longwave photoelastic stress analysis and to illustrate the various future possibilities. The experiments were performed under laboratory conditions with less than acceptable control of temperature and humidity. The properties of plastic materials are known to depend to a large extent upon ambient conditions. Proper calibration in conjunction with accurate model analysis must be accomplished under carefully controlled conditions

so that the relationship between stress-strain-time-temperature-humidity-resin can be properly developed. These tests are tedious to perform at their present stage of development. Attempts to shorten and refine the testing procedure are known to be in progress (64). The results of this investigation, if they may be taken as at least representative, show that the involved relationships are very complex. The very common, greatly simplified approach to the study of the properties of model materials is not necessary and cannot be justified except on the insecure basis of expediency.

The relative retardation which takes place in a birefringent plate, regardless of its nature, was shown to depend upon the absolute index of refraction of the medium (usually air) in which the optical system is immersed. This dependence is ordinarily of no consequence when measurements are made with visible light. But the transmission and refractive properties of air, as well as any other photoelastic material, may vary a great deal over a broader wavelength spectrum and under varying conditions of temperature and humidity. Serious error could result from ignoring the effects of environment upon the photoelastic coefficients in the extended spectral region. In particular, the use of vacuum wavelengths with relative (to air) indices of refraction is inconsistent, although common. Also, failure to account precisely for the variation of the refractive index of air may be apparent in the data as dispersion of birefringence of the refracting plate.

It is hoped that the techniques and apparatus developed for the extension of photomechanics into the longwave spectral region and the results of the investigations into the optical properties of materials in this extended range provide the tools, guidelines, and motivation for

continued exploration. Whatever the results of the additional research, they will be beneficial to the studies of materials structure, material behavior, and the experimental stress and strain analysis.

4.3. Continuation of the Research

Several suggestions for the improvement and extension of the investigation may be formulated. Some of these are enumerated below in the form of specific proposals which should not be considered exclusive of other interesting and potentially profitable possibilities:

(1) The techniques and apparatus for the conducting of photoelastic investigations should be continuously improved, and the upper wavelength limit raised. The infrared spectroscopy region between 0.8μ and 25μ should be considered the minimum limit of the range of infrared photoelasticity. Later extension to the microwave region should prove instructive.

(2) The relationships between stress, strain, birefringence, and dispersion of birefringence for various photoelastic materials in wide ranges of wavelengths of light should be determined. Immediate attention should be given to polycarbonate which has been seriously neglected as a photoelastic material, but which appears promising for use in the analysis of inelastic behavior.

(3) The longwave photoelastic data, including dispersion information, should be carefully compared with infrared transmission spectroscopic data. Both of these classes of information should be viewed in light of what is known about the physics and chemistry of material structure. In this way, models explaining stress and orientational birefringence phenomena may be constructed and improved,

and eventually the physical basis of photoelasticity may be firmly established.

(4) Investigation of the natural and stress-induced birefringence and dichroism of other materials which are not necessarily transparent to visible radiation would contribute to several areas of knowledge and practical endeavor. Of particular scientific and technological interest is a major study of birefringence in semiconductors.

(5) The dependence of double refraction upon sign of stress difference as well as magnitude must be explored as part of the rheological study and also to eliminate the possibility of serious error resulting from the use of simple calibration results in the analysis of more complex stress fields. As a generalization, the empirical relationships between birefringence and stress path must be critically examined to determine whether the simplified relationships are always justified.

(6) The way in which photoelastic measurements are affected by the refractive properties of the medium surrounding the measuring system must be clearly established for all wavelengths. The findings of such a study may form the basis of a critical evaluation of other results, particularly dispersion data.

BIBLIOGRAPHY

1. Ambronn, H., "Dispersion der Doppelbrechung in Zweiphasigen Systemen," Kolloid Zeitschrift 9 (1911), pp. 147-153.

2. American Institute of Physics Handbook, McGraw-Hill, New York, 1957.

3. Appel, A. V., and D. A. Pontarelli, "Infrared Polariscope for Photoelastic Measurements of Semiconductors," Journal Optical Society of America, Vol. 48, p. 289.

4. Besse, A., and Desvignes, F., "An Infrared Polariscope," Rev. Opt., 38, 344 (1959).

5. Bird, George R., and Parrish, M. Jr., "The Wire Grid as a Near-Infrared Polarizer," Journal Optical Society of America, Vol. 50, No. 9, (1960), p. 886.

6. Blout, E. R., Amon, W. F. Jr., Shepherd, R. B., Thomas, A., West, C. D., and Land, E. H., "Near Infrared Transmitting Filters," Jrnl. Optical Soc. of America, Vol. 36, (1946), p. 460.

7. Blumstein, Alexandre, "Photoelastic Properties of Tightly Cross-linked Networks," Journal Polymer Science: Part A, Vol. 2, pp. 769-784, (1964).

8. Born, Max, and Wolf, Emil, Principles of Optics, Pergamon Press, Macmillan Co., New York, 1964.

9. Clark, A. B. J., "Static and Dynamic Calibration of a Photoelastic Model Material CR-39," Proc. of the Soc. for Experimental Stress Analysis, Vol. XIV, No. 1, (1956), pp. 195-204.

10. Coker, E. G., and Filon, L. N. G., A Treatise on Photoelasticity, The University Press, Cambridge, Great Britain, 1957.

11. Condon, E. U., and Odishaw, H., Handbook of Physics, McGraw-Hill, New York, 1958.

12. Coolidge, D. J. Jr., "An Investigation of the Mechanical and Stress-Optical Properties of Columbia Resin CR-39," Proceedings of Society for Experimental Stress Analysis, Vol. VI, No. 1, (1948), pp. 74-82.

13. Dash, W. C., "Birefringence in Silicon," Physical Review, Ser. 2, 98, Apr-June 1955, p. 1536.

14. Den Hartog, J. P., Advanced Strength of Materials, McGraw-Hill, New York, 1952.

15. Dietzel, A., Deeg, E., and Amrhein, E. M., "Die Verwendung Linear Polarisierter Microwellen Zur Zerstorungsfreien Werkstoffprufung," Elektrotechnische Rundschau, No. 4, 1959.

16. Dowd, J. J., "Optical Properties of Selenium, " Proc. Phys. Society (London), B64, 783, 1951.

17. Drechsler, L., and Schreiner, L., "An Investigation of Stresses Using Optical Methods in the Infrared Region," (in Polish) Pomiary-Automatyka Kontrola, Nr 7, 1957.

18. Ellickson, R. T., "Light Storage in Infrared Sensitive Phosphors," Journal American Optical Society, Vol. 36, Sept. 1946, p. 501.

19. Fonda, Gorton R., "Preparation and Characteristics of Zinc-Sulfide Phosphors Sensitive to Infrared," Journal American Optical Society, Vo. 36, No. 7, July 1946, p. 382.

20. Frocht, M. M., Photoelasticity, John Wiley and Sons, New York, 1941.

21. Gebbie, H. A., and Cannon, C. G., "Properties of Amorphous Selenium and its Use as an Optical Material," J. Opt. Soc. Am., 42(4): 277, April, 1952.

22. Gebbie, H. A., and Saker, E. W., "Properties of Amorphous Selenium in the Infrared," Proc. Phys. Society (London) B64, 360, 1951.

23. Giardini, A. A., "Piezobirefringence in Silicon," Am. Mineralog, Vol. 43 (1958), pp. 249/62.

24. Grandjean, C., "Double Refraction of Silicon and Germanium," Philips Research Report, Vol. 16 (1961), pp. 343/55.

25. "The Observation Post," Roscoe Guernsey, Editor, Monthly feature beginning Vol. 5, No. 10, 1965, Experimental Mechanics.

26. Haberlund, G., "Sonderdruck aus Beitrage Zur Spannungs-und Dehnungsanalyse. Part I, Spannungsoptische Ermittlung der Momenten-Einflussfelder elastischer Platten," Akademie Verlag, Berlin, 1965.

27. Hackforth, H. L., Infrared Radiation, McGraw-Hill, New York, 1960.

28. Hausmann, E., and Junghahmel, G., "Zu Spannungsoptischen Versuchen im Ultrarot," Internationales Spannungsoptisches Symposium, Berlin, 10-15, April 1961, Abhandlungen der Deutschen Akademie der Wissenchaften zu Berlin, Akademie Verlag, Berlin, 1962.

29. Hetenyi, M., editor, Handbook of Experimental Stress Analysis, John Wiley and Sons, Inc., New York, 1950.

30. Hornstra, J., and Penning, P., "Birefringence due to Residual Stress in Silicon," Philips Research Report, Vol. 15 (1959), pp. 237/49.

31. Hume-Rothery, W., Atomic Theory for Students of Metallurgy, Institute of Metals, London.

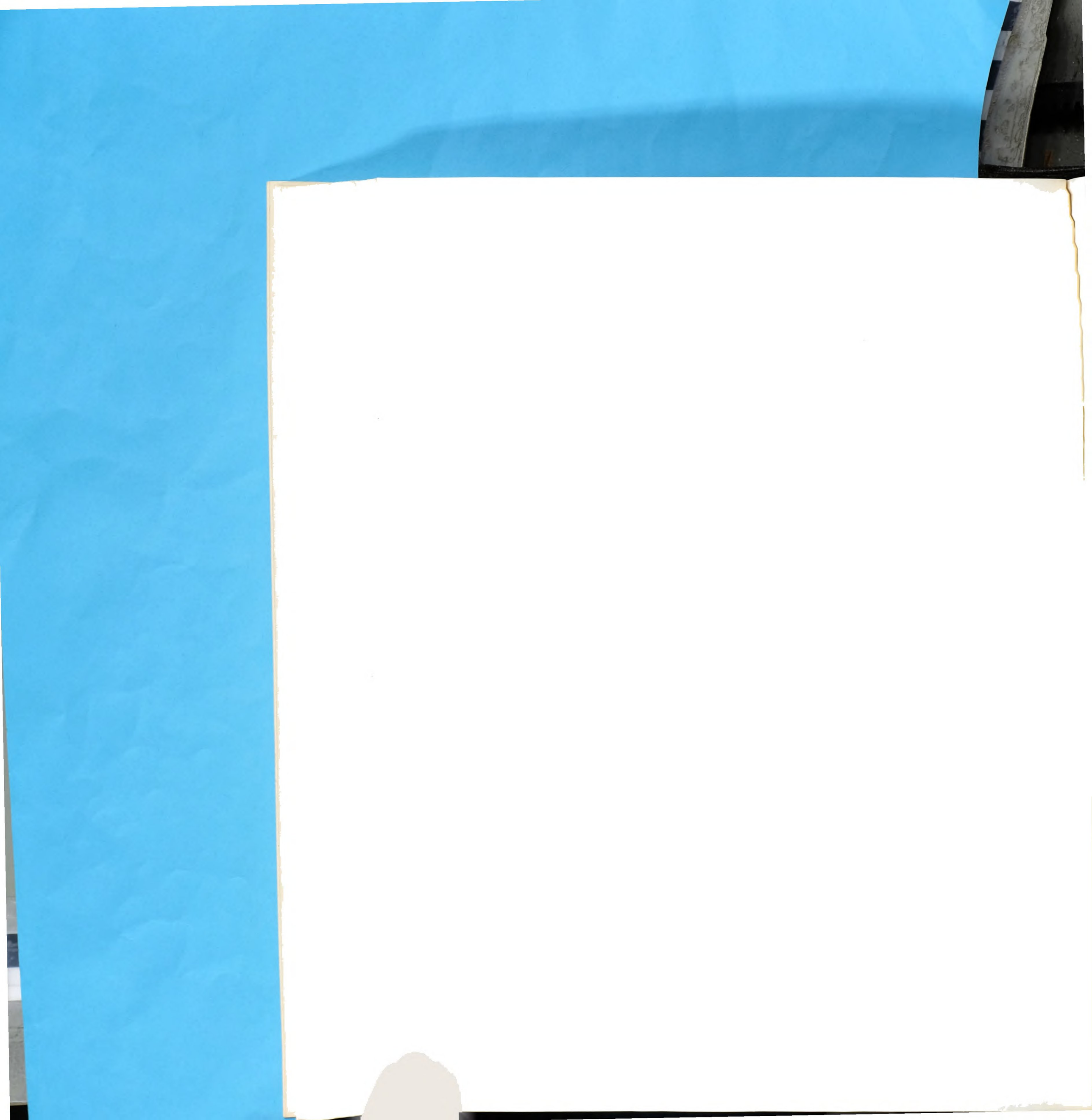

32. Hume-Rothery, W., and Raynor, G. V., The Structure of Metals and Alloys, Institute of Metals, London, 1962.

33. Ito, Katsuhiko, "New Model Materials for Photoelasticity and Photoplasticity," Proceedings SESA, Vol. 19, No. 2, p. 373, December 1962.

34. Jacob, I., Schmidt-Tiedemann, K. J., "Optische Spannungsanalyse Von Hableiter-Barelementen," Proceedings, 3. Internationale Tagung for Experimentelle Spannungsanalyse, Berlin, 1966; VDI-Verlag, Dusseldorf (W. Germany), 1966.

35. Jamieson, J. A., McFee, R. H., Plass, G. N., Grube, R. H., and Richards, R. G., Infrared Physics and Engineering, McGraw-Hill, New York, 1963.

36. Jessop, H. T., "On the Tardy and Senarmont Methods of Measuring Fractional Relative Retardations," British Journal of Applied Physics, Vol. 4, 1953, Suppl. 2, pp. 138-141.

37. Jessop, H. T., and Harris, F. C., Photoelasticity, Principles and Methods, Cleaver-Hume Press Ltd., London (England), 1949.

38. Jira, R., "Das mechanische und spannungsoptische Verhalten von Zelluloid bei zweiachsiger Beanspruchung und der Nachweis seiner Eignung fur ein photoplastisches Verfahren," Konstruktion, Heft 11, 1957.

39. Kodak Wratten Filters, Kodak Scientific and Technical Data Book B-3, 21st ed., Eastman Kodak Co., 1962.

40. Kruse, P. W., McGlauchlin, L. D., and McQuistan, R. B., Elements of Infrared Technology, John Wiley and Sons, New York, 1962.

41. Kuske, Albrecht, "Multiphase Theory of Plastics," Proc. SESA, Vol. 19, No. 2, Sept. 1962, p. 278.

42. Kuske, Albrecht, "Photoelastic Research on Dynamic Stresses," Proceedings of Society for Experimental Stress Analysis, Vol. 6, No. 2, Feb. 1966, p. 105.

43. Landolt, H. H., Landolt-Börnstein, Zahlenwerte und Funktionen aus Physik, Chemie, Astronomie, Geophysik, und Technik, IV Band, 3 Teil, Springer-Verlag, Berlin, 1961.

44. Leverenz, H. W., Luminescence of Solids, John Wiley and Sons, New York, 1950.

45. Lorek, R., "Untersuchung von Polyestergiessharzen und anderen Kunststoffen auf ihre Eignung als photoplastiches Modellmaterial," Kunststoffe, Heft 3, 1962.

46. Maksutova, T. D., "On Optical and Mechanical Properties of Polymers," (in Russian), Issledoranya po Uprogosti i plastichnosti, Leningradsky Universitet, Leningrad, Nr. 2, 1963.

47. Mindlin, R. D., "Analysis of Doubly Refracting Materials with Circularly and Elliptically Polarized Light," Journal Optical Society of America, Vol. 27, (1937), p. 285.

48. Mitsuishi, A., et al., "Polarizer for the Far Infrared Region," Jrnl. Opt. Soc. America, Vol. 50, No. 9, p. 433 (1960).

49. Mönch, E., "Die Dispersion der Doppelbrechung als Plastizitatsmass in der Spannungsoptik," Zeitschrift fur Angewandte Physik, 8 Heft, 1954.

50. Mönch, E., "Der heutige Stand der Photoplastizitat," Schweizer Archiv fur angenwandte Wissenschaft und Technik, Heft 5, 1959.

51. Mönch, E., "Die Dispersion der Doppelbrechung als Mass fur die Plastizitat bei spannungsoptischen Versuchen," Forschung, 21 Band, 1 Heft, 1955.

52. Mönch, E., and Hartmann, Th., "Untersuchung einiger Kunststoffe auf ihre Eignung als photoplastisches Modellmaterial," Zeitschrift fur Angewandte Physik, 11 Band, 1 Heft, 1959.

53. Mönch, E., and Lorek, R., "A Study of the Accuracy and Limits of Application of Plane Photoelastic Experiments," Proceedings of the International Symposium on Photoelasticity, edited by M. M. Frocht, Pergamon Press, New York, 1963.

54. Moss, T. S., Optical Properties of Semiconductors, Butterworths Scientific Publications, London, 1959.

55. Papoular, P., "Far IR Reference Sources for the Evaluation of High Temperatures," Infrared Physics, Vol. 4, No. 2, April 1964, p.137.

56. Persoz, B., "Birefringence du Polystyrene Sous Contraints Constante a Differentes Temperatures," Analyse des Contraintes, Vol. VI, No. 4, October 1961.

57. Philips Spectral Lamps, North American Philips, Technical Brochure No. 10.078BE 3/60.

58. Pindera, J. T., "Einige Rheologische Probleme bei Spannungs-optischen Untersuchungen," Internationales Spannungscoptisches Symposium, Deutsche Akademie der Wissenschaften zu Berlin, Berlin, 10-15 April, 1961, Akademie-Verlag, Berlin, 1962.

59. Pindera, J. T., "Remarks on the Properties of Model Materials," Paper presented at 1963 Annual Meeting of Society for Experimental Analysis (to be published), August 3, 1964.

60. Pindera, J. T., "On Some Criteria of Evaluation of Model Materials," Presented at Second International Conference on Experimental Stress Analysis, Paris, April, 1962.

61. Pindera, J. T., "Recent European Research Work on Photoelasticity," Presented SESA Spring Meeting, Salt Lake City, Utah, May 6-8, 1964.

62. Pindera, J. T., "Investigation of Some Rheological Photoelastic Properties of Some Polyester Resins," Part I, II, III (in Polish), Rozprawy Inzynierskie, No. 3 and 4, 1959.

63. Pindera, J. T., "Rheological Properties of Model Materials," (in Polish, to be published in English), Wydawnictwa Naukowo-Techniczne, Warzawa, 1962.

64. Pindera,J. T., and Kiesling, E. W., "On the Linear Range of Behavior of Photoelastic and Model Materials," Proceedings, 3. Internationale Tagung fur Experimentelle Spannungsanalyse, Berlin, 1966, VDI-Verlag, Dusseldorf (W. Germany), 1966.

65. Plyler, E. K., and Ball, J. J., "Filters for the Infrared Region," Jrnl. Opt. Soc. America, V. 42, No. 4, April 1952, p. 266.

66. Plyler, E. K., and Peters, C. W., "Wavelengths for Calibration of Prism Spectrometers," Paper No. 2159, Journal of Research of National Bureau of Standards, Vol. 45, No. 6, December 1950.

67. Polarized Light, No. F3374, Published by Polaroid Corporation.

68. Prussin, S., and Stevenson, A., "Strain-Optical Coefficients of Silicon for Infrared Light," Journal Applied Physics, Vol. 30, (1959), pp. 452/3.

69. Ramspeck, A., "Anomalien der accidentellen Doppelbrechung bei Zelluloid," Annalen der Physik, 1924, p. 1962.

70. Rao, T. V. K., "Relation Between Photoelastic Properties and Molecular Behavior in Certain Plastics," Ph. D. Thesis, Michigan State University, 1960.

71. Schwieger, H., "A Simple Calculation of the Transverse Impact on Beams and Its Experimental Verification," Proceedings, Society for Experimental Stress Analysis, Vol. 5, No. 11, November 1965, p. 378.

72. Sears, F. W., Optics, Addison-Wesley Press, Inc., Cambridge, Massachusetts, 1949.

73. Seeley, F. B., and Smith, J. O., Advanced Mechanics of Materials, John Wiley and Sons, New York, 1952.

74. Shenk, J. H., Hodge, E. S., Morris, R. J., Pickett, E. E., and Brode, W. R., "Plastic Filters for Visible and Near Infrared Regions," Jrnl. Opt. Soc. America, V. 36, (1946), pp. 569-575.

75. Shurcliff, W. A., Polarized Light Production and Use, Harvard University Press, Cambridge, Massachusetts, 1962.

76. Timoshenko, S., and Goodier, J. N., Theory of Elasticity, McGraw-Hill Company, New York, 1951.

77. Van Geen, R., "Dispersion Cromatique de l'effet photoelastique," Second International Conference on Stress Analysis, Paris, April, 1962.

78. Wolf, H., Spannusungsoptik, Springer-Verlag, Berlin, 1961.

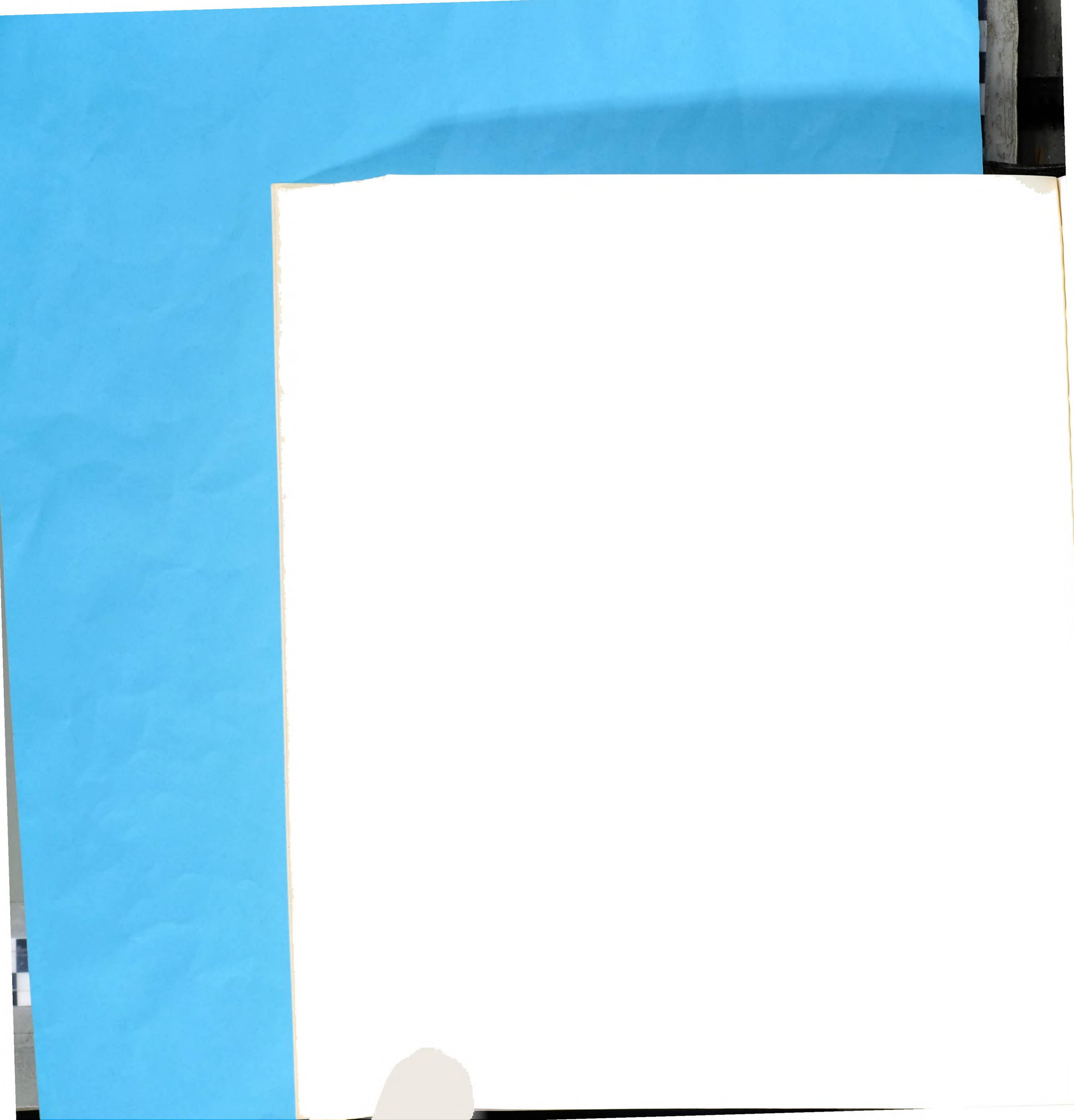

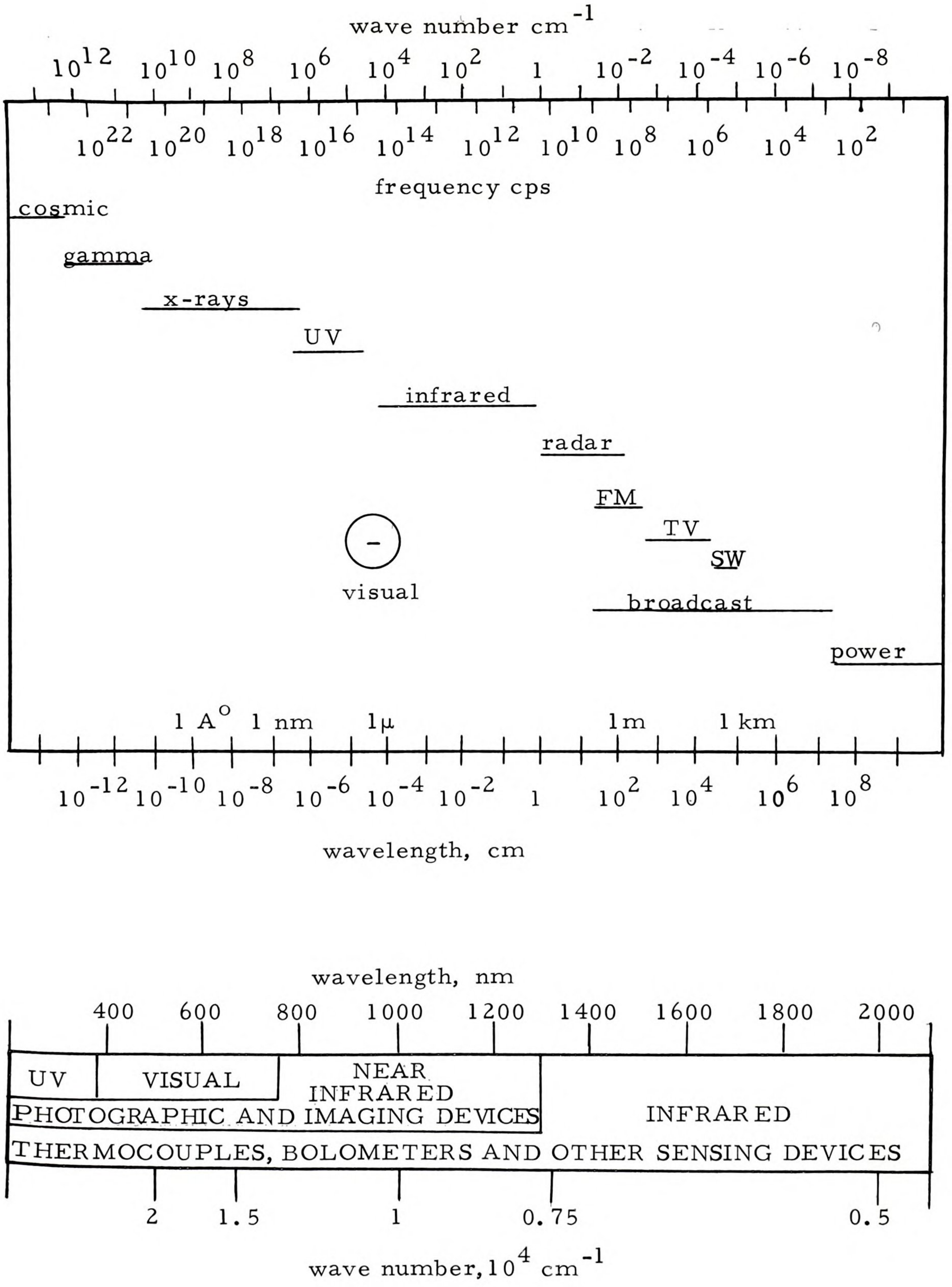

Figure 2.1. The Electromagnetic Spectrum.

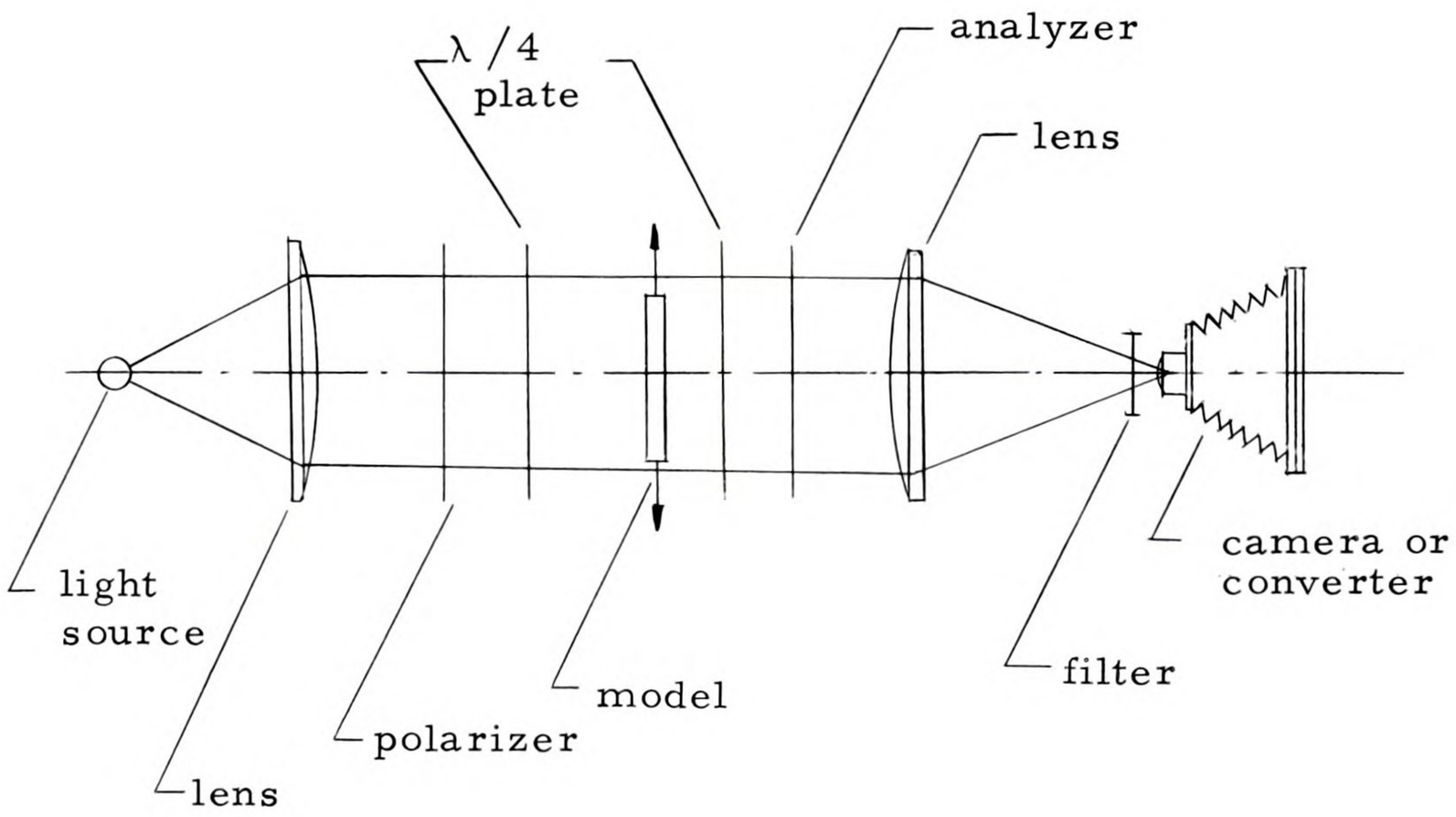

Figure 2.2a. Optical System for Visible and Near Infrared.

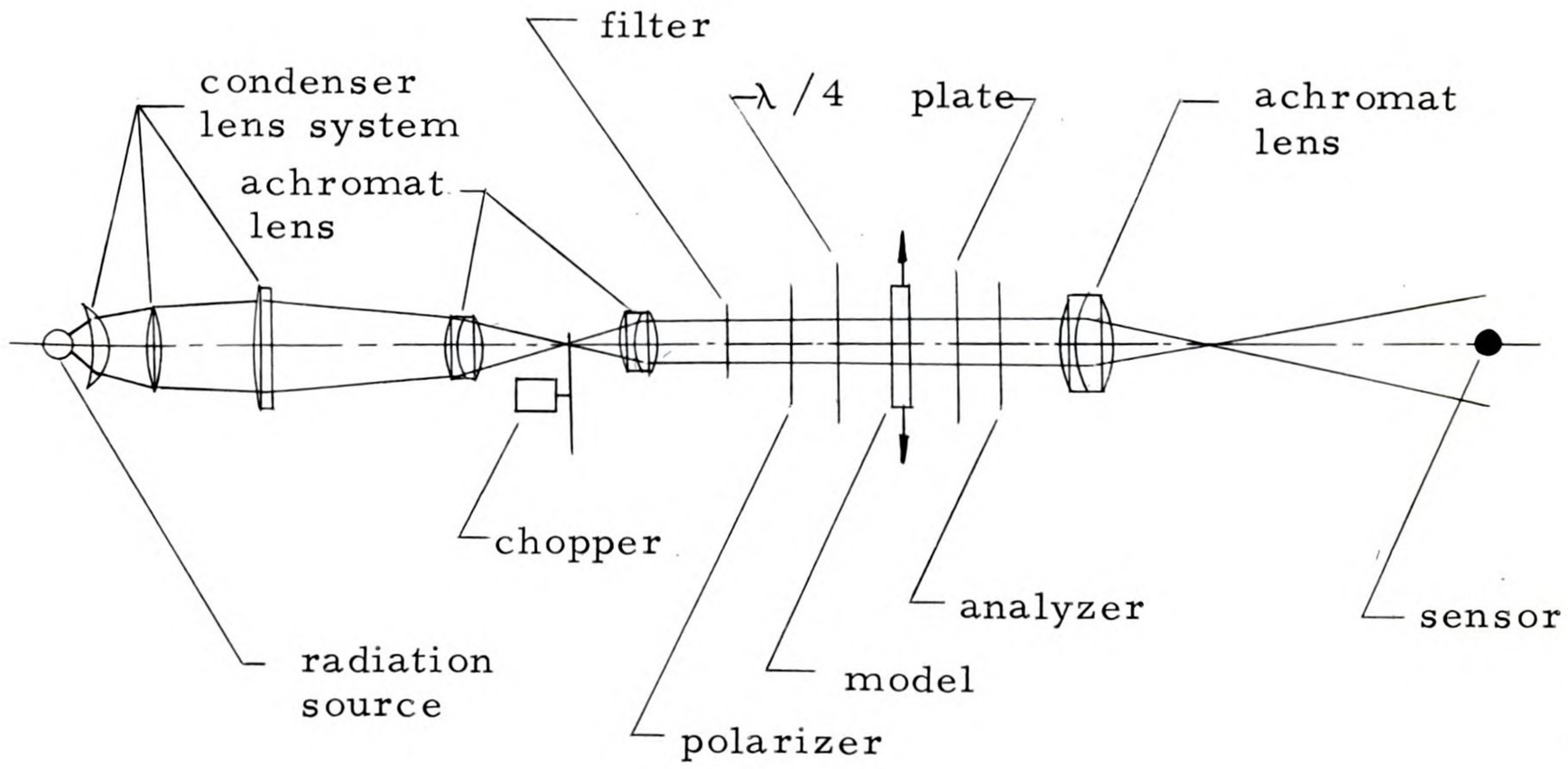

Figure 2.2b. Optical System for Long Wavelengths.

Figure 2.2. Infrared Polariscope Arrangements.

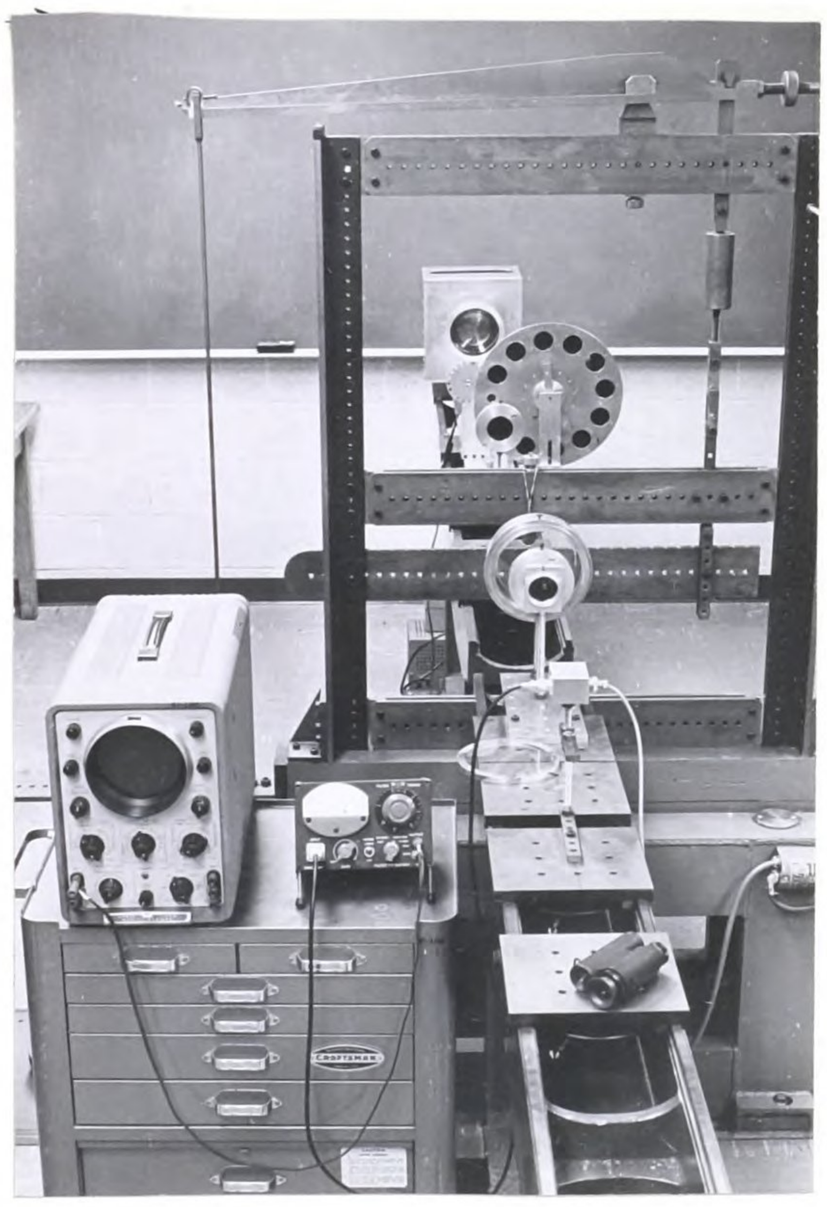

(a) complete optical bench

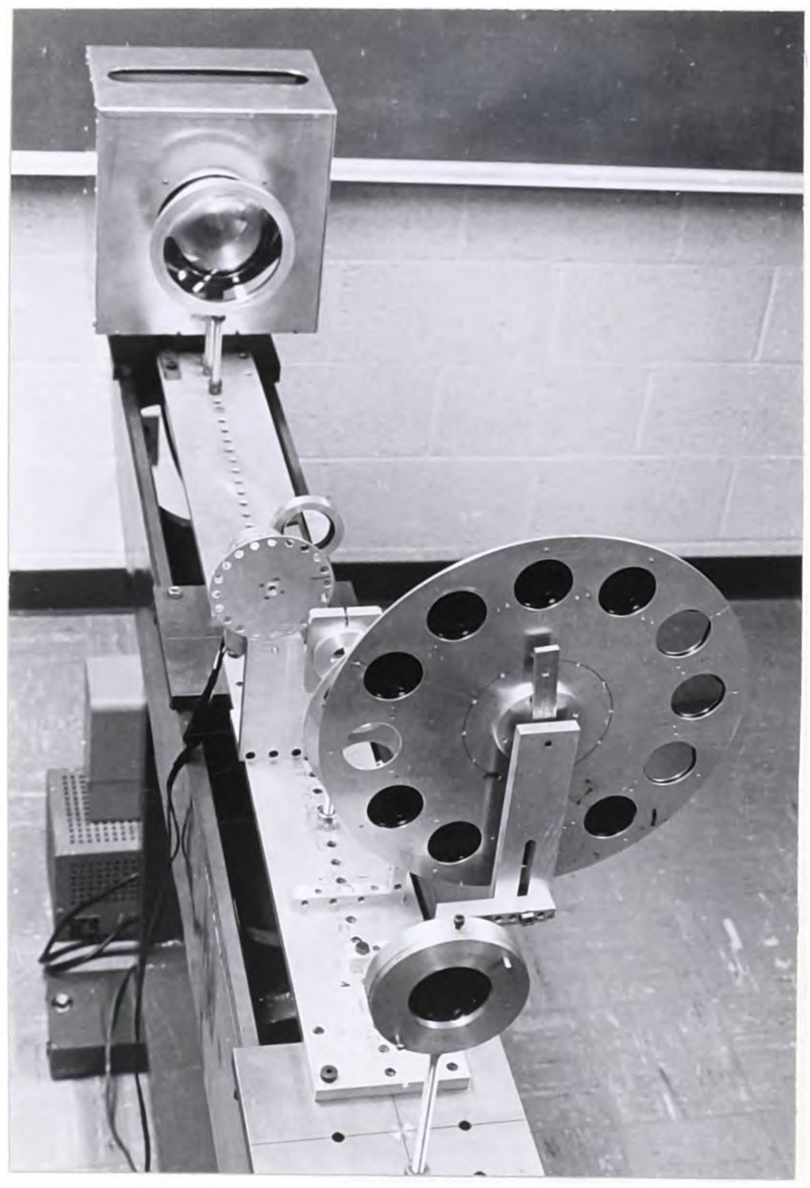

(b) source, chopper, filters

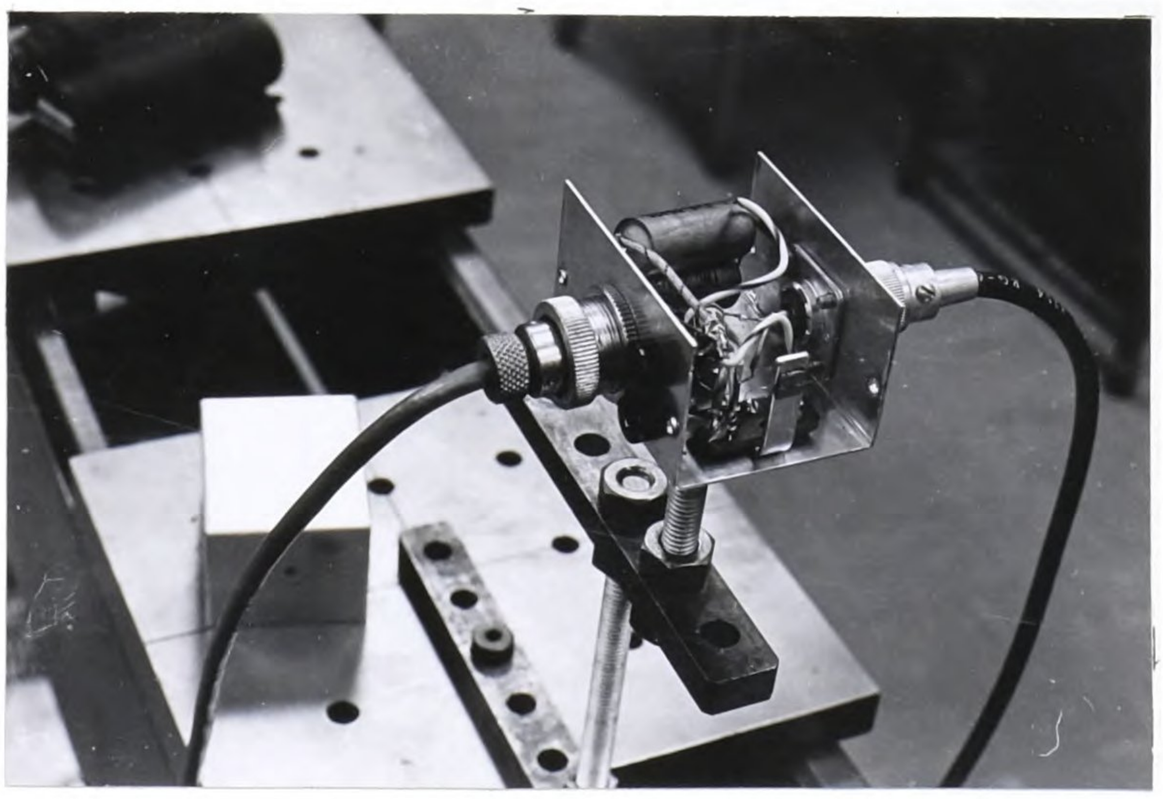

(c) infrared sensing head (cover removed)

Figure 2.3. Photoelastic Apparatus for the One to Two Micron Region.

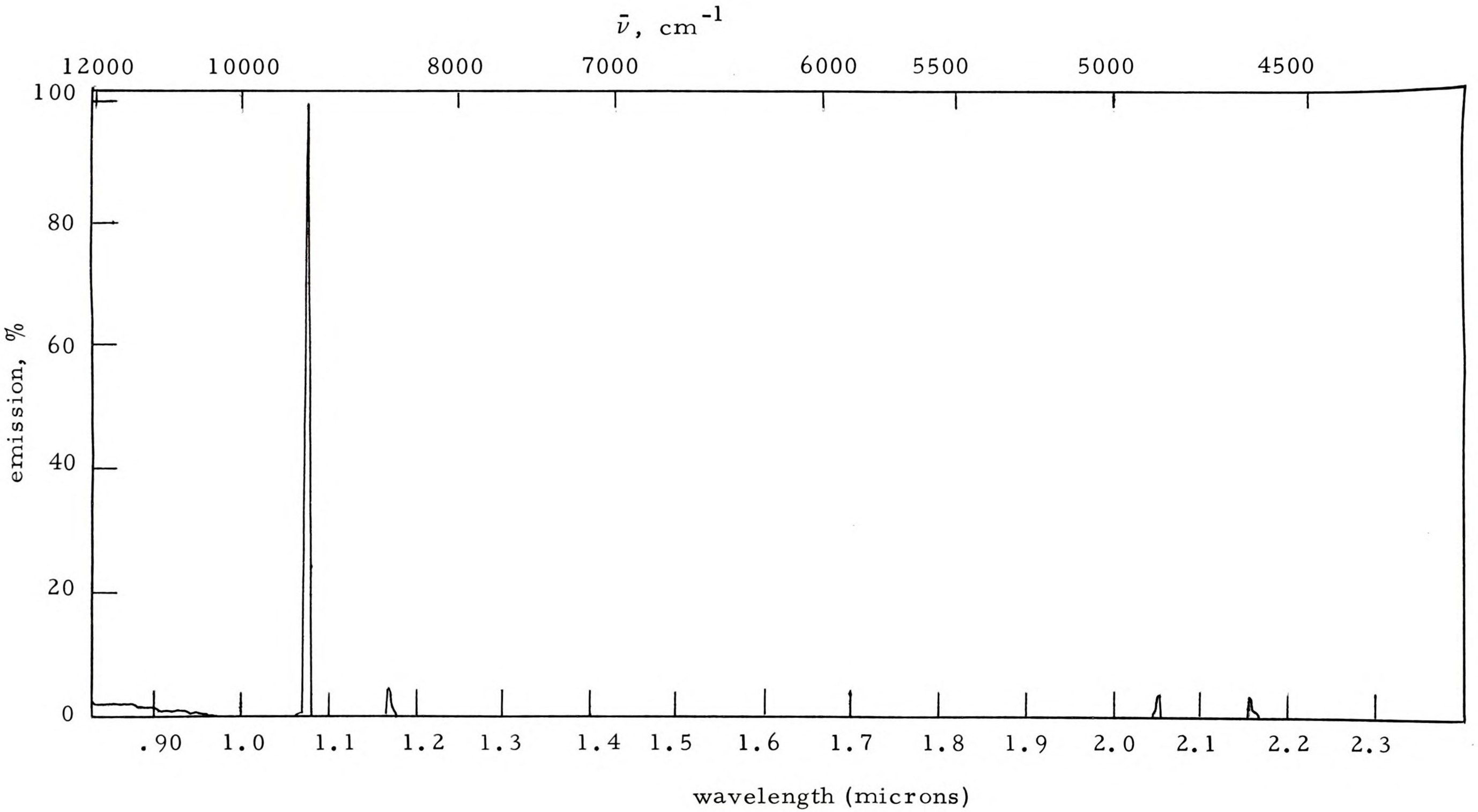

Figure 2.4. Emission of Helium Lamp in Infrared.

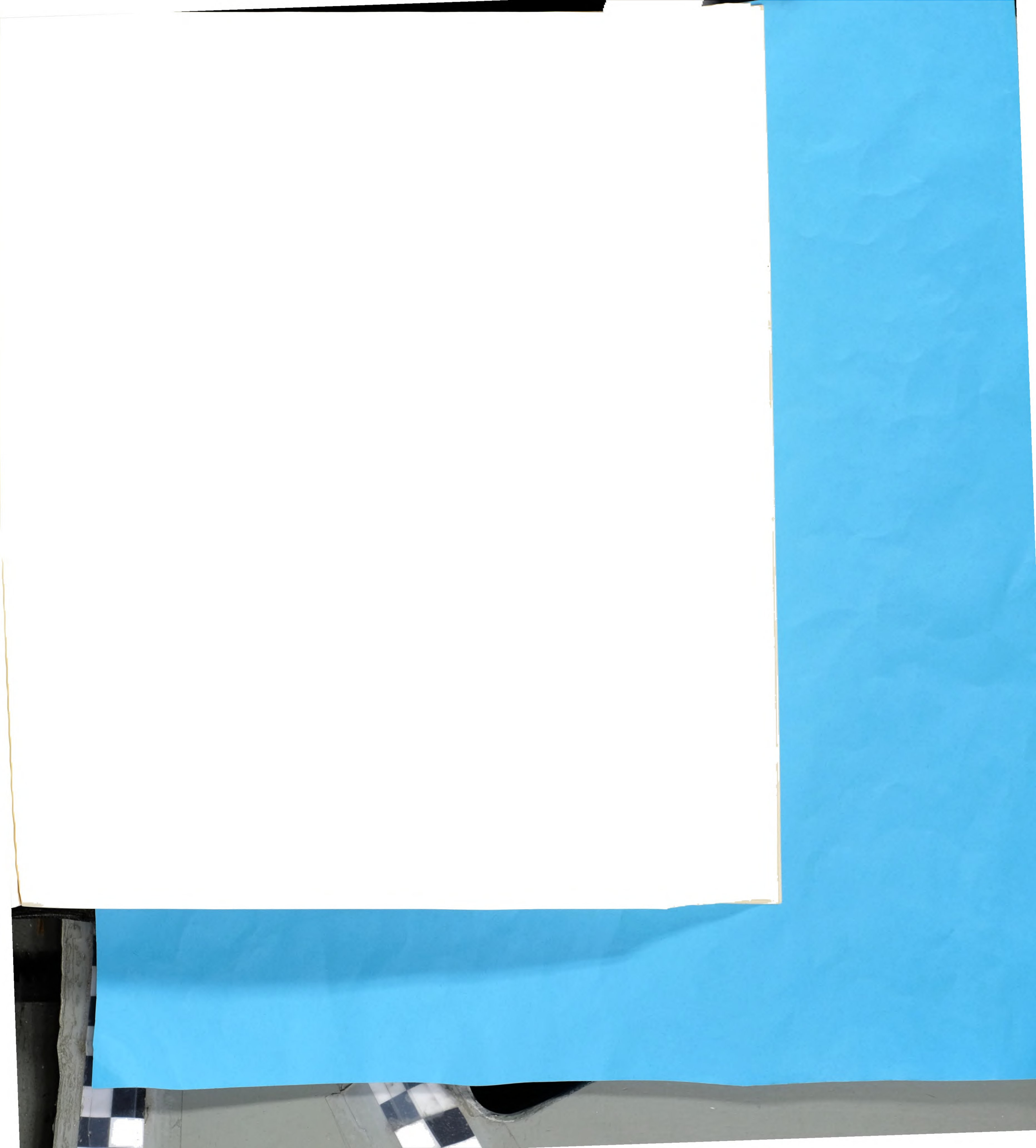

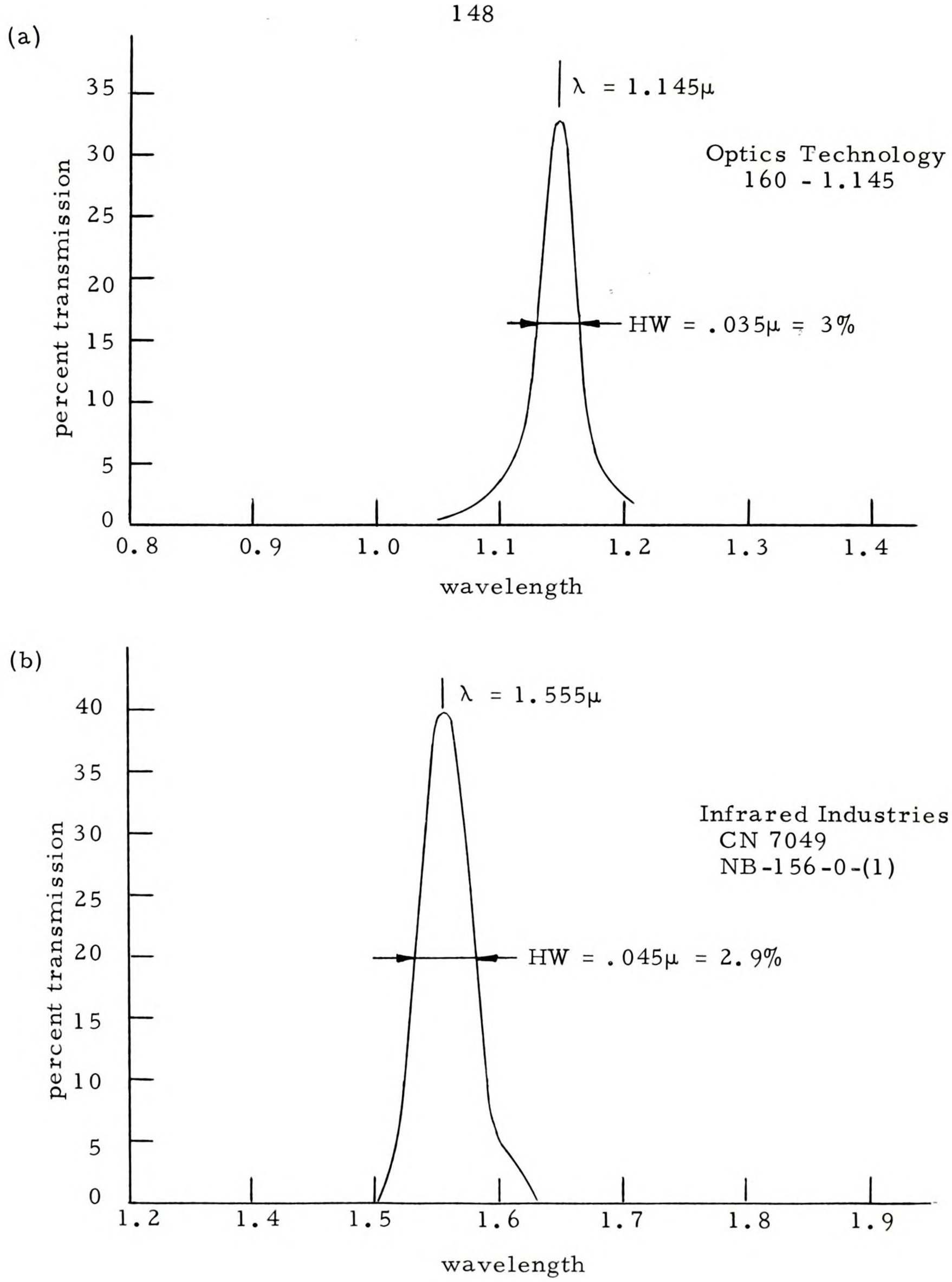

Figure 2.5. Transmission of Representative Interference Filters.

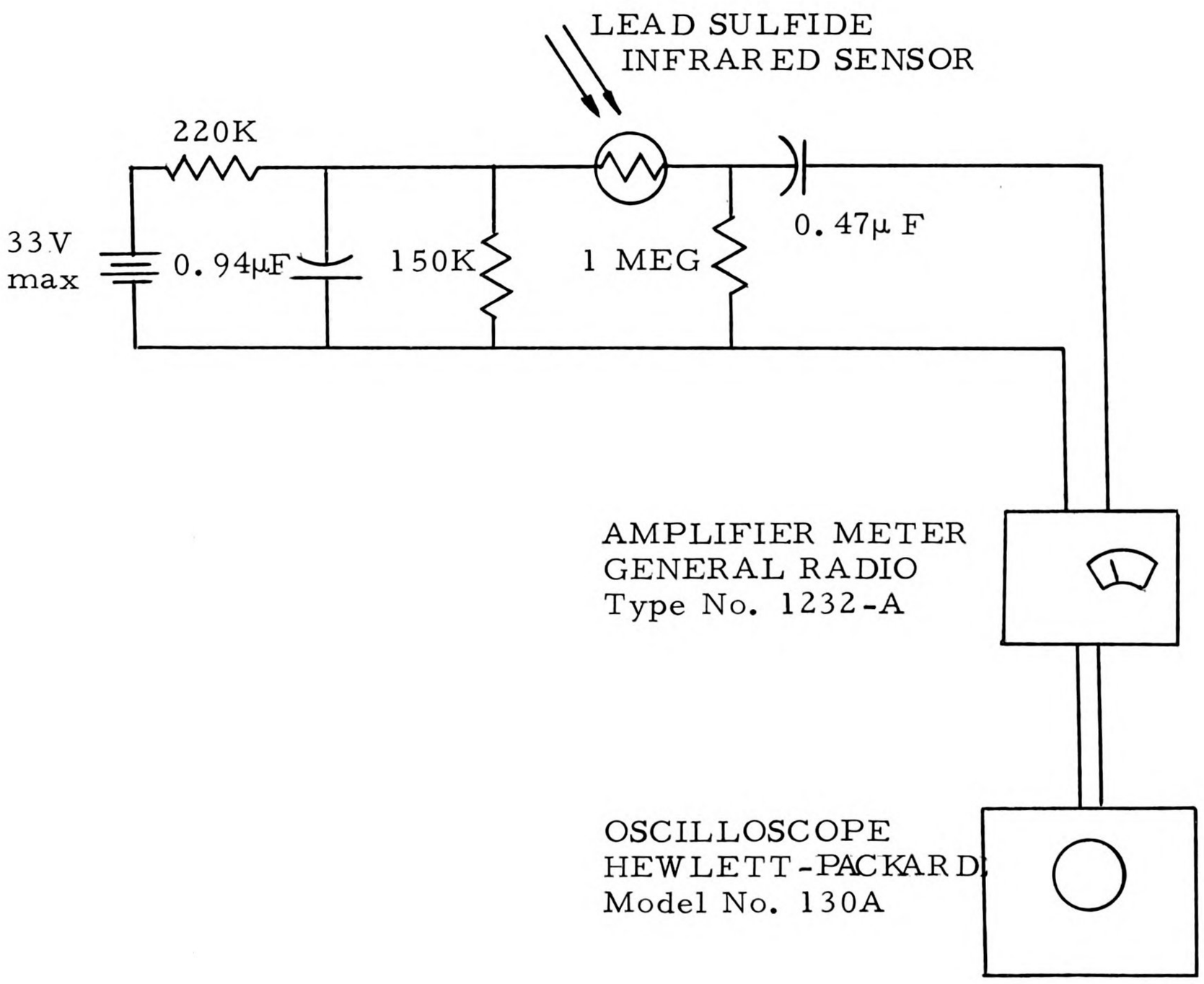

Figure 2.6. Infrared Sensing Circuit.

$$I = \frac{1}{2} A^2 [1 - \cos 2\zeta]$$

where: $\zeta = \frac{\pi(n_1 - n_2)}{\lambda n_o} d - \theta$

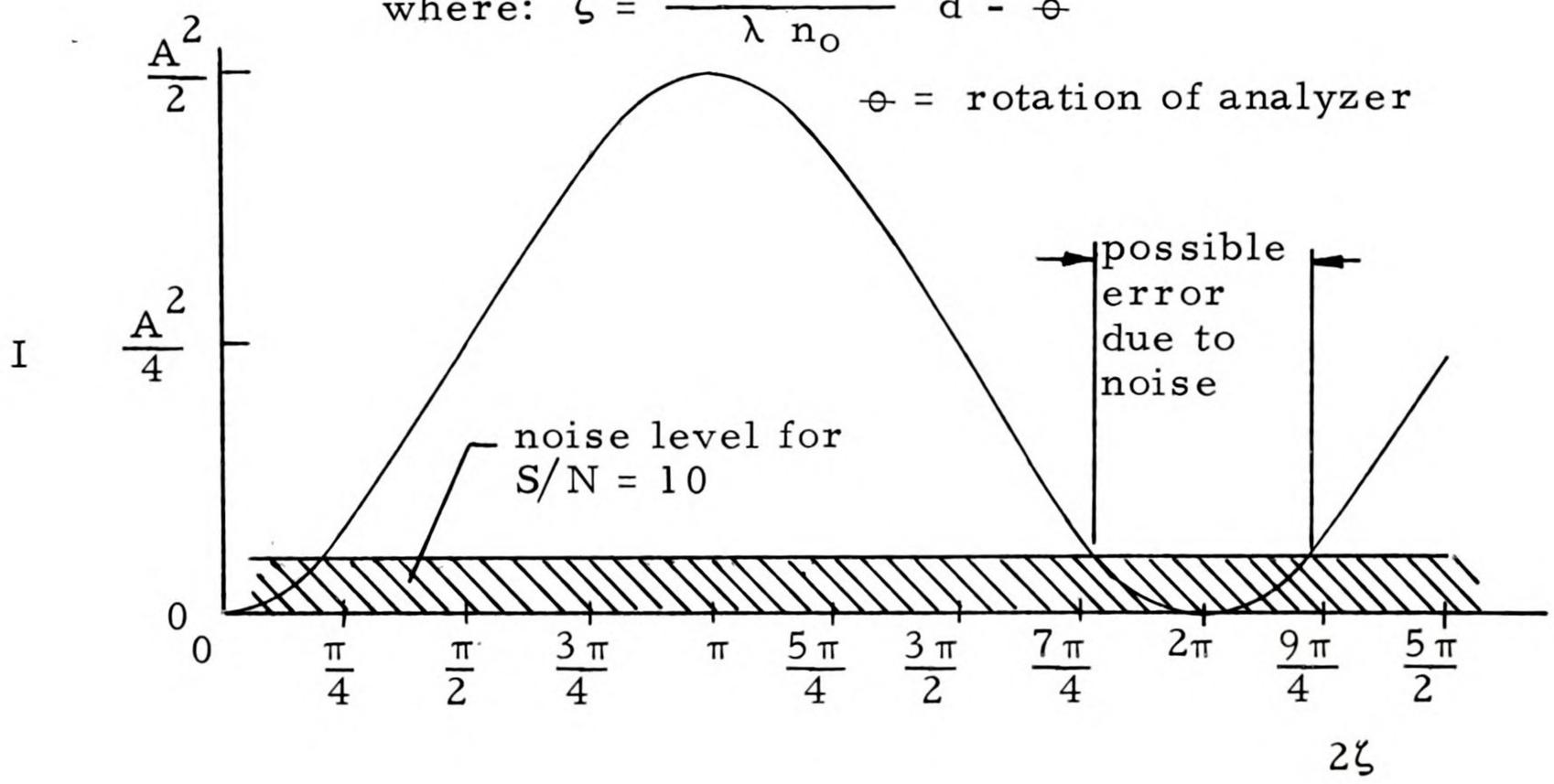

(a) direct detection of minimum intensity angle.

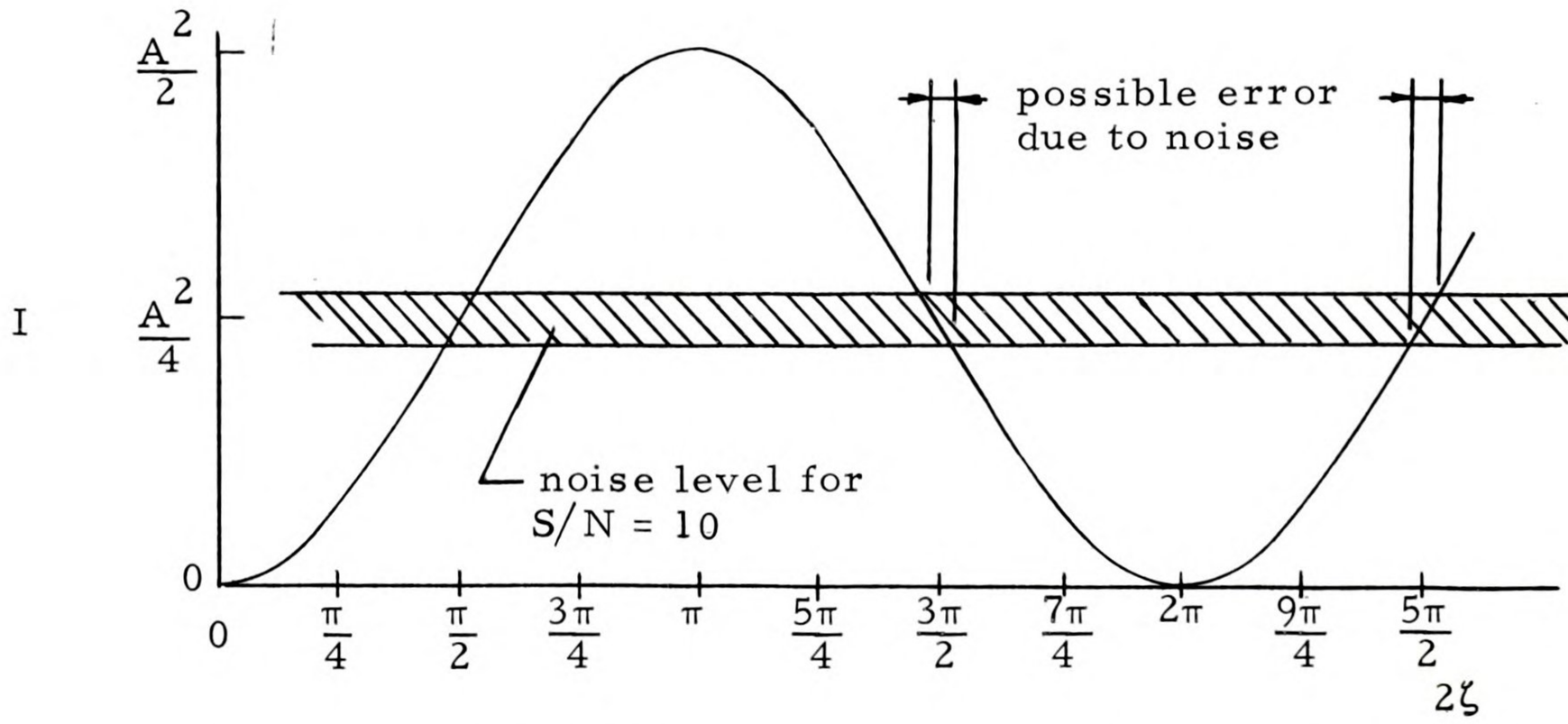

(b) detection of minimum intensity angle by averaging.

Figure 2.7. Reduction of Error in Measurement of Fractional Isochromatic Order.

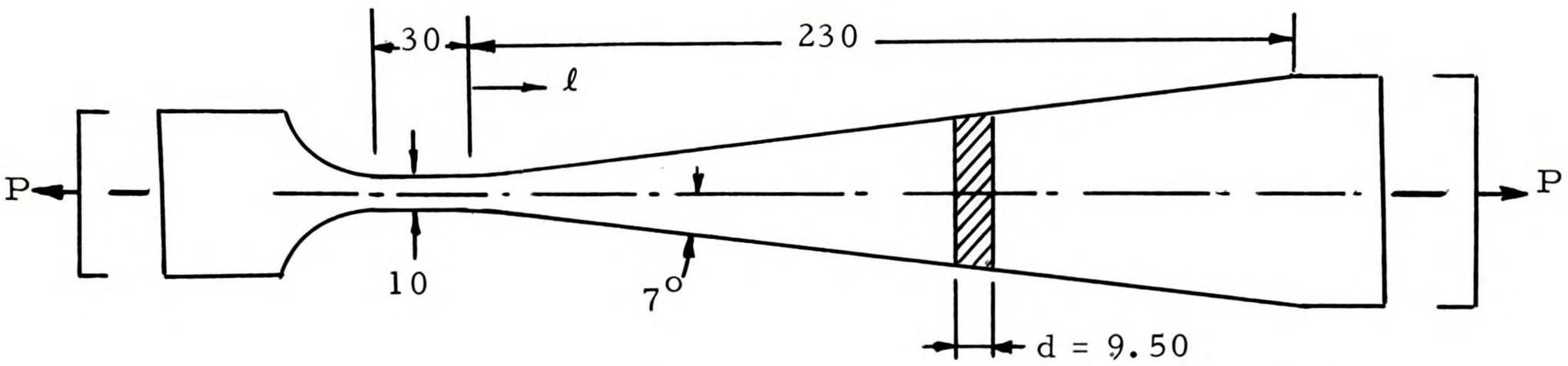

(a) tensile model, CR-39 dimensions millimeters

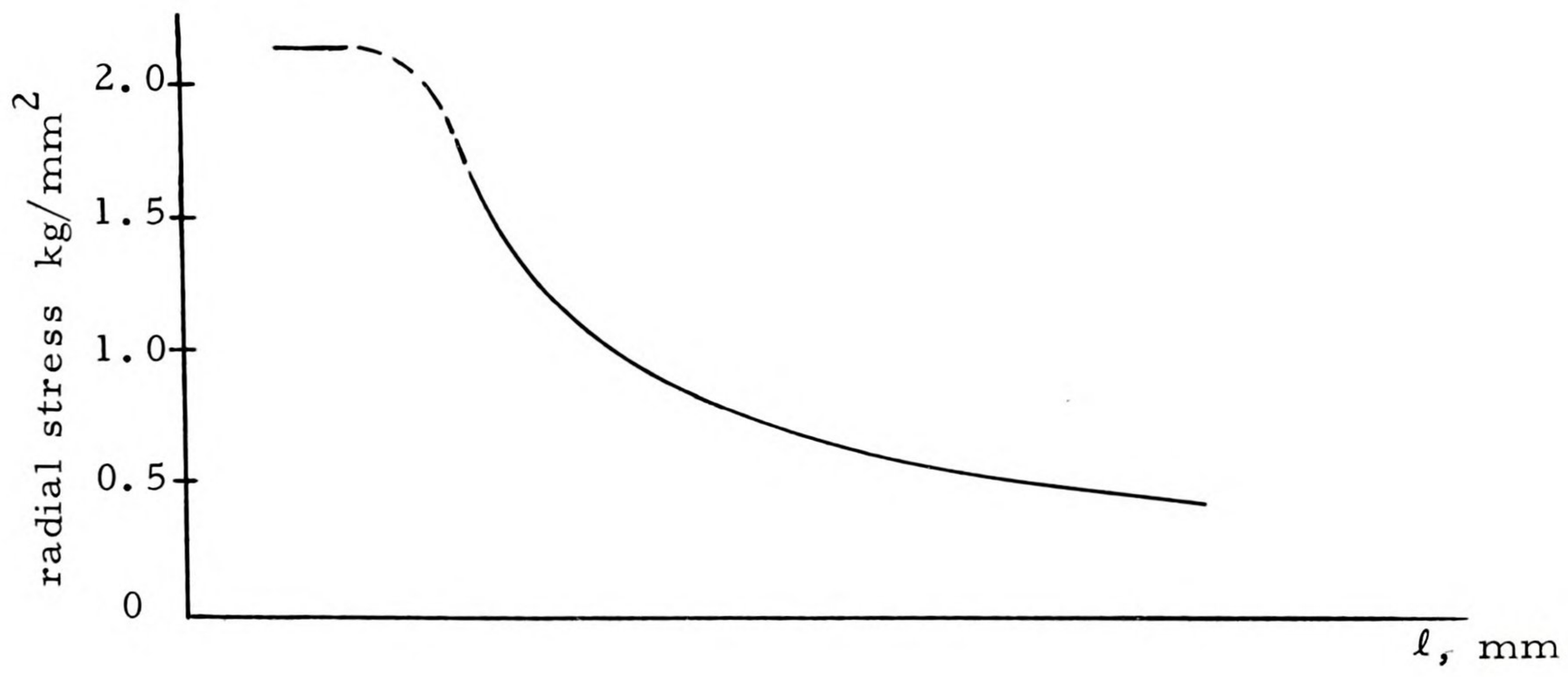

(b) stress distribution

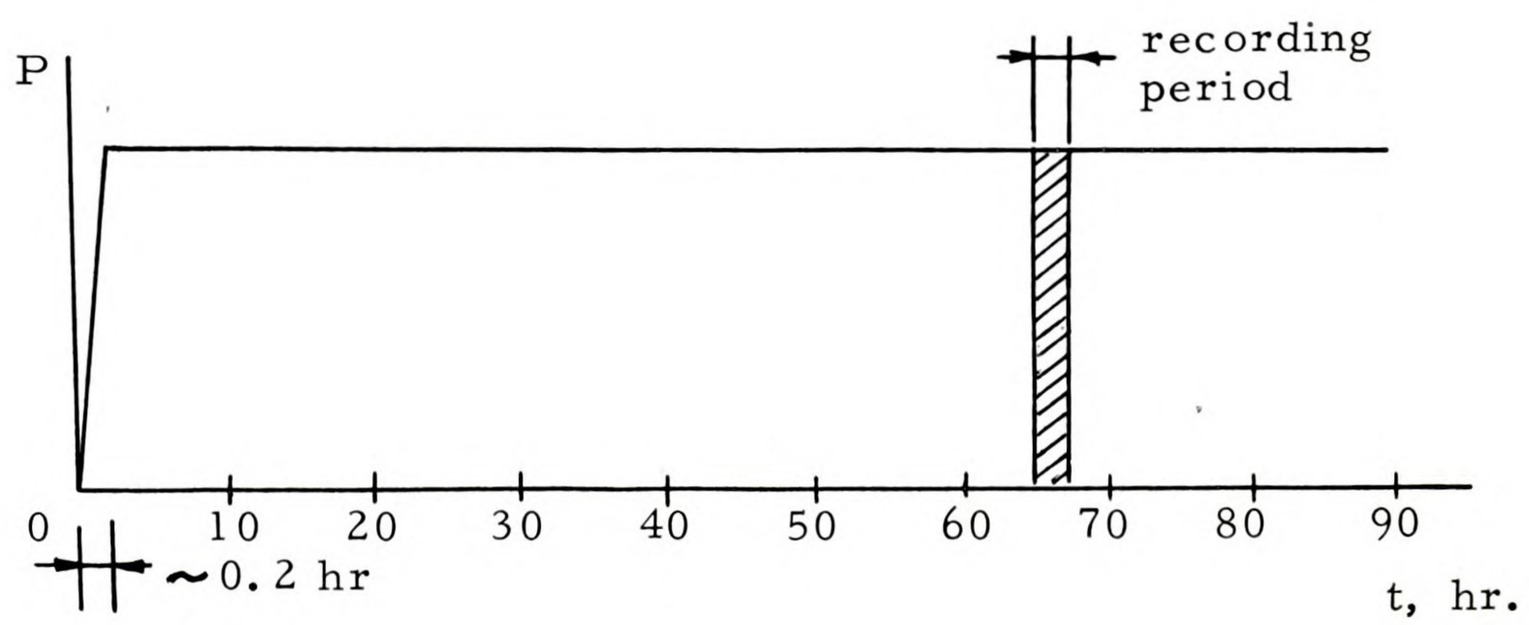

(c) loading history

Figure 3.1. CR-39 Model, Stress Distribution, Load History.

Figure 3.2a. Isochromatic Pattern in CR-39 Model for λ = 546 nm with Linear Polarization.

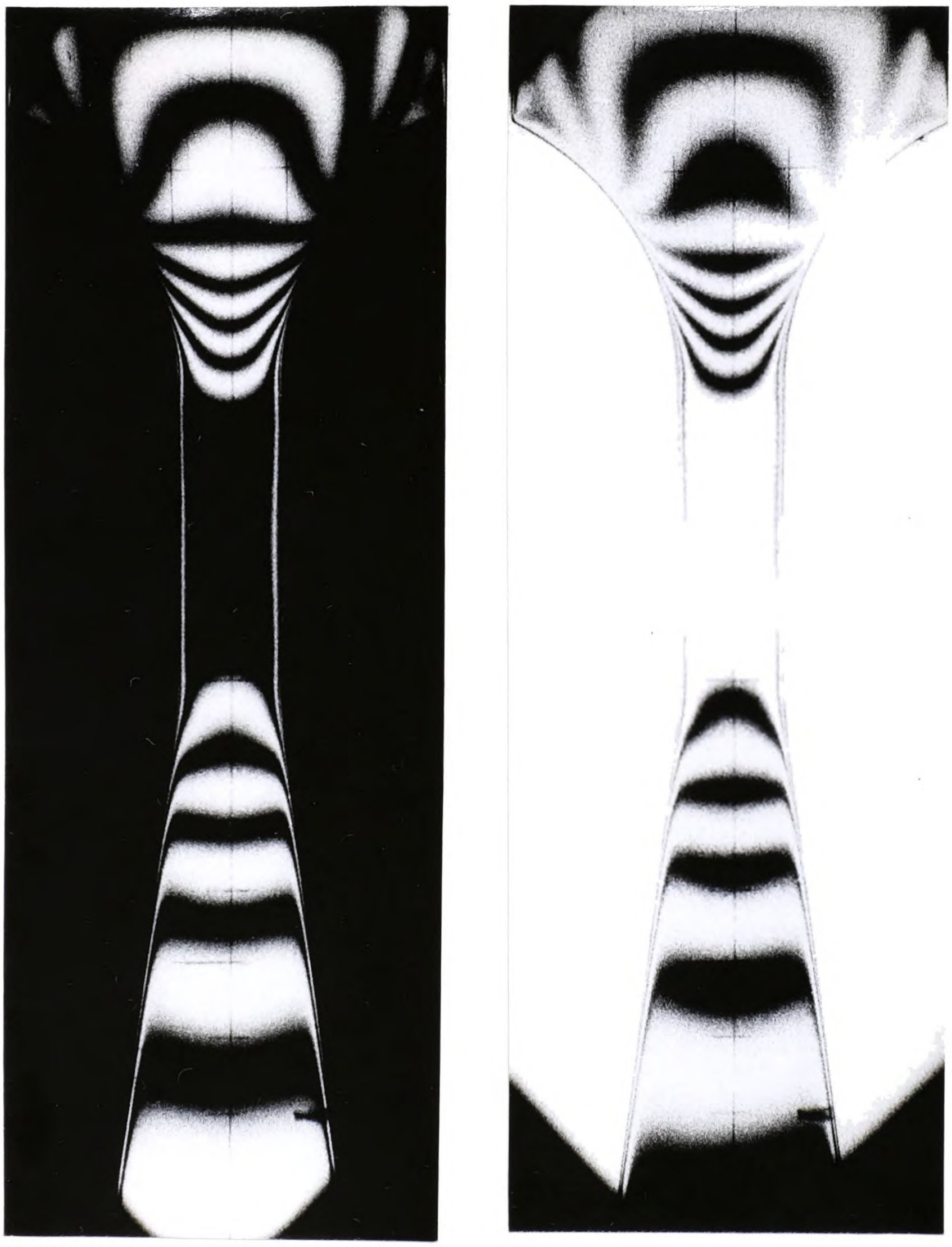

Figure 3.2b. Isochromatic Pattern in CR-39 Model for λ = 1083 nm with Linear Polarization.

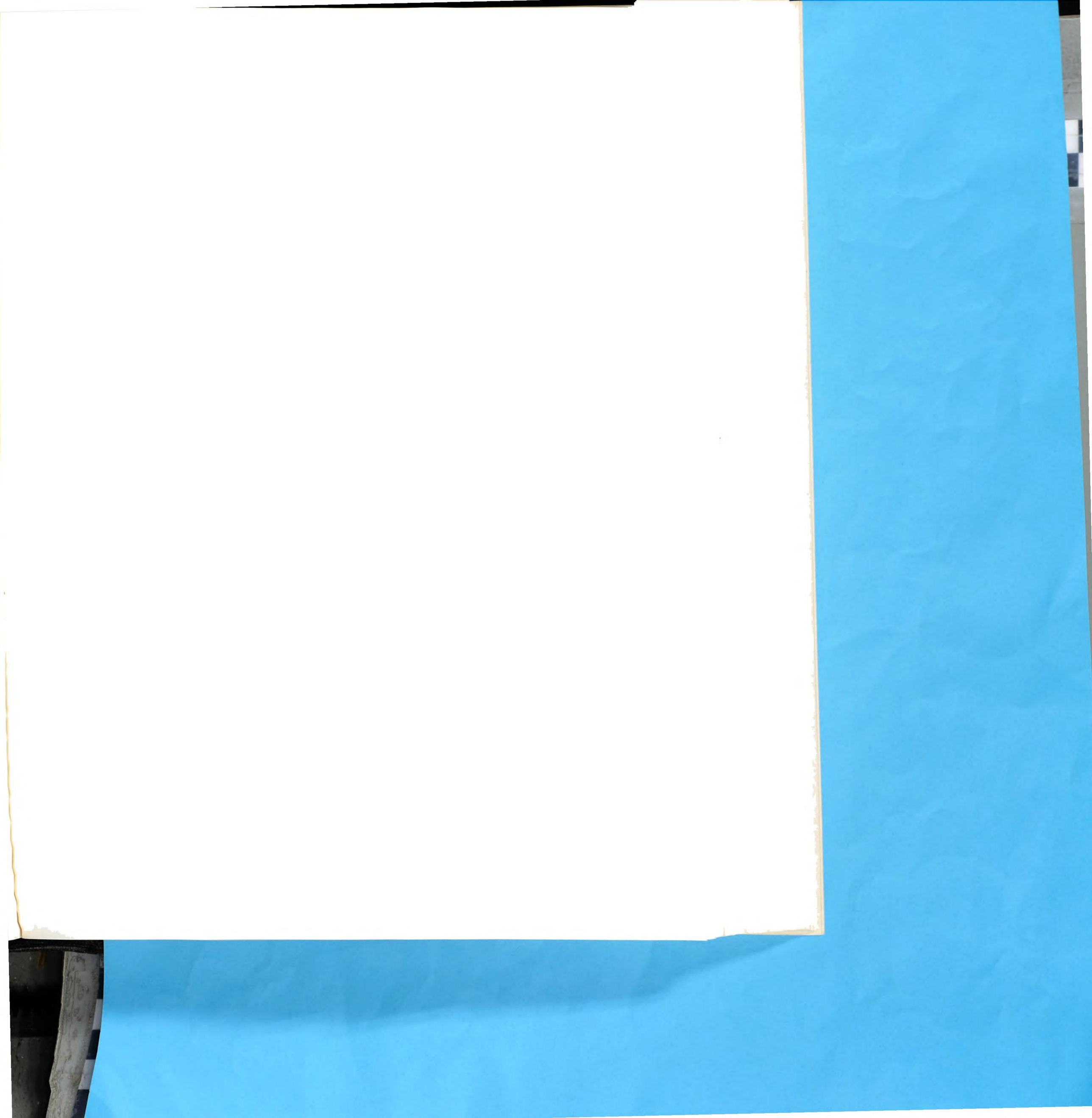

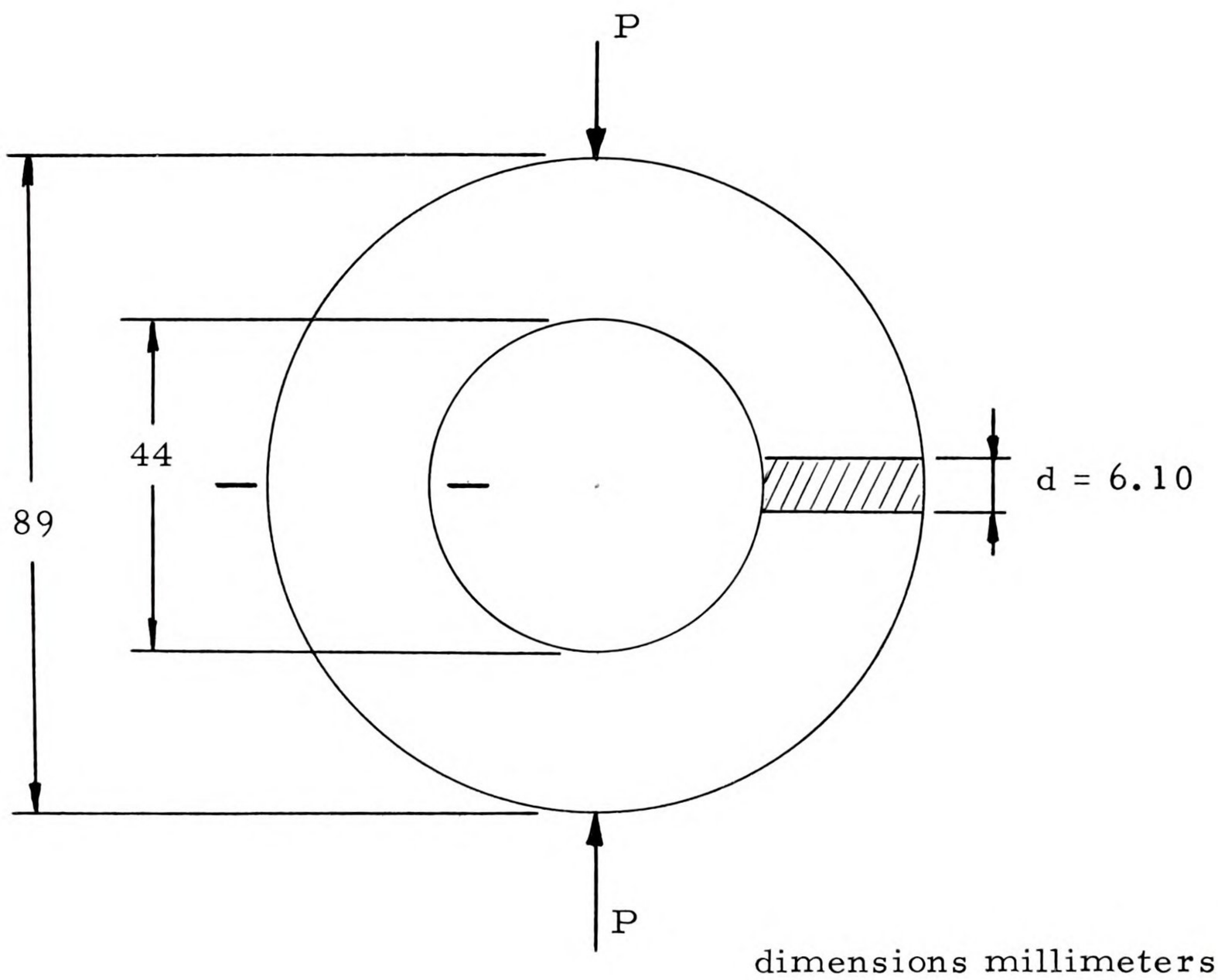

(a) ring model of cured Palatal P-6

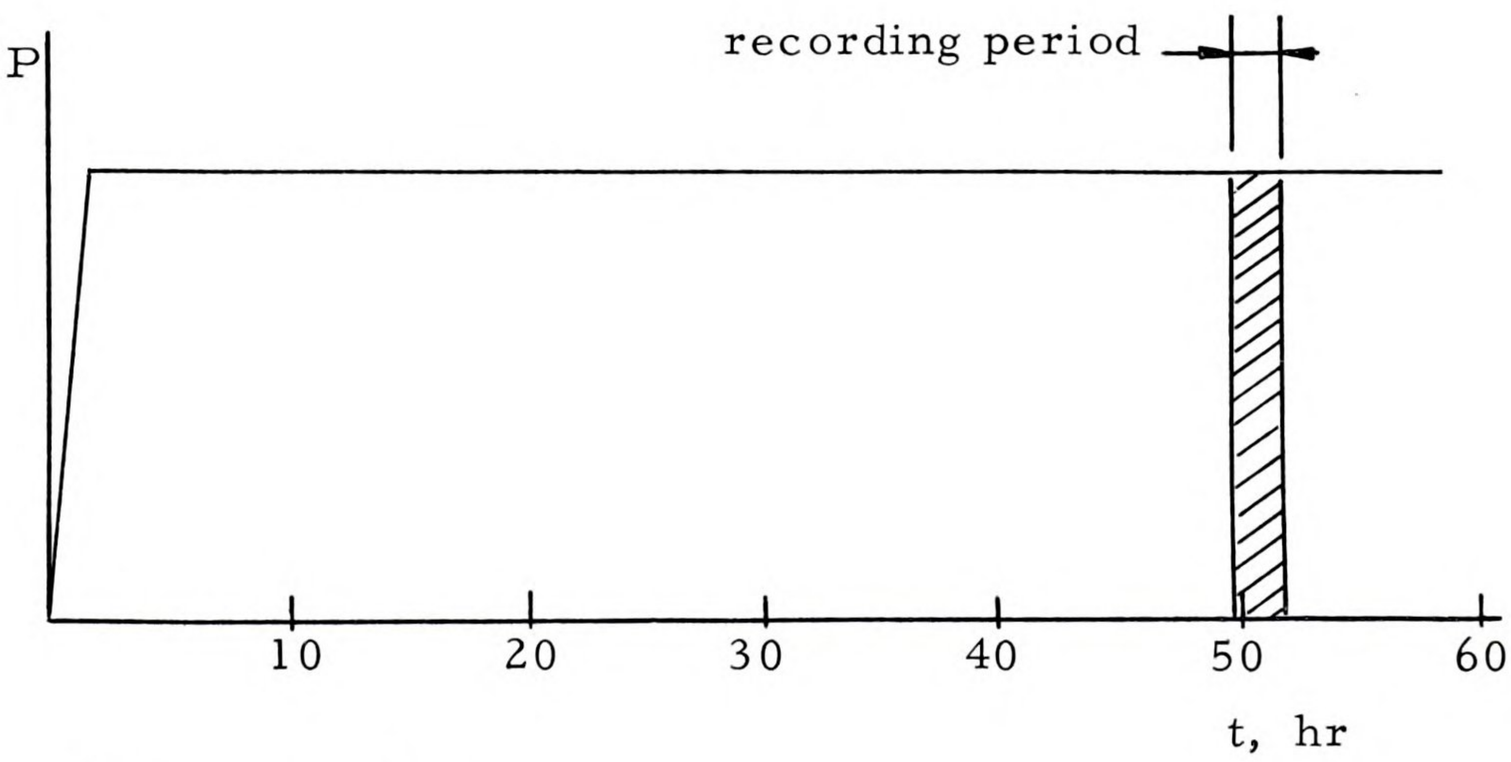

(b) load history

Figure 3.3. Ring Model of Cured Palatal P-6, Load History.

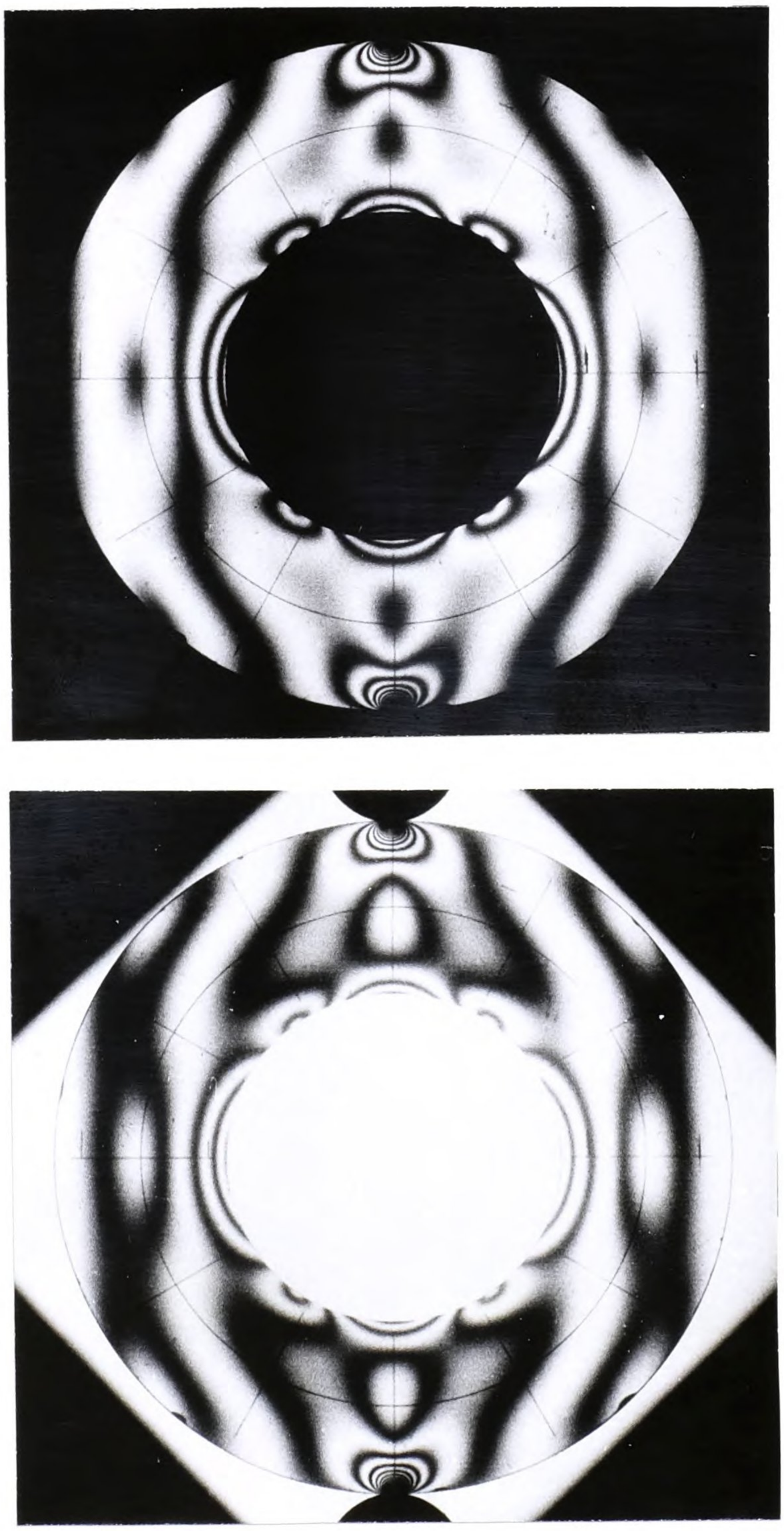

Figure 3.4. Isochromatic Pattern in P-6 Ring for λ = 1083 nm with Circular Polarization.

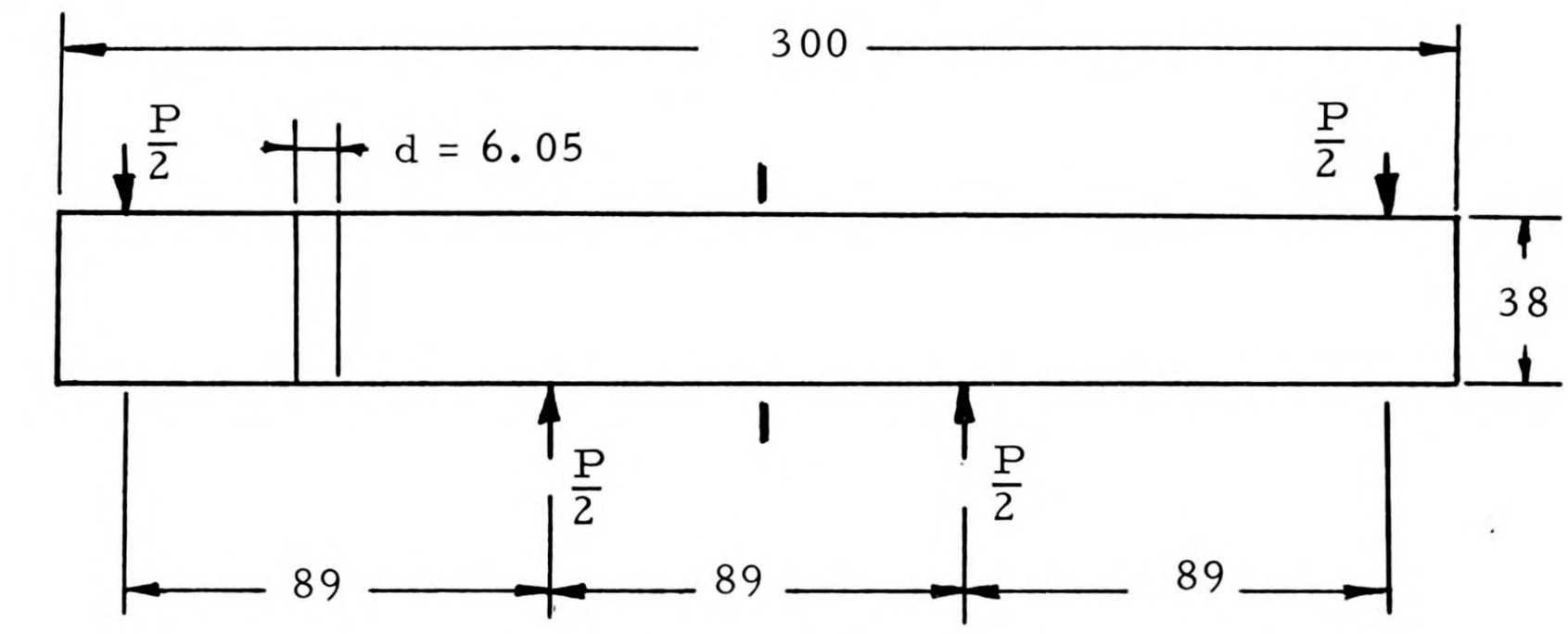

(a) beam model of cured Palatal P-6

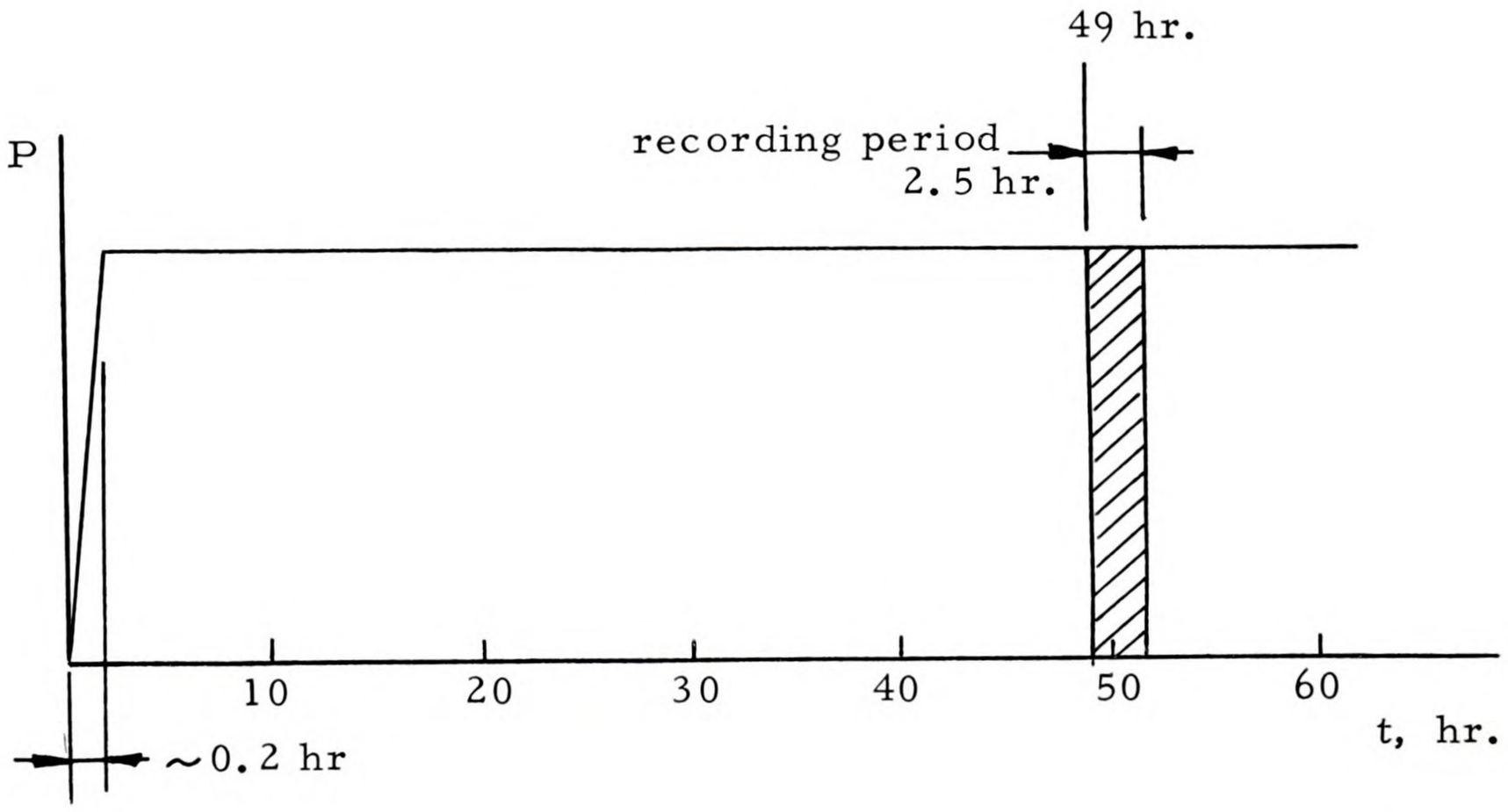

(b) load history

Figure 3.5. Beam Model of Cured P-6, Load History.

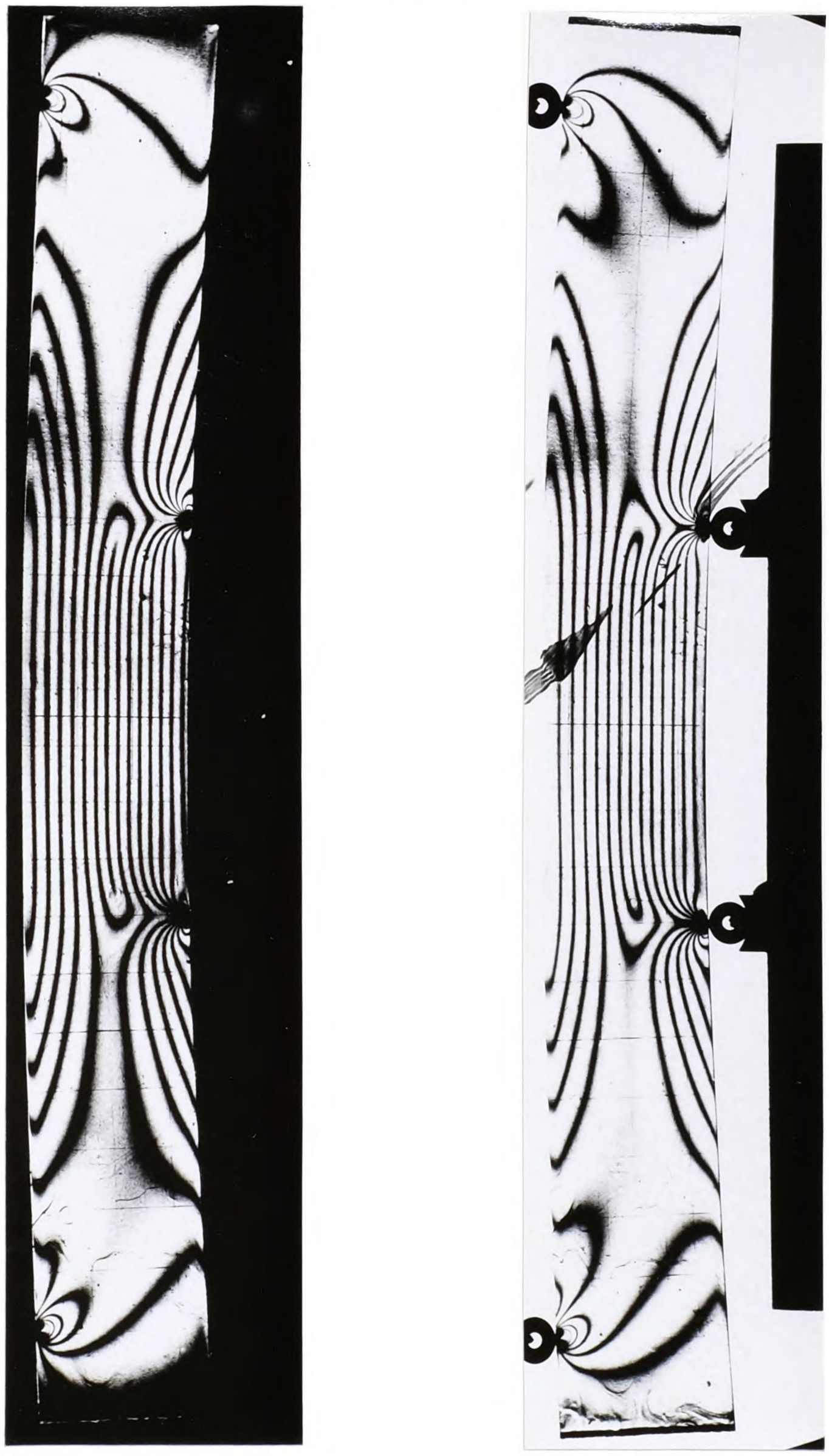

Figure 3.6a. Isochromatic Pattern in P-6 Beam for λ = 546 nm with Circular Polarization.

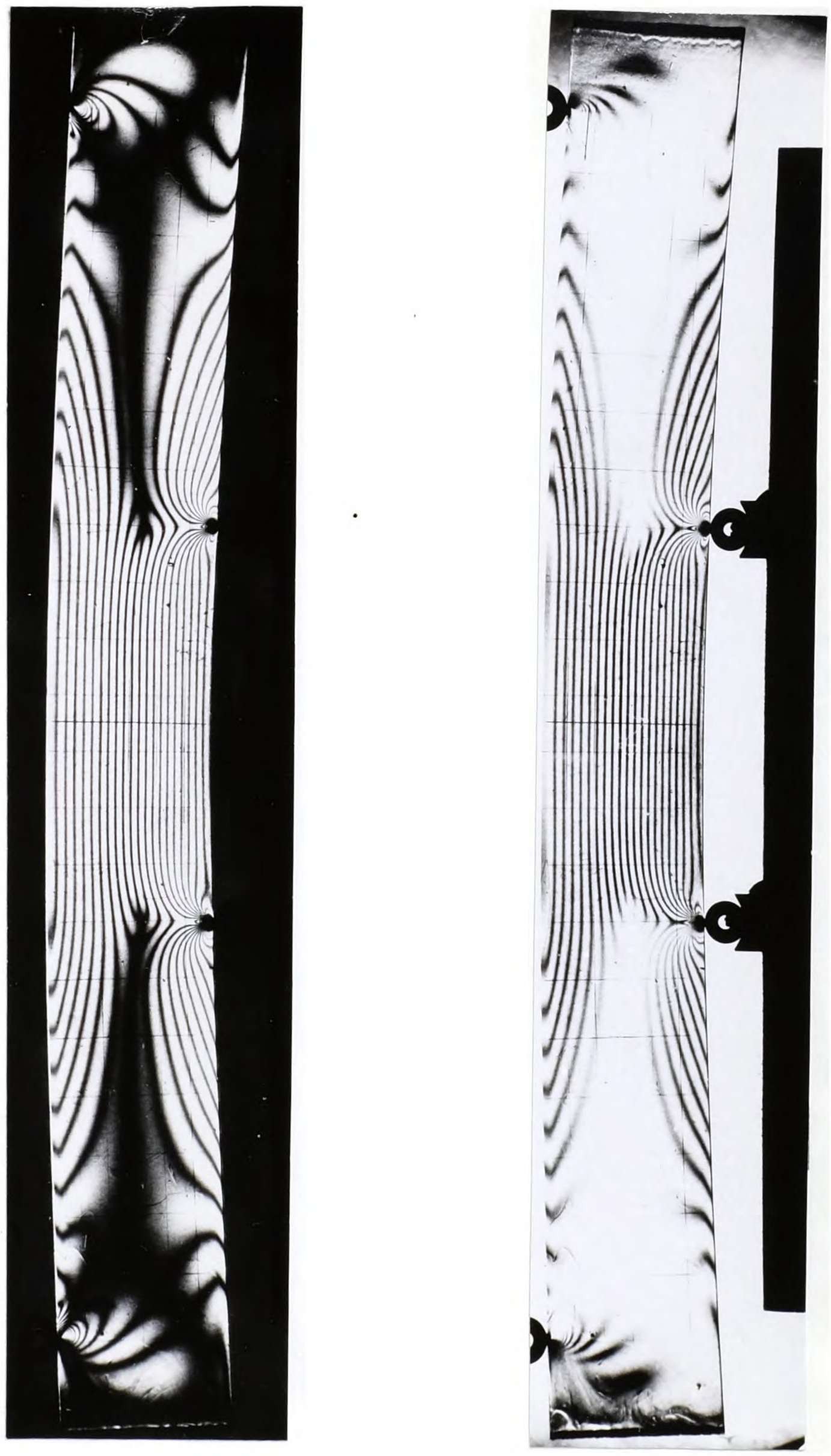

Figure 3.6b. Isochromatic Pattern in P-6 Beam for λ = 405 nm with Linear Polarization.

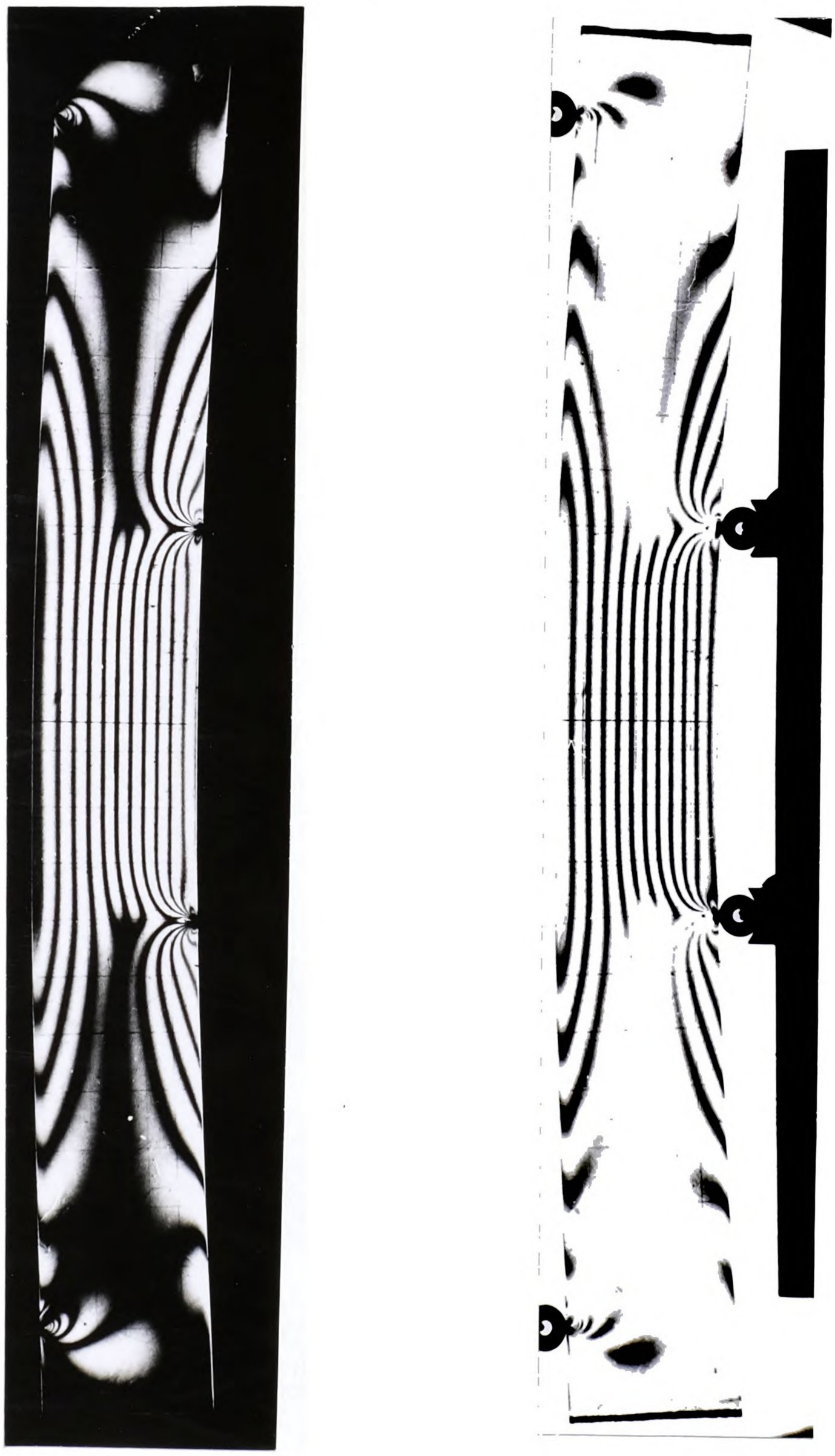

Figure 3.6c. Isochromatic Pattern in P-6 Beam for λ = 668 nm with Linear Polarization.

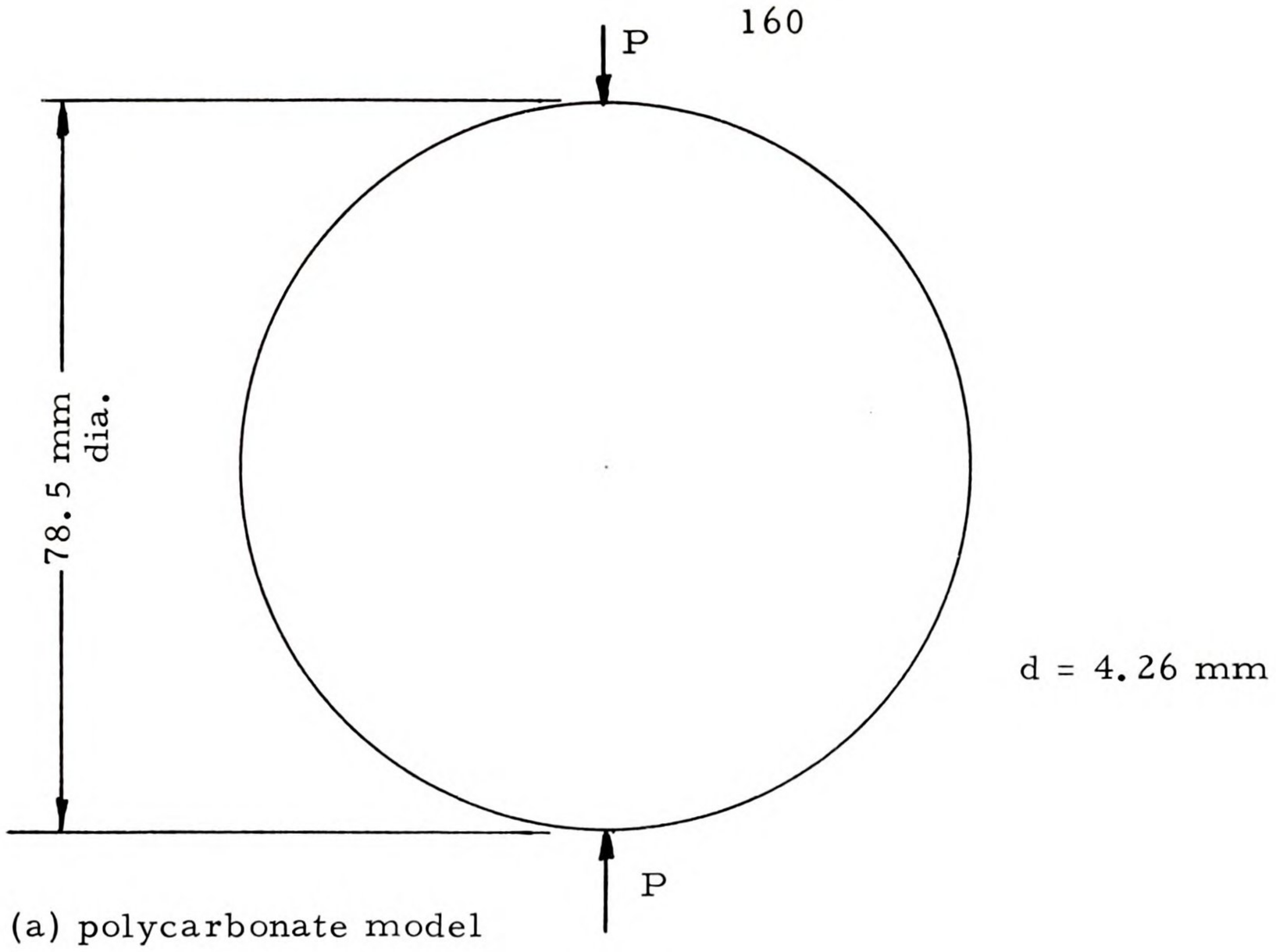

(a) polycarbonate model

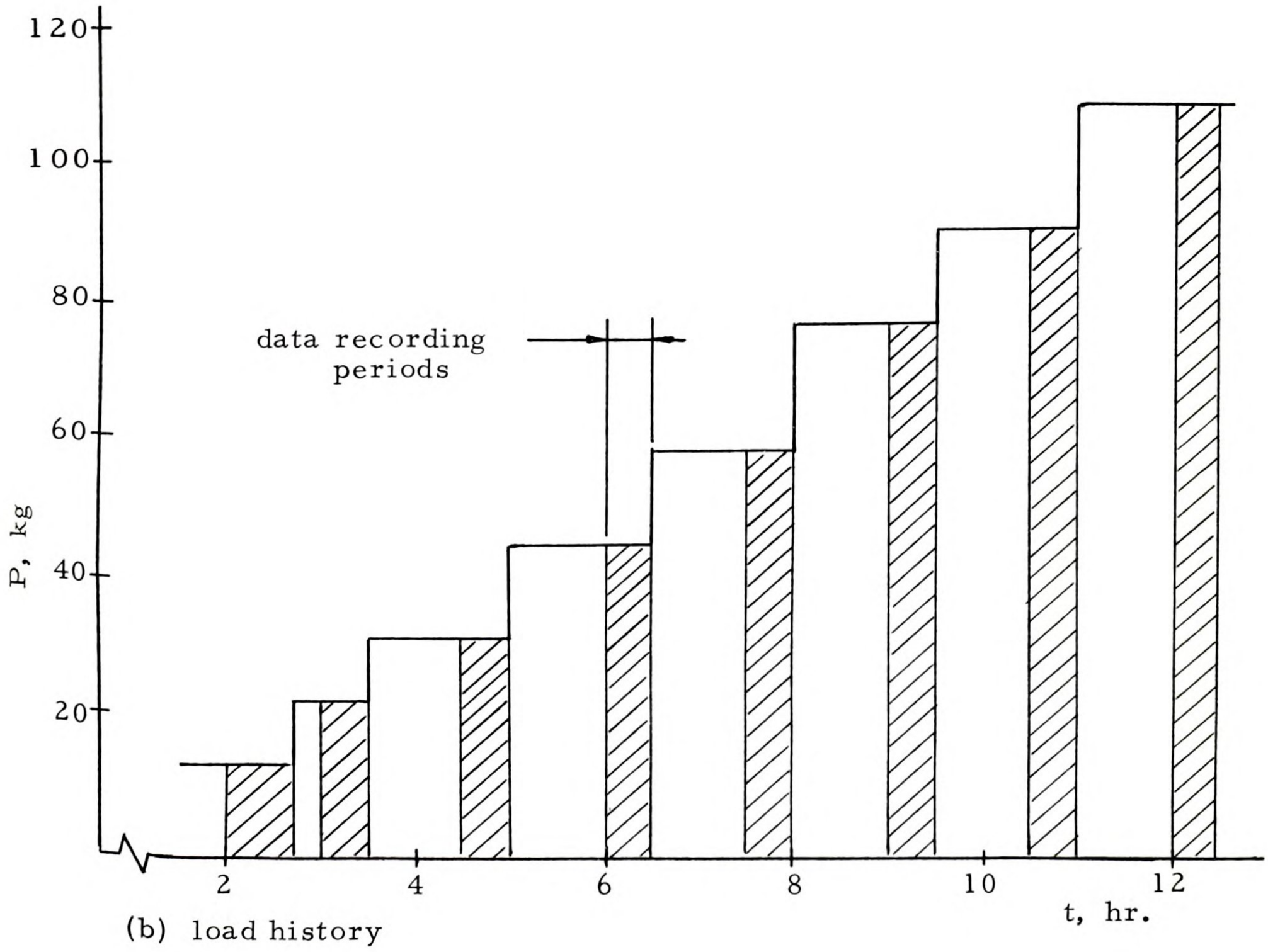

(b) load history

Figure 3.7. Disc Model of Polycarbonate, Load History.

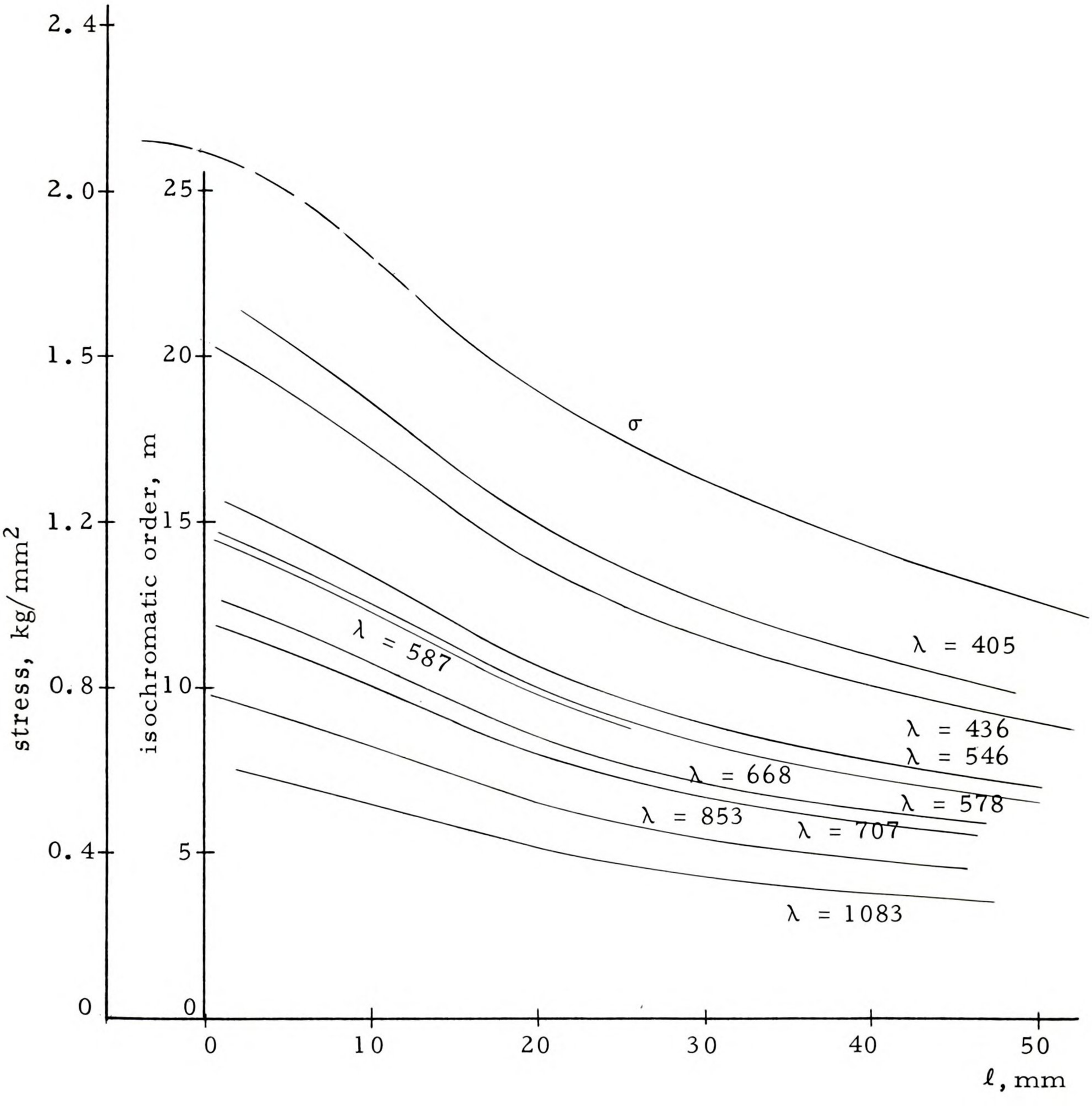

Figure 3.8. Fringe Order for Constant Wavelength and Calculated Stress Along Axis of Portion of CR-39 Model.

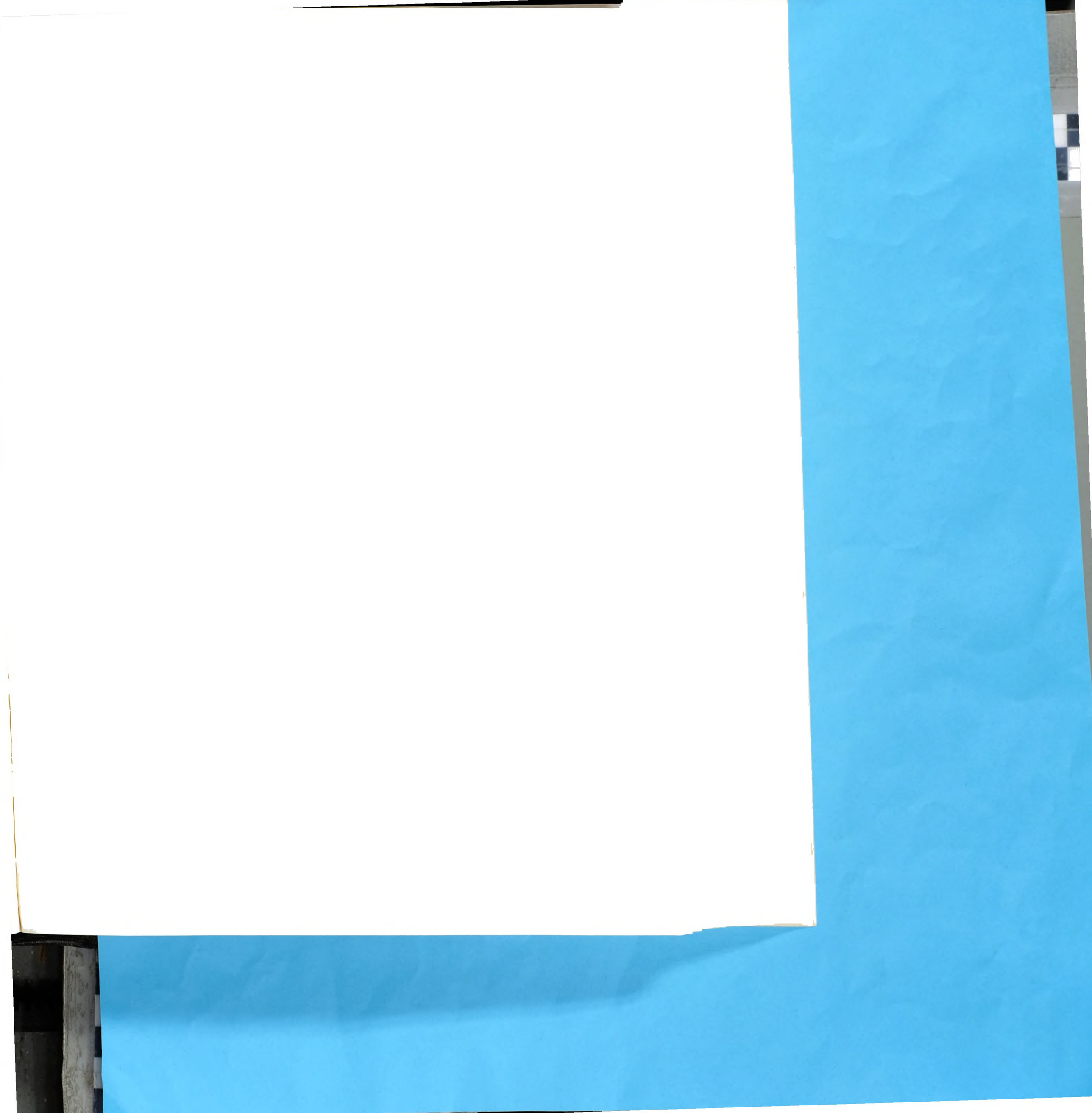

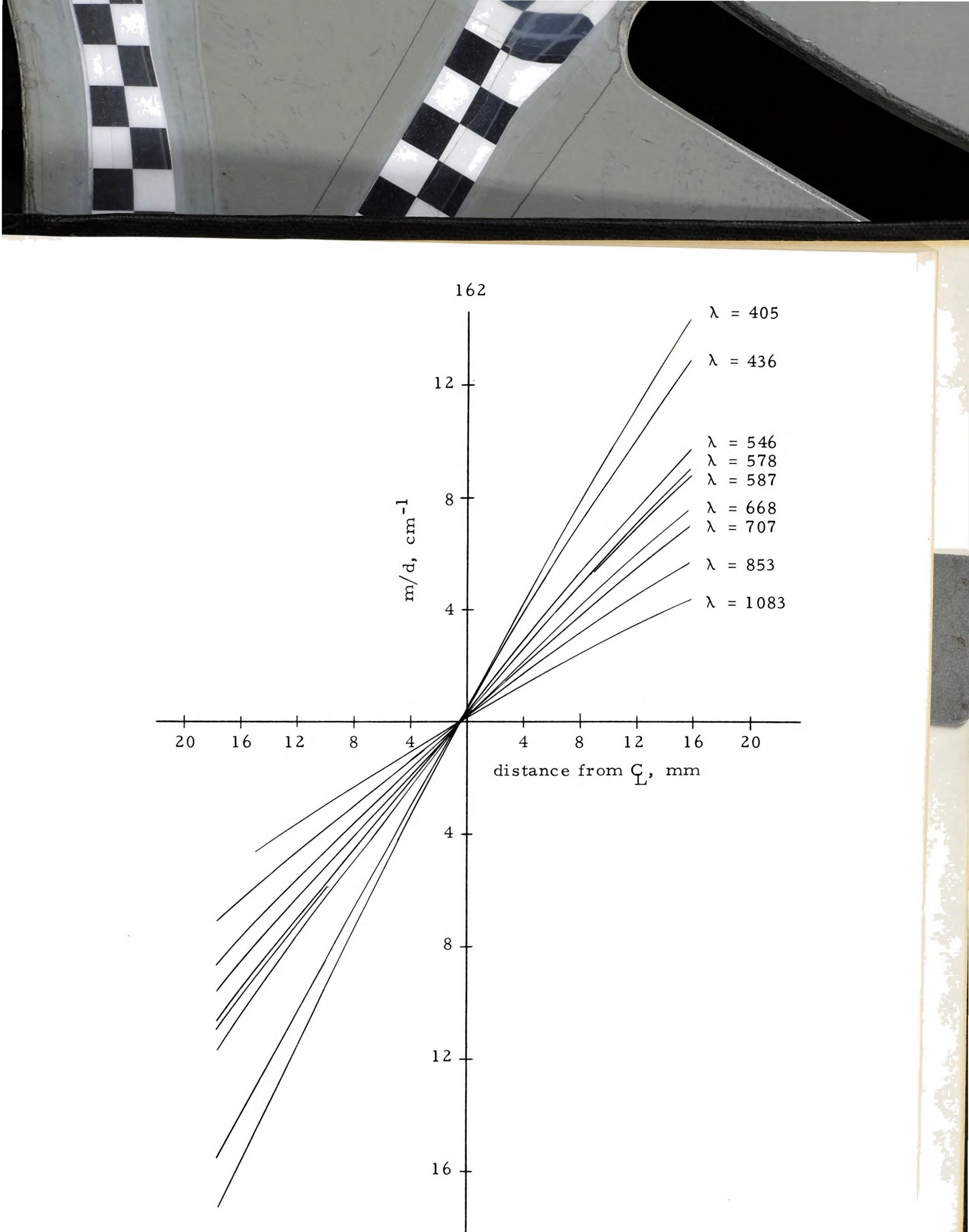

Figure 3.9. Fringe Order per Unit Thickness for Constant Wavelength in P-6 Beam.

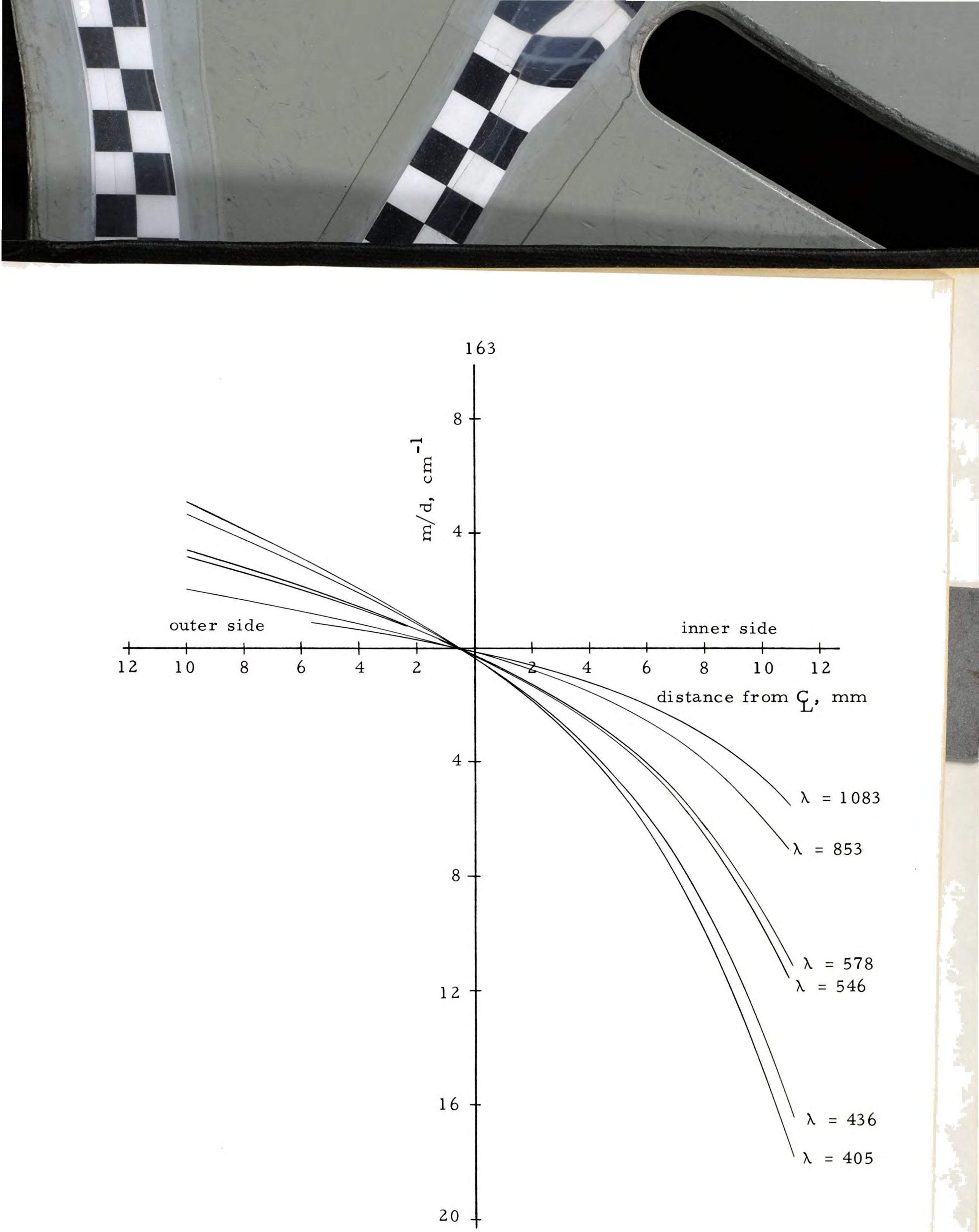

Figure 3.10. Fringe Order Per Unit Thickness for Constant Wavelength in P-6 Ring.

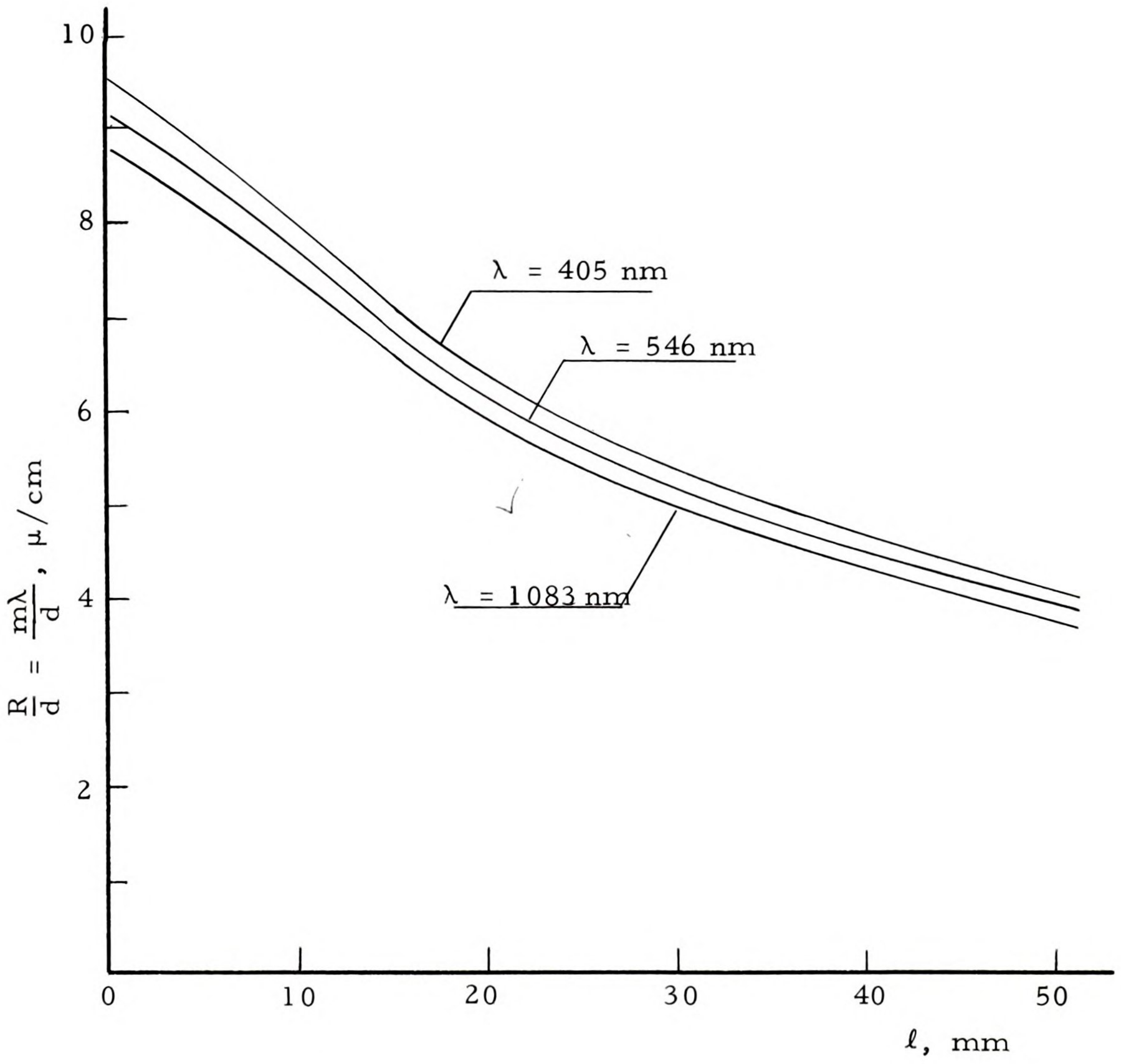

Figure 3.11. Retardation Per Unit Thickness Along Axis of CR-39 Model for Various Wavelengths.

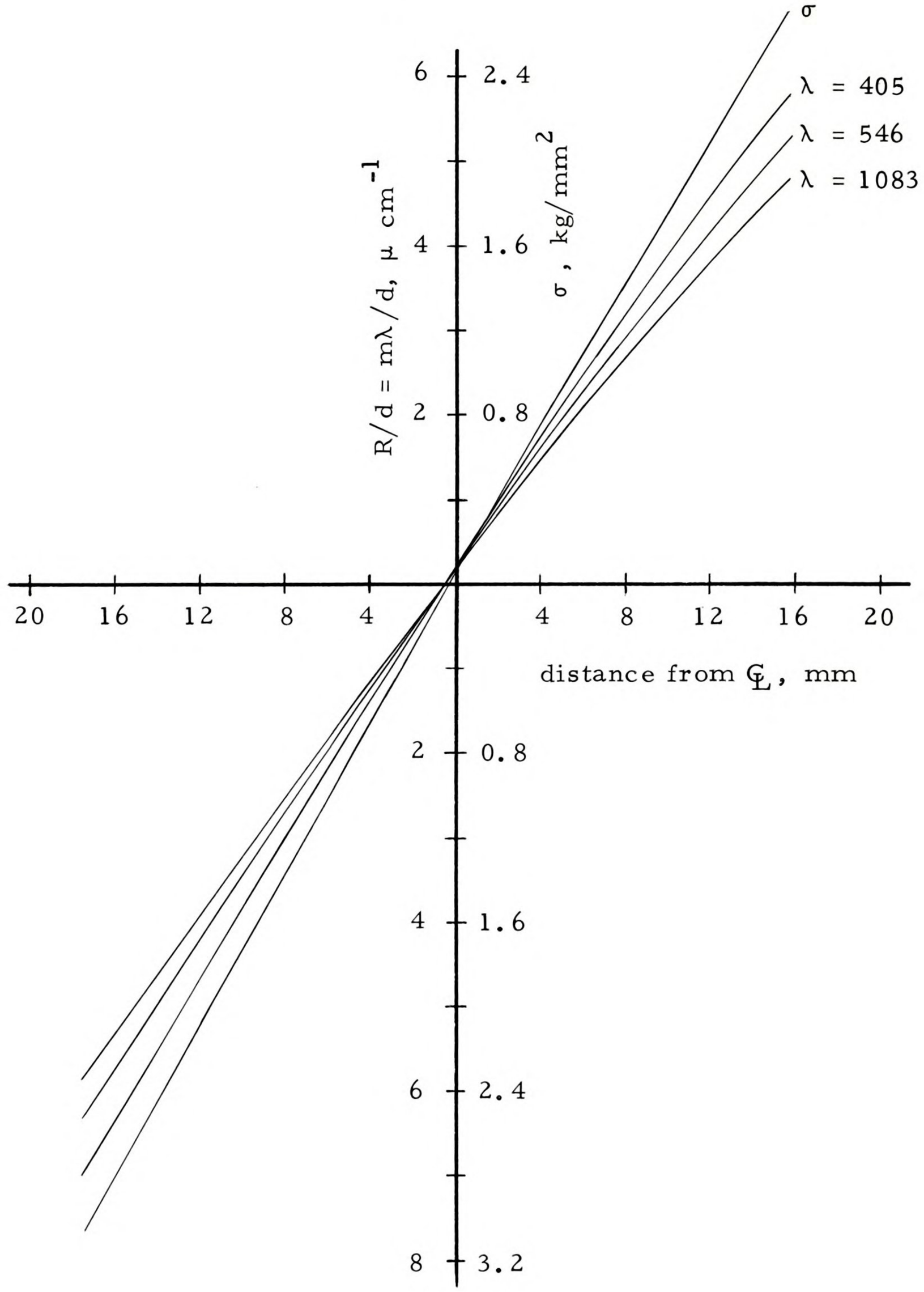

Figure 3.12. Retardation Per Unit Thickness for Constant Wavelengths and Stress by Curved Beam Theory for P-6 Beam.

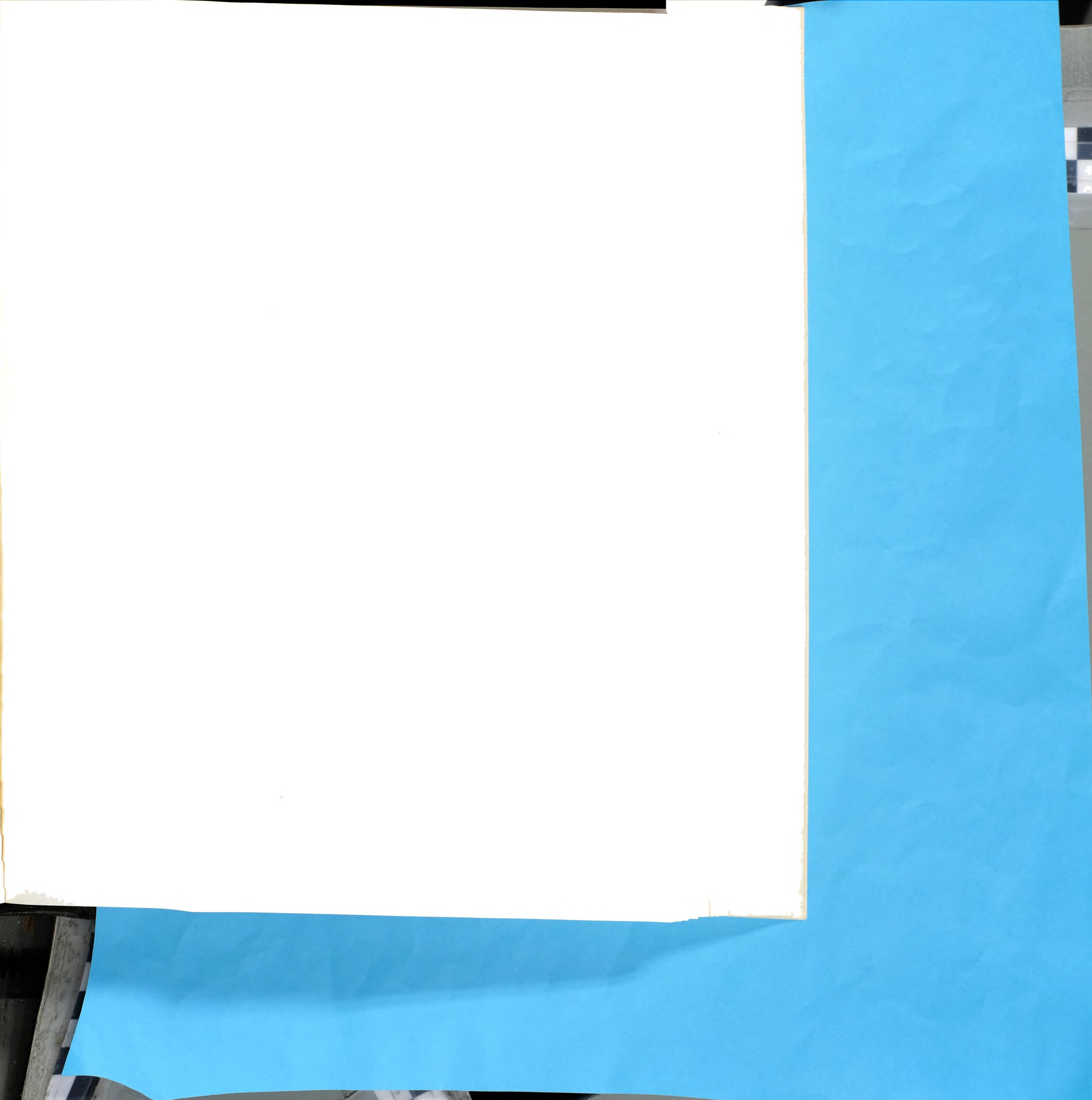

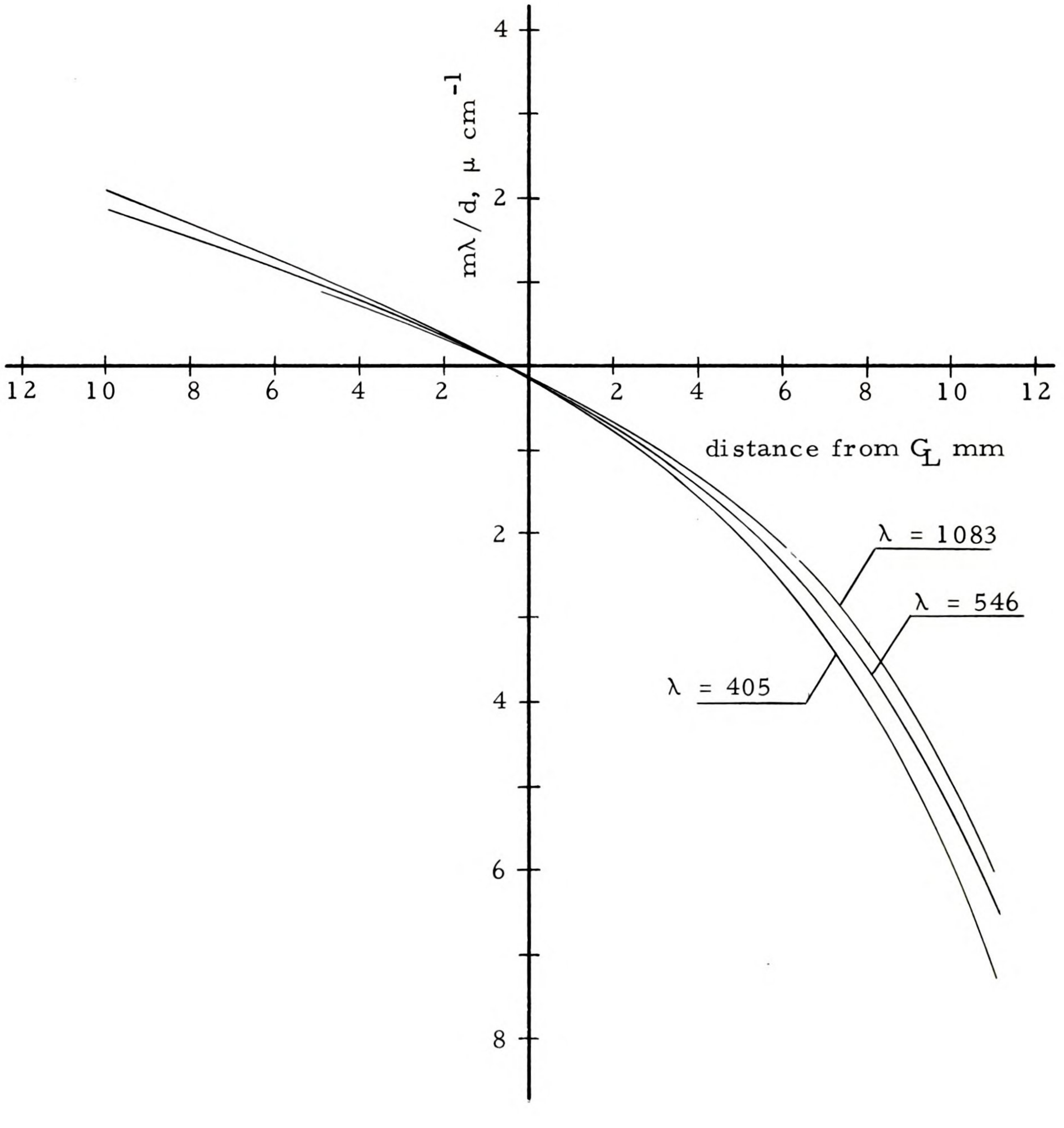

Figure 3.13. Retardation Per Unit Thickness for Constant Wavelengths in P-6 Ring.

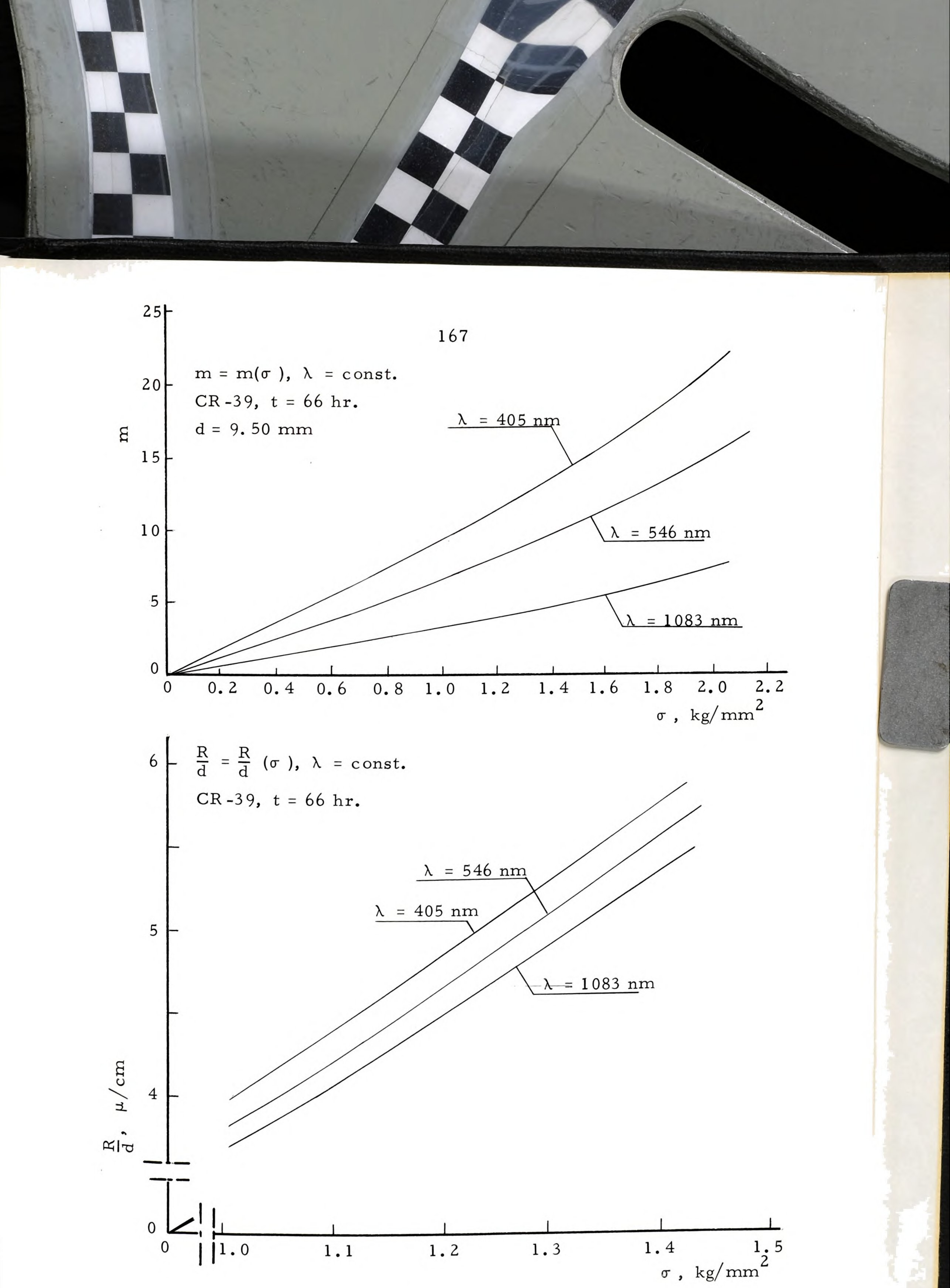

Figure 3.14. Fringe Order and Retardation Per Unit Thickness Versus Stress for Constant Wavelength in CR-39.

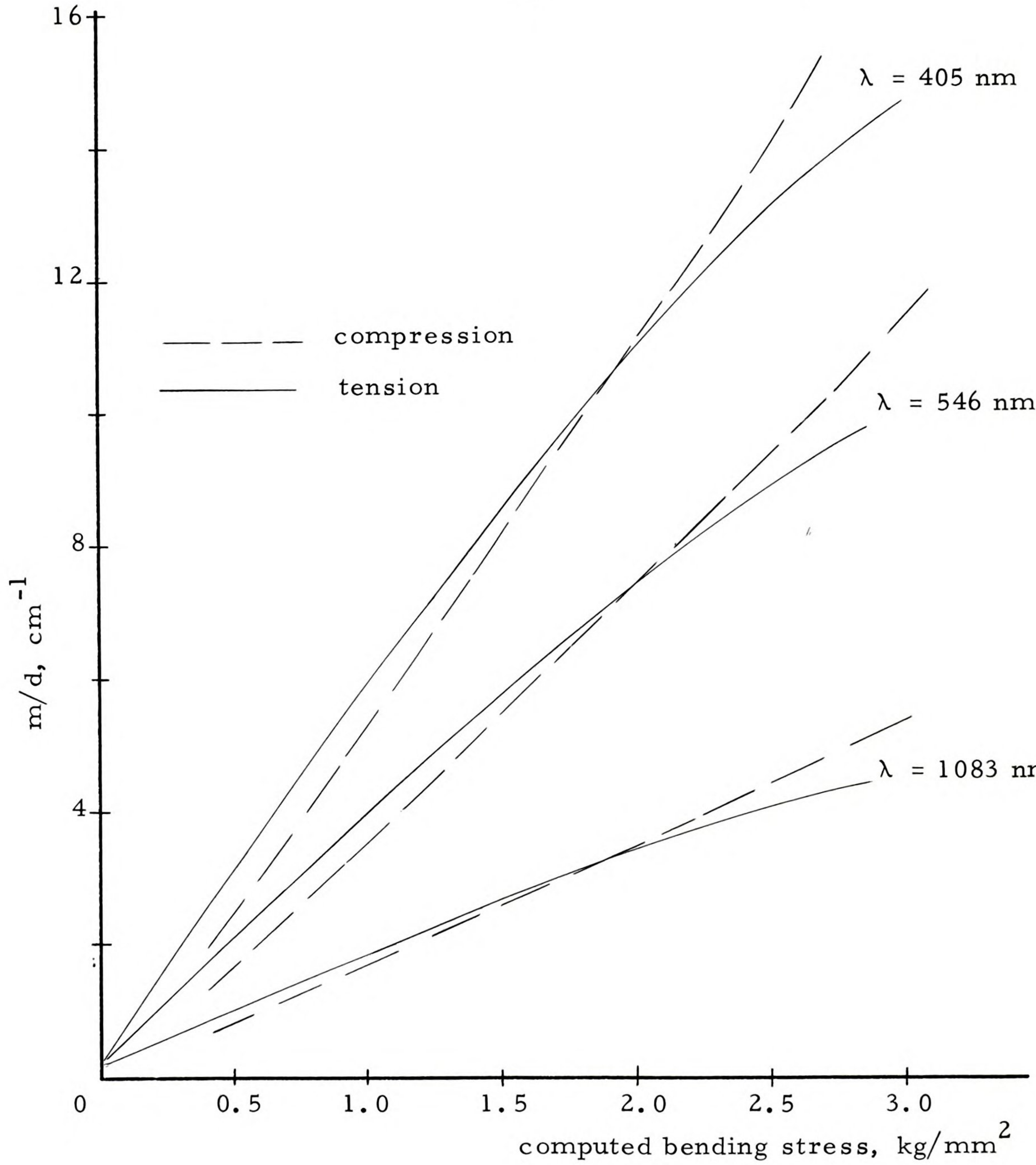

Figure 3.15. Examples of Fringe Order Per Unit Thickness at Constant Wavelength Versus Stress From Curved Beam Theory for P-6 Beam.

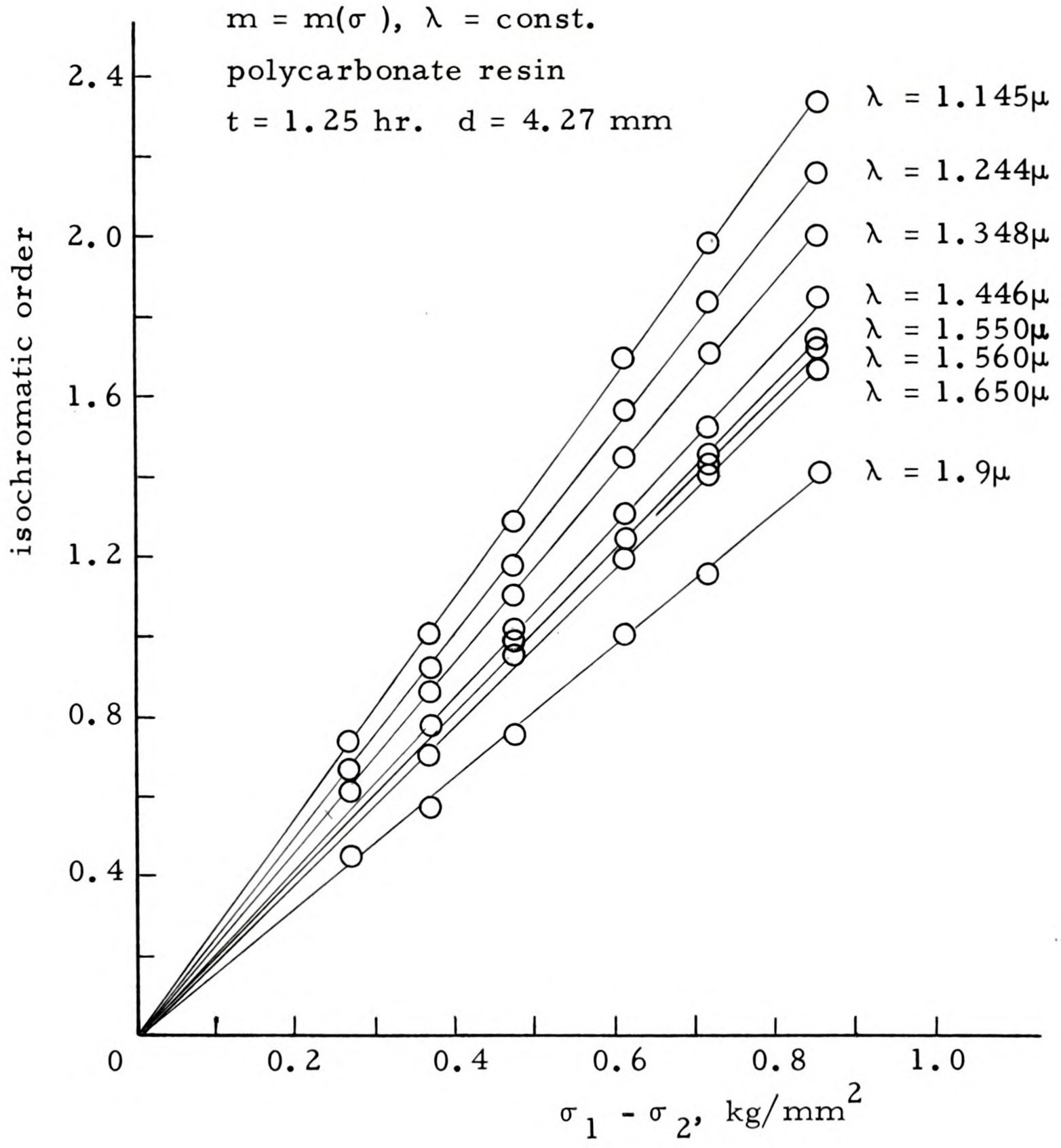

Figure 3.16. Fringe Order for Constant Wavelength Versus Corrected Stress in Polycarbonate.

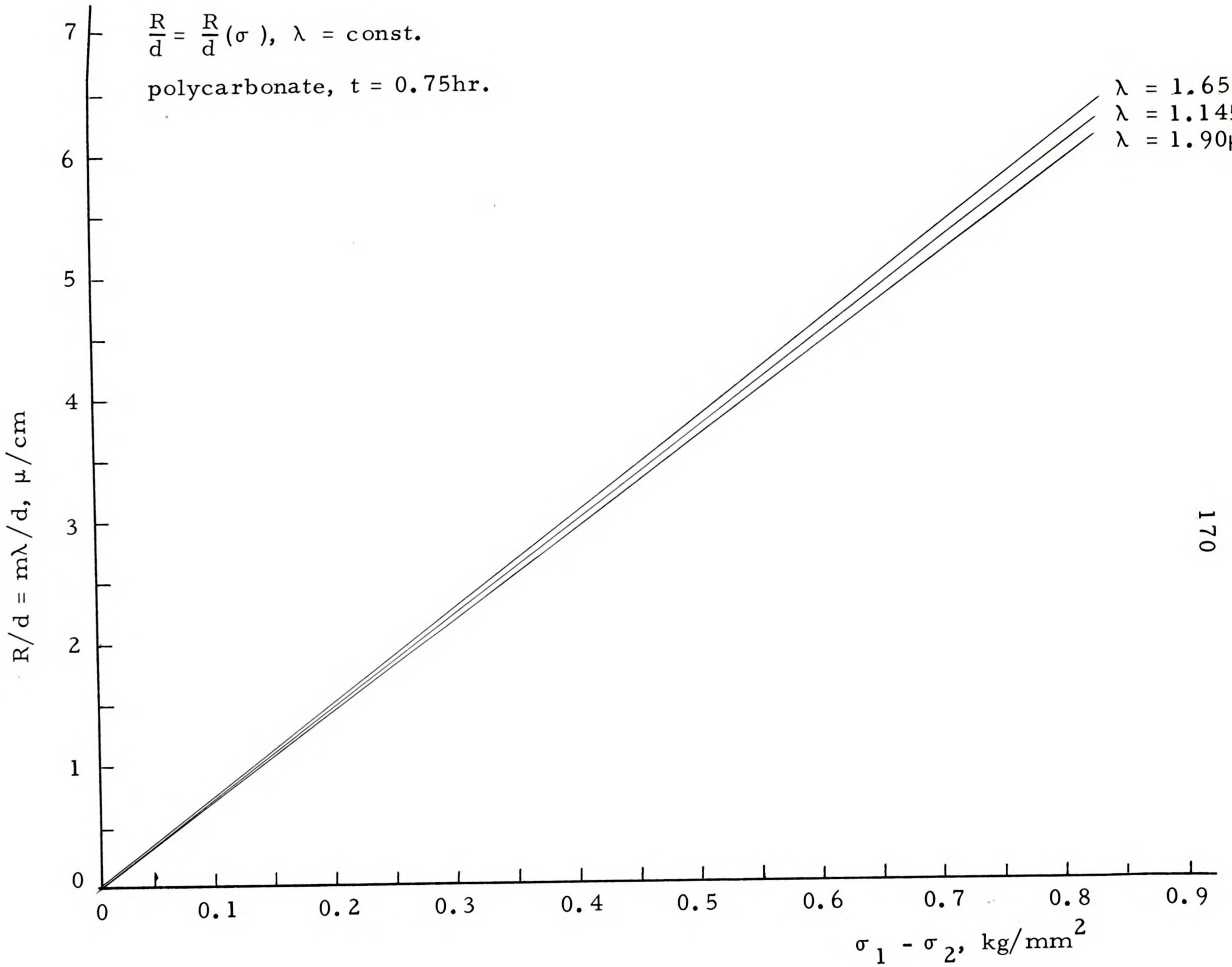

Figure 3.17. Representative Retardation Per Unit Thickness for Constant Wavelength Versus Corrected Stress in Polycarbonate.

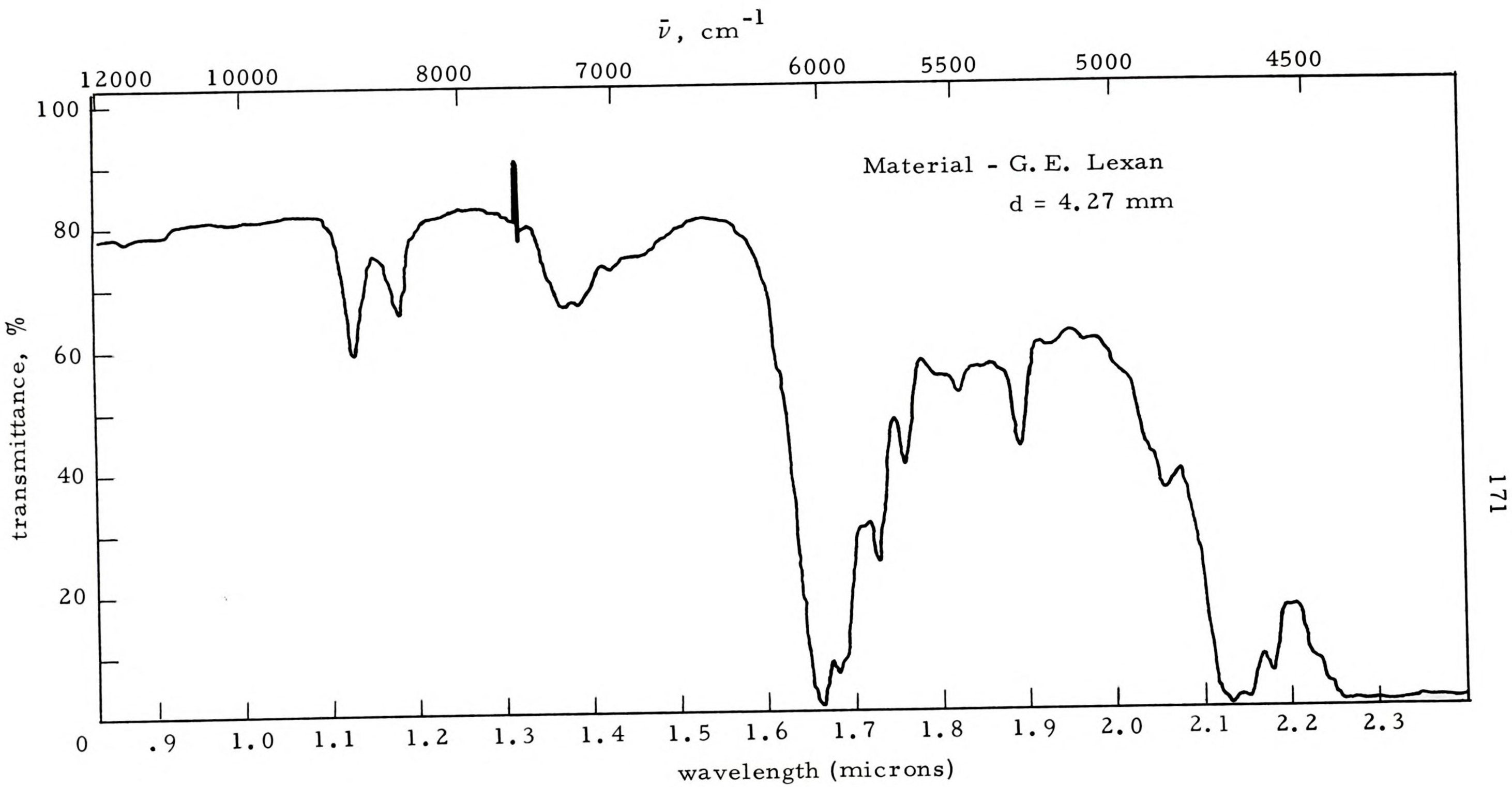

Figure 3.18. Spectral Transmittance of Polycarbonate.

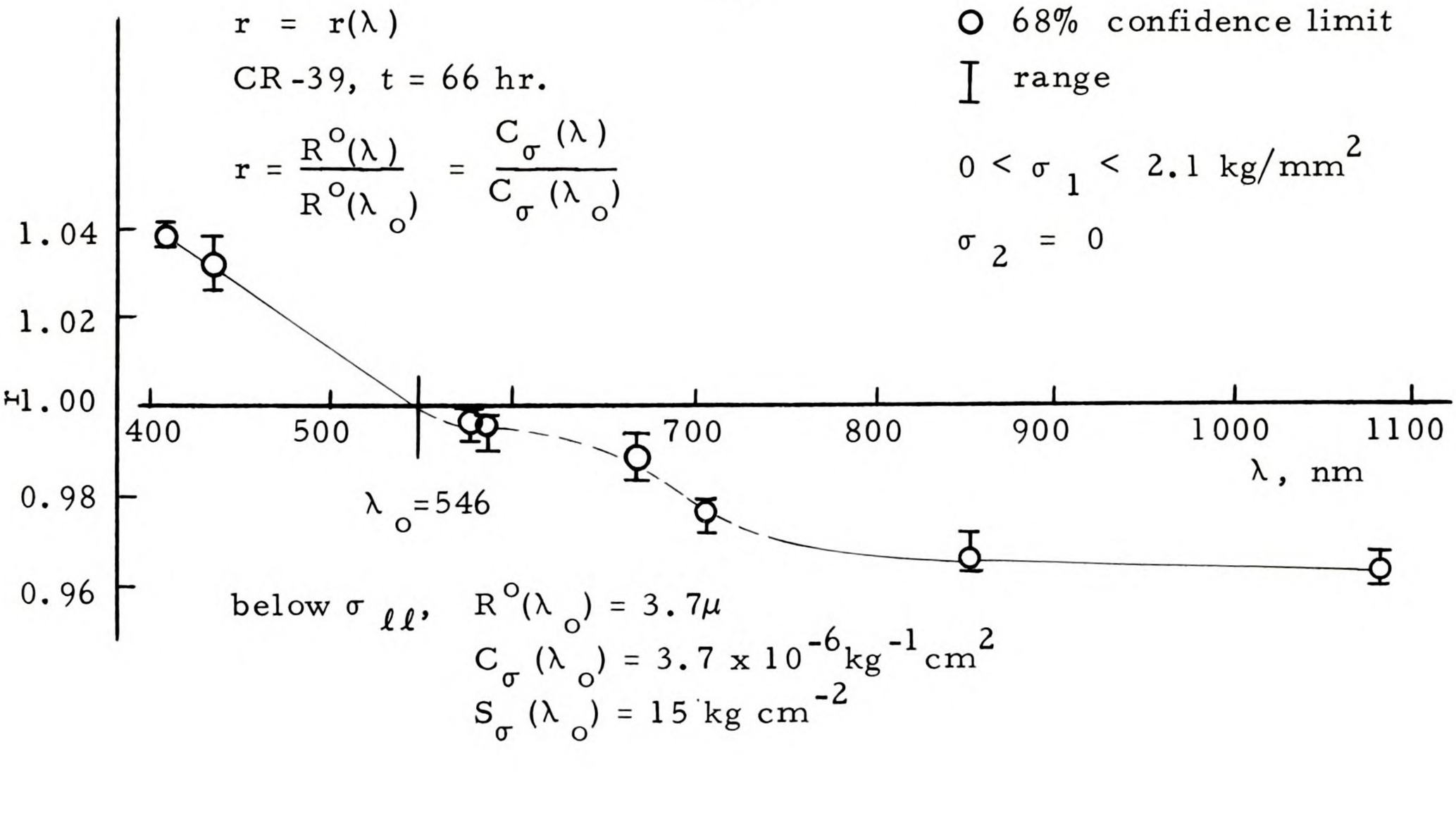

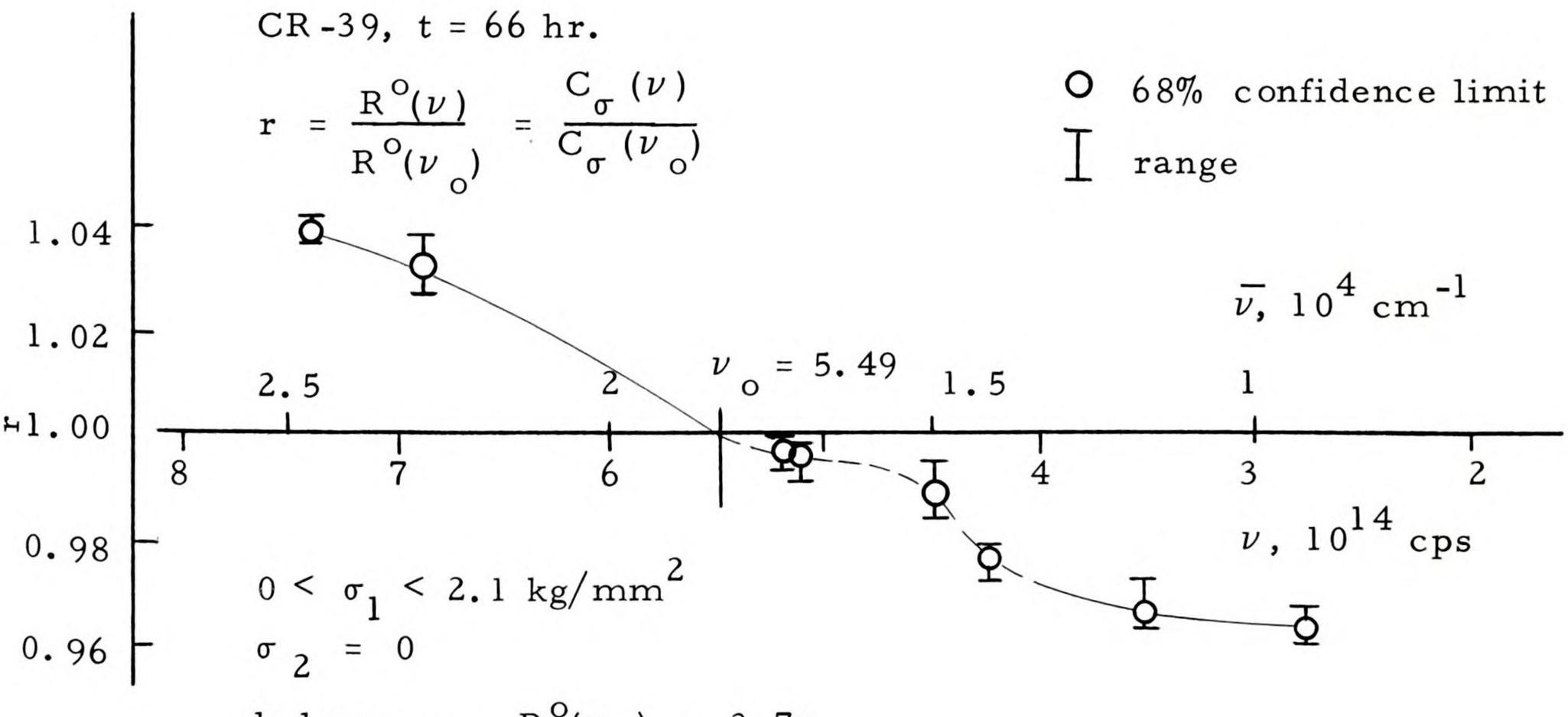

Figure 3.19. Normalized Retardation Versus Wavelength and Frequency for CR-39.

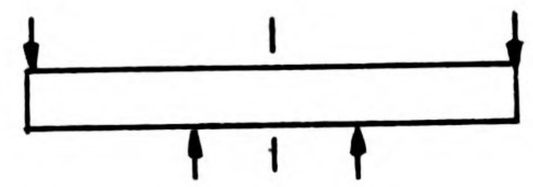

● mean for upper 1/3 of beam (tension)

○ mean for lower 1/3 of beam (compression)

I range

r = r(λ), t = 50 hr.

P-6, cured 90°C 40 hr.*

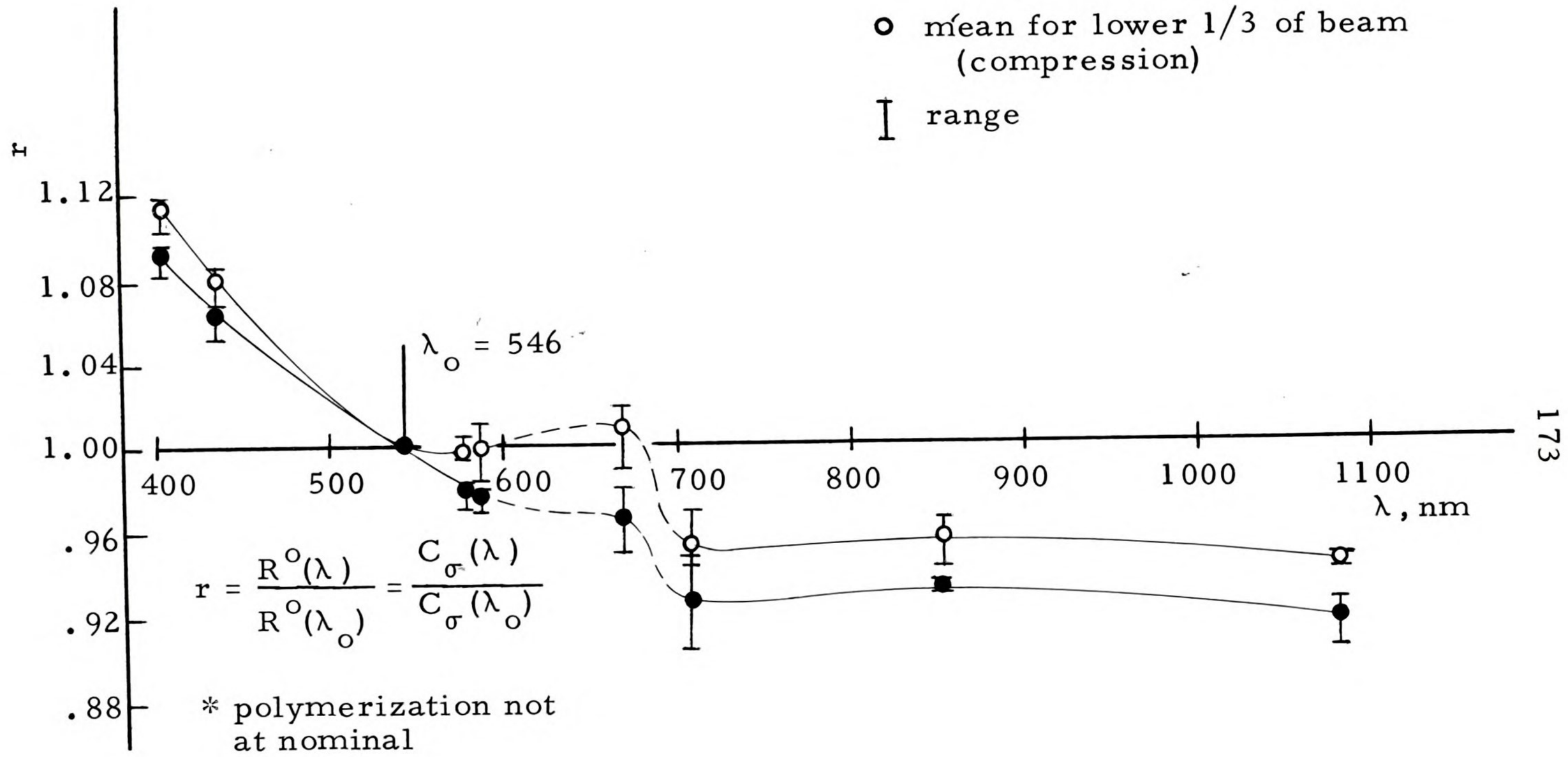

Figure 3.20(a). Representative Normalized Retardation Versus Wavelength for P-6.

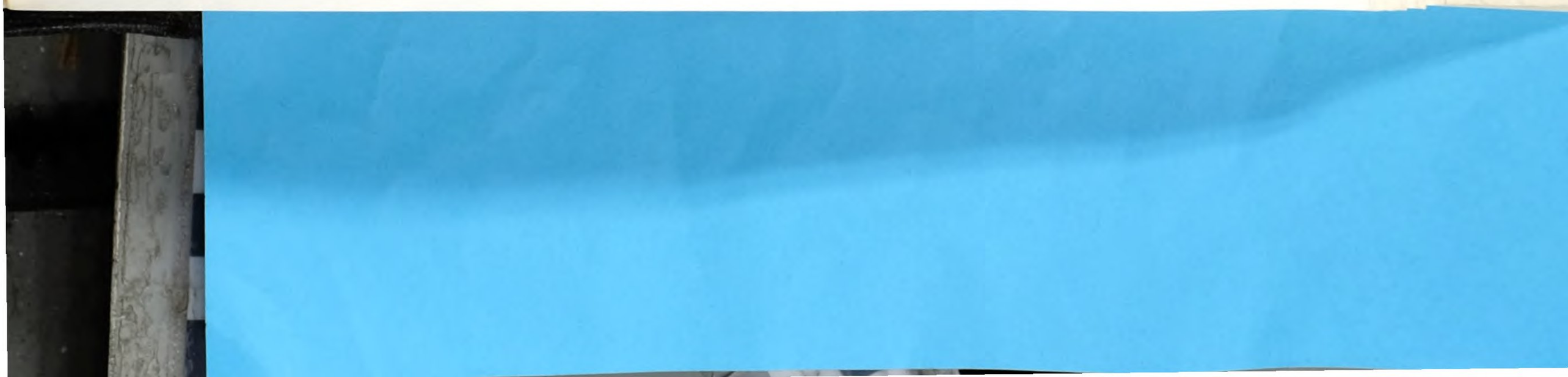

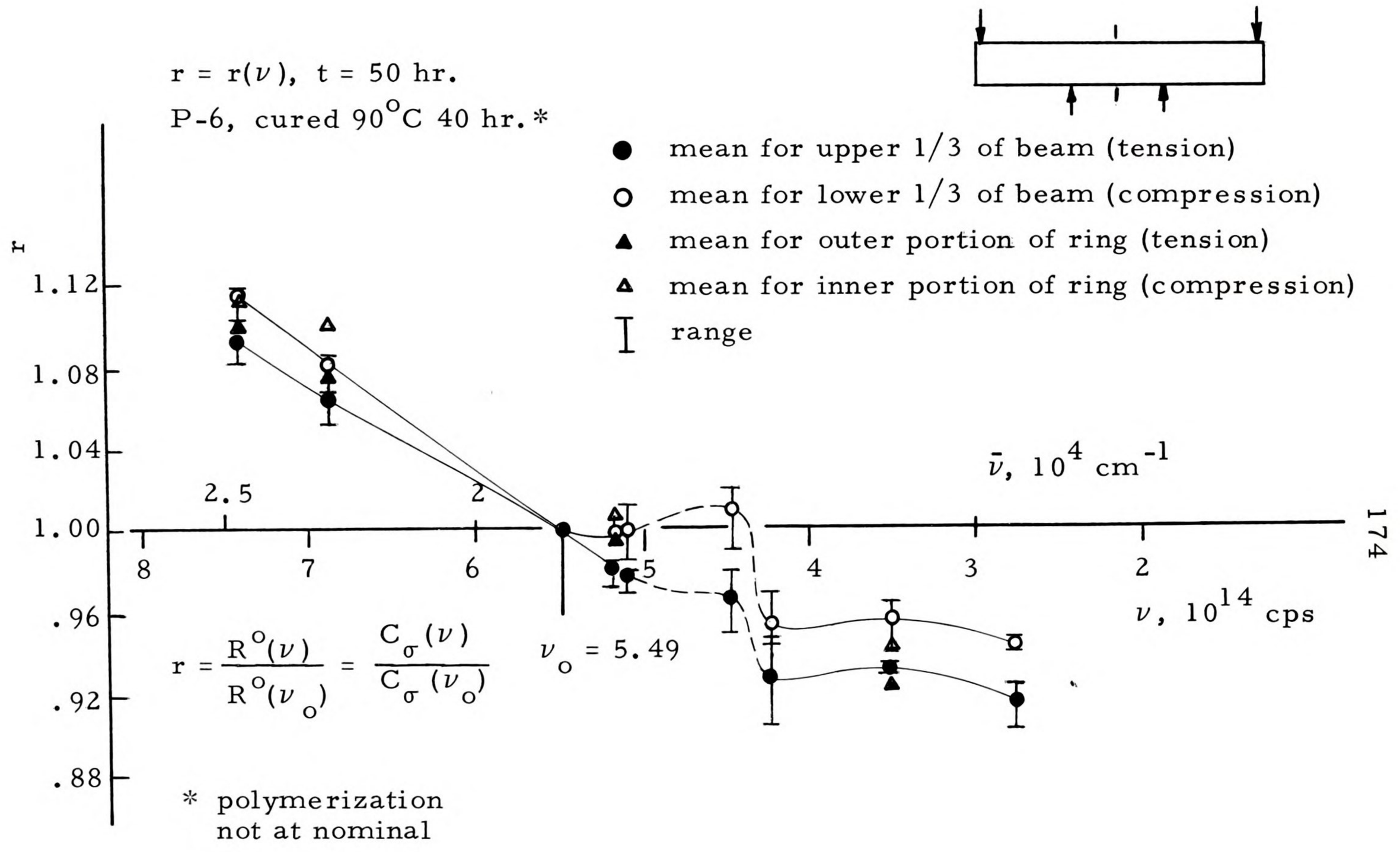

Figure 3.20(b). Representative Normalized Retardation Versus Frequency for P-6.

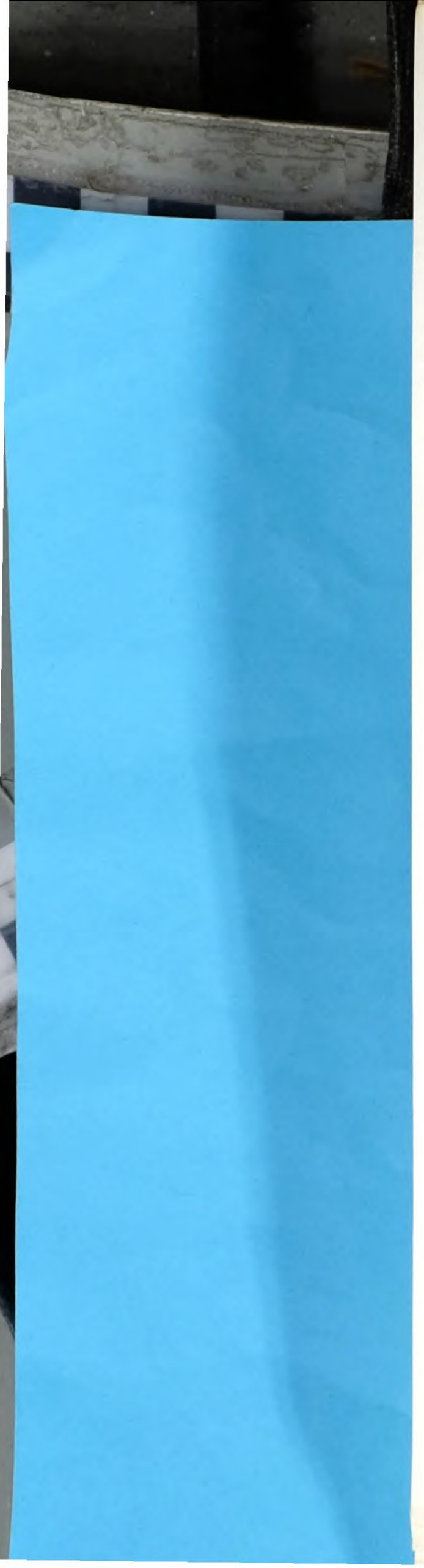

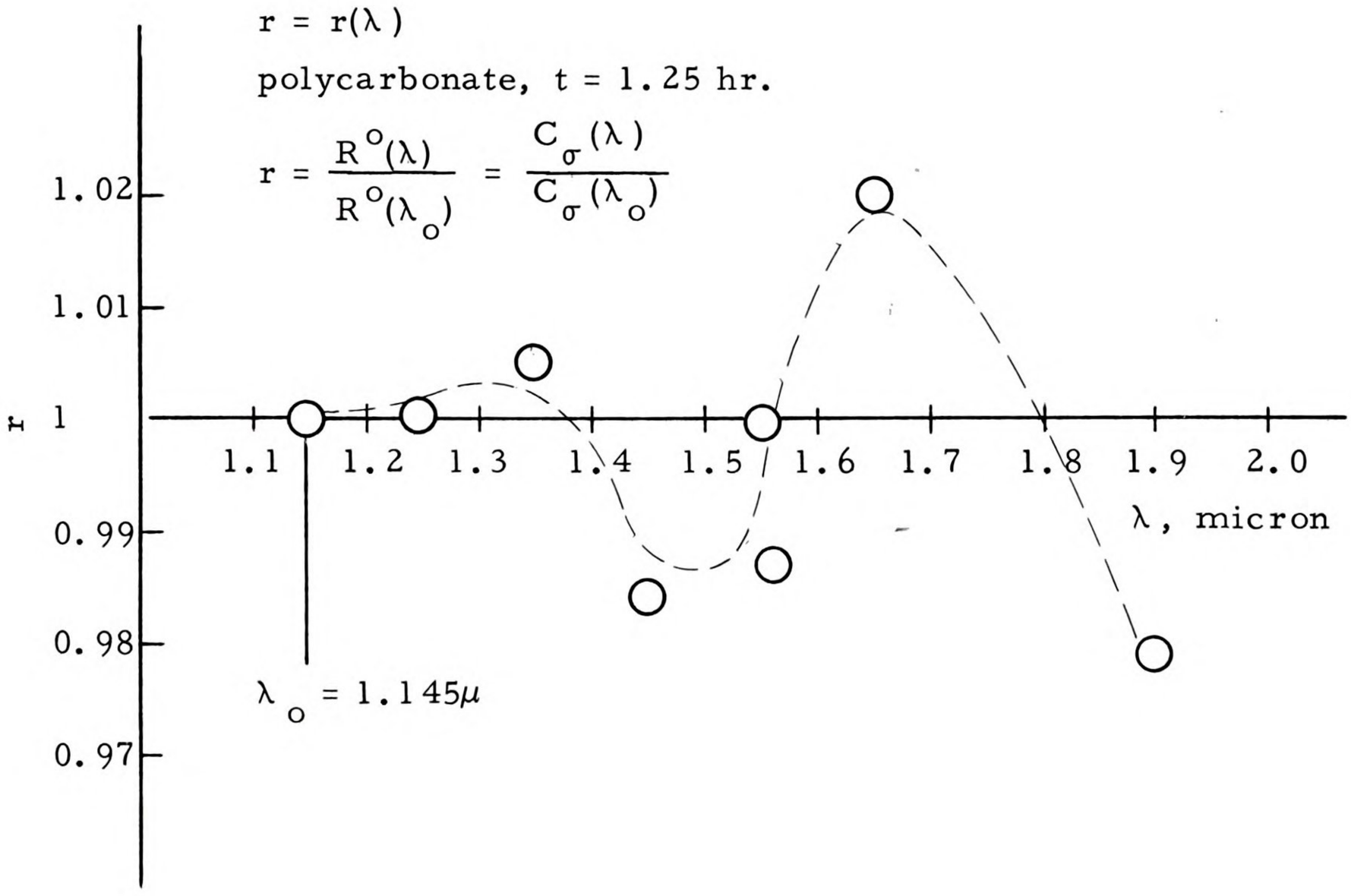

Figure 3.21. Normalized Retardation Versus Wavelength for Polycarbonate for $1\mu < \lambda < 2\mu$.

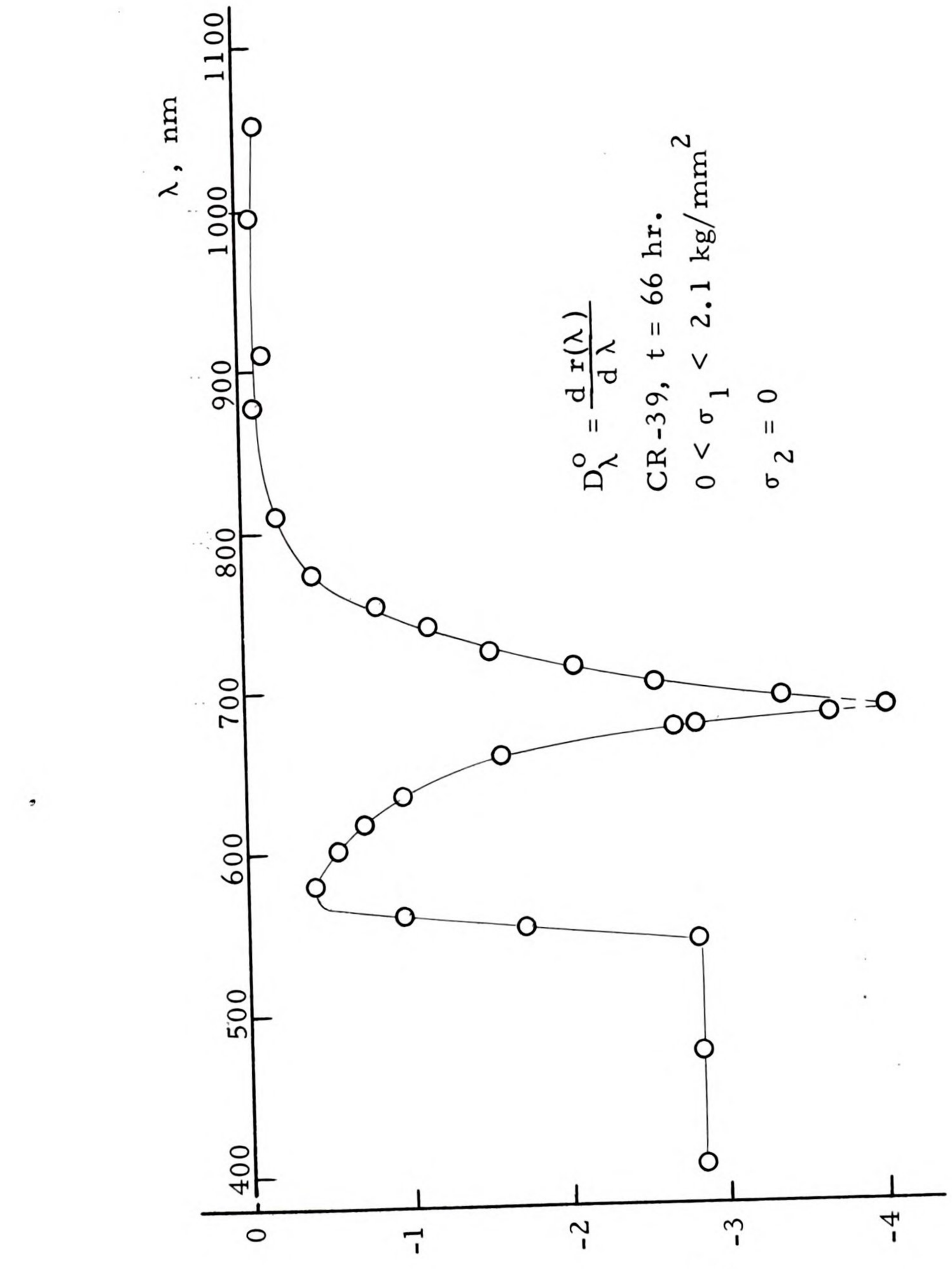

Figure 3.22(a). Dispersion of Birefringence Versus Wavelength for CR-39.

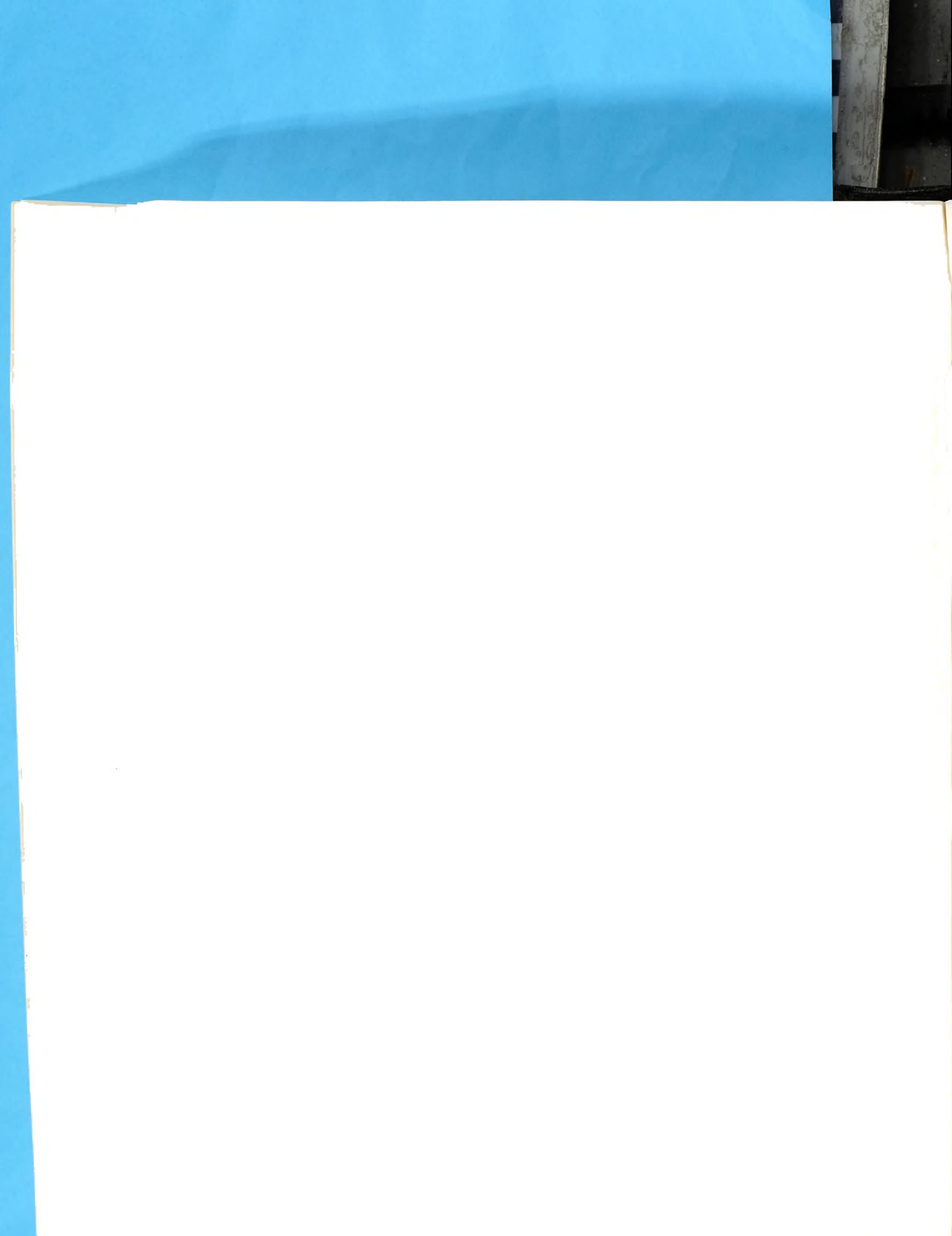

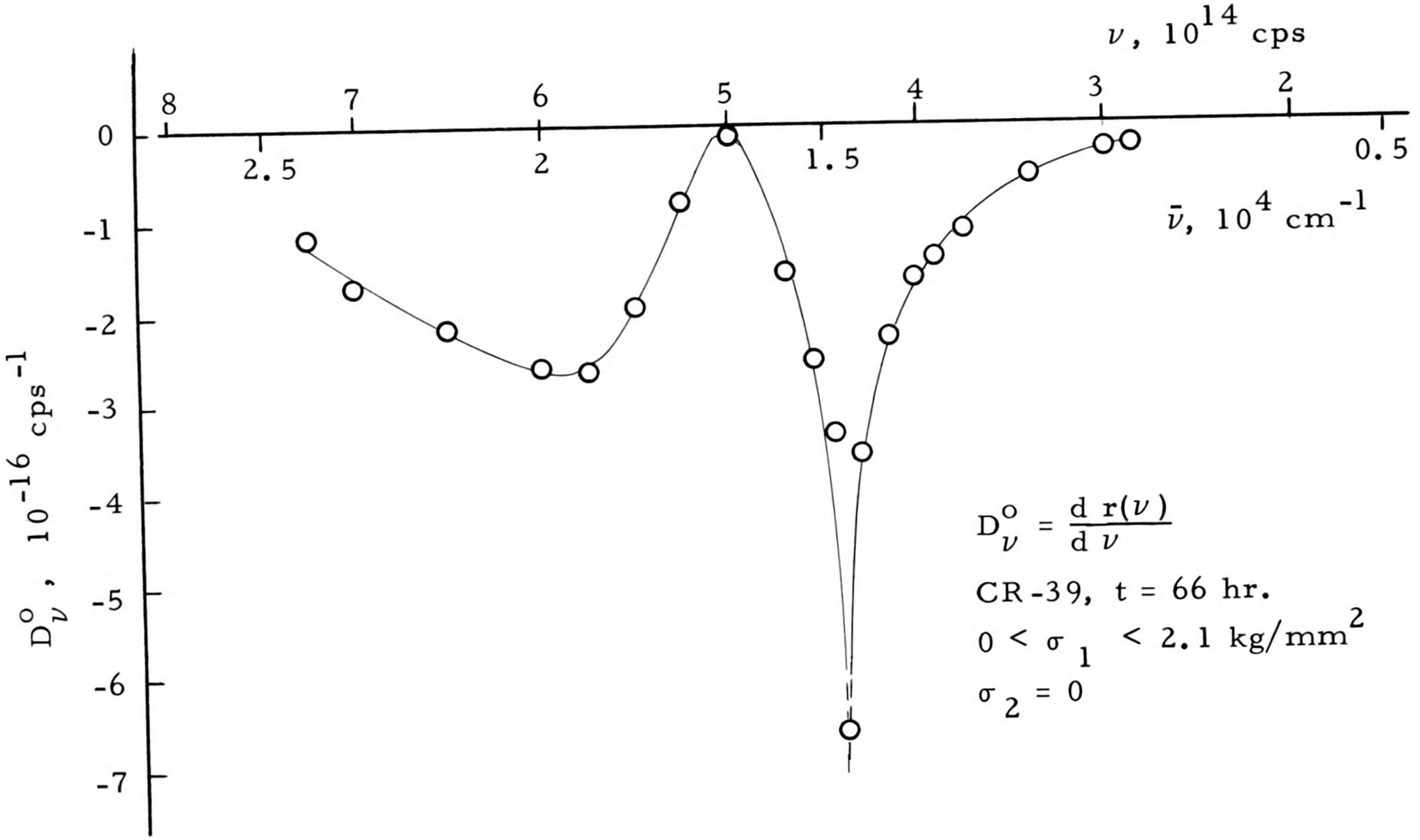

Figure 3.22(b). Dispersion of Birefringence Versus Frequency for CR-39.

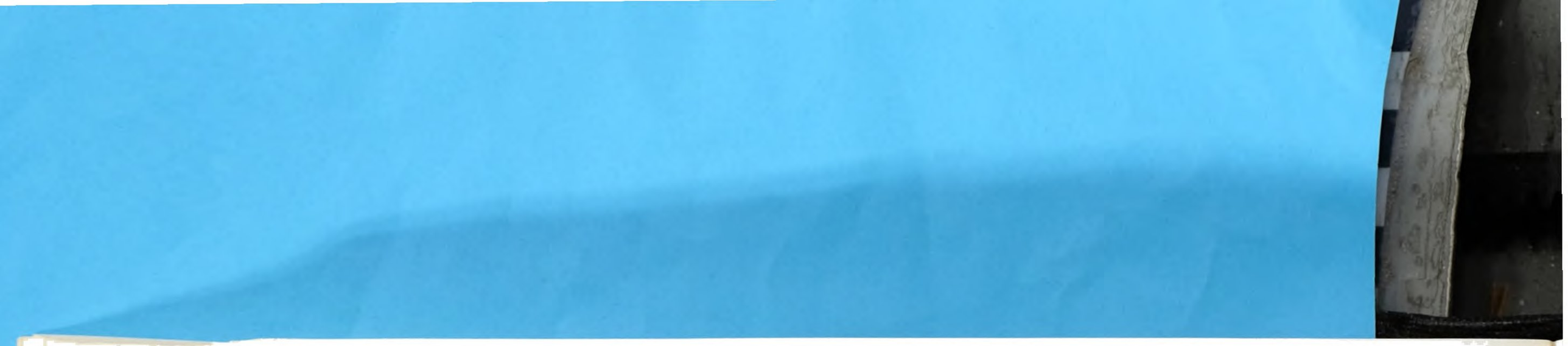

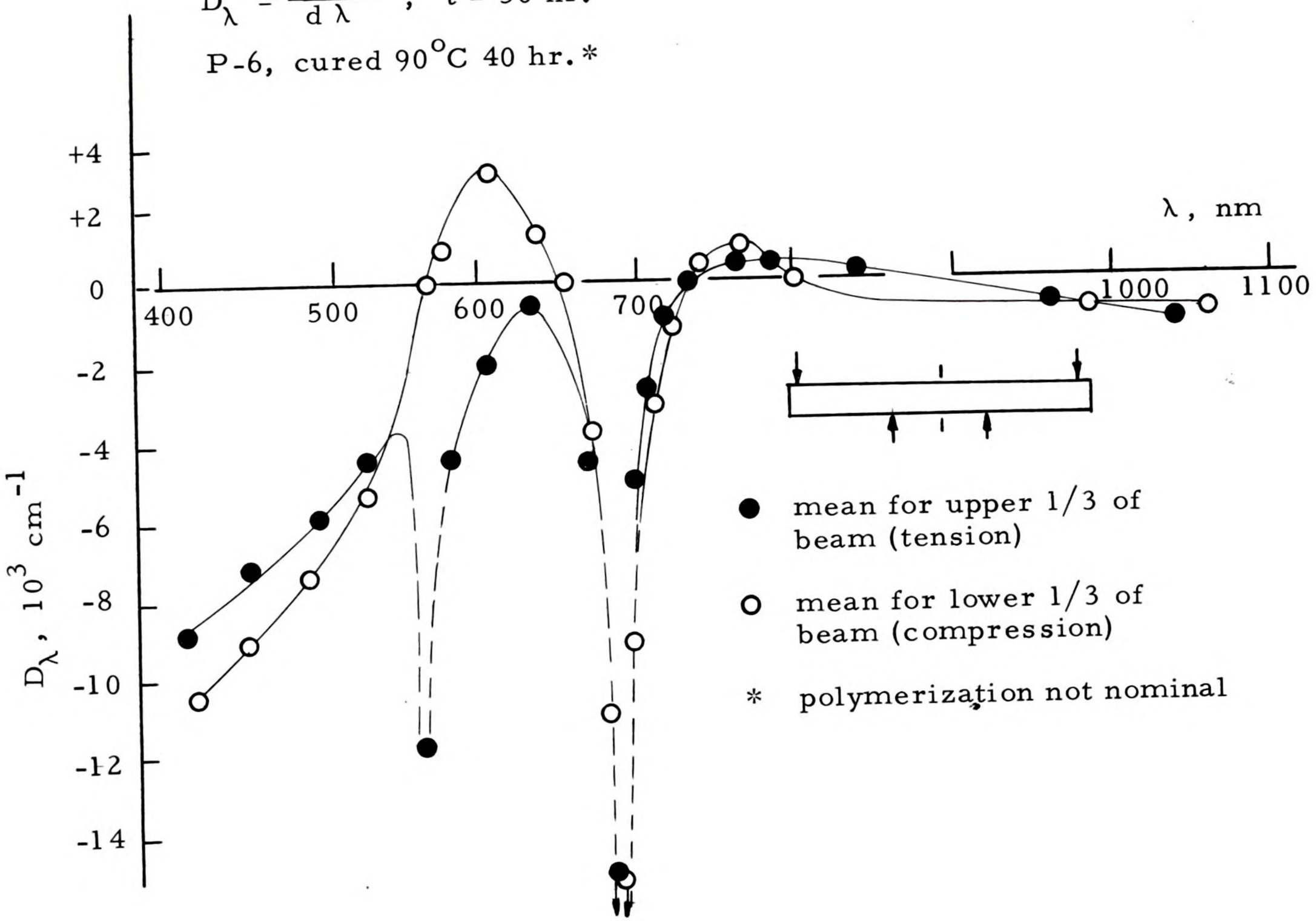

Figure 3.23(a). Dispersion of Birefringence Versus Wavelength for P-6.

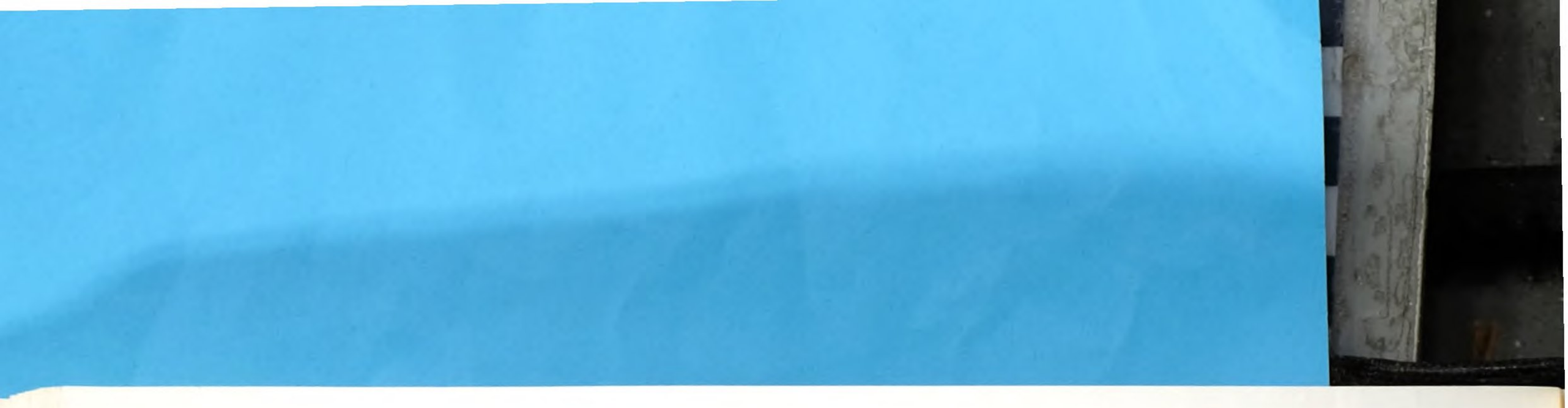

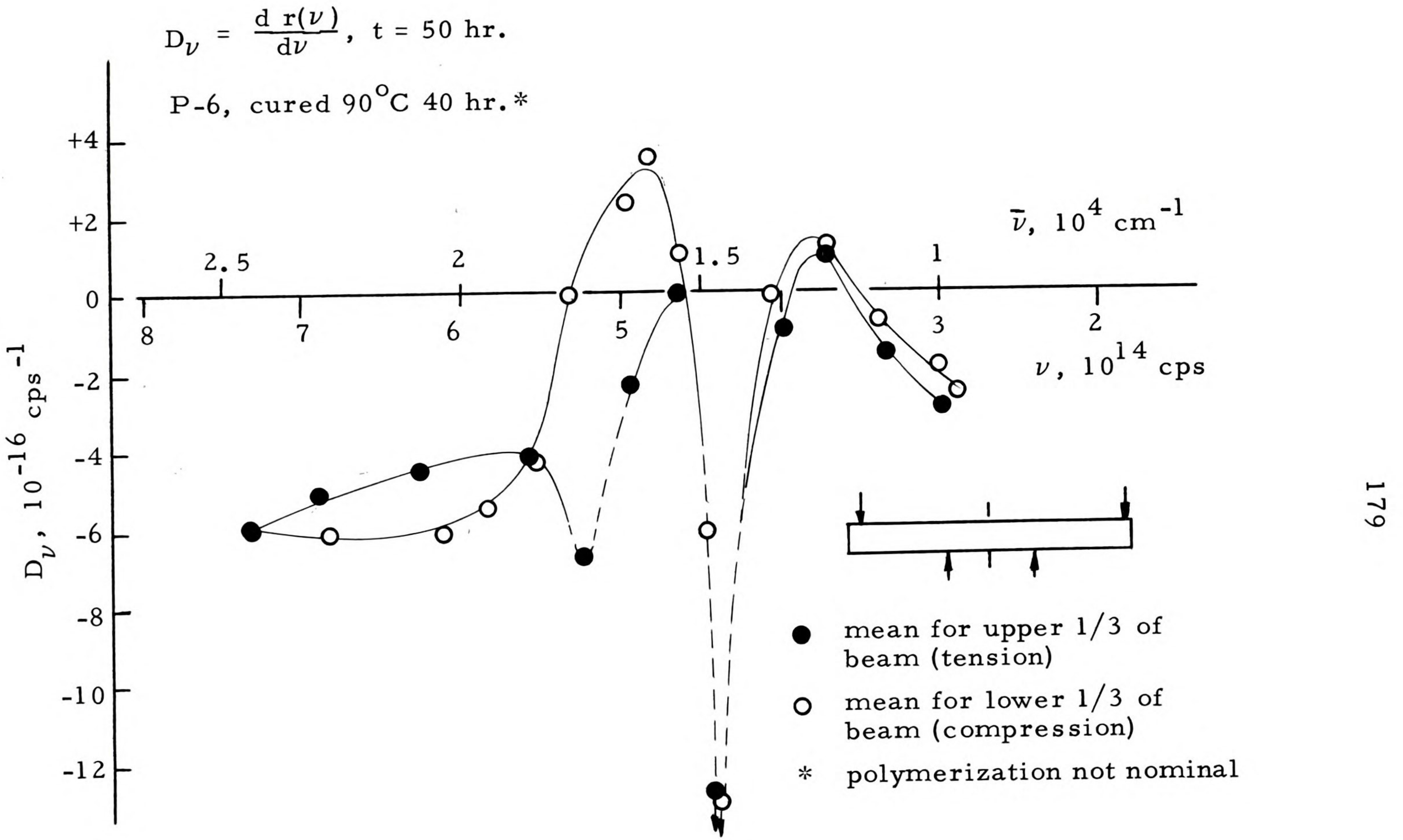

Figure 3.23(b). Dispersion of Birefringence Versus Frequency for P-6.

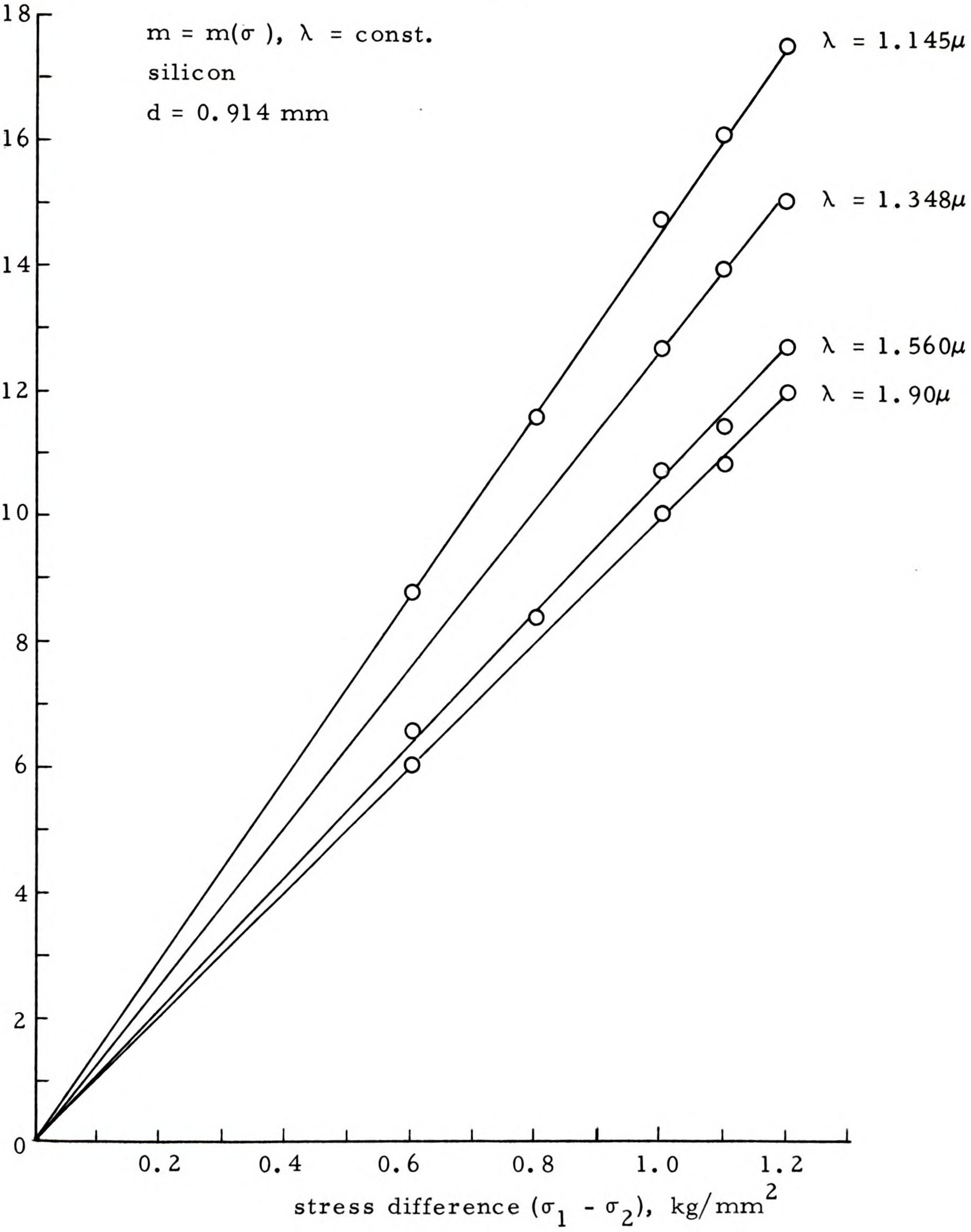

Figure 3.24. Stress Birefringence in Silicon.

APPENDIX A. Representative Measurements and Corrected Data for P-6 Beam at 546 nm.
Test code number CD-4 Film number xxxv111g; 12 A,
λ = 546 nm, light field, linear polarization

Identification	Measurement 10^{-2} mm	Location from Center line	m	m/d	R/d	Corrected location, mm
Edge	12859	184				18.73
Fringe	12819	144	5.5	9.098	4.968	14.66
Line A	12797	122				12.42
Fringe	12788	113	4.5	7.444	4.064	11.51
Fringe	12760	85	3.5	5.780	3.156	8.65
Fringe	12733	58	2.5	4.136	2.258	5.91
Fringe	12707	32	1.5	2.481	1.355	3.26
Fringe	12681	6	0.5	0.827	0.452	0.61
Centerline	12675	0				0
Fringe	12656	19	0.5	0.827	0.452	1.93
Fringe	12631	44	1.5	2.481	1.355	4.48
Line D	12610	65				6.62
Fringe	12607	68	2.5	4.136	2.258	6.92
Fringe	12583	92	3.5	5.780	3.156	9.37
Fringe	12560	115	4.5	7.444	4.064	11.71
Line E	12548	127				12.93
Fringe	12537	138	5.5	9.098	4.968	14.05
Fringe	12514	161	6.5	10.752	5.871	16.39
Edge	12487	188				19.14

Corrected location = location from centerline times magnification factor

Let AE = distance from line A to line E

$$\text{magnification factor} = \frac{\text{AE actual}}{\text{AE measured}} = \frac{3808}{374} = 10.182$$

APPENDIX B. Dimensions of Tapered CR-39 Model and Computation of Stress.

Model thickness = 0.374 in = 9.50 mm
Width of uniform neck = 0.398 in = 10.5 mm
Half angle of tapered portion = α = 6.87° = 0.1199 rad.
Load = 405 lb = 204.08 kg

The equation for the radial normal stress in a wedge of half angle α which is loaded axially at the apex is given in terms of r, the distance from the apex as:

$$\sigma_r = \frac{P \cos \theta}{r\, d\, (\alpha + \frac{1}{2} \sin 2\alpha)}$$

Along the centerline where $\theta = 0$ for the given model:

$$\sigma_r = \frac{204.8}{9.50\, r\, (0.1199 + \frac{1}{2} \sin 0.2398)}$$

$$= \frac{90.15}{r} \quad kg/mm^2$$

in the uniform neck:

$$\sigma_r = \frac{P}{A} = \frac{204.08}{(9.50)(10.15)} = 2.126\ kg/mm^2$$

APPENDIX C. Radius of Curvature and Stress in P-6 Beam.

Since the center segment of the beam is in uniform bending, its curvature is theoretically constant. The equation of the elastic curve is that of a circle of radius r and centered at (a, b):

$$(x - a)^2 + (y - b)^2 = r^2$$

The location of three points on the elastic curve is sufficient for the determination of a, b, and r. From the 35 mm photographic negative, the measured coordinates of three points on the scratched centerline of the given beam while it was deformed are:

Trial 1			Trial 2		
	Film xxxviiij			Film xxxviiif	
Point	x	y	Point	x	y
AL	11134	7409	LS	11793	7347
C	11440	7418	C	12229	7364
EL	11749	7434	RS	12666	7395

Letting the first point be the origin, the coordinates are

Trial 1			Trial 2		
Point	x	y	Point	x	y
AL	0	0	LS	0	0
C	306	9	C	436	17
EL	615	25	RS	873	48

The parameters of the elastic curve are calculated to be

	Trial 1	Trial 2
a	-.252 cm	-.316 cm
b	13.784 cm	13.72 cm
c	13.78 cm	13.73 cm

The ratio between model size and image size on the negative of trials 1 and 2 respectively were 10.33 and 9.89. The average radius of curvature of the beam from the two measurements is R = 139 cm = 54.8 inches.

The stress may be calculated from the approximate energy solution given by Den Hartog (14), since the Winkler-Bach Solution (also approximate) serves poorly for beams of small curvature. The energy solution is known to give superior results which are very near the exact theoretical solution.

$$\sigma = \frac{M}{I}\left(y + \frac{h^2}{12R} - \frac{y^2}{R}\right)$$

here:

$$h = 1.5$$

$$I = \frac{bh^3}{12} = 0.670$$

$$M = \frac{3.5P}{2} = 1.75P$$

$$P = 120$$

$$R = 54.8''$$

so

$$\sigma = 6269\left(y + .00335 - \frac{y^2}{54.8}\right)$$

Since $-.75 \leq y \leq +.75$, the maximum deviation from ordinary beam theory is only slightly greater than 1.5%. A plot of stress versus measured values of y appears in the main body of the report.

APPENDIX D. Computation of Stress Difference in Polycarbonate Disc.

For a disc of radius "a" and thickness "d" compressed along a vertical diameter by load "P", the horizontal and vertical normal stresses at the center of the disc are given by the equations (25a):

$$\sigma_x = \frac{P}{\pi a d}$$

$$\sigma_y = -\frac{3P}{\pi a d}$$

and also $\tau_{xy} = 0$

so,

$$\sigma_1 - \sigma_2 = \sigma_x - \sigma_y = \frac{4P}{\pi a d}$$

For the experiment, $d = 0.168$in, $a = 1.540$ in

$$\sigma_1 - \sigma_2 = 4.921\ P \text{ psi}$$

$$= 0.3460 \times 10^{-2}\ P \text{ kg/mm}^2$$

APPENDIX E. Illustrative Determination of Fractional Isochromatic Order in Polycarbonate Disc.

β_1 = position of analyzer at which transmitted light is minimum

$\alpha_1 \alpha_2$ = positions of analyzer on either side of β_1 at which transmitted intensity reaches arbitrary but equal values

Load = 170 kg, Analyzer and Polarizer initially at 45^o

λ micron	β_1 degrees	α_1 degrees	α_2 degrees	$\beta_2 = \frac{\alpha_1 + \alpha_2}{2}$	$\theta = 45^o - \beta_2$	m_f $\theta/180$	m_i	m
1.145	-13	+17	-37	-10	-55	-.306	2	1.694
1.244	-36	- 5	-62	-33.5	-78.5	-.432	2	1.568
1.348	-54	-23	-84	-53.5	-98.5	-.546	2	1.454
1.446	+100	+131	+70	+100.5	+55.5	+.308	1	1.308
1.550	+87	+116	+61	+88.5	+43.5	+.242	1	1.242
1.560	+82	+115	+57	+86	+41	+.228	1	1.228
1.650	+76	+107	+52	+79.5	+34.5	+.192	1	1.192
1.9	+48	+82	+ 8	+45	0	0	1	1.000

APPENDIX F. Illustrative Normalized Retardation Data and Its Statistical Treatment for CR-39.

For a population of N values of some quantity r, the average, $\bar{r}$, is given by

$$\bar{r} = \frac{1}{N} \sum_{1}^{N} r_i$$

The standard deviation, σ, (root mean square of deviation from average) is then:

$$\sigma = \left[\frac{1}{N} \sum_{1}^{N} (r_i - \bar{r})^2 \right]^{1/2}$$

For λ = 707 nm, the normalized retardation for N = 18 different stress levels is listed below as quantity r. Statistically, approximately 68% of the values which might be measured for stresses within the given limits would lie within the range encompassed by the average plus and minus the standard deviation. Sample calculations follow:

$r \times 10^{-3}$	$\lvert r_i - \bar{r} \rvert \times 10^{-3}$	$(r_i - \bar{r})^2 \times 10^{-6}$
980	3	9
979	2	4
977	0	0
974	3	9
976	1	1
977	0	0
975	2	4
972	5	25
978	1	1
976	1	1
977	0	0
975	2	4

$r \times 10^{-3}$	$\lvert r_i - \bar{r} \rvert \times 10^{-3}$	$(r_i - \bar{r})^2 \times 10^{-6}$
973	4	16
980	3	9
977	0	0
974	3	9
977	0	0
978	1	1
		93

sum = 17577

N = 18

$\bar{r}$ = 977

$$\sigma = \left(\frac{93 \times 10^{-6}}{18}\right)^{1/2}$$

σ = .0022 = 0.2%

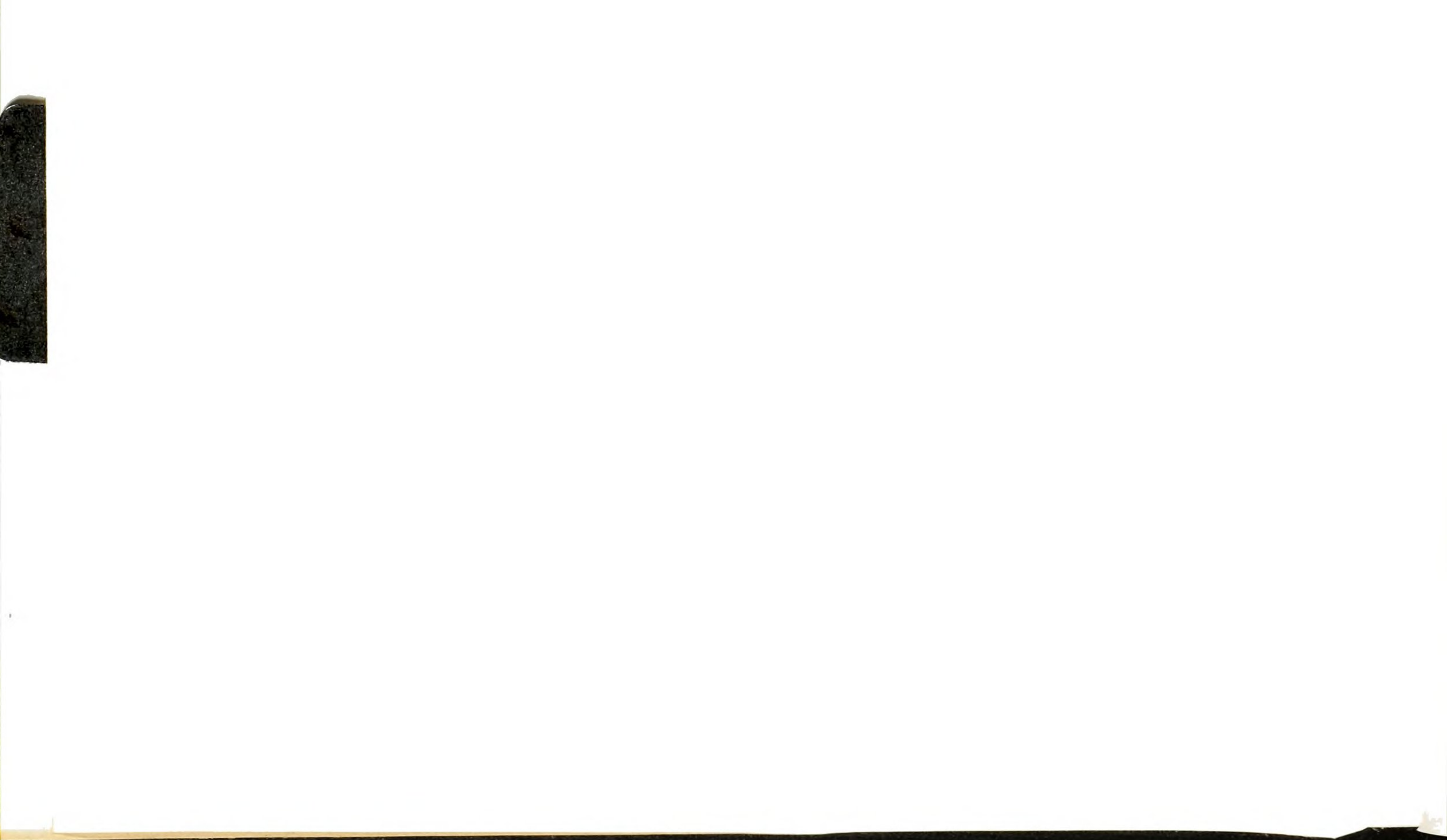

MICHIGAN STATE UNIVERSITY LIBRARIES
3 1293 03046 5649